

**UC Davis**

**UC Davis Electronic Theses and Dissertations**

**Title**

Aqueous-Phase Chemistry of Secondary Organic Aerosol and Brown Carbon from Biomass Burning Emissions

**Permalink**

<https://escholarship.org/uc/item/4hb0q7qd>

**Author**

Jiang, Wenqing

**Publication Date**

2022

Peer reviewed|Thesis/dissertation

Aqueous-Phase Chemistry of Secondary Organic Aerosol and Brown Carbon from  
Biomass Burning Emissions

By

WENQING JIANG

DISSERTATION

Submitted in partial satisfaction of the requirements for the degree of

DOCTOR OF PHILOSOPHY

in Agricultural and Environmental Chemistry

in the

OFFICE OF GRADUATE STUDIES

of the

UNIVERSITY OF CALIFORNIA DAVIS

Approved by:

---

Qi Zhang, Chair

---

Cort Anastasio

---

Tran B. Nguyen

Committee in Charge

2022

## Abstract

Secondary organic aerosol (SOA), formed from atmospheric transformation of primary organic emissions, is an important component of atmospheric aerosol. A great effort has been made to understand SOA sources, composition, and properties over the last decade; however, our understanding of SOA is still limited, and especially, SOA formation in atmospheric aqueous-phase remains poorly interpreted. A thorough characterization of the composition and properties of SOA and a better understanding of the formation and fate of SOA are critical for predicting the impact of SOA on climate and human health. This dissertation takes advantage of advanced techniques such as high-resolution time-of-flight aerosol mass spectrometer (HR-ToF-AMS) and aims to understand the formation and aging of SOA generated from phenolic precursors which are emitted in significant quantities from biomass burning, as well as to investigate brown carbon (BrC) formation in phenolic SOA.

Chapter 2 presents phenolic aqueous-phase SOA (aqSOA) formation from the photosensitized reaction of guaiacyl acetone (a phenolic carbonyl model compound) with a triplet excited states of organic carbon ( $^3C^*$ ). Rapid and efficient aqSOA production were observed with mass yield ~80%. The composition of phenolic aqSOA continuously evolves, with oligomerization and functionalization dominating the initial formation while fragmentation taking over during extended periods. BrC chromophores produced in initial aqSOA formation are identified as oligomers and functionalized monomers of the phenolic precursor. Additionally, significant carboxylic acid formation was observed in phenolic aqSOA formation.

In chapter 3, photochemical aging of phenolic aqSOA generated from different oxidants (i.e.,  $\bullet OH$  and  $^3C^*$ ) were studied. The aqSOA generated from  $\bullet OH$  reaction ( $\bullet OH$ -aqSOA) is more

oxidized and shows lower amounts of oligomeric products than the aqSOA generated from  $^3\text{C}^*$  reaction ( $^3\text{C}^*$ -aqSOA), and accordingly, BrC formation is less significant in  $\bullet\text{OH}$ -aqSOA. Prolonged photochemical aging extended up to 21 days of equivalent atmospheric sunlight results in a significant loss of aqSOA mass and decay of BrC absorption, suggesting fragmentation and evaporation of oxidized volatile species dominates the prolonged photo-aging. Additionally, the effects of increased oxidant concentration during aging were investigated. Accelerated chemical evolution, specifically, promoted fragmentation and evaporation of volatile species and facilitated photobleaching were observed with increased oxidant concentration.

Chapter 4 compares phenolic SOA generated from gas-phase reactions (gasSOA) with that from aqueous-phase reactions. Significant chemical differences were observed between phenolic gasSOA and aqSOA. The initially formed gasSOA is more oxidized than the initially formed aqSOA, and there is negligible change of oxidation degree during gasSOA formation, while aqSOA continuously gets more oxidized during formation. Oligomerization plays an important role in the initial formation of phenolic aqSOA, whereas is not observed in phenolic gasSOA. Additionally, aqSOA shows more pronounced carboxylic formation. The chemical differences observed between gasSOA and aqSOA indicate the importance of incorporating both gas-phase and aqueous-phase reaction pathways in models for better prediction of SOA formation.

Another important part of this dissertation is to explore the sources, composition, and optical properties of ambient water-soluble BrC (WS-BrC) aerosol in North California. In Chapter 5, the water-soluble components of  $\text{PM}_{2.5}$  samples collected in Davis were analyzed by HR-ToF-AMS and UV-vis spectroscopy (UV-vis). Positive matrix factorization (PMF) was applied to the combined AMS and UV-vis data and resolved five water-soluble organic aerosol (WSOA) factors (including a fresh and an aged water-soluble biomass burning organic aerosol (WS-BBOA) and

three water-soluble oxygenated organic aerosol (WS-OOA) factors) with distinctive mass spectral and UV-vis spectral profiles. The fresh WS-BBOA is the most light-absorbing and contributes the most to the total light absorption of WS-BrC in Davis. Additionally, the BrC chromophores in WS-BBOA and WS-OOA appear to be important sources of aqueous-phase oxidants (i.e.,  $^3\text{C}^*$  and singlet oxygen ( $^1\text{O}_2^*$ )) in the atmosphere.

## Acknowledgements

Davis has been a nice place to do my Ph.D, and there are many to thank. First, to my advisor Dr. Qi Zhang, I've really appreciated the advice and resources I was given to pursue my research interests. Without the scientific guidance and mentorship she has provided, I would not have been able to complete this research. Working with such an intelligent and supportive mentor has added wonderful depth to my graduate school career. The Zhang Research Group was also a huge support network over the years, special thanks to Shan Zhou, Caroline Parworth, Sonya Collier, Christopher Niedek, Ryan Farley, and Justin Trousdell.

Next, a sincerely thanks to Dr. Cort Anastasio and Dr. Tran Nguyen, for their valuable insights as both members of my qualifying exam and dissertation committees. I also thank the other members of my qualifying exam committee, Dr. Christopher Cappa, Dr. Ann Dillner, and Dr. Peter Green.

I would also like to thank the collaborators from Anastasio Research Group: Richie Kaur, Alex McFall, Lan Ma, and Stephanie Arciva.

Special thanks to my sources of funding: the US National Science Foundation (Grant AGS-1649212 and AGS-2220307), the California Agricultural Experiment Station (Projects CA-D-ETX-2102-H and CA-D-LAW-6403-RR), and the US Department of Energy (DOE) Atmospheric System Research Program (Grant DESC0022140). Additional funding was provided by Jastro-Shields Graduate Research Award (UC Davis), Donald G. Crosby Fellowship (UC Davis), James & Rita Seiber International Graduate Student Support Award (UC Davis), Matsumura Memorial Fellowship (UC Davis) and Chinese Scholarship Council Scholarship (China).

Finally, and with the deepest love and gratitude, I thank my family who have been listening, encouraging me, inspiring me to pursue my goals. Thank you for the love and support.

## Table of Contents

<b>Abstract.....</b>	<b>i</b>
<b>Acknowledgements .....</b>	<b>iv</b>
<b>Chapter 1: Introduction .....</b>	<b>1</b>
1.1 Atmospheric Aerosol and Secondary Organic Aerosol .....	1
1.2 Aqueous-phase Chemistry and its Role in SOA Formation.....	3
1.3 Phenolic SOA.....	4
1.4 Atmospheric Brown Carbon.....	7
1.5 Dissertation Organization.....	8
1.6 Publications associated with this dissertation .....	10
References .....	11
<b>Chapter2: Photosensitized Reactions of a Phenolic Carbonyl from Wood Combustion in the Aqueous Phase – Chemical Evolution and Light Absorption Properties of AqSOA.....</b>	<b>17</b>
2.1 Abstract .....	17
2.2 Introduction .....	18
2.3 Experimental Methods .....	21
2.3.1 Aqueous-phase Photochemical Reaction.....	21
2.3.2 Sample Analyses.....	22
2.4 Results and Discussion.....	27
2.4.1 Photosensitized Oxidation of Guaiacyl Acetone and aqSOA Formation.....	27
2.4.2 Photochemical Evolution of GA aqSOA Composition and Light Absorption.....	29
2.4.3 Molecular Characterization of BrC in GA aqSOA.....	35
2.5 Atmospheric Implication.....	36
Figures.....	39
Reference.....	48
Supporting Information.....	55
<b>Chapter3: Photochemical Aging of Phenolic Secondary Organic Aerosol in Aqueous Phase: Evolution of Chemical and Optical Properties and Effects of Different Oxidants.....</b>	<b>65</b>
3.1 Abstract .....	65
3.2 Introduction .....	66
3.3 Experimental .....	69
3.3.1 Formation and Aging of Phenolic AqSOA.....	69

3.3.2 Chemical and Optical Analyses.....	70
3.4 Results and Discussion.....	72
3.4.1 AqSOA Formation in •OH- and <sup>3</sup> C* -initiated Photoreactions of Guaiacyl Acetone....	72
3.4.2 Photo-transformation of AqSOA and Evolution of SOA Yield and Composition during Prolonged Aging.....	75
3.4.3 Evolution of AqSOA Optical Properties during Prolonged Aging .....	78
3.4.4 Effects of Additional Oxidant Exposure on AqSOA Aging.....	79
3.5 Conclusions.....	80
Figures.....	83
Reference.....	92
Supporting Information.....	99
<b>Chapter 4: Chemical Differences between Phenolic Secondary Organic Aerosol Formed through Gas-phase and Aqueous-phase Reactions.....</b>	<b>105</b>
4.1 Abstract .....	105
4.2 Introduction .....	106
4.3 Experimental Methods .....	108
4.3.1 Overview of Photooxidation Experiments .....	108
4.3.2 Chemical Analysis.....	109
4.4 Results and Discussion.....	109
4.4.1 Comparison of chemical composition between gasSOA and aqSOA at t <sub>0.5</sub> and t <sub>0.25</sub> .	109
4.4.2 Chemical evolution of gasSOA and aqSOA.....	111
4.4.3 Formation of oligomers and high molecular weight species .....	112
4.4.4 Formation of organic acids .....	113
4.4.5 Molecular level comparison .....	114
Reference.....	117
Figures.....	121
Supporting Information.....	129
<b>Chapter 5: Chemical and Absorption Properties of Water-Soluble Organic Aerosols in Northern California and Insights into the Photooxidant Production Potentials of Brown Carbon Components.....</b>	<b>139</b>
5.1 Abstract .....	139
5.2 Introduction .....	140
5.3 Materials and Methods.....	143
5.3.1 PM sample collection and extraction.....	143



5.3.2 Chemical and optical analyses of PM extracts .....	143
5.3.3 Measurements of photooxidants .....	144
5.3.4 Data analysis .....	145
5.4 Results and Discussions .....	148
5.4.1 Bulk compositions and light absorption properties of WSOA in PM <sub>2.5</sub> .....	148
5.4.2 Chemical compositions and light absorption of WSOA factors.....	149
5.4.3 Relationship between WSOA components and condensed-phase oxidants ( $\bullet\text{OH}$ , $^3\text{C}^*$ and $^1\text{O}_2^*$ ).....	154
5.4.4 Estimation of global aqueous-phase oxidant concentrations.....	156
5.5 Conclusions .....	157
Figures .....	160
Reference.....	168
Supporting Information .....	176
<b>Chapter 6: Conclusions .....</b>	<b>188</b>

## **Chapter 1: Introduction**

### **1.1 Atmospheric Aerosol and Secondary Organic Aerosol**

Atmospheric aerosols, composed of suspended solid and liquid particles with size ranging from nanometers to micrometers in air, originate from a wide variety of nature and anthropogenic sources and can have significant impacts on climate, air quality and human health (Kanakidou et al., 2005; Nel, 2005). Aerosol particles can alter the energy balance of the climate system directly by scattering and absorbing solar radiation, and indirectly by acting as cloud condensation nuclei (CCN) and ice nuclei or by modifying the optical properties and lifetime of clouds (Haywood and Boucher, 2000). For example, light colored aerosols such as sulfate and most organic aerosols typically reflect and scatter sunlight, whereas black carbon (BC), mineral dust, and brown carbon (BrC) can absorb sunlight and warm the atmosphere. The aerosol-cloud interaction can exert a negative perturbation on radiation by increasing cloud optical depth and cloud cover, whereas it may also contribute to warming by reducing cloud amount through increased precipitation or promoted cloud water evaporation (Lohmann and Feichter, 2005). Currently, aerosols are generally considered to have global cooling effects, however, there is still a large uncertainty in aerosols' impacts on the radiation balance of the earth, due to the complex sources, composition, and transformation of aerosols and the complexity in aerosol-cloud interactions. Apart from climate impacts, aerosols also have adverse effects on human health. Fine particulate matters with diameter less than  $2.5 \mu\text{M}$  ( $\text{PM}_{2.5}$ ) can be deposited deep into the pulmonary system, leading to inflammation of the lungs, and inducing oxidative stress and respiratory diseases (Happo et al., 2013; MohanKumar et al., 2008; R. et al., 2017). Epidemiological studies have shown that exposure to PM leads to a consistent increase in cardiac and respiratory morbidity and mortality,

and global analyses have estimated that air pollution can result in about 4.3 million of deaths per year (Cohen et al., 2017; Shiraiwa et al., 2017).

Organic aerosols contribute for a substantial fraction of atmospheric aerosols, accounting for 20-90% of the particulate mass in the lower troposphere (Kanakidou et al., 2005; Murphy et al., 2006; Zhang et al., 2007). The sources of organic aerosols include both primary emissions (i.e., POA) from combustion sources and secondary formation (i.e., SOA) through chemical reactions in the atmosphere. Studies have shown that SOA makes up a large fraction (65-95%) of the ambient organic mass (De Gouw and Jimenez, 2009; Zhang et al., 2007), and due to the variety of the precursors and different physical and chemical processes, the composition, properties and climate and health effects of SOA are highly uncertain. One of the most common SOA formation mechanisms is through the gas-phase reactions of volatile, semi-volatile and intermediate-volatile organic compounds (VOCs, SVOCs and IVOCs) with oxidants such as ozone ( $O_3$ ), hydroxyl radical ( $\bullet OH$ ), and nitrate ( $NO_3$ ), followed by the condensation or nucleation of the less volatile products (Kroll and Seinfeld, 2008). The major classes of SOA precursors include alkenes (e.g., isoprene, monoterpenes, and sesquiterpenes) which are mainly emitted from biogenic sources dominated by vegetation, and alkanes and aromatic hydrocarbons which are mainly emitted from anthropogenic sources such as traffic and industry (Henze and Seinfeld, 2006; Kroll et al., 2006; Ng et al., 2007). Recent studies have also found that biomass burning (BB) emits a significant amount of oxygenated aromatic compounds, including phenol and methoxyphenols, which can be important SOA precursors, accounting for 60% of the SOA formation in BB emissions (Akherati et al., 2020). While gas-phase oxidation of VOCs is an important pathway, it cannot fully explain the SOA formation in the atmosphere: models involving only gas-phase reaction pathways tend to underestimate organic aerosol concentrations, and lab-generated SOA from gas-phase reactions is

usually less oxidized than aged ambient organic aerosols (Aiken et al., 2008; Heald et al., 2005). Heterogeneous oxidations, in which gas-phase radicals diffuse to the aerosol surface and react with surface-bound aerosol constituents, and aqueous-phase reactions, in which water-soluble precursors react with oxidants in atmospheric waters (e.g., cloud/fog droplets and particle water), are also significant contributors to SOA formation (George and Abbatt, 2010; Herrmann et al., 2015).

## **1.2 Aqueous-phase Chemistry and its Role in SOA Formation**

Atmospheric aqueous phase exists in different forms, such as cloud droplets, fog water, rain, and aerosol particle water, and there are huge variations in microphysical (e.g., size and liquid water content (LWC)) and chemical (e.g., pH and ionic strength) characteristics (McNeill, 2015) between different forms of atmospheric waters. The LWC can range from 0.001-0.01 g m<sup>-3</sup> for deliquescent aerosol particles to 0.05-3 g m<sup>-3</sup> for cloud and fog water, and the pH varies between 0-9 for aerosol particles and 2-7 for cloud and fog water. The ionic strength varies from 10<sup>-4</sup> M for dilute cloud and fog droplets to > 10 M for deliquescent aerosol particles (Herrmann et al., 2015; McNeill, 2015). These variations in liquid water conditions could affect phase transfer and the chemical reactions in aqueous-phase (Herrmann et al., 2015).

Research on atmospheric aqueous-phase reactions has been developed since the early 1980s (Graedel and Weschler, 1981), and at that time, aqueous-phase chemistry was identified to include acid generation through efficient SO<sub>2</sub> oxidation in cloud droplets. Later, a wide range of organic reactions, including organic acid formation, accretion reactions (such as aldol reactions, acetal and hemiacetal formation, and other oligomerizations where small molecules combine under the

formation of C-C or C-O-C bond sequences), and hydrolysis reactions have been studied (Altieri et al., 2008; Carlton et al., 2006; Nguyen et al., 2012; Sareen et al., 2010).

Recently, aqueous-phase reactions have been hypothesized to be an important source of SOA (Blando and Turpin, 2000), which affect not only the mass concentration but also the properties of SOA. Studies have shown that SOA formed from aqueous-phase reactions (aqSOA) can be more oxygenated and more hygroscopic than the SOA produced from gas-phase reactions (gasSOA) (Ervens et al., 2011). Additionally, gasSOA particles are usually in the condensation mode, whereas aqSOA can contribute significantly to the droplet mode, and thus can modify the aerosol size distributions differently (Ervens et al., 2011). AqSOA formation initiates with the partition of water-soluble precursors to atmospheric waters, followed by reactions in the aqueous phase to form low-volatility products such as organic acids, oligomers, and organosulfates which can remain in the particle phase upon water evaporation. For example, methylglyoxal can undergo aqueous-phase oxidation to produce pyruvic acid which subsequently reacts to form low-volatility oxalic and glyoxylic acids and oligomerization products (Carlton et al., 2006; Ervens et al., 2004; Guzmán et al., 2006). Perri et al. has reported that aqueous-phase  $\bullet\text{OH}$  oxidation of glycolaldehyde in the presence of sulfuric acid can produce low-volatility organosulfates through radical-radical reactions (Perri et al., 2010). In addition, several studies have demonstrated that phenolic compounds (such as phenol, catechol, cresols, methoxyphenols, and phenolic carbonyls), which usually have high Henry's law constants, can go fast aqueous-phase photoreactions with oxidants (such as  $\bullet\text{OH}$ ,  $\text{NO}_3$ , and the triplet excited states of organic carbon ( $^3\text{C}^*$ )) in atmospheric waters to produce aqSOA with high mass yields (Huang et al., 2018; Pang et al., 2019; Smith et al., 2014; Sun et al., 2010; Yu et al., 2014).

### **1.3 Phenolic SOA**

Phenols are an important class of aromatic compounds ubiquitous in the atmosphere. The concentration of phenols in the air is in the  $\text{ng m}^{-3}$  rang, and it can get up to  $\sim 100 \mu\text{g L}^{-1}$  in atmospheric waters (Trempe 1993). The major sources of atmospheric phenols include biomass burning, vehicle emissions, and oxidation from aromatic hydrocarbons (Schauer et al., 2001; Trempe et al., 1993; Volkamer et al., 2002). Studies have shown that wood combustion emits a variety of phenolic compounds (such as phenol, guaiacol and substituted guaiacols, and syringol and substituted syringols) from the pyrolysis of lignin, with emission rates ranging from 400 to  $900 \text{ mg kg}^{-1}$  fuel (Hawthorne et al., 1989; Schauer et al., 2001). Guaiacol and syringol have been proposed as important aerosol markers for wood combustion (Simpson et al., 2005).

In the gas phase, phenols can react with oxidants (such as ozone,  $\bullet\text{OH}$  and  $\text{NO}_3$ ) to produce SOA with mass yield ranging from 17%- 86% (Coeur-Tourneur et al., 2009; Yee et al., 2013). The gas-phase rate coefficients for the  $\bullet\text{OH}$  oxidation of phenols range from 5 to  $10 \times 10^{-11} \text{ cm}^3 \text{ molecule}^{-1} \text{ s}^{-1}$  (Coeur-Tourneur et al., 2010; Lauraguais et al., 2015), and the ozonolysis rate coefficients are in the range of  $9 \times 10^{-18}$  -  $3 \times 10^{-17} \text{ cm}^3 \text{ molecule}^{-1} \text{ s}^{-1}$  (Tomas et al., 2003). The gas-phase  $\bullet\text{OH}$  reaction of phenols initiates by H-atom abstraction from the hydroxyl group to form a phenoxy radical or by  $\bullet\text{OH}$  radical addition to the aromatic ring followed by reaction with  $\text{O}_2$  to form an organic peroxy radical ( $\text{RO}_2\bullet$ ) (Olariu et al., 2002). This  $\text{RO}_2\bullet$  radical have three major fates: 1) to react with  $\text{HO}_2\bullet$  to form a hydroperoxide; 2) to eliminate  $\text{HO}_2\bullet$  to form OH-adducts and benzoquinones; and 3) to isomerize to a bicyclic radical which can further reacts to form ring-opening products (e.g., aldehydes, ketones, esters, small organic acids, and epoxides) (Olariu et al., 2002; Yee et al., 2013). In addition, under high  $\text{NO}_x$  conditions, nitrophenols can be formed through the reaction of  $\text{NO}_2$  with phenoxy radical (Atkinson et al., 1992; Olariu et al., 2002). The

SOA mass yield from gas-phase •OH reaction of phenols has been reported in the range of 25-49% under low NO<sub>x</sub> conditions (Yee et al., 2013).

In addition to gas-phase reactions, phenolic compounds can have high Henry's law constant up to  $10^8 \text{ M atm}^{-1}$  (McFall et al., 2020), and thus readily partition to the aqueous phase and undergo fast photochemical reactions therein. Studies have shown that the rate of aqueous-phase photolysis and photooxidation of phenols can be comparable to that in the gas phase (Coeur-Tourneur et al., 2010; Li et al., 2014a; Sun et al., 2010). Direct photolysis of phenols in the aqueous has been found to produce hydroxylated compounds (e.g., hydroquinones) and dimer products (e.g., dihydroxybiphenyls and hydroxydiphenyl ethers) (Rayne et al., 2009; Sun et al., 2010). Besides this, phenols also react with aqueous-phase oxidants effectively to produce aqSOA. For example, •OH, which is typically considered the dominant oxidant for organics in the aqueous phase, reacts with phenols rapidly with rate constant in the range of  $1.9\text{-}25 \times 10^9 \text{ M}^{-1} \text{ s}^{-1}$ , and produces aqSOA with mass yield ranging from 67-140% (Arciva et al., 2022; Sun et al., 2010; Yu et al., 2014, 2016). Hydroxylation, oligomerization, demethoxylation, and fragmentation have been proposed to be important reaction pathways in the aqueous-phase •OH photooxidation of phenols (Sun et al., 2010; Yu et al., 2014). Compared with direct photolysis, •OH oxidation tends to produce more oxidized aqSOA, higher amount of fragmented ring-opening products and more small organic acids (e.g., oxalic acid) (Li et al., 2014a; Sun et al., 2010), and this compositional difference in turn results in differences in SOA properties (e.g., hygroscopicity and light absorptivity) (Li et al., 2014a). Another important type of aqueous-phase reactions of phenols is the photosensitized reactions with  $^3\text{C}^*$  produced from the sunlight absorption by organic chromophores (Hawthorne et al., 1989; Simoneit, 1999). Upon sunlight absorption, the ground state organic chromophore can be promoted to the excited singlet state which is not stable and can be converted to the triplet state

through intersystem crossing (Anastasio 1997; McNeill 2016), and the formed triplet state can further undergo energy transfer (e.g., react with O<sub>2</sub> to form singlet oxygen (<sup>1</sup>O<sub>2</sub>)) and electron transfer (e.g., react with phenols to form phenoxy radical) processes. Studies have shown that the reaction rates of phenols with <sup>3</sup>C\* (ranging from 2-11 × 10<sup>9</sup>) are comparable to or even faster than that of •OH reactions (Ma et al., 2021; Smith et al., 2014), especially under conditions with high abundance of organic chromophores such as biomass burning impacted cloud and fog water. Similar to •OH oxidation, the <sup>3</sup>C\* reactions of phenols have been proposed to undergo oligomerization, functionalization, and fragmentation (Yu et al., 2014, 2016) to form aqSOA with high mass yield ranging from 59% to 120% (Ma et al., 2021; Yu et al., 2016). Compared with •OH oxidation, <sup>3</sup>C\* reactions tend to produce higher amount of high molecular weight products (e.g., phenolic oligomers and oxygenated oligomeric derivatives) which can possibly affect the volatility and optical properties of the aqSOA. Indeed, in this dissertation, we find the functionalized and oligomeric products from the aqueous-phase reactions of phenolic compound can absorb near-UV and visible light and contribute to BrC in the atmosphere.

## 1.4 Atmospheric Brown Carbon

Although organic aerosols are typically considered to scatter light, some organics absorb sunlight efficiently in near-UV and visible range and are termed brown carbon (BrC) (Andreae and Gelencsér, 2006; Laskin et al., 2015). Different from black carbon (BC) which strongly absorbs light over a broad range (from UV extended to infrared) with negligible wavelength dependence, BrC typically show an absorption spectrum that gradually decreases from UV to visible. The sources of BrC are complex, including both primary emissions (e.g., biomass and coal combustions and biogenic release of fungi, plant debris, and humic substances) (Claeys et al., 2012; Hecobian et al., 2010; Jo et al., 2016; Rizzo et al., 2011) and secondary formations such as



organonitrate formation from gas-phase photooxidation of aromatic hydrocarbons in the presence of NO<sub>x</sub> (Liu et al., 2015), evaporation-driven oligomer formation in limonene SOA in the presence of ammonium sulfate (Nguyen et al., 2012), aqueous-phase imidazole formation from dicarbonyl reactions with ammonia or amines (Kampf et al., 2016), and aqueous oxidation of phenolic compounds (Smith et al., 2016). Primary BrC from high temperature combustions generally appears to be more light-absorbing than secondary BrC (Saleh, 2020). Although many studies have been done to understand BrC, its composition, properties, and atmospheric lifetime remain poorly understood, due to the complex sources and formation mechanisms in the atmosphere.

## **1.5 Dissertation Organization**

The major goal of this dissertation is to thoroughly characterize the formation and aging of phenolic SOA. Several specific scientific questions this dissertation tries to answer includes:

1. What are the composition and optical properties of phenolic aqSOA?
2. What are the BrC chromophores formed in phenolic aqSOA?
3. How does long-duration of photochemical aging modify the composition and light absorption properties of phenolic aqSOA?
4. How does oxidant level influence the aging of phenolic aqSOA?
5. Is there any chemical difference between phenolic gasSOA and aqSOA?

In Chapter 2, lab experiments were conducted to investigate aqSOA and BrC formation from the photosensitized reactions of guaiacyl acetone with <sup>3</sup>C\* under biomass burning influenced cloud and fog water conditions. The results demonstrate efficient aqSOA formation and continuously chemical and optical property evolution of the aqSOA. Oligomerization and functionalization

occurring in the initial aqSOA generation can contribute to BrC formation, whereas fragmentation occurring in the later periods contributes to significant small carboxylic acid formation.

In Chapter 3, phenolic aqSOA formation from OH and  $^3\text{C}^*$  were compared. Long-duration of photo-aging extended up to 21 days of atmospheric sunlight were studied. In addition, the impact of increased oxidant concentration during prolonged aging were investigated. The results show differences between initially formed OH- and  $^3\text{C}^*$ -aqSOA. Prolonged photo-aging leads to significant aqSOA mass loss and photobleaching. Additionally, increased oxidant concentration accelerates the chemical evolution of phenolic aqSOA, promoting fragmentation and evaporation of volatile products.

Chapter 4 compares the phenolic SOA generated from gas-phase photoreactions with the phenolic aqSOA. Significant compositional differences were observed between the initially formed gasSOA and aqSOA, although these differences gradually become less noticeable in extended aging. This study highlights the importance of involving both gas-phase and aqueous-phase reactions in model predictions for SOA formation

As BrC chromophores represent an important portion of phenolic aqSOA, following the laboratory studies on BrC formation from phenols, this dissertation further explores the composition and properties ambient BrC aerosol.

In Chapter 5, the water-soluble components in  $\text{PM}_{2.5}$  samples collected in Davis over one year were characterized by AMS and UV-vis. The results suggest the water-soluble biomass burning organic aerosol (WS-BBOA) represents the most light-absorbing portion of the water-soluble organic aerosol (WSOA), and due to its high abundance, WS-BBOA appears to be the most important source of water-soluble BrC in Davis.

## 1.6 Publications associated with this dissertation

As listed below, Chapter 2 is published, and Chapter 3-5 are in preparation for submission.

Chapter 2: Jiang, W., Misovich, M. V, Hettiyadura, A. P. S., Laskin, A., McFall, A. S., Anastasio, C. and Zhang, Q.: Photosensitized Reactions of a Phenolic Carbonyl from Wood Combustion in the Aqueous Phase—Chemical Evolution and Light Absorption Properties of AqSOA, *Environ. Sci. Technol.*, 55(8), 5199–5211, doi:10.1021/acs.est.0c07581, 2021.

Chapter 3: Jiang, W. et al.: Photochemical Aging of Phenolic Secondary Organic Aerosol in Aqueous Phase: Evolution of Chemical and Optical Properties and Effects of Different Oxidants, In preparation.

Chapter 4: Jiang, W. et al.: Chemical Differences between Phenolic Secondary Organic Aerosol Formed through Gas-phase and Aqueous-phase Reactions, In preparation.

Chapter 5: Jiang, W., Ma, L., Niedek, C., Anastasio, C., Zhang, Q.: Chemical and Absorption Properties of Water-Soluble Organic Aerosols in Northern California and Insights into the Photooxidant Production Potentials of Brown Carbon Components, In preparation.

## References

- Aiken, A. C., DeCarlo, P. F., Kroll, J. H., Worsnop, D. R., Huffman, J. A., Docherty, K. S., Ulbrich, I. M., Mohr, C., Kimmel, J. R., Sueper, D., Sun, Y., Zhang, Q., Trimborn, A., Northway, M., Ziemann, P. J., Canagaratna, M. R., Onasch, T. B., Alfarra, M. R., Prevot, A. S. H., Dommen, J., Duplissy, J., Metzger, A., Baltensperger, U. and Jimenez, J. L.: O/C and OM/OC Ratios of Primary, Secondary, and Ambient Organic Aerosols with High-Resolution Time-of-Flight Aerosol Mass Spectrometry, *Environ. Sci. Technol.*, 42(12), 4478–4485, doi:10.1021/es703009q, 2008.
- Akherati, A., He, Y., Coggon, M. M., Koss, A. R., Hodshire, A. L., Sekimoto, K., Warneke, C., de Gouw, J., Yee, L., Seinfeld, J. H., Onasch, T. B., Herndon, S. C., Knighton, W. B., Cappa, C. D., Kleeman, M. J., Lim, C. Y., Kroll, J. H., Pierce, J. R. and Jathar, S. H.: Oxygenated Aromatic Compounds are Important Precursors of Secondary Organic Aerosol in Biomass-Burning Emissions, *Environ. Sci. Technol.*, 54(14), 8568–8579, doi:10.1021/acs.est.0c01345, 2020.
- Altieri, K. E., Seitzinger, S. P., Carlton, A. G., Turpin, B. J., Klein, G. C. and Marshall, A. G.: Oligomers formed through in-cloud methylglyoxal reactions: Chemical composition, properties, and mechanisms investigated by ultra-high resolution FT-ICR mass spectrometry, *Atmos. Environ.*, 42(7), 1476–1490, doi:https://doi.org/10.1016/j.atmosenv.2007.11.015, 2008.
- Andreae, M. O. and Gelencsér, A.: Black carbon or brown carbon? The nature of light-absorbing carbonaceous aerosols, *Atmos. Chem. Phys.*, 6(10), 3131–3148, doi:10.5194/acp-6-3131-2006, 2006.
- Arciva, S., Niedeck, C., Mavis, C., Yoon, M., Sanchez, M. E., Zhang, Q. and Anastasio, C.: Aqueous ·OH Oxidation of Highly Substituted Phenols as a Source of Secondary Organic Aerosol, *Environ. Sci. Technol.*, 56(14), 9959–9967, doi:10.1021/acs.est.2c02225, 2022.
- Atkinson, R., Aschmann, S. M. and Arey, J.: Reactions of hydroxyl and nitrogen trioxide radicals with phenol, cresols, and 2-nitrophenol at 296±2 K, *Environ. Sci. Technol.*, 26(7), 1397–1403, 1992.
- Blando, J. D. and Turpin, B. J.: Secondary organic aerosol formation in cloud and fog droplets: a literature evaluation of plausibility, *Atmos. Environ.*, 34(10), 1623–1632, doi:https://doi.org/10.1016/S1352-2310(99)00392-1, 2000.
- Carlton, A. G., Turpin, B. J., Lim, H.-J., Altieri, K. E. and Seitzinger, S.: Link between isoprene and secondary organic aerosol (SOA): Pyruvic acid oxidation yields low volatility organic acids in clouds, *Geophys. Res. Lett.*, 33(6), doi:https://doi.org/10.1029/2005GL025374, 2006.
- Claeys, M., Vermeylen, R., Yasmeen, F., Gómez-González, Y., Chi, X., Maenhaut, W., Mészáros, T. and Salma, I.: Chemical characterisation of humic-like substances from urban, rural and tropical biomass burning environments using liquid chromatography with UV/vis photodiode array detection and electrospray ionisation mass spectrometry, *Environ. Chem.*, 9(3), 273–284 [online] Available from: https://doi.org/10.1071/EN11163, 2012.

- Coeur-Tourneur, C., Tomas, A., Guilloteau, A., Henry, F., Ledoux, F., Visez, N., Riffault, V., Wenger, J. C. and Bedjanian, Y.: Aerosol formation yields from the reaction of catechol with ozone, *Atmos. Environ.*, 43(14), 2360–2365, doi:<https://doi.org/10.1016/j.atmosenv.2008.12.054>, 2009.
- Coeur-Tourneur, C., Cassez, A. and Wenger, J. C.: Rate Coefficients for the Gas-Phase Reaction of Hydroxyl Radicals with 2-Methoxyphenol (Guaiacol) and Related Compounds, *J. Phys. Chem. A*, 114(43), 11645–11650, doi:[10.1021/jp1071023](https://doi.org/10.1021/jp1071023), 2010.
- Cohen, A. J., Brauer, M., Burnett, R., Anderson, H. R., Frostad, J., Estep, K., Balakrishnan, K., Brunekreef, B., Dandona, L., Dandona, R., Feigin, V., Freedman, G., Hubbell, B., Jobling, A., Kan, H., Knibbs, L., Liu, Y., Martin, R., Morawska, L., Pope, C. A., Shin, H., Straif, K., Shaddick, G., Thomas, M., van Dingenen, R., van Donkelaar, A., Vos, T., Murray, C. J. L. and Forouzanfar, M. H.: Estimates and 25-year trends of the global burden of disease attributable to ambient air pollution: an analysis of data from the Global Burden of Diseases Study 2015, *Lancet*, 389(10082), 1907–1918, doi:[https://doi.org/10.1016/S0140-6736\(17\)30505-6](https://doi.org/10.1016/S0140-6736(17)30505-6), 2017.
- Ervens, B., Feingold, G., Frost, G. J. and Kreidenweis, S. M.: A modeling study of aqueous production of dicarboxylic acids: 1. Chemical pathways and speciated organic mass production, *J. Geophys. Res. Atmos.*, 109(D15), doi:<https://doi.org/10.1029/2003JD004387>, 2004.
- Ervens, B., Turpin, B. J. and Weber, R. J.: Secondary organic aerosol formation in cloud droplets and aqueous particles (aqSOA): a review of laboratory, field and model studies, *Atmos. Chem. Phys.*, 11(21), 11069–11102, doi:[10.5194/acp-11-11069-2011](https://doi.org/10.5194/acp-11-11069-2011), 2011.
- George, I. J. and Abbatt, J. P. D.: Chemical evolution of secondary organic aerosol from OH-initiated heterogeneous oxidation, *Atmos. Chem. Phys.*, 10(12), 5551–5563, doi:[10.5194/acp-10-5551-2010](https://doi.org/10.5194/acp-10-5551-2010), 2010.
- De Gouw, J. and Jimenez, J. L.: Organic Aerosols in the Earth's Atmosphere, *Environ. Sci. Technol.*, 43(20), 7614–7618, doi:[10.1021/es9006004](https://doi.org/10.1021/es9006004), 2009.
- Graedel, T. E. and Weschler, C. J.: Chemistry within aqueous atmospheric aerosols and raindrops, *Rev. Geophys.*, 19(4), 505–539, doi:<https://doi.org/10.1029/RG019i004p00505>, 1981.
- Guzmán, M. I., Colussi, A. J. and Hoffmann, M. R.: Photoinduced Oligomerization of Aqueous Pyruvic Acid, *J. Phys. Chem. A*, 110(10), 3619–3626, doi:[10.1021/jp056097z](https://doi.org/10.1021/jp056097z), 2006.
- Happo, M. S., Uski, O., Jalava, P. I., Kelz, J., Brunner, T., Hakulinen, P., Mäki-Paakkanen, J., Kosma, V.-M., Jokiniemi, J., Obernberger, I. and Hirvonen, M.-R.: Pulmonary inflammation and tissue damage in the mouse lung after exposure to PM samples from biomass heating appliances of old and modern technologies, *Sci. Total Environ.*, 443, 256–266, doi:<https://doi.org/10.1016/j.scitotenv.2012.11.004>, 2013.
- Hawthorne, S. B., Krieger, M. S., Miller, D. J. and Mathiason, M. B.: Collection and quantitation of methoxylated phenol tracers for atmospheric pollution from residential wood stoves, *Environ. Sci. Technol.*, 23(4), 470–475, doi:[10.1021/es00181a013](https://doi.org/10.1021/es00181a013), 1989.
- Haywood, J. and Boucher, O.: Estimates of the direct and indirect radiative forcing due to tropospheric aerosols: A review, *Rev. Geophys.*, 38(4), 513–543,

doi:<https://doi.org/10.1029/1999RG000078>, 2000.

- Heald, C. L., Jacob, D. J., Park, R. J., Russell, L. M., Huebert, B. J., Seinfeld, J. H., Liao, H. and Weber, R. J.: A large organic aerosol source in the free troposphere missing from current models, *Geophys. Res. Lett.*, 32(18), doi:<https://doi.org/10.1029/2005GL023831>, 2005.
- Hecobian, A., Zhang, X., Zheng, M., Frank, N., Edgerton, E. S. and Weber, R. J.: Water-Soluble Organic Aerosol material and the light-absorption characteristics of aqueous extracts measured over the Southeastern United States, *Atmos. Chem. Phys.*, 10(13), 5965–5977, doi:10.5194/acp-10-5965-2010, 2010.
- Henze, D. K. and Seinfeld, J. H.: Global secondary organic aerosol from isoprene oxidation, *Geophys. Res. Lett.*, 33(9), doi:<https://doi.org/10.1029/2006GL025976>, 2006.
- Herrmann, H., Schaefer, T., Tilgner, A., Styler, S. A., Weller, C., Teich, M. and Otto, T.: Tropospheric Aqueous-Phase Chemistry: Kinetics, Mechanisms, and Its Coupling to a Changing Gas Phase, *Chem. Rev.*, 115(10), 4259–4334, doi:10.1021/cr500447k, 2015.
- Huang, D. D., Zhang, Q., Cheung, H. H. Y., Yu, L., Zhou, S., Anastasio, C., Smith, J. D. and Chan, C. K.: Formation and Evolution of aqSOA from Aqueous-Phase Reactions of Phenolic Carbonyls: Comparison between Ammonium Sulfate and Ammonium Nitrate Solutions, *Environ. Sci. Technol.*, doi:10.1021/acs.est.8b03441, 2018.
- Jo, D. S., Park, R. J., Lee, S., Kim, S.-W. and Zhang, X.: A global simulation of brown carbon: implications for photochemistry and direct radiative effect, *Atmos. Chem. Phys.*, 16(5), 3413–3432, doi:10.5194/acp-16-3413-2016, 2016.
- Kampf, C. J., Filippi, A., Zuth, C., Hoffmann, T. and Opatz, T.: Secondary brown carbon formation via the dicarbonyl imine pathway: nitrogen heterocycle formation and synergistic effects, *Phys. Chem. Chem. Phys.*, 18(27), 18353–18364, doi:10.1039/C6CP03029G, 2016.
- Kanakidou, M., Seinfeld, J. H., Pandis, S. N., Barnes, I., Dentener, F. J., Facchini, M. C., Van Dingenen, R., Ervens, B., Nenes, A., Nielsen, C. J., Swietlicki, E., Putaud, J. P., Balkanski, Y., Fuzzi, S., Horth, J., Moortgat, G. K., Winterhalter, R., Myhre, C. E. L., Tsigaridis, K., Vignati, E., Stephanou, E. G. and Wilson, J.: Organic aerosol and global climate modelling: a review, *Atmos. Chem. Phys.*, 5(4), 1053–1123, doi:10.5194/acp-5-1053-2005, 2005.
- Kroll, J. H. and Seinfeld, J. H.: Chemistry of secondary organic aerosol: Formation and evolution of low-volatility organics in the atmosphere, *Atmos. Environ.*, 42(16), 3593–3624, doi:<http://dx.doi.org/10.1016/j.atmosenv.2008.01.003>, 2008.
- Kroll, J. H., Ng, N. L., Murphy, S. M., Flagan, R. C. and Seinfeld, J. H.: Secondary Organic Aerosol Formation from Isoprene Photooxidation, *Environ. Sci. Technol.*, 40(6), 1869–1877, doi:10.1021/es0524301, 2006.
- Laskin, A., Laskin, J. and Nizkorodov, S. A.: Chemistry of Atmospheric Brown Carbon, *Chem. Rev.*, 115(10), 4335–4382, doi:10.1021/cr5006167, 2015.
- Lauraguais, A., Bejan, I., Barnes, I., Wiesen, P. and Coeur, C.: Rate Coefficients for the Gas-Phase Reactions of Hydroxyl Radicals with a Series of Methoxylated Aromatic Compounds, *J. Phys. Chem. A*, 119(24), 6179–6187, doi:10.1021/acs.jpca.5b03232, 2015.

- Li, Y. J., Huang, D. D., Cheung, H. Y., Lee, A. K. Y. and Chan, C. K.: Aqueous-phase photochemical oxidation and direct photolysis of vanillin – a model compound of methoxy phenols from biomass burning, *Atmos. Chem. Phys.*, 14(6), 2871–2885, doi:10.5194/acp-14-2871-2014, 2014.
- Liu, P. F., Abdelmalki, N., Hung, H.-M., Wang, Y., Brune, W. H. and Martin, S. T.: Ultraviolet and visible complex refractive indices of secondary organic material produced by photooxidation of the aromatic compounds toluene and *m*-xylene, *Atmos. Chem. Phys.*, 15(3), 1435–1446, doi:10.5194/acp-15-1435-2015, 2015.
- Lohmann, U. and Feichter, J.: Global indirect aerosol effects: a review, *Atmos. Chem. Phys.*, 5(3), 715–737, doi:10.5194/acp-5-715-2005, 2005.
- Ma, L., Guzman, C., Niedek, C., Tran, T., Zhang, Q. and Anastasio, C.: Kinetics and Mass Yields of Aqueous Secondary Organic Aerosol from Highly Substituted Phenols Reacting with a Triplet Excited State, *Environ. Sci. Technol.*, 55(9), 5772–5781, doi:10.1021/acs.est.1c00575, 2021.
- McFall, A. S., Johnson, A. W. and Anastasio, C.: Air–Water Partitioning of Biomass-Burning Phenols and the Effects of Temperature and Salinity, *Environ. Sci. Technol.*, 54(7), 3823–3830, doi:10.1021/acs.est.9b06443, 2020.
- McNeill, V. F.: Aqueous Organic Chemistry in the Atmosphere: Sources and Chemical Processing of Organic Aerosols, *Environ. Sci. Technol.*, 49(3), 1237–1244, doi:10.1021/es5043707, 2015.
- MohanKumar, S. M. J., Campbell, A., Block, M. and Veronesi, B.: Particulate matter, oxidative stress and neurotoxicity, *Neurotoxicology*, 29(3), 479–488, doi:https://doi.org/10.1016/j.neuro.2007.12.004, 2008.
- Murphy, D. M., Cziczko, D. J., Froyd, K. D., Hudson, P. K., Matthew, B. M., Middlebrook, A. M., Peltier, R. E., Sullivan, A., Thomson, D. S. and Weber, R. J.: Single-particle mass spectrometry of tropospheric aerosol particles, *J. Geophys. Res. Atmos.*, 111(D23), doi:https://doi.org/10.1029/2006JD007340, 2006.
- Nel, A.: Air Pollution-Related Illness: Effects of Particles, *Science (80-. )*, 308(5723), 804–806, doi:10.1126/science.1108752, 2005.
- Ng, N. L., Kroll, J. H., Chan, A. W. H., Chhabra, P. S., Flagan, R. C. and Seinfeld, J. H.: Secondary organic aerosol formation from *m*-xylene, toluene, and benzene, *Atmos. Chem. Phys.*, 7(14), 3909–3922, doi:10.5194/acp-7-3909-2007, 2007.
- Nguyen, T. B., Lee, P. B., Updyke, K. M., Bones, D. L., Laskin, J., Laskin, A. and Nizkorodov, S. A.: Formation of nitrogen- and sulfur-containing light-absorbing compounds accelerated by evaporation of water from secondary organic aerosols, *J. Geophys. Res. Atmos.*, 117(D1), doi:https://doi.org/10.1029/2011JD016944, 2012.
- Olariu, R. I., Klotz, B., Barnes, I., Becker, K. H. and Mocanu, R.: FT–IR study of the ring-retaining products from the reaction of OH radicals with phenol, *o*-, *m*-, and *p*-cresol, *Atmos. Environ.*, 36(22), 3685–3697, doi:https://doi.org/10.1016/S1352-2310(02)00202-9, 2002.
- Pang, H., Zhang, Q., Lu, X., Li, K., Chen, H., Chen, J., Yang, X., Ma, Y., Ma, J. and Huang, C.: Nitrite-Mediated Photooxidation of Vanillin in the Atmospheric Aqueous Phase, *Environ. Sci.*

- Technol., 53(24), 14253–14263, doi:10.1021/acs.est.9b03649, 2019.
- Perri, M. J., Lim, Y. B., Seitzinger, S. P. and Turpin, B. J.: Organosulfates from glycolaldehyde in aqueous aerosols and clouds: Laboratory studies, *Atmos. Environ.*, 44(21), 2658–2664, doi:<https://doi.org/10.1016/j.atmosenv.2010.03.031>, 2010.
- R., K. J., A., M. J., G., R. A., Sivaraman, B., Andrea, W., E., T. P., A., W. L. and Ebel, S. S.: Associations between Source-Specific Fine Particulate Matter and Emergency Department Visits for Respiratory Disease in Four U.S. Cities, *Environ. Health Perspect.*, 125(1), 97–103, doi:10.1289/EHP271, 2017.
- Rayne, S., Forest, K. and Friesen, K. J.: Mechanistic aspects regarding the direct aqueous environmental photochemistry of phenol and its simple halogenated derivatives. A review, *Environ. Int.*, 35(2), 425–437, doi:10.1016/j.envint.2008.09.004, 2009.
- Rizzo, L. V, Correia, A. L., Artaxo, P., Procópio, A. S. and Andreae, M. O.: Spectral dependence of aerosol light absorption over the Amazon Basin, *Atmos. Chem. Phys.*, 11(17), 8899–8912, doi:10.5194/acp-11-8899-2011, 2011.
- Saleh, R.: From Measurements to Models: Toward Accurate Representation of Brown Carbon in Climate Calculations, *Curr. Pollut. Reports*, 6(2), 90–104, doi:10.1007/s40726-020-00139-3, 2020.
- Sareen, N., Schwier, A. N., Shapiro, E. L., Mitroo, D. and McNeill, V. F.: Secondary organic material formed by methylglyoxal in aqueous aerosol mimics, *Atmos. Chem. Phys.*, 10(3), 997–1016, doi:10.5194/acp-10-997-2010, 2010.
- Schauer, J. J., Kleeman, M. J., Cass, G. R. and Simoneit, B. R. T.: Measurement of Emissions from Air Pollution Sources. 3. C1–C29 Organic Compounds from Fireplace Combustion of Wood, *Environ. Sci. Technol.*, 35(9), 1716–1728, doi:10.1021/es001331e, 2001.
- Shiraiwa, M., Ueda, K., Pozzer, A., Lammel, G., Kampf, C. J., Fushimi, A., Enami, S., Arangio, A. M., Fröhlich-Nowoisky, J., Fujitani, Y., Furuyama, A., Lakey, P. S. J., Lelieveld, J., Lucas, K., Morino, Y., Pöschl, U., Takahama, S., Takami, A., Tong, H., Weber, B., Yoshino, A. and Sato, K.: Aerosol Health Effects from Molecular to Global Scales, *Environ. Sci. Technol.*, 51(23), 13545–13567, doi:10.1021/acs.est.7b04417, 2017.
- Simoneit, B. R. T.: A review of biomarker compounds as source indicators and tracers for air pollution, *Environ. Sci. Pollut. Res.*, 6(3), 159–169, doi:10.1007/bf02987621, 1999.
- Simpson, C. D., Paulsen, M., Dills, R. L., Liu, L.-J. S. and Kalman, D. A.: Determination of Methoxyphenols in Ambient Atmospheric Particulate Matter: Tracers for Wood Combustion, *Environ. Sci. Technol.*, 39(2), 631–637, doi:10.1021/es0486871, 2005.
- Smith, J. D., Sio, V., Yu, L., Zhang, Q. and Anastasio, C.: Secondary Organic Aerosol Production from Aqueous Reactions of Atmospheric Phenols with an Organic Triplet Excited State, *Environ. Sci. Technol.*, 48(2), 1049–1057, doi:10.1021/es4045715, 2014.
- Smith, J. D., Kinney, H. and Anastasio, C.: Phenolic carbonyls undergo rapid aqueous photodegradation to form low-volatility, light-absorbing products, *Atmos. Environ.*, 126, 36–44, doi:<http://dx.doi.org/10.1016/j.atmosenv.2015.11.035>, 2016.



- Sun, Y. L., Zhang, Q., Anastasio, C. and Sun, J.: Insights into secondary organic aerosol formed via aqueous-phase reactions of phenolic compounds based on high resolution mass spectrometry, *Atmos. Chem. Phys.*, 10(10), 4809–4822, doi:10.5194/acp-10-4809-2010, 2010.
- Tomas, A., Olariu, R. I., Barnes, I. and Becker, K. H.: Kinetics of the reaction of O<sub>3</sub> with selected benzenediols, *Int. J. Chem. Kinet.*, 35(6), 223–230, doi:https://doi.org/10.1002/kin.10121, 2003.
- Tremp, J., Mattrel, P., Fingler, S. and Giger, W.: Phenols and nitrophenols as tropospheric pollutants: Emissions from automobile exhausts and phase transfer in the atmosphere, *Water. Air. Soil Pollut.*, 68(1), 113–123, doi:10.1007/BF00479396, 1993.
- Volkamer, R., Klotz, B., Barnes, I., Imamura, T., Wirtz, K., Washida, N., Becker, K. H. and Platt, U.: OH-initiated oxidation of benzene Part I. Phenol formation under atmospheric conditions, *Phys. Chem. Chem. Phys.*, 4(9), 1598–1610, doi:10.1039/B108747A, 2002.
- Yee, L. D., Kautzman, K. E., Loza, C. L., Schilling, K. A., Coggon, M. M., Chhabra, P. S., Chan, M. N., Chan, A. W. H., Hersey, S. P., Crouse, J. D., Wennberg, P. O., Flagan, R. C. and Seinfeld, J. H.: Secondary organic aerosol formation from biomass burning intermediates: phenol and methoxyphenols, *Atmos. Chem. Phys.*, 13(16), 8019–8043, doi:10.5194/acp-13-8019-2013, 2013.
- Yu, L., Smith, J., Laskin, A., Anastasio, C., Laskin, J. and Zhang, Q.: Chemical characterization of SOA formed from aqueous-phase reactions of phenols with the triplet excited state of carbonyl and hydroxyl radical, *Atmos. Chem. Phys.*, 14(24), 13801–13816, doi:10.5194/acp-14-13801-2014, 2014.
- Yu, L., Smith, J., Laskin, A., George, K. M., Anastasio, C., Laskin, J., Dillner, A. M. and Zhang, Q.: Molecular transformations of phenolic SOA during photochemical aging in the aqueous phase: competition among oligomerization, functionalization, and fragmentation, *Atmos. Chem. Phys.*, 16(7), 4511–4527, doi:10.5194/acp-16-4511-2016, 2016.
- Zhang, Q., Jimenez, J. L., Canagaratna, M. R., Allan, J. D., Coe, H., Ulbrich, I., Alfarra, M. R., Takami, A., Middlebrook, A. M., Sun, Y. L., Dzepina, K., Dunlea, E., Docherty, K., DeCarlo, P. F., Salcedo, D., Onasch, T., Jayne, J. T., Miyoshi, T., Shimojo, A., Hatakeyama, S., Takegawa, N., Kondo, Y., Schneider, J., Drewnick, F., Borrmann, S., Weimer, S., Demerjian, K., Williams, P., Bower, K., Bahreini, R., Cottrell, L., Griffin, R. J., Rautiainen, J., Sun, J. Y., Zhang, Y. M. and Worsnop, D. R.: Ubiquity and dominance of oxygenated species in organic aerosols in anthropogenically-influenced Northern Hemisphere midlatitudes, *Geophys. Res. Lett.*, 34(13), n/a-n/a, doi:10.1029/2007GL029979, 2007.

## Chapter 2: Photosensitized Reactions of a Phenolic Carbonyl from Wood Combustion in the Aqueous Phase – Chemical Evolution and Light Absorption Properties of AqSOA

This chapter has been published in the journal *Environmental Science and Technology*: [Jiang, W.](#), Misovich, M. V, Hettiyadura, A. P. S., Laskin, A., McFall, A. S., Anastasio, C. and Zhang, Q.: Photosensitized Reactions of a Phenolic Carbonyl from Wood Combustion in the Aqueous Phase—Chemical Evolution and Light Absorption Properties of AqSOA, *Environ. Sci. Technol.*, 55(8), 5199–5211, doi:10.1021/acs.est.0c07581, 2021.

### 2.1 Abstract

Guaiacyl acetone (GA) is a phenolic carbonyl emitted in significant quantities by wood combustion that undergoes rapid aqueous-phase oxidation to produce aqueous secondary organic aerosol (aqSOA). We investigate the photosensitized oxidation of GA by an organic triplet excited state ( $^3C^*$ ) and the formation and aging of the resulting aqSOA in wood smoke-influenced fog/cloud water. The chemical transformations of the aqSOA were characterized in situ using a high-resolution time-of-flight aerosol mass spectrometer (AMS). Additionally, aqSOA samples collected over different time periods were analyzed using high-performance liquid chromatography coupled with a photodiode array detector and a high-resolution Orbitrap mass spectrometer (HPLC-PDA-HRMS) to provide details on the molecular composition and optical properties of brown carbon (BrC) chromophores. Our results show efficient formation of aqSOA from GA, with an average mass yield around 80%. The composition and BrC properties of the aqSOA changed significantly over the course of reaction. Three generations of aqSOA products were identified via Positive Matrix Factorization analysis of the AMS data. Oligomerization and functionalization dominated the production of the first-generation aqSOA, whereas fragmentation and ring-opening reactions controlled the formation of more oxidized second- and third-generation

products. Significant formation of BrC was observed in the early stages of the photoreaction, while organic acids were produced throughout the experiment. High-molecular-weight molecules ( $m/z > 180$ ) with high aromaticity were identified via HPLC-PDA-HRMS and were found to account for a majority of the UV-vis absorption of the aqSOA.

## **2.2 Introduction**

Biomass burning (BB) emissions – from residential stoves and fireplaces, wildland fires and prescribed agricultural burns – are a major source of particulate matter (PM) in the atmosphere, contributing approximately 10–50% of the total organic aerosol (OA) mass (De Gouw and Jimenez, 2009; Schauer and Cass, 2000). Aerosols from BB sources have significant impacts on climate, air quality, and human health (Cordell et al., 2016; E. et al., 2016; Jaffe et al., 2020; O’Dell et al., 2019; Sommers et al., 2014; Yadav et al., 2017). Emissions from residential wood burning are frequently a major contributor to fine PM pollution in urban regions in winter (Chen et al., 2018; Gaston et al., 2016; Ge et al., 2012b; Jeong et al., 2008; Sullivan et al., 2019; Ward et al., 2006; Young et al., 2016). Wildfires, a major natural hazard, have been reported to emit more PM than anthropogenic sources in many parts of the world (Jaffe et al., 2020; Knorr et al., 2017; McClure and Jaffe, 2018). BB aerosols contribute significantly to global warming due to their light-absorbing properties (Adler et al., 2019; Xie et al., 2019). Previous studies have reported that brown carbon (BrC) chromophores observed in BB aerosols include lignin pyrolysis products, distillation products (coumarins and flavonoids), nitroaromatics, and polycyclic aromatic hydrocarbons (PAHs) (Fleming et al., 2019). In addition, exposure to wood smoke particles cause health problems such as acute respiratory infections, tuberculosis, lung cancer, and cataracts (Scott and Reilly, 2019).

BB smoke consists of complex mixtures of particles and gases. Oxidation of volatile organic compounds (VOCs) emitted from BB is an important source of secondary organic aerosol (SOA) in the atmosphere (Bruns et al., 2016; Gilardoni et al., 2016; Gilman et al., 2015; Hatch et al., 2017; Liu et al., 2019). During the photooxidation of BB emissions, both chromophore formation and sunlight bleaching can occur, leading to changes of aerosols optical properties (Cappa et al., 2020; Hems et al., 2020; Pang et al., 2019; Zhong and Jang, 2014). Previous studies have reported that aqueous-phase photo-oxidation of BB emissions can increase the absorbance of BrC through the formation of aromatic dimer compounds and functionalized products (Hems et al., 2020). On the other hand, longer aging generally leads to photobleaching of the BrC in BB emissions, which can be mainly attributed to decomposition of chromophoric aromatics, nitrogen-containing organics, and high-molecular weight components (Li et al., 2019). Also, the wavelength dependence of BrC absorption generally increases with prolonged aging (Cappa et al., 2020).

Phenols are emitted from BB in significant quantities through lignin pyrolysis. Aldehyde- and ketone-functionalized phenols (i.e., phenolic carbonyls) account for 18% and 22% of total phenol emissions from the burning of hardwood and softwood, respectively (Schauer et al., 2001; Simpson et al., 2005). Most of the phenolic carbonyls emitted from BB are of intermediate volatility and have high Henry's law constants (McFall et al., 2020; Smith et al., 2016). They readily partition into atmospheric aqueous phases (e.g., deliquesced aerosol, cloud and fog droplets), where reactions can occur to form low-volatility materials which remain in the particle phase upon water evaporation, yielding aqSOA (Smith et al., 2016). Conjugated phenolic carbonyls, i.e., phenols with the carbonyl groups directly connected to the aromatic ring, tend to have high solar absorbance and a propensity to form aqSOA and brown carbon (BrC) through

direct photochemical reactions at fast rates (Chang and Thompson, 2010a; Huang et al., 2018; Li et al., 2014b; Smith et al., 2016).

Guaiacyl acetone (GA; 4-Hydroxy-3-methoxyphenylacetone;  $C_{10}H_{12}O_3$ ) is a phenolic carbonyl released from BB with emission rates of 12 - 41  $\mu\text{g g}_{\text{fuel}}^{-1}$ . This compound was detected in the atmosphere in the range of 0.3 - 0.6  $\text{ng m}^{-3}$  (Nolte et al., 2001), which is comparable to the concentrations of the most common phenols (e.g., guaiacol and syringol). The high Henry's law constant of GA ( $1.2 \times 10^6 \text{ M atm}^{-1}$ ) (McFall et al., 2020) suggests that aqueous reactions are an important atmospheric sink for this molecule in cloud/fog conditions. For example, within a cloud/fog with a liquid water content of 0.3  $\text{g-H}_2\text{O m}^{-3}$ , ~ 90% of GA is estimated to present in the aqueous phase at Henry's law equilibrium. Additionally, since the replenishment of the aqueous-phase GA by partitioning from the gas phase is very fast (time scale of minutes) compared to aqueous reaction (time scale of hours) (Feigenbrugel et al., 2004), aqueous reactions are likely major pathways for GA transformation under cloudy or foggy conditions. Compared with conjugated phenolic carbonyls, such as vanillin, acetovanillone, acetosyringone and syringaldehyde, GA absorbs little sunlight and therefore is more resilient to direct photodegradation (Smith et al., 2016). Aqueous-phase aging of GA may occur through oxidation by hydroxyl radical ( $\bullet\text{OH}$ ), triplet excited states of carbon ( $^3\text{C}^*$ ), and singlet molecular oxygen ( $^1\text{O}_2^*$ ).  $^3\text{C}^*$  is a particularly important oxidant for phenols as the reactions usually generate aqSOA at faster rates and higher mass yields compared to OH oxidation of phenols (Anastasio et al., 1997; Kaur et al., 2018; Smith et al., 2014, 2015, 2016; Sun et al., 2010; Yu et al., 2014). Furthermore, there is evidence (Yu et al., 2014, 2016) that  $^3\text{C}^*$  oxidation of phenols produces light-absorbing oligomers and high molecular weight derivatives more efficiently compared to OH oxidation or direct photodegradation.

One important source of atmospheric  $^3\text{C}^*$  is light-absorbing organic compounds emitted from BB (Simoneit, 1999). Sunlight absorption by the organics can promote the ground states of chromophores to the triplet excited states in the aqueous phase (Anastasio et al., 1997; Smith et al., 2014, 2016). Significant formation of  $^3\text{C}^*$  has been observed in fog droplets and particle-bound water under solar irradiation (Kaur et al., 2019; Kaur and Anastasio, 2018) and the reactions of phenols with  $^3\text{C}^*$  have been shown to be an effective formation pathway for highly oxidized aqSOA with average oxygen-to-carbon ratio close to 1 (Smith et al., 2014, 2016; Sun et al., 2010; Yu et al., 2014, 2016).

In this study, we investigate the photochemical formation and aging of aqSOA through the aqueous reactions of GA with  $^3\text{C}^*$  under solar irradiation in wood smoke-influenced fog and cloud waters. We perform aqueous-phase photoreaction experiments of GA in the presence of  $^3\text{C}^*$ , characterize the chemical composition and light absorption properties of the formed aqSOA and examine the formation pathways, molecular composition, and optical properties of the BrC chromophores within the aqSOA. Although many studies on the photo-oxidation of biomass burning emissions have been done previously, this study uses GA as a model compound to investigate the aqueous photosensitized reactions of phenolic carbonyls and their potential to produce aqSOA and BrC, which have not been thoroughly investigated before.

## **2.3 Experimental Methods**

### **2.3.1 Aqueous-phase Photochemical Reaction**

Experimental solutions were prepared with 100  $\mu\text{M}$  (18 mg/L) of GA and 5  $\mu\text{M}$  (0.83 mg/L) of 3,4-DMB (3,4-dimethoxybenzaldehyde;  $\text{C}_9\text{H}_{10}\text{O}_3$ ) as a source of  $^3\text{C}^*$ , with the pH adjusted to 4.6 using sulfuric acid to mimic the wood burning-impacted cloud and fog waters (Anastasio et

al., 1997; Collett et al., 1998; Kaur and Anastasio, 2018; Raja et al., 2008). In addition, 10 mg/L of ammonium sulfate was added into the solution as an internal standard for quantification of SOA mass concentration using a high-resolution time-of-flight aerosol mass spectrometer (AMS, Aerodyne Res. Inc.) (Sun et al., 2010). The prepared solution was placed in 110 mL Pyrex tubes, continuously magnetically stirred, and illuminated with simulated sunlight inside an RPR-200 photoreactor system described elsewhere (George et al., 2015b) (Fig. S1). Note that for  $^{3}\text{C}^*$  exposure, the rate of light absorption was  $\sim 7$  times faster in our Photoreactor System than that in the midday winter solstice sunlight in Davis. A dark control sample was prepared in the same manner, wrapped with aluminum foil, and placed inside the photoreactor during the illumination experiment.

### **2.3.2 Sample Analyses**

Throughout the course of each experiment, a Shimadzu LC-10AD HPLC pump was used to draw solution at a constant flow rate (1.0 mL/min) alternatively from the illuminated and the dark control tubes. The solution was delivered to a constant output atomizer and atomized continuously in purified pressurized air. The resulting particles were dried to  $\text{RH} < 5\%$  using a diffusion dryer and analyzed by AMS in real-time. The excess solution dripping from the atomizer was collected at different time intervals over the course of each experiment and the aliquots were stored frozen ( $-20\text{ }^{\circ}\text{C}$ ) for offline analysis of: 1) GA and 3,4-DMB concentrations using HPLC-PDA (Agilent Technologies Inc.) (McFall et al., 2020); 2) concentrations of organic anions, including formate, acetate, malate, malonate, and oxalate, using a Metrohm anion ion chromatograph (IC) (Ge et al., 2014); 3) UV-visible absorption using a Shimadzu UV-2501PC spectrophotometer; and 4) molecular composition and optical properties of aqSOA chromophores using HPLC-PDA-HRMS (Lin et al., 2018).

### 2.3.2.1 Real-time AMS Analysis of aqSOA Bulk Composition and Yield Calculation

Real-time changes in the mass concentration and bulk chemical composition of the aqSOA were measured by an AMS operated alternatively between “V” and “W” modes (mass resolution ( $m/\Delta m$ ) of  $\sim 3000$  and  $\sim 5000$ , respectively) to acquire mass spectra up to 485 and 280 amu, respectively. The data was processed using the standard AMS data analysis toolkits (SQUIRREL v1.56D and PIKA 1.15D). According to our previous studies, we assume the particles are effectively dried by the diffusion drier, which led to  $RH < 5\%$  at the AMS inlet, and the contribution of particle water in the AMS mass spectra was negligible (Yu et al., 2014). The organic  $H_2O^+$  signal (org- $H_2O^+$  hereafter) was thus determined as the difference between the measured  $H_2O^+$  signal and the sulfate-associated  $H_2O^+$  signal. The derived org- $H_2O^+$  signal was somewhat noisy, but it showed a good correlation ( $r^2 = 0.66$ ) with the measured organic  $CO_2^+$  signal with a slope of 0.4 (Fig. S2). To reduce noise in the calculated elemental ratios, we thus parameterized the org- $H_2O^+$  related signals of aqSOA according to the measured  $CO_2^+$  signal, i.e.,  $org-H_2O^+ = 0.4 \times CO_2^+$ ,  $org-OH^+ = 0.25 \times org-H_2O^+$  and  $org-O^+ = 0.04 \times org-H_2O^+$  (Aiken et al., 2008; Yu et al., 2014). The atomic oxygen-to-carbon (O/C) ratio, hydrogen-to-carbon (H/C) ratio, and organic mass-to-organic-carbon (OM/OC) ratio were subsequently determined. The average oxidation state of carbon ( $OS_C$ ) in aqSOA is determined as  $OS_C = 2 O/C - H/C$ , (Kroll et al., 2011) since the aqSOA studied here mainly consisted of C, H, and O atoms with a negligible contribution from peroxide groups (Yee et al., 2013).

The aqSOA mass yield was calculated using Equation 1:

$$SOA \text{ yield} = \frac{[Org]_t - [Org]_0}{[GA]_t - [GA]_0} = \frac{[Org_{AMS}]_t \times \frac{[AS]_t}{[AS_{AMS}]_t} - [Org_{AMS}]_0 \times \frac{[AS]_0}{[AS_{AMS}]_0}}{[GA]_t - [GA]_0} \quad (1)$$



where [Org], [AS], and [GA] denote the aqSOA, sulfate and GA concentrations ( $\text{mg L}^{-1}$ ) in the solution, respectively. The  $[\text{Org}]_{\text{AMS}}$  and  $[\text{AS}]_{\text{AMS}}$  denote the apparent concentrations ( $\mu\text{g m}^{-3}$ ) of aqSOA and sulfate measured by AMS. The subscripts indicate irradiation time, e.g.,  $[\text{GA}]_0$  is the initial concentration of GA. Here, the concentration of sulfate in the solution is assumed to be constant during irradiation (i.e.,  $[\text{AS}]_t = [\text{AS}]_0$ ).

Positive matrix factorization (PMF) analysis was performed to investigate the chemical evolution of the aqSOA. The input data were the organic mass spectral matrix and the corresponding error matrix generated within PIKA. The PMF results were evaluated using the PMF Evaluation Toolkit (PET v3.05 downloaded from: [http://cires1.colorado.edu/jimenez-group/wiki/index.php/PMF-AMS\\_Analysis\\_Guide](http://cires1.colorado.edu/jimenez-group/wiki/index.php/PMF-AMS_Analysis_Guide)) (Ulbrich et al., 2009). A four-factor solution was chosen based on the evaluation criteria outlined in a previous study (Zhang et al., 2011). A summary of the diagnostic plots for the 4-factor PMF solution is presented in Fig. S3. Selecting fewer or more factors leads to either high residuals or splitting of the factors. Among the four resolved factors, three are representative of different generations of aqSOA and the fourth is a background factor likely due to chemical impurities present in the reagents. The time series and mass spectrum of the background factor are shown in Fig. S4. The mass spectrum of the background factor looks very different than the spectra of the aqSOA factors and its concentration remained nearly constant throughout the experiment. This factor only accounts for a minor fraction of the organic aerosol mass measured by AMS (3%), and therefore likely has a negligible effect on the bulk composition of the aqSOA.

### 2.3.2.2 Offline UV-vis Absorption Measurements

The light absorption coefficient ( $\alpha_\lambda, \text{cm}^{-1}$ ) of the solution was calculated using Equation 2:

$$\alpha_{\lambda} = \frac{A_{\lambda}}{l} \quad (2)$$

where  $A_{\lambda}$  is the base-10 light absorbance of the aqSOA solution at wavelength  $\lambda$  (i.e.,  $A_{\lambda}$  = total measured absorbance at  $\lambda$  – the absorbance contributed by GA and 3,4-DMB at  $\lambda$ ) and  $l$  is the pathlength of the cuvette (cm).

The mass absorption coefficient for the aqSOA ( $MAC_{\lambda}$ ,  $\text{cm}^2 \text{g}^{-1}$ ) was then calculated as:

$$MAC_{\lambda} = \frac{2.303 \alpha_{\lambda}}{C} \times 10^{-6} \quad (3)$$

where  $C$  is the aqSOA mass concentration in  $\text{mg L}^{-1}$ , and 2.303 is a base conversion factor between  $\lg$  and  $\ln$ . The carbon-based  $MAC_{\lambda}$ ,  $\text{cm}^2 \text{g-C}^{-1}$ , can be derived by multiplying  $MAC_{\lambda}$  by the OM/OC ratio of the aqSOA.

Additionally, the rate of sunlight absorption ( $R_{abs}$ ,  $\text{mol-photon} \text{L}^{-1} \text{s}^{-1}$ ) of the aqSOA solution was calculated using:

$$R_{abs} = 2.303 \times 10^3 \times N_A \times \int_{300\text{nm}}^{700\text{nm}} \alpha_{\lambda} \times I_{\lambda} \times d\lambda \quad (4)$$

where 2.303 is a base conversion,  $10^3$  is a units conversion factor ( $\text{cm}^3 \text{L}^{-1}$ ),  $N_A$  is Avogadro's number,  $I_{\lambda}$  is the winter-solstice actinic flux ( $\text{photons cm}^{-2} \text{s}^{-1} \text{nm}^{-1}$ ) in Davis, CA, calculated using the Tropospheric Ultraviolet and Visible (TUV) Radiation Model ([http://cprm.acom.ucar.edu/Models/TUV/Interactive\\_TUV/](http://cprm.acom.ucar.edu/Models/TUV/Interactive_TUV/)), and  $d\lambda$  is the interval between adjacent wavelengths in the TUV output (2 nm).

### 2.3.2.3 HPLC-PDA-HRMS analysis of BrC in aqSOA

The aqSOA samples were analyzed using an HPLC system coupled with a PDA detector (Vanquish™, Thermo Scientific Inc) and a high resolution Orbitrap mass spectrometer, Q

Exactive™ HF-X (Thermo Scientific Inc) to identify and characterize BrC chromophores. LC-MS grade water was used as a blank. All solvents, including mobile phases, were Optima™ LC/MS grade, purchased from Fisher Chemical. The HPLC separation was performed according to Lin et al., 2018.(Lin et al., 2018) Briefly, organic compounds were separated on a reversed-phase column (Luna® C18(2), 150 × 2 mm, 5 µm particles, 100 Å pores; Phenomenex Inc.) using water with 0.1% (v/v) formic acid (A) and acetonitrile with 0.1% (v/v) formic acid (B) as mobile phases at a flow rate of 0.200 mL min<sup>-1</sup>, 0-3 min at 10% B, 3-63 min a linear increase to 90% B; 63-75 min hold at 90% B, 75-90 min a linear gradient to 100% B, 90-100 hold at 100% B, 100-101 min a linear decrease to 10% B, 101-120 min equilibration at 10% B to prepare for the next run. A sample injection volume of 15 µL was used. Light absorption between 250 – 680 nm was recorded by the PDA detector. The HPLC separated organic compounds were ionized using an electrospray ionization (ESI) source operated in alternating positive and negative ion modes. This study reports the data acquired in negative mode. The analysis was performed in the full scan mode in the mass range m/z 80 – 1200 at a mass resolution of 24,000 at 200 m/z. A spray voltage of 2.5 kV was used in the negative ion mode. A capillary temperature of 250 °C was used. A sheath gas flow rate of 30 arbitrary units (arb), auxiliary gas flow rate of 10 arb and a sweep gas flow rate of 1 arb were used. The mass calibration was performed using Thermo Scientific™ Pierce™ negative ion calibration solution (PI-88324). The highly polar CHO components of aqSOA were mostly observed as deprotonated ions [M-H]<sup>-</sup>, while some of them were also observed as cluster ions with sodium formate [M+(HCOONa)<sub>x</sub>-H]<sup>-</sup>. Xcalibur (Thermo Scientific) was used to acquire raw data. MZmine 2.39 (<http://mzmine.github.io/>) software was used to select peaks (Pluskal et al., 2010). Peaks that occurred in the blank sample were subtracted from the sample signal. Carbon-13 isotopes were removed and MS peaks were grouped in homologues series using a suite of

Microsoft Excel macros (Roach et al., 2011). Formula assignments were performed using the MIDAS formula calculator (<http://magnet.fsu.edu/~midas/>) with the following constraints applicable for deprotonated ions:  $C \leq 50$ ,  $H \leq 100$ ,  $O \leq 50$ ,  $N \leq 3$ , and  $S \leq 1$ . Formulas containing both nitrogen and sulfur were not considered. Since the mobile phase contained formic acid, additional assignments allowed  $1 \leq Na \leq 3$  to account for sodium formate clustering. Na-containing formulas were not considered if there were too few carbon, hydrogen, or oxygen atoms to account for sodium formate. All ESI-HRMS data shown in this work correspond to neutral analyte species inferred from these assignments. The neutral formulas were characterized by the double-bond equivalent (DBE) calculated as  $DBE = c - h/2 + n/2 + 1$  and aromaticity index (AI) calculated as  $AI = (1 + c - o - 0.5h)/(c - o - n)$ , where  $c$ ,  $h$ ,  $o$ , and  $n$  are the numbers of C, H, O and N atoms in the neutral formula.

## 2.4 Results and Discussion

### 2.4.1 Photosensitized Oxidation of Guaiacyl Acetone and aqSOA Formation

Fig. 1 provides an overview of the loss of GA, formation of aqSOA, and evolution of aqSOA chemical properties over the course of photoreaction. GA decays quickly upon irradiation following pseudo-first-order kinetics with a fitted rate constant ( $k$ ) of  $1.28 \text{ h}^{-1}$  and a half-life of 32.5 min (Fig. 1a). The aqSOA mass concentration increases in sync with the decrease of GA, and plateaus after ~ 3 hours of irradiation after all GA has reacted (Fig. 1b). The aqSOA mass yield is in the range of 76 ~ 91%, which is slightly lower than those reported for the photoreactions of phenol, guaiacol (2-methoxyphenol), and syringol (2, 6-dimethoxyphenol) with  $^3\text{C}^*$  (Smith et al., 2014). The comparatively lower SOA yield of GA is likely due to the presence of the acetone group on its *para* position. Compared to the *meta* and *ortho* positions on phenols, the *para* position

is usually more reactive for electrophilic substitution due to relatively higher electron density and less steric hindrance. Thus, the occupancy of the *para* position on GA may lower the rates of substitution reactions and reduce the production of low volatility compounds.

Previous studies reported that conjugated phenolic carbonyls (e.g., vanillin, acetovanillone, acetosyringone and syringaldehyde) undergo direct photodegradation to produce aqSOA with aqueous phase mass yields around 80% (Huang et al., 2018; Smith et al., 2016). However, because GA absorbs weakly at wavelengths above 300 nm (Fig. S5), direct photodegradation of GA is expected to be negligible (Smith et al., 2016) compared to oxidation by  $^3\text{C}^*$ . Additionally, here we observed that 3,4-DMB decreases nearly linearly during illumination and 80% of the initial 3,4-DMB is lost after 5.5 hrs of irradiation (Fig. S6). No detectable loss of GA or 3,4-DMB is observed in the dark (Fig. 1a). On the other hand, consistent with previous reported aqueous photo-oxidation of guaiacol and syringol using 3,4-DMB as the source of  $^3\text{C}^*$  (Yu et al., 2016), these results indicate that 3,4-DMB transforms during the oxidation of GA, and the range of products formed may potentially contain low volatility compounds. However, since the initial concentration of 3,4-DMB is 20 times lower than that of GA, the contribution of 3,4-DMB oxidation products to aqSOA is expected to be minimal.

The bulk chemical composition of the aqSOA evolves continuously during illumination and becomes increasingly more oxidized (Fig. 1c). The O/C ratio of the aqSOA increases from 0.43 to 0.67 while the H/C ratio decreases from 1.60 to 1.41, leading to a rise of  $\text{OS}_\text{C}$  from  $-0.75$  to  $-0.074$  over  $\sim 6$  hours of photoreaction. Note that H/C, O/C and  $\text{OS}_\text{C}$  are not reported for the first 24 min of the reactions because of insufficient aqSOA mass. Both the O/C and H/C ratios of the aqSOA are higher than those of the precursor (O/C = 0.3 and H/C = 1.2 for GA), suggesting the occurrence of hydrogen incorporation and oxygenation pathways such as electrophilic addition of the OH

radical to the aromatic ring and carboxylic acid formation. Previous studies have shown that the reactions of  $^3\text{C}^*$  with phenols form  $\text{H}_2\text{O}_2$  (Anastasio et al., 1997) which can be a source of OH radical. In this work, AMS tracer ions for hydroxylated GA compounds, such as  $\text{C}_{10}\text{H}_{12}\text{O}_4^+$  and  $\text{C}_{10}\text{H}_{12}\text{O}_5^+$ , are observed in the mass spectra of the aqSOA. In addition, LC-MS analysis detects the presence of hydroxylated products of GA in the aqSOA, such as  $\text{C}_{10}\text{H}_{12}\text{O}_6$ , which is identified as a product of GA resulting from the addition of three OH groups to the aromatic ring (Table 1). This is consistent with previous findings that OH radical addition is an important pathway in aqueous-phase oxidation of phenols (Chen et al., 2020; Huang et al., 2018; Pillar et al., 2014; Sun et al., 2010; Yu et al., 2014, 2016).

Significant formation of carboxylic acids during the photoreaction of GA is suggested by the Van Krevelen diagram of H/C vs. O/C (Heald et al., 2010), where the aqSOA evolves along a slope of around  $-1$  over the course of the photooxidation (Fig. S7). The  $\text{CHO}_2^+$  ion in the aqSOA AMS spectra, which is an indicator for the carboxyl functional group, also rises constantly over the course of the photoreaction (Fig. 1d). Furthermore, IC analysis of offline samples indicates continuous formation of five small organic acids (formic acid, acetic acid, malic acid, malonic acid, and oxalic acid) in the aqSOA (Fig. 1d), with acetic acid, formic acid, and oxalic acid being the major small acid products. In the later periods of the photoreaction ( $\sim 5.5$  hrs), the measured total small acids account for 10.9% of the original organic carbon mass. In addition, there is a tight correlation between the total concentration of organic acids measured by IC and the organic-equivalent concentration of  $\text{CHO}_2^+$  measured by AMS. Together, these results indicate that carboxylic acids are important reaction products from the photooxidation of GA.

#### **2.4.2 Photochemical Evolution of GA aqSOA Composition and Light Absorption**

### 2.4.2.1 Formation and Evolution of Three Generations of aqSOA

To investigate the chemical evolution of aqSOA, we performed PMF analysis of the AMS spectra and resolved three distinct factors that are referred to as different generations of the aqSOA products. Fig. 2 shows the mass spectra of the aqSOA factors and their evolution as a function of irradiation time. The least oxidized factor ( $O/C = 0.42$  and  $H/C = 1.68$ ; Fig. 2c1) appears to represent the first generation aqSOA products. It rises rapidly at the beginning of the illumination with an initial formation rate of  $3.5 \text{ mg L}^{-1} \text{ h}^{-1}$  and gradually declines after peaking at 42 min (Fig. 2a). The 1<sup>st</sup> generation products dominate aqSOA composition within the first hour of the photoreaction but their contribution then decreases and disappears once the precursor is completely depleted (Fig. 2b). Oligomerization appears to be a prominent process in the formation of the 1<sup>st</sup> generation aqSOA materials from GA as this factor correlates tightly with  $C_{20}H_{22}O_6^+$  ( $m/z$  358) and  $C_{18}H_{19}O_5^+$  ( $m/z$  315), which are AMS tracer ions for GA dimers (Fig. 2a). Specifically,  $C_{20}H_{22}O_6^+$  is the molecular ion of the GA dimer and  $C_{18}H_{19}O_5^+$  is a major fragment ion of the dimer (after losing  $-C_2H_3O$  from the molecular ion). In addition, the LC-PDA-ESI/HRMS analysis of the samples collected at 15 – 33 min and 65-82 min of irradiation, confirms the presence of molecules representative of GA dimer and trimer products (e.g.  $C_{20}H_{22}O_6$ ,  $C_{20}H_{22}O_7$ ,  $C_{20}H_{22}O_8$ ,  $C_{20}H_{22}O_9$ ,  $C_{30}H_{32}O_9$ , and  $C_{30}H_{32}O_{10}$  - see Fig. 3 panel a1 and a2).

The 2<sup>nd</sup> generation aqSOA is more oxidized ( $O/C = 0.56$ ,  $H/C = 1.46$ ) and presents a time trend which starts to rise after 23 min of illumination and increases at a slower rate and peaks at a later time than the 1<sup>st</sup> generation aqSOA (Fig. 2a). In the mass spectrum of this factor, the dimer molecular ion ( $C_{20}H_{22}O_6^+$ ) disappears and the relative intensity of  $C_{18}H_{19}O_5^+$  is substantially reduced (Fig. 2c2). However, smaller fragment ions from dimer derivatives, such as  $C_{18}H_{17}O_5^+$  ( $m/z$  313),  $C_{15}H_{11}O_4^+$  ( $m/z$  255) and  $C_{14}H_{11}O_3^+$  ( $m/z$  227), become more prominent (Fig. 2c).

$C_{18}H_{17}O_5^+$  is likely produced from the demethylation and demethoxylation products of the GA dimer, whereas  $C_{15}H_{11}O_4^+$  and  $C_{14}H_{11}O_3^+$  are probably produced from the functionalized products of GA monomer or ring opening products of GA dimers. These results, as well as the similarities in the time trends of 2<sup>nd</sup> generation aqSOA and  $C_{18}H_{17}O_5^+$  (Fig. 2a), suggest that the 1<sup>st</sup> generation products are transformed via hydroxylation, demethylation, demethoxylation, and partial ring-opening to form functionalized monomers and dimers (Scheme S1). Indeed, the molecules identified in the sample collected between 68 – 82 min of irradiation, which is composed of ~ 40% 1<sup>st</sup> generation and 60% 2<sup>nd</sup> generation aqSOA, show a wider range of MW and  $OS_C$  values than those in the 15 – 33 min sample, which is composed completely of 1<sup>st</sup> generation aqSOA (Fig. 3). These results suggest that oligomerization and functionalization may occur in parallel and compete in the early stages of the photoreaction, although oligomerization is more predominant at the very beginning of the photoreaction, likely because such reactions are more favored under higher precursor concentrations.

The 3<sup>rd</sup> generation aqSOA starts to rise after ~ 1 hour of irradiation and continues to increase over the entire period of irradiation (Fig. 2a). It is the most oxidized of the three identified aqSOA factors (O/C of 0.68 and H/C of 1.46) and contains the lowest fraction of ions with  $m/z > 100$ . The mass spectrum of this factor is overall similar to the semivolatile oxygenated organic aerosols (SV-OOA) commonly observed in the atmosphere (Zhang et al., 2011). Furthermore, the concentration of this factor correlates very well with the mass spectral signals of highly oxygenated smaller ions such as  $C_4H_5O_3^+$  ( $m/z = 101$ ;  $r^2 = 0.96$ ),  $CH_3O_2^+$  ( $m/z = 47$ ;  $r^2 = 0.94$ ) and  $CHO_2^+$  ( $m/z = 45$ ;  $r^2 = 0.98$ ) (Fig. S8), suggesting that fragmentation is a major pathway in the later periods of the photochemical reactions. Also, the good correlation ( $r^2 = 0.88$ ; Fig. S8) between the time trends of the 3<sup>rd</sup> generation aqSOA and the IC-measured total acid concentration suggests that carboxylic



acid formation plays an important role in the later periods of the reactions. This is consistent with the HPLC-PDA-HRMS results for the final time point (313-345 min), which is almost completely 3<sup>rd</sup> generation aqSOA (Fig. 2b), and shows increased abundance of small molecules (e.g. C<sub>4</sub>H<sub>4</sub>O<sub>4</sub>, C<sub>5</sub>H<sub>6</sub>O<sub>4</sub>, C<sub>6</sub>H<sub>6</sub>O<sub>2</sub>, C<sub>6</sub>H<sub>8</sub>O<sub>3</sub>, and C<sub>6</sub>H<sub>10</sub>O<sub>3</sub>). These results are also consistent with previous finds that, in phenolic aqSOA production, fragmentation can occur through demethoxylation and the cleavage of aromatic rings (Huang et al., 2018; O'Neill et al., 1978; Sun et al., 2010; Yu et al., 2014), and lead to the formation of ketones, carboxylic acids, and other highly oxygenated aliphatic products. Fragmentation may convert aqSOA species into semi-volatile and volatile molecules. However, in this study, we did not observe a decrease of aqSOA mass yield in the 6 hrs of irradiation. It suggests that even in the late period of the photoreaction, the production of low-volatility compounds in the aqSOA outweighs the loss of semi-volatile and volatile species. Also, it may suggest that some of the low-volatility products in the aqSOA are quite recalcitrant to fragmentation.

#### **2.4.2.2 Photochemical Evolution of the Molecular Composition of aqSOA**

The molecular compositions of aqSOA sampled during three time periods of irradiation, i.e., 15-33 min, 65-82 min, and 313-345 min, were analyzed using LC-PDA-ESI/HRMS (Lin et al., 2015a, 2016, 2018). Fig. 3, panels a1-a3 show all the assigned features in the aqSOA mass spectra. The identified compounds include the hydroxylation products of GA (e.g., C<sub>10</sub>H<sub>12</sub>O<sub>4</sub>, C<sub>10</sub>H<sub>12</sub>O<sub>5</sub>, and C<sub>10</sub>H<sub>12</sub>O<sub>6</sub>), GA dimers (e.g., C<sub>20</sub>H<sub>22</sub>O<sub>6</sub>, C<sub>20</sub>H<sub>22</sub>O<sub>7</sub>, C<sub>20</sub>H<sub>22</sub>O<sub>8</sub>, and C<sub>20</sub>H<sub>22</sub>O<sub>9</sub>), and GA trimers (e.g., C<sub>30</sub>H<sub>32</sub>O<sub>9</sub>, C<sub>30</sub>H<sub>32</sub>O<sub>10</sub>).

Fig. 4 shows the distributions of OS<sub>C</sub> and carbon number (n<sub>C</sub>) of all the CHO compounds identified by the LC-PDA-ESI/HRMS in the aqSOA samples. The aqSOA formed during the initial stages of photoreaction (i.e., in 15-33 min and 65-82 min samples) contains a significant

number of large molecules with  $n_C > 20$  and  $OS_C > -1$ , while the aqSOA composition towards the end of the reaction (i.e., in the 313-345 min sample) contains more smaller molecules with  $n_C < 10$ . The abundance of large molecules ( $n_C > 20$ ) significantly decreases at the end of the photoreaction. The van Krevelen diagrams of the aqSOA samples (Fig. 3b1-b3) illustrate the molecular transformation of the aqSOA components. For all three samples a majority of the detected species are located in the region of  $O/C \leq 1.0$  and  $H/C \leq 2.0$ . Molecules with  $H/C \leq 1.0$  and  $O/C \leq 0.5$  are typical for aromatic species, while molecules with  $H/C \geq 1.5$  and  $O/C \leq 0.5$  correspond to more aliphatic compounds (Kourtchev et al., 2014; Mazzoleni et al., 2012). DBE and AI values of the aqSOA products cover a wide range. Fig. 3 panels b1-b3 indicate that products with high AI dominate at the initial stages of the photoreaction but decrease in later periods. In particular, compounds with extremely high unsaturation degrees, such as  $C_{30}H_{30}O_{10}$  (AI = 0.30),  $C_{30}H_{32}O_9$  (AI = 0.29),  $C_{30}H_{32}O_{10}$  (AI = 0.25) and  $C_{28}H_{28}O_9$  (AI = 0.32), are only observed in the aqSOA sample irradiated for 65-82 min, and disappeared at the end of the photoreaction.

The signal-weighted average molecular formulas of the molecules detected by LC-PDA-ESI/HRMS are calculated to be  $C_{15.8}H_{17.5}O_{5.5}$  in the 15-33 min sample,  $C_{18.8}H_{20.7}O_{5.9}$  in the 65-82 min sample, and  $C_{12.8}H_{14.9}O_{5.1}$  in the 313-345 min sample. The changes of  $n_C$  in these three samples are consistent with the AMS findings that oligomers are formed at initial stages of the reaction and small fragmentation products are more predominant in late periods. Also, consistent with the AMS findings of a continuous increase of aqSOA oxidation over the course of photoreaction, the signal-weighted average O/C ratio of the aqSOA molecules are found to increase from 0.35 to 0.40. Note that the signal-weighted average O/C ratios of aqSOA determined by the LC-PDA-ESI/HRMS are systematically lower than the average O/C ratio measured by the AMS, probably due to the difference between the ESI/HRMS and AMS methodology in terms of sample analysis, data

processing, and O/C calculations (Yu et al., 2014). Overall, these results indicate that oligomerization and functionalization dominate in early stages of the photoreaction, contributing significantly to the composition of aqSOA, while fragmentation becomes more important after photochemical aging, leading to the formation of highly oxidized smaller species. Nevertheless, some high MW oligomeric compounds appear to be recalcitrant to photoreaction and can survive after 5 hours of irradiation (Fig. 3a3).

### 2.4.2.3 Light Absorbance by aqSOA

During illumination, the aqueous solution changed from colorless to yellow, indicating the formation of light-absorbing compounds (i.e., BrC). Fig. 5 shows the absorption coefficient ( $\text{cm}^{-1}$ ) and the mass absorption coefficient (MAC,  $\text{cm}^2 \text{g}^{-1}$ ) of the aqSOA in the wavelength range of 300-550 nm (the absorbance due to GA and 3,4-DMB has been removed). The aqSOA UV-vis absorption spectra exhibit general exponential shapes in the range of 300-550 nm. The calculated MAC values at 350 nm are in the range of 4300 and 8800  $\text{cm}^2 \text{g}^{-1}$ , similar to the MAC values previously reported for phenolic aqSOA (Smith et al., 2016). Absorption Angstrom Exponents (AAE) for the illuminated reaction solution increases from 5.1 ( $\pm 0.48$ ) to 9.4 ( $\pm 0.15$ ) (Fig. 5 and Fig. S9). The AAE values measured in this study are similar to the previous values observed for BrC from biomass burning (Hecobian et al., 2010; Kirchstetter and Thatcher, 2012). Also, the increasing trend of the AAE value during the photoreaction indicates that the wavelength-dependence of the absorption of the aqSOA becomes more pronounced as reactions progress.

Both the absorption coefficient and the MAC of the aqSOA increase with time at the beginning of the photoreactions but decrease slightly in later periods (Fig. 5). This trend is more clearly shown in the plot of the sunlight absorption rate ( $R_{\text{abs}}$ ) of aqSOA as a function of irradiation time (Fig. 6). In the first 3 hours of irradiation, the  $R_{\text{abs}}$  increases 4.6 folds from  $7.1 \times 10^{-7}$  ( $\pm 1.1 \times 10^{-8}$ )

to  $3.3 \times 10^{-6}$  ( $\pm 1.1 \times 10^{-8}$ ) mol-photons  $L^{-1}s^{-1}$ , and the aqSOA-mass-normalized  $R_{\text{abs}}$  increases 1.7 folds from  $1.2 \times 10^{-7}$  ( $\pm 1.9 \times 10^{-9}$ ) to  $2.1 \times 10^{-7}$  ( $\pm 7.1 \times 10^{-10}$ ) mol-photons  $mg^{-1}s^{-1}$ . During the same period, the total concentration of the 1<sup>st</sup> and 2<sup>nd</sup> generation aqSOA products rises and reaches a maximum, indicating that the formation of GA oligomers and functionalized products contributes to the formation of chromophores. From 3 to 6 hours of irradiation, the  $R_{\text{abs}}$  of the aqSOA decreases by 20% while the total aqSOA mass remains constant (Fig. 6), resulting in a 20% decrease of the mass normalized  $R_{\text{abs}}$  (from  $2.1 \times 10^{-7}$  to  $1.7 \times 10^{-7}$  mol-photons  $mg^{-1}s^{-1}$ ). This decrease of the aqSOA light absorption correlates with a continuous increase of the 3<sup>rd</sup> generation aqSOA products, which are composed of a higher mass fraction of smaller fragmentation products compared to the 1<sup>st</sup> and the 2<sup>nd</sup> generation aqSOA. This is an indication that the transformation of the early generation products may cause the degradation of chromophores and an overall photobleaching of the aqSOA.

### 2.4.3 Molecular Characterization of BrC in GA aqSOA

Table 1 summarizes the UV-vis spectra, chemical structures, and proposed formation mechanisms of the major BrC chromophores identified using HPLC-PDA-HRMS. Hydroxylation and dimerization of GA appear to be important pathways in the formation of chromophores. GA (#6 in Table 1) shows significant absorption around 280 nm but nearly no absorption in the solar range (i.e., above 290 nm). However, hydroxylated GA ( $C_{10}H_{12}O_6$ , #3 in Table 1) show strong light absorbance at wavelengths above 290 nm and exhibit a significant absorption band around 310 nm. Three dimerization products of GA (#9, 10 and 11 in Table 1) formed through C-C linkage were identified, which exhibit significant absorption bands at wavelengths around 320, 330, and 390 nm. Here, since C-O dimerization can break the conjugation system and would produce less absorbing products, thus the detected BrC chromophores are more likely to be C-C dimers rather than C-O dimers.  $C_{19}H_{22}O_6$  (#11 in Table 1) could be a derivative of  $C_{20}H_{22}O_7$  (#9 in Table 1)

produced from Norrish photochemical reaction with a loss of CO.(Mang et al., 2008) Hydroxylation and dimerization of GA can extend the conjugation of the  $\pi$ -bonds in the aromatic ring, causing red shifts of the absorption bands. In addition, hydroxylation and dimerization of 3,4-DMB may also contribute to the chromophore formation in this study (#1, 4, and 8 in Table 1). Although the products from DMB-participated reactions are only a minor contributor to the aqSOA mass due to the low initial DMB concentration, the contribution of DMB products to the absorption of aqSOA may still be important.

Using LC-PDA-ESI/HRMS, some of the structural isomers with the same formula can be separated on the LC column. For a significant number of the assigned formulas, structural isomers were observed and some of them undergo different transformations during the photoreaction. For example,  $C_{20}H_{22}O_6$  shows three isomers eluted at RT values of 20.3 min, 20.9 min, and 24.5 min, respectively. Possible structures for  $C_{20}H_{22}O_6$  may include GA dimers and other species such as derivatives of GA functionalized products and oligomers.  $C_{20}H_{22}O_6$  (RT = 20.3 min) and  $C_{20}H_{22}O_6$  (RT 20.9 = min) were observed at the very beginning of the reaction, but quickly disappeared.  $C_{20}H_{22}O_6$  (RT = 24.5 min, #11 in Table 1) was not present at the very beginning of the reaction but was observed in later samples and decreased with increased reactions time. As phenolic dimers can be formed through both C-C and C-O coupling of phenoxy radicals, and the reaction could occur at the *meta* or *ortho* positions to the hydroxyl group of GA, the observed structural isomers of  $C_{20}H_{22}O_6$  could therefore be GA dimers formed through different mechanisms, and may also be other structural isomers.

## 2.5 Atmospheric Implication

This study reveals that the aqueous-phase photosensitized reaction of GA, a phenolic carbonyl emitted from wood burning, can be an effective source of aqSOA and BrC. The fast reaction rate and high aqSOA yield of GA suggest that aqueous-phase photosensitized reactions of phenolic carbonyls in biomass burning emissions may play an important role in atmospheric SOA production. Our results show that oligomerization and functionalization dominate in the early stages of the reaction, while fragmentation becomes increasingly more important with aging. This finding is consistent with prior studies, which have also observed oligomerization, functionalization and fragmentation competing in aqSOA formation during photodegradation of phenols (Sun et al., 2010; Yu et al., 2014, 2016). The O/C ratio of the GA-derived aqSOA increases from 0.42 to 0.67, and the  $OS_C$  increases from  $-0.75$  to  $-0.073$  over the 5.6 hrs of photoreaction. The significant increases in the O/C ratio and  $OS_C$  of aqSOA compared to the precursor indicate that aqueous processing of GA and similar phenols could be an effective source of oxygenated organic aerosols (OOA) in areas impacted by biomass burning emissions. In addition, BrC compounds, which mainly include GA oligomers and functionalized products, are formed at the initial stages of the photosensitized reaction of GA. The light absorption of the aqSOA in the range of 300 – 550 nm increases initially, when the 1<sup>st</sup> generation aqSOA dominates the composition, reaches a plateau as the aqSOA composition is primarily composed of 2<sup>nd</sup> and 3<sup>rd</sup> generation products, and decreases slightly by the end of the reaction when the aqSOA is composed completely of the 3<sup>rd</sup> generation products. This finding may help elucidating how phenolic aqSOA influences the radiative balance of the atmosphere, and may have important implications for understanding the climate impacts of phenolic aqSOA during atmospheric aging.

## **Acknowledgements**

This work was supported by the U.S. National Science Foundation, Grant No. AGS-1649212 and the California Agricultural Experiment Station (Projects CA-D-ETX-2102-H and CA-D-LAW-6403-RR). PU group acknowledges additional support from discretionary startup funds allocated to A.L. WJ and AM acknowledge additional funding from the Jastro-Shields Graduate Research Award and the Donald G. Crosby Fellowship at UC Davis.

## Figures

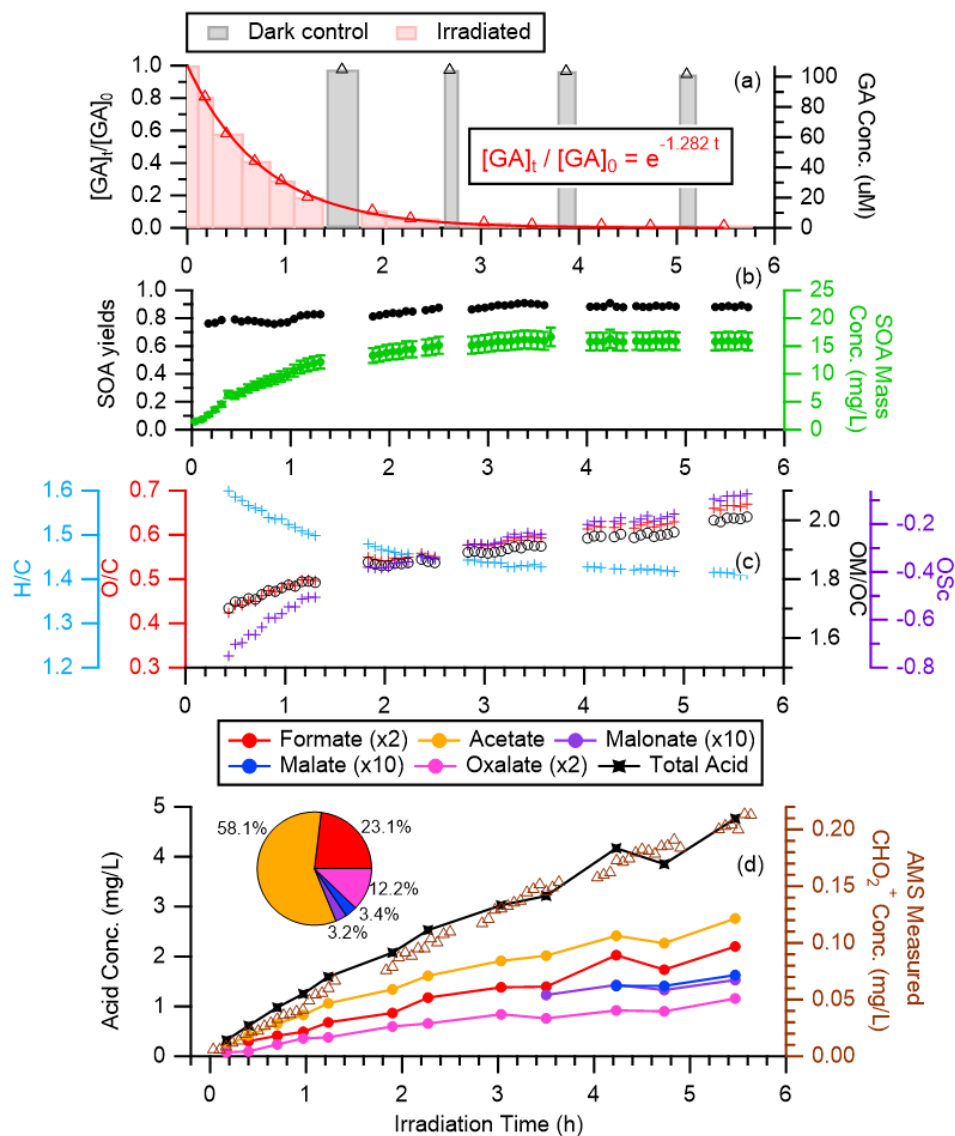


Figure 1. Overview of the aqueous photoreaction of guaiacyl acetone (GA) with the triplet excited state of 3,4-DMB and aqSOA formation over the course of simulated sunlight illumination. (a) Apparent first-order decay of GA measured by HPLC in offline samples.  $[GA]_0$  and  $[GA]_t$  are the concentrations of GA measured initially and at time  $t$  of illumination. Evolution trends of (b) aqSOA concentration and mass yield (error bars represent  $1\sigma$  (10%) of uncertainty in AMS quantification of aqSOA mass) and (c) H/C, O/C, OM/OC and OS<sub>C</sub> determined by HR-ToF-AMS. Evolution trends of (d) organic-equivalent concentrations of CHO<sub>2</sub><sup>+</sup> (HR-ToF-AMS tracer ion for carboxylic acids) and concentrations of organic acids measured by IC. The total acid concentration in (d) represents the sum of the five acids and the pie chart shows the mass contributions of individual acids measured in the last offline sample. The sampling duration for each offline sample



is marked on (a) and the irradiation time for each offline sample symbol is displayed as the mean of the sampling start time and end time.

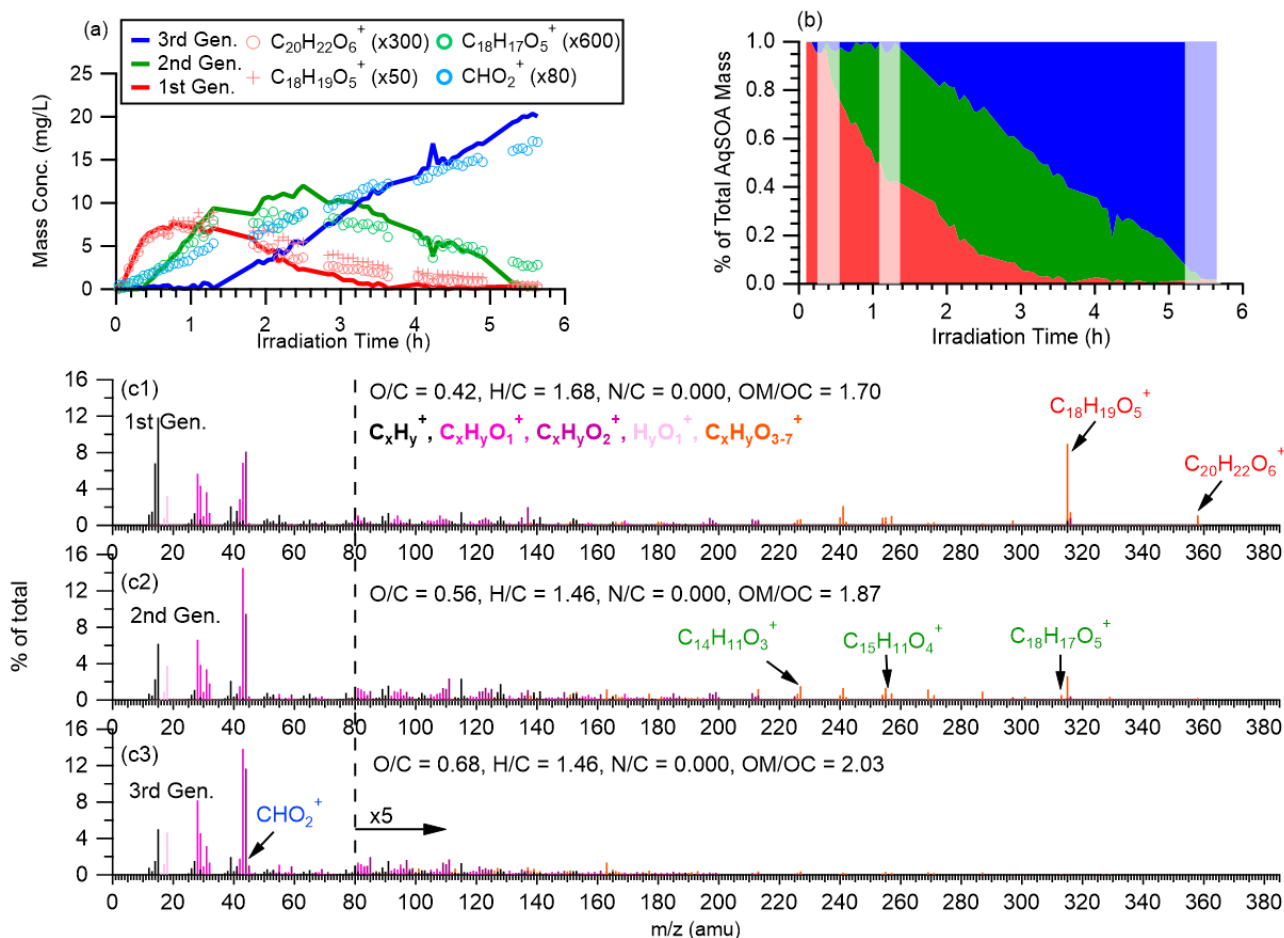


Figure 2. (a) Time series (b) fraction time series and (c) MS profiles for the three generations of aqSOA products obtained from PMF analysis. The shaded areas in (b) show the offline samples for LC-MS analysis. The peaks in the mass spectra are color-coded according to five ion categories:  $C_xH_y^+$ ,  $C_xH_yO^+$ ,  $C_xH_yO_2^+$ ,  $H_yO_1^+$ ,  $C_xH_yO_{3-7}^+$  ( $x > 1$ ,  $y \geq 0$ ). The tracer ions representative of the 1st generation (red), 2nd generation (green), and 3rd generation (blue) products are marked on the mass spectra in c1-c3.

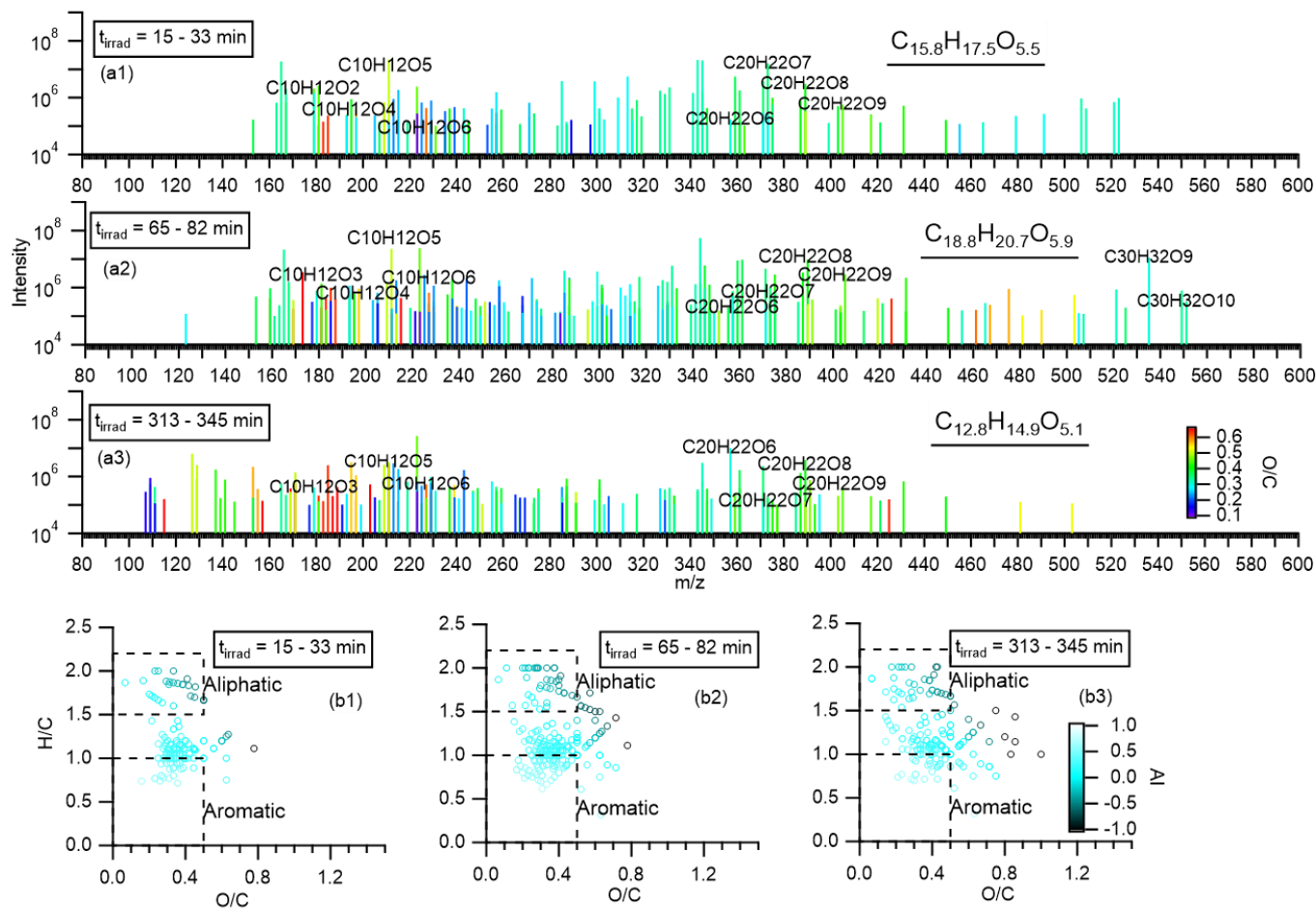


Figure 3. (a1-a3) Molecules detected by negative ion mode LC-ESI-HRMS in aqSOA samples at different stages of the photoreaction. Signals are colored by the O/C ratios of the formulas. The underlined molecular formular is the intensity-weighted average formular for the sample; and (b1-b3) Van Krevelen diagrams of the aqSOA components formed at different stages of photoreaction. Each data point is colored by the aromaticity index (AI) value of the formula.

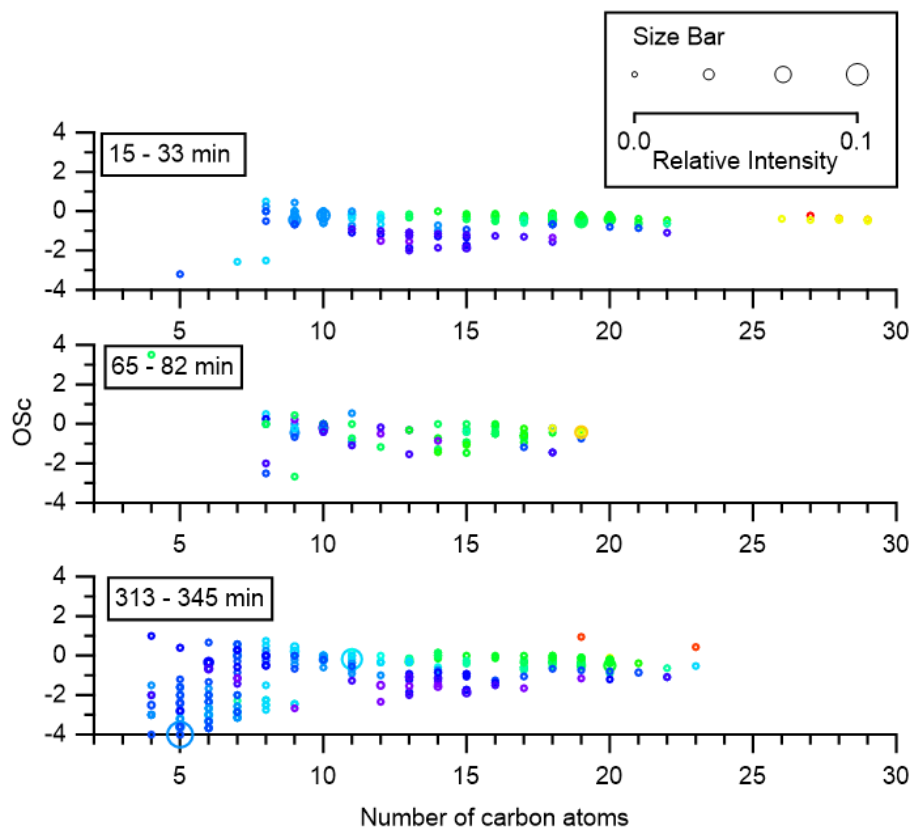


Figure 4. OSC and carbon number of chromophores detected in the irradiated samples determined by LC-PDA-ESI/HRMS, colored by DBE and size by the peak relative intensity in the mass spectrum (size 1-4 represents 0.0001-0.1).

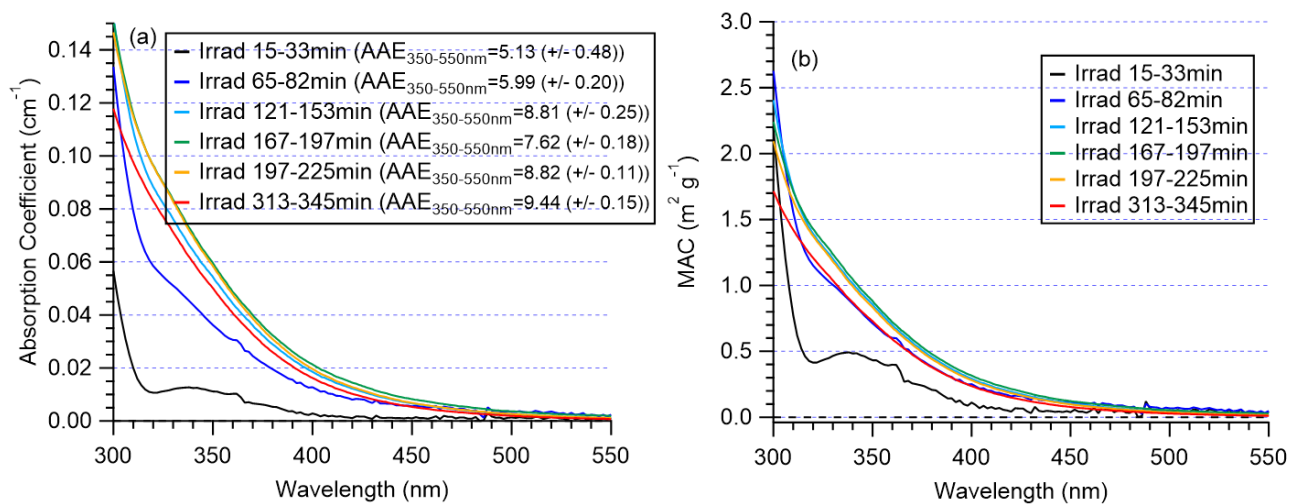


Figure 5. (a) Absorption coefficient and (b) mass absorption coefficients (MAC) of 6 offline samples collected throughout the course of the photoreaction of GA with 3C\* ( $t_0$  data subtracted). The AAE value for each sample is reported in the legend of (a).

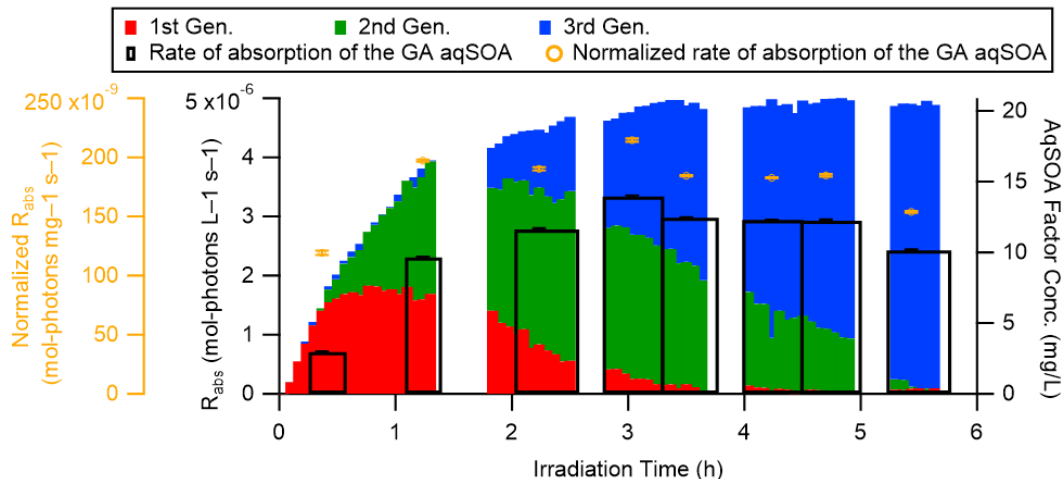
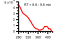
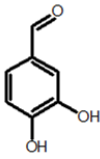
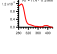
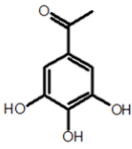
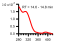
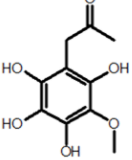
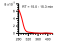
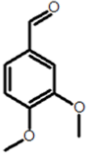
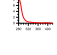
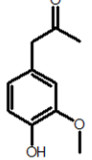
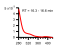
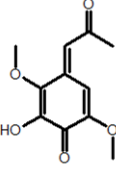
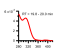
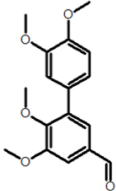
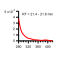
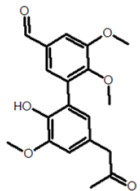
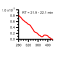
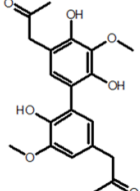
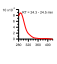
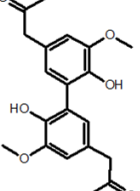
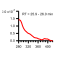
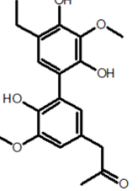


Figure 6. Change in the rate of sunlight absorption (black bars) and the organic mass normalized rate of sunlight absorption (black triangles) ( $\square = 300-550$  nm) of the aqSOA of GA as a function of irradiation time, together with the time series of the three generations of aqSOA. Error bars represent  $\pm 1$  standard error (SE) calculated by propagating the uncertainties.

Table 1. Information for the identified aqSOA chromophores, GA, and DMB detected by LC-PDA(-)ESI-HRMS in four offline samples collected during the photoreaction. The compounds are numbered in the order of their retention times. The y-axis of the UV-Vis spectrum is the absorbance detected by PDA (AU).

#	UV-Vis spectrum and RT	Neutral Formula and Nominal Mass	Possible structures	Proposed Formation Mechanisms
1		C <sub>7</sub> H <sub>6</sub> O <sub>3</sub> , 138.0317 amu		Formed by methoxy displacement of DMB. Both methoxy groups are replaced by hydroxyl groups
2		C <sub>8</sub> H <sub>8</sub> O <sub>4</sub> , 168.0423 amu		Mechanism is not apparent. Proposed structure is chosen for its stability.
3		C <sub>10</sub> H <sub>12</sub> O <sub>6</sub> , 228.0634 amu		Monomeric product of GA resulting from addition of three OH radicals to the aromatic ring.
4		C <sub>9</sub> H <sub>10</sub> O <sub>3</sub> , 166.0630 amu		<b>DMB – the photosensitizer.</b> Source of triplet carbon used to oxidize GA.
5		C <sub>10</sub> H <sub>12</sub> O <sub>3</sub> , 180.0786 amu		<b>GA – the phenol precursor.</b>
6		C <sub>11</sub> H <sub>12</sub> O <sub>5</sub> , 224.0685 amu		Monomeric product of GA resulting from addition of an OH radical and a methoxy radical and to the aromatic ring. Another OH radical abstracts a proton, resulting in a water byproduct. Rearrangement of double bonds to form a quinoidal system in conjugation with the ketone group.
7		C <sub>17</sub> H <sub>18</sub> O <sub>5</sub> , 302.1154 amu		DMB+DMB dimeric product resulting from photolysis leading to the formation of CHO and dimethoxybenzyl radicals and addition to an DMB unit. Hydrogen abstraction is then achieved by OH.

8		$C_{19}H_{20}O_6$ , 344.1260 amu		GA+DMB dimeric product formed by C-C linkage of a GA radical to a DMB unit. Hydrogen abstraction is achieved by OH.
9		$C_{20}H_{22}O_7$ , 374.1365 amu		GA+GA dimeric product, formed by linking two C radicals; formed either before or after OH radical addition to one aromatic ring.
10		$C_{20}H_{22}O_6$ , 358.1416 amu		GA+GA dimeric product, formed by linking two C radicals.
11		$C_{19}H_{22}O_6$ , 346.1416 amu		GA+GA dimeric product resulting from Norrish photochemistry with product 9. A CO unit is removed from the molecule.



## Reference

- Adler, G., Wagner, N. L., Lamb, K. D., Manfred, K. M., Schwarz, J. P., Franchin, A., Middlebrook, A. M., Washenfelder, R. A., Womack, C. C., Yokelson, R. J. and Murphy, D. M.: Evidence in biomass burning smoke for a light-absorbing aerosol with properties intermediate between brown and black carbon, *Aerosol Sci. Technol.*, 53(9), 976–989, doi:10.1080/02786826.2019.1617832, 2019.
- Aiken, A. C., DeCarlo, P. F., Kroll, J. H., Worsnop, D. R., Huffman, J. A., Docherty, K. S., Ulbrich, I. M., Mohr, C., Kimmel, J. R., Sueper, D., Sun, Y., Zhang, Q., Trimborn, A., Northway, M., Ziemann, P. J., Canagaratna, M. R., Onasch, T. B., Alfarra, M. R., Prevot, A. S. H., Dommen, J., Duplissy, J., Metzger, A., Baltensperger, U. and Jimenez, J. L.: O/C and OM/OC Ratios of Primary, Secondary, and Ambient Organic Aerosols with High-Resolution Time-of-Flight Aerosol Mass Spectrometry, *Environ. Sci. Technol.*, 42(12), 4478–4485, doi:10.1021/es703009q, 2008.
- Anastasio, C., Faust, B. C. and Rao, C. J.: Aromatic Carbonyl Compounds as Aqueous-Phase Photochemical Sources of Hydrogen Peroxide in Acidic Sulfate Aerosols, Fogs, and Clouds. 1. Non-Phenolic Methoxybenzaldehydes and Methoxyacetophenones with Reductants (Phenols), *Environ. Sci. Technol.*, 31(1), 218–232, doi:10.1021/es960359g, 1997.
- Bruns, E. A., El Haddad, I., Slowik, J. G., Kilic, D., Klein, F., Baltensperger, U. and Prévôt, A. S. H.: Identification of significant precursor gases of secondary organic aerosols from residential wood combustion, , 6, 27881, doi:10.1038/srep27881, 2016.
- Cappa, C. D., Lim, C. Y., Hagan, D. H., Coggon, M., Koss, A., Sekimoto, K., de Gouw, J., Onasch, T. B., Warneke, C. and Kroll, J. H.: Biomass-burning-derived particles from a wide variety of fuels – Part 2: Effects of photochemical aging on particle optical and chemical properties, *Atmos. Chem. Phys.*, 20(14), 8511–8532, doi:10.5194/acp-20-8511-2020, 2020.
- Chang, J. L. and Thompson, J. E.: Characterization of colored products formed during irradiation of aqueous solutions containing H<sub>2</sub>O<sub>2</sub> and phenolic compounds, *Atmos. Environ.*, 44(4), 541–551, doi:10.1016/J.ATMOSENV.2009.10.042, 2010.
- Chen, C.-L., Chen, S., Russell, L. M., Liu, J., Price, D. J., Betha, R., Sanchez, K. J., Lee, A. K. Y., Williams, L., Collier, S. C., Zhang, Q., Kumar, A., Kleeman, M. J., Zhang, X. and Cappa, C. D.: Organic Aerosol Particle Chemical Properties Associated With Residential Burning and Fog in Wintertime San Joaquin Valley (Fresno) and With Vehicle and Firework Emissions in Summertime South Coast Air Basin (Fontana), *J. Geophys. Res. Atmos.*, 123(18), 10,707–710,731, doi:10.1029/2018JD028374, 2018.
- Chen, Y., Li, N., Li, X., Tao, Y., Luo, S., Zhao, Z., Ma, S., Huang, H., Chen, Y., Ye, Z. and Ge, X.: Secondary organic aerosol formation from 3C\*-initiated oxidation of 4-ethylguaiaicol in atmospheric aqueous-phase, *Sci. Total Environ.*, 723, 137953, doi:https://doi.org/10.1016/j.scitotenv.2020.137953, 2020.
- Collett, J. L., Hoag, K. J., Sherman, D. E., Bator, A. and Richards, L. W.: Spatial and temporal variations in San Joaquin Valley fog chemistry, *Atmos. Environ.*, 33(1), 129–140, doi:https://doi.org/10.1016/S1352-2310(98)00136-8, 1998.
- Cordell, R. L., Mazet, M., Dechoux, C., Hama, S. M. L., Staelens, J., Hofman, J., Stroobants, C.,

- Roekens, E., Kos, G. P. A., Weijers, E. P., Frumau, K. F. A., Panteliadis, P., Delaunay, T., Wyche, K. P. and Monks, P. S.: Evaluation of biomass burning across North West Europe and its impact on air quality, *Atmos. Environ.*, 141, 276–286, doi:10.1016/J.ATMOSENV.2016.06.065, 2016.
- E., R. C., Michael, B., H., J. F., Michael, J., R., B. J. and T., E. C.: Critical Review of Health Impacts of Wildfire Smoke Exposure, *Environ. Health Perspect.*, 124(9), 1334–1343, doi:10.1289/ehp.1409277, 2016.
- Feigenbrugel, V., Le Calvé, S., Mirabel, P. and Louis, F.: Henry's law constant measurements for phenol, o-, m-, and p-cresol as a function of temperature, *Atmos. Environ.*, 38(33), 5577–5588, doi:10.1016/j.atmosenv.2004.06.025, 2004.
- Fleming, L. T., Lin, P., Roberts, J. M., Selimovic, V., Yokelson, R., Laskin, J., Laskin, A. and Nizkorodov, S. A.: Molecular composition and photochemical lifetimes of brown carbon chromophores in biomass burning organic aerosol, *Atmos. Chem. Phys. Discuss.*, 2019, 1–38, doi:10.5194/acp-2019-523, 2019.
- Gaston, C. J., Lopez-Hilfiker, F. D., Whybrew, L. E., Hadley, O., McNair, F., Gao, H., Jaffe, D. A. and Thornton, J. A.: Online molecular characterization of fine particulate matter in Port Angeles, WA: Evidence for a major impact from residential wood smoke, *Atmos. Environ.*, 138, 99–107, doi:https://doi.org/10.1016/j.atmosenv.2016.05.013, 2016.
- Ge, X., Setyan, A., Sun, Y. and Zhang, Q.: Primary and secondary organic aerosols in Fresno, California during wintertime: Results from high resolution aerosol mass spectrometry, *J. Geophys. Res. Atmos.*, 117(D19), doi:10.1029/2012JD018026, 2012.
- Ge, X., Shaw, S. L. and Zhang, Q.: Toward Understanding Amines and Their Degradation Products from Postcombustion CO<sub>2</sub> Capture Processes with Aerosol Mass Spectrometry, *Environ. Sci. Technol.*, 48(9), 5066–5075, doi:10.1021/es4056966, 2014.
- George, K. M., Ruthenburg, T. C., Smith, J., Yu, L., Zhang, Q., Anastasio, C. and Dillner, A. M.: FT-IR quantification of the carbonyl functional group in aqueous-phase secondary organic aerosol from phenols, *Atmos. Environ.*, 100, 230–237, doi:10.1016/j.atmosenv.2014.11.011, 2015.
- Gilardoni, S., Massoli, P., Paglione, M., Giulianelli, L., Carbone, C., Rinaldi, M., Decesari, S., Sandrini, S., Costabile, F., Gobbi, G. P., Pietrogrande, M. C., Visentin, M., Scotto, F., Fuzzi, S. and Facchini, M. C.: Direct observation of aqueous secondary organic aerosol from biomass-burning emissions, *Proc. Natl. Acad. Sci.*, 113(36), 10013–10018, doi:10.1073/pnas.1602212113, 2016.
- Gilman, J. B., Lerner, B. M., Kuster, W. C., Goldan, P. D., Warneke, C., Veres, P. R., Roberts, J. M., de Gouw, J. A., Burling, I. R. and Yokelson, R. J.: Biomass burning emissions and potential air quality impacts of volatile organic compounds and other trace gases from fuels common in the US, *Atmos. Chem. Phys.*, 15(24), 13915–13938, doi:10.5194/acp-15-13915-2015, 2015.
- De Gouw, J. and Jimenez, J. L.: Organic Aerosols in the Earth's Atmosphere, *Environ. Sci. Technol.*, 43(20), 7614–7618, doi:10.1021/es9006004, 2009.
- Hatch, L. E., Yokelson, R. J., Stockwell, C. E., Veres, P. R., Simpson, I. J., Blake, D. R., Orlando, J. J. and Barsanti, K. C.: Multi-instrument comparison and compilation of non-methane organic gas emissions from biomass burning and implications for smoke-derived secondary organic

- aerosol precursors, *Atmos. Chem. Phys.*, 17(2), 1471–1489, doi:10.5194/acp-17-1471-2017, 2017.
- Heald, C. L., Kroll, J. H., Jimenez, J. L., Docherty, K. S., DeCarlo, P. F., Aiken, A. C., Chen, Q., Martin, S. T., Farmer, D. K. and Artaxo, P.: A simplified description of the evolution of organic aerosol composition in the atmosphere, *Geophys. Res. Lett.*, 37(8), L08803, doi:10.1029/2010GL042737, 2010.
- Hecobian, A., Zhang, X., Zheng, M., Frank, N., Edgerton, E. S. and Weber, R. J.: Water-Soluble Organic Aerosol material and the light-absorption characteristics of aqueous extracts measured over the Southeastern United States, *Atmos. Chem. Phys.*, 10(13), 5965–5977, doi:10.5194/acp-10-5965-2010, 2010.
- Hems, R. F., Schnitzler, E. G., Bastawrous, M., Soong, R., Simpson, A. J. and Abbatt, J. P. D.: Aqueous Photoreactions of Wood Smoke Brown Carbon, *ACS Earth Sp. Chem.*, 4(7), 1149–1160, doi:10.1021/acsearthspacechem.0c00117, 2020.
- Huang, D. D., Zhang, Q., Cheung, H. H. Y., Yu, L., Zhou, S., Anastasio, C., Smith, J. D. and Chan, C. K.: Formation and Evolution of aqSOA from Aqueous-Phase Reactions of Phenolic Carbonyls: Comparison between Ammonium Sulfate and Ammonium Nitrate Solutions, *Environ. Sci. Technol.*, doi:10.1021/acs.est.8b03441, 2018.
- Jaffe, D. A., O'Neill, S. M., Larkin, N. K., Holder, A. L., Peterson, D. L., Halofsky, J. E. and Rappold, A. G.: Wildfire and prescribed burning impacts on air quality in the United States, *J. Air Waste Manage. Assoc.*, 70(6), 583–615, doi:10.1080/10962247.2020.1749731, 2020.
- Jeong, C.-H., Evans, G. J., Dann, T., Graham, M., Herod, D., Dabek-Zlotorzynska, E., Mathieu, D., Ding, L. and Wang, D.: Influence of biomass burning on wintertime fine particulate matter: Source contribution at a valley site in rural British Columbia, *Atmos. Environ.*, 42(16), 3684–3699, doi:10.1016/J.ATMOENV.2008.01.006, 2008.
- Kaur, R. and Anastasio, C.: First Measurements of Organic Triplet Excited States in Atmospheric Waters, *Environ. Sci. Technol.*, 52(9), 5218–5226, doi:10.1021/acs.est.7b06699, 2018.
- Kaur, R., Labins, J. R., Helbock, S. S., Jiang, W., Bein, K., Zhang, Q. and Anastasio, C.: Photooxidants from Brown Carbon and Other Chromophores in Illuminated Particle Extracts, *Atmos. Chem. Phys. Discuss.*, 2018, 1–34, doi:10.5194/acp-2018-1258, 2018.
- Kaur, R., Labins, J. R., Helbock, S. S., Jiang, W., Bein, K. J., Zhang, Q. and Anastasio, C.: Photooxidants from brown carbon and other chromophores in illuminated particle extracts, *Atmos. Chem. Phys.*, 19(9), 6579–6594, doi:10.5194/acp-19-6579-2019, 2019.
- Kirchstetter, T. W. and Thatcher, T. L.: Contribution of organic carbon to wood smoke particulate matter absorption of solar radiation, *Atmos. Chem. Phys.*, 12(14), 6067–6072, doi:10.5194/acp-12-6067-2012, 2012.
- Knorr, W., Dentener, F., Lamarque, J.-F., Jiang, L. and Arneeth, A.: Wildfire air pollution hazard during the 21st century, *Atmos. Chem. Phys.*, 17(14), 9223–9236, doi:10.5194/acp-17-9223-2017, 2017.
- Kourtchev, I., Fuller, S. J., Giorio, C., Healy, R. M., Wilson, E., O'Connor, I., Wenger, J. C., McLeod, M., Aalto, J., Ruuskanen, T. M., Maenhaut, W., Jones, R., Venables, D. S., Sodeau, J. R., Kulmala, M. and Kalberer, M.: Molecular composition of biogenic secondary organic

- aerosols using ultrahigh-resolution mass spectrometry: comparing laboratory and field studies, *Atmos. Chem. Phys.*, 14(4), 2155–2167, doi:10.5194/acp-14-2155-2014, 2014.
- Kroll, J. H., Donahue, N. M., Jimenez, J. L., Kessler, S. H., Canagaratna, M. R., Wilson, K. R., Altieri, K. E., Mazzoleni, L. R., Wozniak, A. S., Bluhm, H., Mysak, E. R., Smith, J. D., Kolb, C. E. and Worsnop, D. R.: Carbon oxidation state as a metric for describing the chemistry of atmospheric organic aerosol, *Nat Chem*, 3(2), 133–139, doi:10.1038/nchem.948, 2011.
- Li, C., He, Q., Schade, J., Passig, J., Zimmermann, R., Meidan, D., Laskin, A. and Rudich, Y.: Dynamic changes in optical and chemical properties of tar ball aerosols by atmospheric photochemical aging, *Atmos. Chem. Phys.*, 19(1), 139–163, doi:10.5194/acp-19-139-2019, 2019.
- Li, Y. J., Huang, D. D., Cheung, H. Y., Lee, A. K. Y. and Chan, C. K.: Aqueous-phase photochemical oxidation and direct photolysis of vanillin – a model compound of methoxy phenols from biomass burning, *Atmos. Chem. Phys.*, 14(6), 2871–2885, doi:10.5194/acp-14-2871-2014, 2014.
- Lin, P., Liu, J., Shilling, J. E., Kathmann, S. M., Laskin, J. and Laskin, A.: Molecular characterization of brown carbon (BrC) chromophores in secondary organic aerosol generated from photo-oxidation of toluene, *Phys. Chem. Chem. Phys.*, 17(36), 23312–23325, doi:10.1039/C5CP02563J, 2015.
- Lin, P., Aiona, P. K., Li, Y., Shiraiwa, M., Laskin, J., Nizkorodov, S. A. and Laskin, A.: Molecular Characterization of Brown Carbon in Biomass Burning Aerosol Particles, *Environ. Sci. Technol.*, 50(21), 11815–11824, doi:10.1021/acs.est.6b03024, 2016.
- Lin, P., Fleming, L. T., Nizkorodov, S. A., Laskin, J. and Laskin, A.: Comprehensive Molecular Characterization of Atmospheric Brown Carbon by High Resolution Mass Spectrometry with Electrospray and Atmospheric Pressure Photoionization, *Anal. Chem.*, 90(21), 12493–12502, doi:10.1021/acs.analchem.8b02177, 2018.
- Liu, C., Liu, J., Liu, Y., Chen, T. and He, H.: Secondary organic aerosol formation from the OH-initiated oxidation of guaiacol under different experimental conditions, *Atmos. Environ.*, 207, 30–37, doi:10.1016/j.atmosenv.2019.03.021, 2019.
- Mang, S. A., Henricksen, D. K., Bateman, A. P., Andersen, M. P. S., Blake, D. R. and Nizkorodov, S. A.: Contribution of Carbonyl Photochemistry to Aging of Atmospheric Secondary Organic Aerosol, *J. Phys. Chem. A*, 112(36), 8337–8344, doi:10.1021/jp804376c, 2008.
- Mazzoleni, L. R., Saranjampour, P., Dalbec, M. M., Samburova, V., Hallar, A. G., Zielinska, B., Lowenthal, D. H. and Kohl, S.: Identification of water-soluble organic carbon in non-urban aerosols using ultrahigh-resolution FT-ICR mass spectrometry: organic anions, *Environ. Chem.*, 9(3), 285–297 [online] Available from: <https://doi.org/10.1071/EN11167>, 2012.
- McClure, C. D. and Jaffe, D. A.: US particulate matter air quality improves except in wildfire-prone areas, *Proc. Natl. Acad. Sci.*, 115(31), 7901 LP – 7906, doi:10.1073/pnas.1804353115, 2018.
- McFall, A. S., Johnson, A. W. and Anastasio, C.: Air–Water Partitioning of Biomass-Burning Phenols and the Effects of Temperature and Salinity, *Environ. Sci. Technol.*, 54(7), 3823–3830, doi:10.1021/acs.est.9b06443, 2020.

- Nolte, C. G., Schauer, J. J., Cass, G. R. and Simoneit, B. R. T.: Highly Polar Organic Compounds Present in Wood Smoke and in the Ambient Atmosphere, *Environ. Sci. Technol.*, 35(10), 1912–1919, doi:10.1021/es001420r, 2001.
- O'Dell, K., Ford, B., Fischer, E. V and Pierce, J. R.: Contribution of Wildland-Fire Smoke to US PM<sub>2.5</sub> and Its Influence on Recent Trends, *Environ. Sci. Technol.*, 53(4), 1797–1804, doi:10.1021/acs.est.8b05430, 2019.
- O'Neill, P., Steenken, S., van der Linde, H. and Schulte-Frohlinde, D.: Reaction of OH radicals with nitrophenols in aqueous solution, *Radiat. Phys. Chem.*, 12(1), 13–17, doi:https://doi.org/10.1016/0146-5724(78)90070-5, 1978.
- Pang, H., Zhang, Q., Lu, X., Li, K., Chen, H., Chen, J., Yang, X., Ma, Y., Ma, J. and Huang, C.: Nitrite-Mediated Photooxidation of Vanillin in the Atmospheric Aqueous Phase, *Environ. Sci. Technol.*, 53(24), 14253–14263, doi:10.1021/acs.est.9b03649, 2019.
- Pillar, E. A., Camm, R. C. and Guzman, M. I.: Catechol Oxidation by Ozone and Hydroxyl Radicals at the Air–Water Interface, *Environ. Sci. Technol.*, 48(24), 14352–14360, doi:10.1021/es504094x, 2014.
- Pluskal, T., Castillo, S., Villar-Briones, A. and Orešič, M.: MZmine 2: Modular framework for processing, visualizing, and analyzing mass spectrometry-based molecular profile data, *BMC Bioinformatics*, 11(1), 395, doi:10.1186/1471-2105-11-395, 2010.
- Raja, S., Raghunathan, R., Yu, X.-Y., Lee, T., Chen, J., Kommalapati, R. R., Murugesan, K., Shen, X., Qingzhong, Y., Valsaraj, K. T. and Collett, J. L.: Fog chemistry in the Texas–Louisiana Gulf Coast corridor, *Atmos. Environ.*, 42(9), 2048–2061, doi:https://doi.org/10.1016/j.atmosenv.2007.12.004, 2008.
- Roach, P. J., Laskin, J. and Laskin, A.: Higher-Order Mass Defect Analysis for Mass Spectra of Complex Organic Mixtures, *Anal. Chem.*, 83(12), 4924–4929, doi:10.1021/ac200654j, 2011.
- Schauer, J. J. and Cass, G. R.: Source Apportionment of Wintertime Gas-Phase and Particle-Phase Air Pollutants Using Organic Compounds as Tracers, *Environ. Sci. Technol.*, 34(9), 1821–1832, doi:10.1021/es981312t, 2000.
- Schauer, J. J., Kleeman, M. J., Cass, G. R. and Simoneit, B. R. T.: Measurement of Emissions from Air Pollution Sources. 3. C<sub>1</sub>–C<sub>29</sub> Organic Compounds from Fireplace Combustion of Wood, *Environ. Sci. Technol.*, 35(9), 1716–1728, doi:10.1021/es001331e, 2001.
- Scott, A. F. and Reilly, C. A.: Wood and Biomass Smoke: Addressing Human Health Risks and Exposures, *Chem. Res. Toxicol.*, 32(2), 219–221, doi:10.1021/acs.chemrestox.8b00318, 2019.
- Simoneit, B. R. T.: A review of biomarker compounds as source indicators and tracers for air pollution, *Environ. Sci. Pollut. Res.*, 6(3), 159–169, doi:10.1007/bf02987621, 1999.
- Simpson, C. D., Paulsen, M., Dills, R. L., Liu, L.-J. S. and Kalman, D. A.: Determination of Methoxyphenols in Ambient Atmospheric Particulate Matter: Tracers for Wood Combustion, *Environ. Sci. Technol.*, 39(2), 631–637, doi:10.1021/es0486871, 2005.
- Smith, J. D., Sio, V., Yu, L., Zhang, Q. and Anastasio, C.: Secondary Organic Aerosol Production from Aqueous Reactions of Atmospheric Phenols with an Organic Triplet Excited State, *Environ. Sci. Technol.*, 48(2), 1049–1057, doi:10.1021/es4045715, 2014.

- Smith, J. D., Kinney, H. and Anastasio, C.: Aqueous benzene-diols react with an organic triplet excited state and hydroxyl radical to form secondary organic aerosol, *Phys. Chem. Chem. Phys.*, 17(15), 10227–10237, doi:10.1039/c4cp06095d, 2015.
- Smith, J. D., Kinney, H. and Anastasio, C.: Phenolic carbonyls undergo rapid aqueous photodegradation to form low-volatility, light-absorbing products, *Atmos. Environ.*, 126, 36–44, doi:http://dx.doi.org/10.1016/j.atmosenv.2015.11.035, 2016.
- Sommers, W. T., Loehman, R. A. and Hardy, C. C.: Wildland fire emissions, carbon, and climate: Science overview and knowledge needs, *For. Ecol. Manage.*, 317, 1–8, doi:10.1016/j.foreco.2013.12.014, 2014.
- Sullivan, A. P., Guo, H., Schroder, J. C., Campuzano-Jost, P., Jimenez, J. L., Campos, T., Shah, V., Jaeglé, L., Lee, B. H., Lopez-Hilfiker, F. D., Thornton, J. A., Brown, S. S. and Weber, R. J.: Biomass Burning Markers and Residential Burning in the WINTER Aircraft Campaign, *J. Geophys. Res. Atmos.*, 124(3), 1846–1861, doi:10.1029/2017JD028153, 2019.
- Sun, Y. L., Zhang, Q., Anastasio, C. and Sun, J.: Insights into secondary organic aerosol formed via aqueous-phase reactions of phenolic compounds based on high resolution mass spectrometry, *Atmos. Chem. Phys.*, 10(10), 4809–4822, doi:10.5194/acp-10-4809-2010, 2010.
- Ulbrich, I. M., Canagaratna, M. R., Zhang, Q., Worsnop, D. R. and Jimenez, J. L.: Interpretation of organic components from Positive Matrix Factorization of aerosol mass spectrometric data, *Atmos. Chem. Phys.*, 9(9), 2891–2918, doi:10.5194/acp-9-2891-2009, 2009.
- Ward, T. J., Rinehart, L. R. and Lange, T.: The 2003/2004 Libby, Montana PM<sub>2.5</sub> Source Apportionment Research Study, *Aerosol Sci. Technol.*, 40(3), 166–177, doi:10.1080/02786820500494536, 2006.
- Xie, M., Chen, X., Hays, M. D. and Holder, A. L.: Composition and light absorption of N-containing aromatic compounds in organic aerosols from laboratory biomass burning, *Atmos. Chem. Phys.*, 19(5), 2899–2915, doi:10.5194/acp-19-2899-2019, 2019.
- Yadav, I. C., Linthoingambi Devi, N., Li, J., Syed, J. H., Zhang, G. and Watanabe, H.: Biomass burning in Indo-China peninsula and its impacts on regional air quality and global climate change-a review, *Environ. Pollut.*, 227, 414–427, doi:10.1016/J.ENVPOL.2017.04.085, 2017.
- Yee, L. D., Kautzman, K. E., Loza, C. L., Schilling, K. A., Coggon, M. M., Chhabra, P. S., Chan, M. N., Chan, A. W. H., Hersey, S. P., Crouse, J. D., Wennberg, P. O., Flagan, R. C. and Seinfeld, J. H.: Secondary organic aerosol formation from biomass burning intermediates: phenol and methoxyphenols, *Atmos. Chem. Phys.*, 13(16), 8019–8043, doi:10.5194/acp-13-8019-2013, 2013.
- Young, D. E., Kim, H., Parworth, C., Zhou, S., Zhang, X., Cappa, C. D., Seco, R., Kim, S. and Zhang, Q.: Influences of emission sources and meteorology on aerosol chemistry in a polluted urban environment: results from DISCOVER-AQ California, *Atmos. Chem. Phys.*, 16(8), 5427–5451, doi:10.5194/acp-16-5427-2016, 2016.
- Yu, L., Smith, J., Laskin, A., Anastasio, C., Laskin, J. and Zhang, Q.: Chemical characterization of SOA formed from aqueous-phase reactions of phenols with the triplet excited state of carbonyl and hydroxyl radical, *Atmos. Chem. Phys.*, 14(24), 13801–13816, doi:10.5194/acp-14-13801-2014, 2014.

- Yu, L., Smith, J., Laskin, A., George, K. M., Anastasio, C., Laskin, J., Dillner, A. M. and Zhang, Q.: Molecular transformations of phenolic SOA during photochemical aging in the aqueous phase: competition among oligomerization, functionalization, and fragmentation, *Atmos. Chem. Phys.*, 16(7), 4511–4527, doi:10.5194/acp-16-4511-2016, 2016.
- Zhang, Q., Jimenez, J. L., Canagaratna, M. R., Ulbrich, I. M., Ng, N. L., Worsnop, D. R. and Sun, Y.: Understanding atmospheric organic aerosols via factor analysis of aerosol mass spectrometry: a review, *Anal. Bioanal. Chem.*, 401(10), 3045–3067, doi:10.1007/s00216-011-5355-y, 2011.
- Zhong, M. and Jang, M.: Dynamic light absorption of biomass-burning organic carbon photochemically aged under natural sunlight, *Atmos. Chem. Phys.*, 14(3), 1517–1525, doi:10.5194/acp-14-1517-2014, 2014.

## Supporting Information

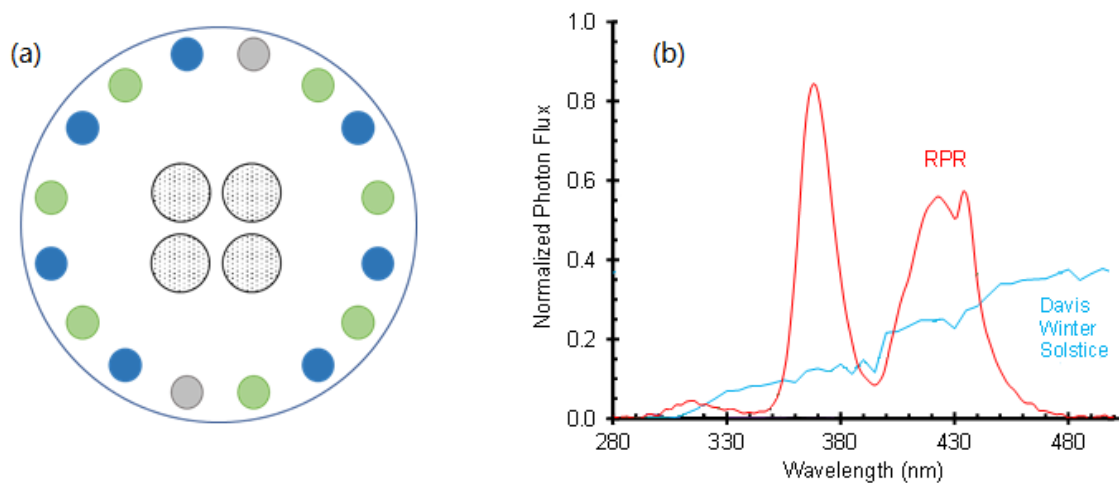


Figure S1. (a) Top-down diagram of the bulb and samples in the RPR-200 photoreactor. The four central, dotted circles are the Pyrex tubes containing samples for illumination, and the peripheral grey, green, and blue circles are RPR-3000, RPR-3500, and RPR-4190 bulbs, respectively. The fan and stir plates are located directly beneath the sample tubes, and each illuminated sample tube contains a stir bar; (b) Normalized distribution of the photon flux inside the RPR-200 photoreactor, and for comparison, the actinic flux in Davis, CA at winter solstice. (George et al., 2015b) Photon fluxes are normalized such that the area under each curve between 280 and 500 nm is equal.



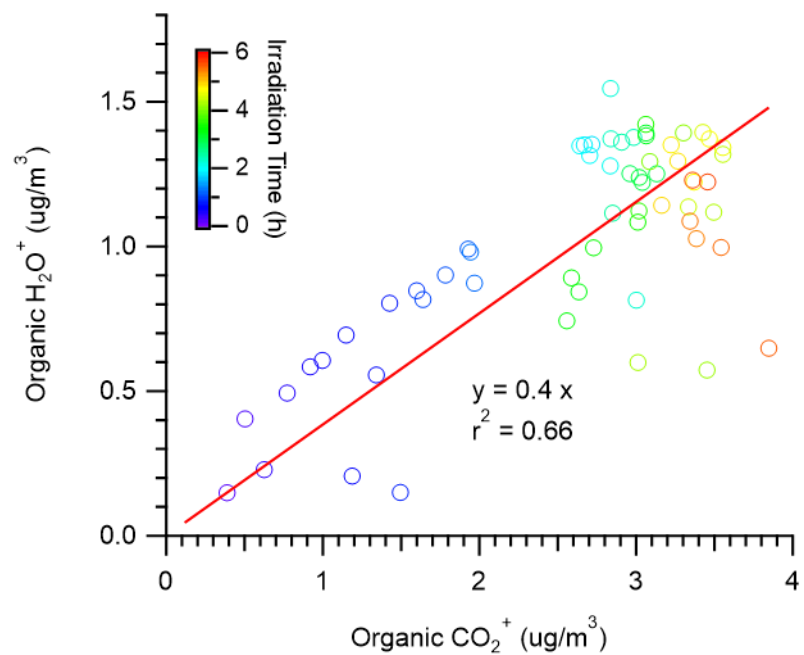


Figure S2. Correlation between the organic H<sub>2</sub>O<sup>+</sup> signal (= total H<sub>2</sub>O<sup>+</sup> signal - sulfate H<sub>2</sub>O<sup>+</sup> signal) and the CO<sub>2</sub><sup>+</sup> signal measured in the AMS spectra of the aqSOA samples

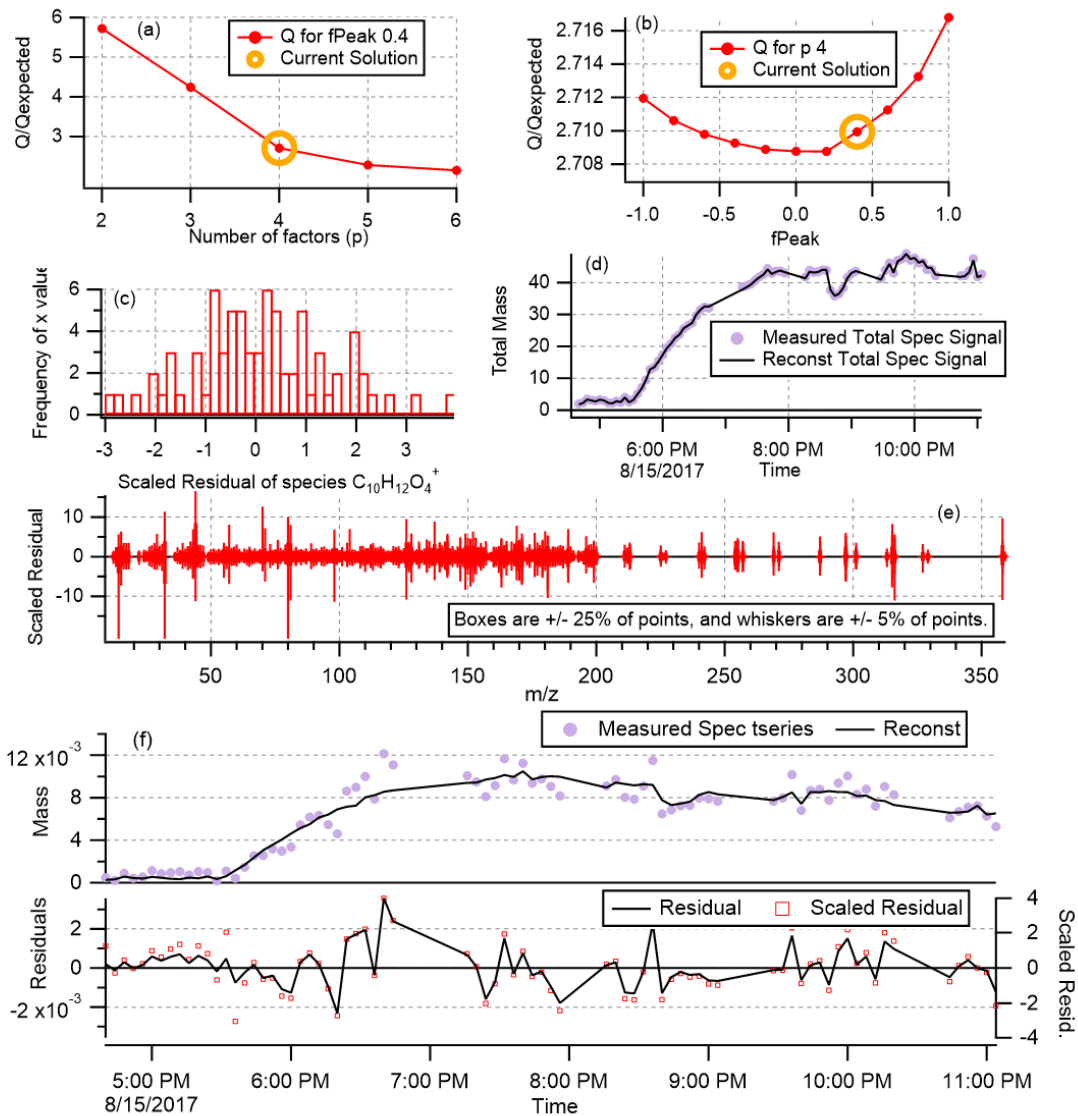


Figure S3. Summary of diagnostic plots for the four-factor solution for PMF analysis: (a)  $Q/Q_{exp}$  as a function of number of factors selected for PMF modeling; (b)  $Q/Q_{exp}$  as a function of  $f_{Peak}$ ; (c) Histogram of scaled residuals for species  $C_{10}H_{12}O_4^+$ ; (d) Reconstructed and measured total species signal for all species; (e) box and whisker plot showing the distributions of scaled residuals for each  $m/z$ ; and (f) Reconstructed and measured signals and residuals for species  $C_{10}H_{12}O_4^+$

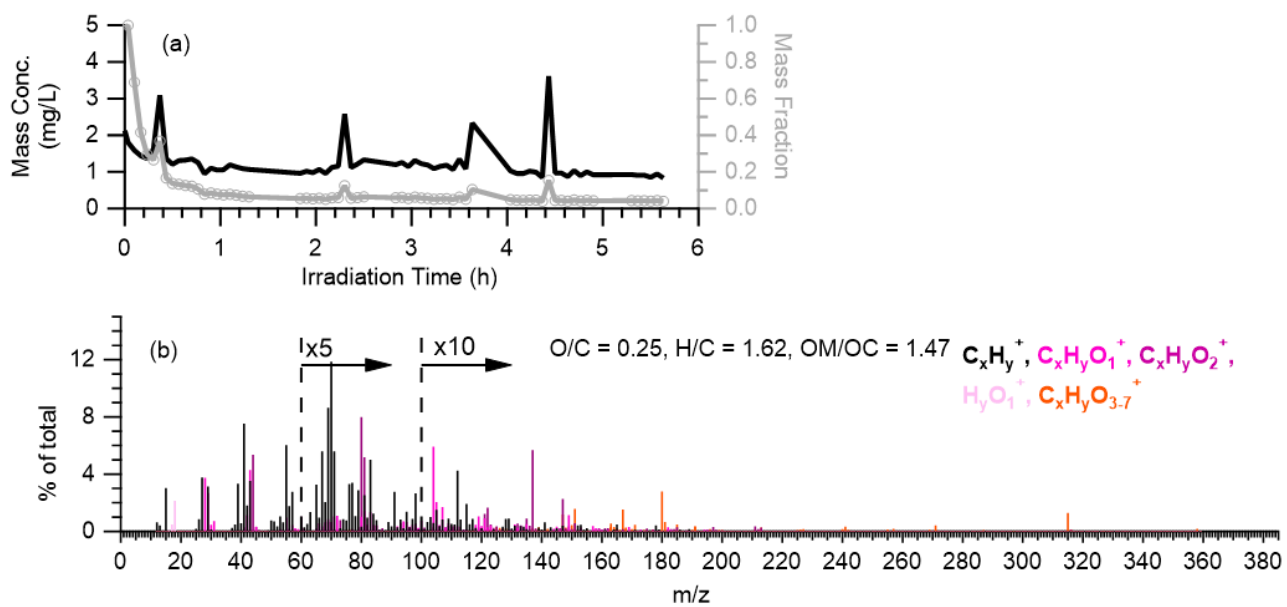


Figure S4. (a) Mass concentration and fraction time series and (b) MS profile of the background factor obtained from PMF analysis

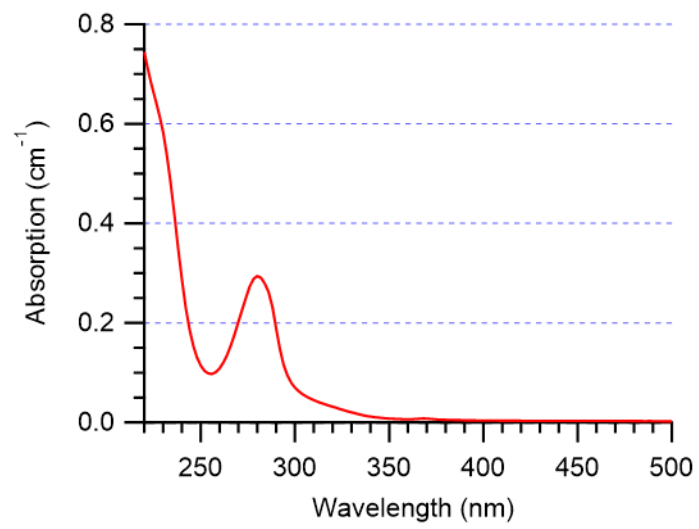


Figure S5. UV-vis absorption spectrum of 100 μM of GA standard

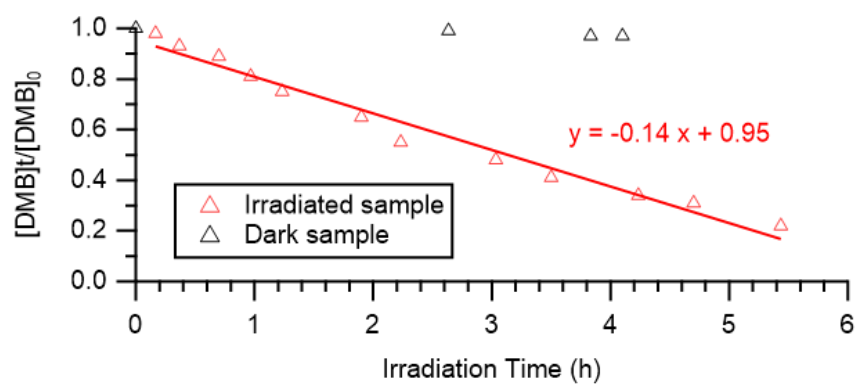


Figure S6. Loss of 3,4-DMB in the reaction solution. The irradiation time for each sample was calculated as the mean of the sampling start time and end time.

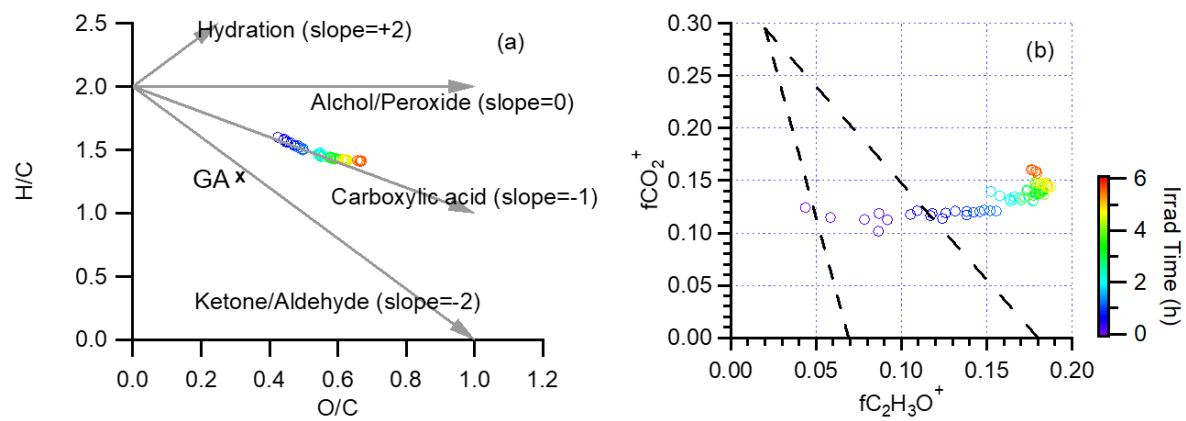


Figure S7. (a) Van Krevelen Diagram and (b) AMS measured mass fraction of C<sub>2</sub>H<sub>3</sub>O<sup>+</sup> and CO<sub>2</sub><sup>+</sup> of aqSOA products formed in the photoreaction experiment of GA with <sup>3</sup>C\*

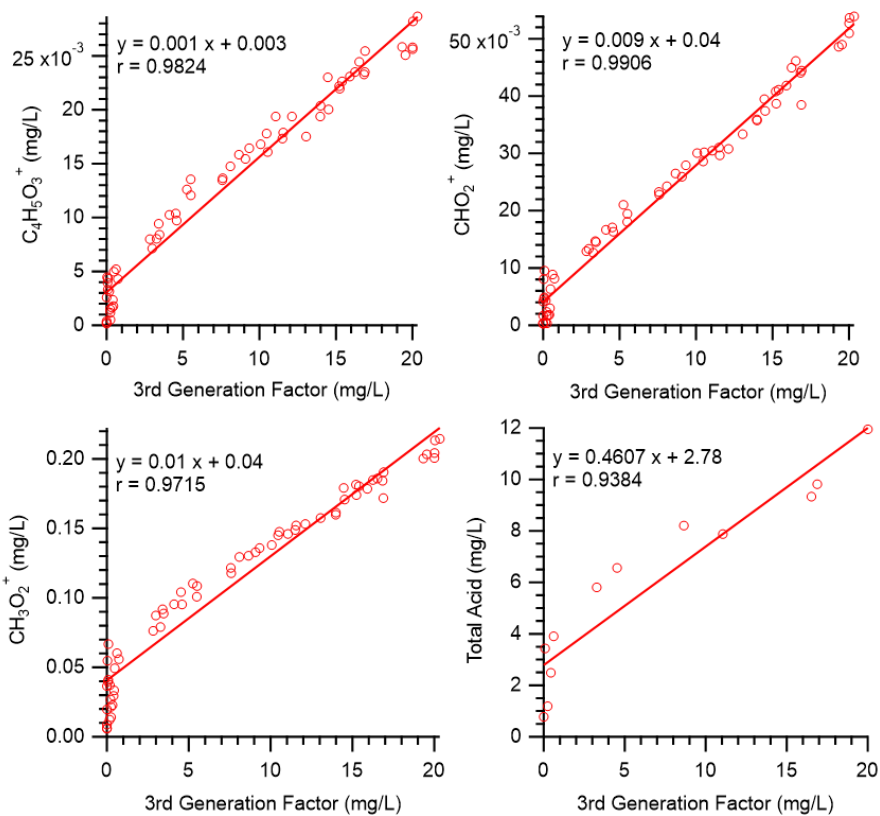


Figure S8. Correlation between the time series of selected ions and the 3rd generation products factor from PMF analysis.

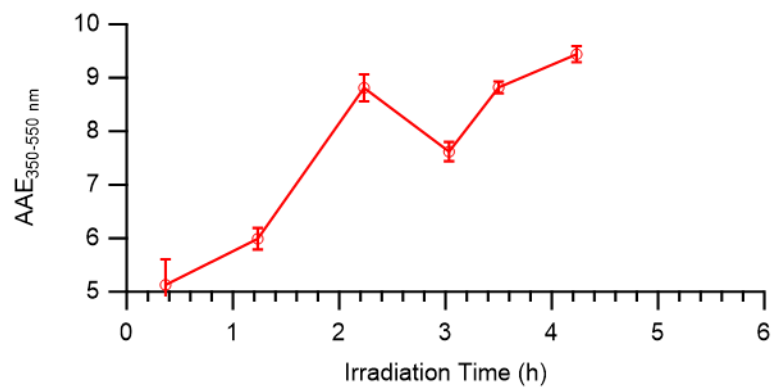
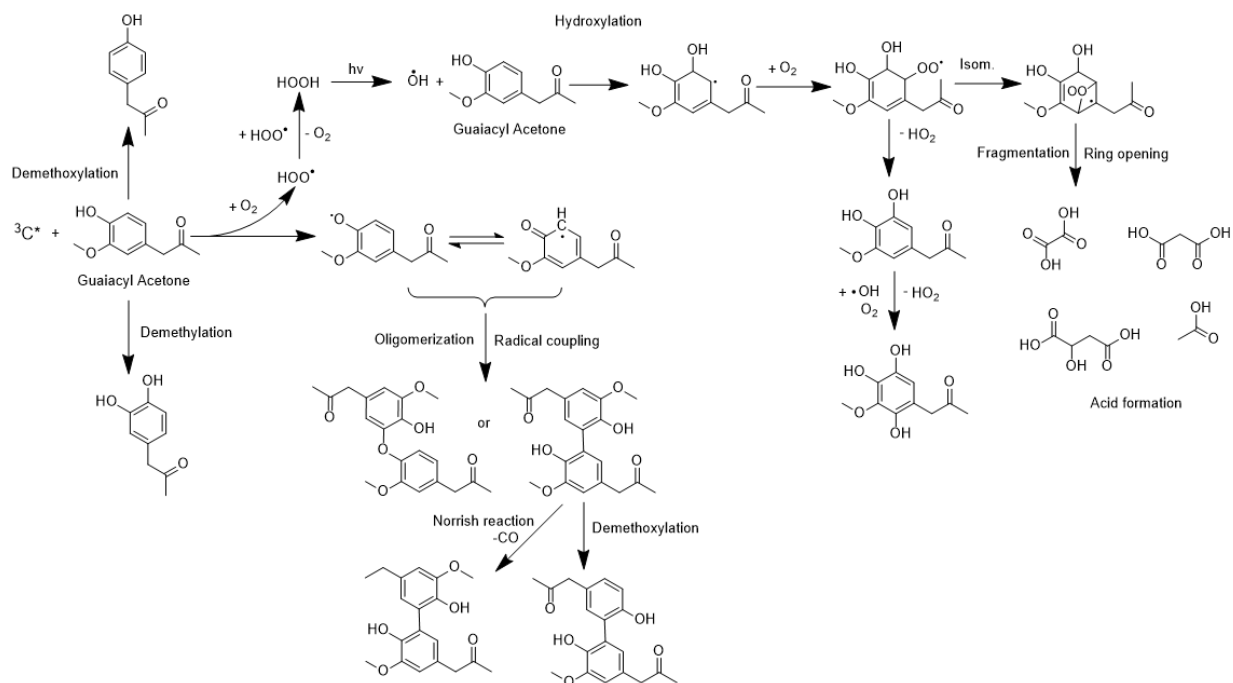


Figure S9. Time series of the Absorption Angstrom Exponents (AAE) for the illuminated reaction solution. Error bars represent  $\pm 1$  standard error (SE) calculated by propagating the uncertainties.





Scheme S1. Possible products produced during photooxidation of GA through oligomerization, hydroxylation, and demethoxylation.

# Chapter 3: Photochemical Aging of Phenolic Secondary Organic Aerosol in the Aqueous Phase: Evolution of Chemical and Optical Properties and Effects of Oxidants

## 3.1 Abstract

Gas-phase reactions strongly influence the mass concentration, chemical composition, and optical properties of secondary organic aerosol (SOA), but relatively little is known about the aqueous-phase aging of SOA. In this study, we performed a series of long-duration photochemical aging experiments to investigate the evolution of the composition and light absorption properties of the aqueous SOA (aqSOA) of guaiacyl acetone (GA), a highly water-soluble phenolic carbonyl common in biomass burning plumes. The aqSOA was produced from reactions of GA with hydroxyl radical ( $\bullet\text{OH}$ ) or a triplet excited state of organic carbon ( $^3\text{C}^*$ ) and was aged for up to 21 days of equivalent northern California sunlight. Additionally, photo-aging under the conditions of elevated aqueous-phase  $\bullet\text{OH}$  or  $^3\text{C}^*$  concentration was studied. The composition and the light absorptivity of aqSOA were characterized using high resolution aerosol mass spectrometry (HR-AMS) and UV-vis spectroscopy.

AqSOA of GA formed from  $^3\text{C}^*$  reaction ( $^3\text{C}^*$ -aqSOA) is less oxidized, more oligomer-rich, and more light-absorbing than aqSOA formed from  $\bullet\text{OH}$  ( $\bullet\text{OH}$ -aqSOA). Prolonged photo-aging promotes fragmentation and the formation of more volatile and less light-absorbing products. Close to 50% of the initial aqSOA mass was lost and substantial photobleaching occurred after 14 and 72 hours of simulated sunlight illumination for  $^3\text{C}^*$ - and  $\bullet\text{OH}$ -aqSOA, respectively. Positive matrix factorization (PMF) analysis of the combined HR-AMS and UV-vis spectral data resolved

three generations of aqSOA with distinctly different chemical composition and optical properties. The second-generation aqSOA is moderately oxidized and enriched in functionalized GA species with enhanced light absorption in the near UV and visible wavelengths. While photochemical aging generally increases the oxidation degree of aqSOA, a slight decrease in the O/C of •OH-aqSOA was observed after 60 hours of illumination with additional •OH exposure, likely due to greater fragmentation and evaporation of highly oxidized compounds. Elevated oxidant concentrations accelerate the transformation of aqSOA and promote the decay of BrC chromophores, leading to faster mass reduction and photobleaching. In addition, compared with •OH, <sup>3</sup>C\* exposure during photo-aging produces more low-volatility functionalized products, which counterbalance part of the mass loss due to fragmentation and evaporation.

## 3.2 Introduction

Phenols, emitted from biomass burning (BB) through lignin pyrolysis (Hawthorne et al., 1989; Schauer et al., 2001; Simpson and Naeher, 2010) and formed from the oxidation of aromatic hydrocarbons (Berndt and Böge, 2006; Volkamer et al., 2002), are important precursors for atmospheric secondary organic aerosol (SOA) and brown carbon (BrC) (Bruns et al., 2016; Jiang et al., 2021; Misovich et al., 2021; Smith et al., 2016; Yee et al., 2013; Yu et al., 2014). Aqueous phase SOA (aqSOA) is rapidly and efficiently formed from photoreactions of phenols with oxidants such as hydroxyl radical (•OH), excited triplet states (<sup>3</sup>C\*) of organic carbon, and nitrate radical (NO<sub>3</sub>). Mass yields range from 80% to 140%, and proposed formation pathways include oligomerization, hydroxylation, functionalization, demethoxylation and fragmentation (Huang et al., 2018; Jiang et al., 2021; Misovich et al., 2021; Sun et al., 2010; Yu et al., 2014, 2016). Reactions involving reactive nitrogen species also lead to nitration and nitrophenol formation (Pang et al., 2019; Yang et al., 2021). The phenolic oligomers, multifunctional derivatives and

nitrophenols formed through aqueous-phase reactions can absorb near-UV and visible light and contribute significantly to BrC formation in biomass burning emissions (Gilardoni et al., 2016; Misovich et al., 2021; Palm et al., 2020; Pang et al., 2019). In addition, humic-like substances (HULIS), which can induce oxidative stress and cause adverse health effects (Li et al., 2022; McWhinney et al., 2013), are observed in phenolic aqSOA (Chang and Thompson, 2010b).

While the formation of phenolic aqSOA has been investigated extensively, the aging and loss processes of phenolic aqSOA are poorly characterized. Atmospheric lifetimes of SOA range from hours to weeks (Tsigaridis et al., 2014; Wagstrom and Pandis, 2009), during which chemical aging can occur and lead to continuous evolution of SOA. Fragmentation, for example, is an important reaction pathway during SOA aging, and it is usually followed by evaporation of volatile products, causing SOA mass loss (Kroll et al., 2015). Lab studies have shown that photolysis of  $\alpha$ -pinene SOA results in a rapid transformation of highly functionalized species to small volatile compounds and a decrease of SOA mass (Henry and Donahue, 2012). In addition, Yu et al. (2016) demonstrated that phenolic aqSOA gets more oxidized during photochemical aging, with fragmentation becoming more important than oligomerization and functionalization, although a fraction of the low-volatility SOA appears to be recalcitrant to fragmentation (Yu et al., 2016). Similarly, O'Brien and Kroll (2019) observed 70–90% of the  $\alpha$ -pinene SOA mass remaining in particles after an initial SOA decay during photochemical aging. Field observations have also demonstrated the effects of aging on SOA loading and properties in the atmosphere. For example, substantial losses of SOA mass and increases of SOA oxidation occur in aged wildfire plumes (Farley et al., 2022; Sedlacek et al., 2022; Zhou et al., 2017). In addition, in remote areas, where aerosols are usually highly aged, organic aerosols are significantly more oxidized, less volatile,

and more hygroscopic (Jimenez et al., 2009; Morgan et al., 2010; Ng et al., 2011; Zhang et al., 2011; Zhou et al., 2019).

Chemical aging can also influence the optical properties of SOA, as some reactions increase the light absorptivity while others cause photobleaching by destroying chromophores (Hems et al., 2021).  $\text{NH}_4^+$ -mediated aging of terpene SOA produces imidazoles and pyridines, which are strong absorbers and fluorophores (Bones et al., 2010), while oxidative aging of methylglyoxal aqSOA increases light absorption due to the formation of carbonyl compounds (Sareen et al., 2013). Hems and Abbatt (2018) observed an increase of absorption during the early  $\bullet\text{OH}$  aging of nitrophenols, but photodegradation of BrC eventually took over, decreasing light absorptivity (Hems and Abbatt, 2018). Similarly,  $\bullet\text{OH}$  and  $\text{NO}_3$  aging of catechol SOA results in continuous loss of nitrocatechol as well as a decrease in visible light absorption (Fredrickson et al., 2022).

Light intensity and oxidant concentration are crucial factors influencing the chemical aging of SOA. Sunlight-triggered reactions in particles, such as direct photolysis of organics, nitrate, nitrite and hydrogen peroxide, as well as energy and charge-transfer reactions driven by  $^3\text{C}^*$ , play an important role in SOA aging and can alter the composition and properties of particles (Corral Arroyo et al., 2018; George et al., 2015a; Herrmann et al., 2015). Oxidant exposure of SOA varies widely due to differences in oxidant concentration and residence time in the atmosphere. For example, the steady state concentration of  $\bullet\text{OH}$  ranges from  $10^{-16}$  to  $10^{-12}$  M (Herrmann et al., 2010) and  $^3\text{C}^*$  concentrations range from  $10^{-14}$  to  $10^{-11}$  M (Kaur et al., 2019) in atmospheric waters. Increased oxidant exposure can promote formation of highly oxygenated SOA (Daumit et al., 2016; Kang et al., 2011; Lambe et al., 2015; Ng et al., 2010a), but can also decrease SOA mass and facilitate the transition from functionalization to fragmentation (Lambe et al., 2012).

This study focuses on the long timescale aqueous aging of phenolic aqSOA formed from the photooxidation of guaiacyl acetone (GA), a phenolic model compound from BB emissions. In our previous work (Jiang et al. 2021), we explored aqSOA formation from  $^3\text{C}^*$  reactions with GA. Here, we investigate aqSOA formation from reactions of GA with  $\bullet\text{OH}$  and  $^3\text{C}^*$ , with a focus on exploring how prolonged aqueous aging (up to 15 half-lives of GA) impacts the chemical composition and optical properties of the aqSOA. Moreover, we also studied the effects of light and additional oxidant exposure during aqSOA aging.

### 3.3 Experimental

#### 3.3.1 Formation and Aging of Phenolic AqSOA

The initial reaction solution was prepared with 100  $\mu\text{M}$  of guaiacyl acetone (GA) and either 100  $\mu\text{M}$  of  $\text{H}_2\text{O}_2$  (hydrogen peroxide; as a source of  $\bullet\text{OH}$ ) or 5  $\mu\text{M}$  of 3,4-DMB (3,4-dimethoxybenzaldehyde; as a source of  $^3\text{C}^*$ ) in Milli-Q water. The pH of the solution was adjusted to 4.6 using sulfuric acid. These conditions were set to mimic wood burning-influenced cloud and fog waters (Anastasio et al., 1997; Arakaki et al., 2013; Collett et al., 1998; Kaur et al., 2019; Kaur and Anastasio, 2018; Nolte et al., 2001; Raja et al., 2008; Schauer et al., 2001). The reaction solution was placed in a 400 mL Pyrex tube, continuously stirred and illuminated inside a RPR-200 photoreactor system equipped with three different types of bulbs to roughly mimic sunlight (George et al., 2015b). For a given solution, steady-state concentrations of oxidants ( $\bullet\text{OH}$  and  $^3\text{C}^*$ ) in the photoreactor are approximately 7 times higher than during exposure to midday winter solstice sunlight in Davis (George et al., 2015b; Yu et al., 2016). When ~95% of the initial GA has reacted (after 24 h for  $\bullet\text{OH}$ -initiated reactions and 3.5 h for  $^3\text{C}^*$ -initiated reactions), the reaction solution was separated into four aliquots and moved into separate 110 mL Pyrex tubes for further

aging. This occurred under four different conditions: 1) aging in the dark aging (tube wrapped with aluminum foil); 2) continued illumination without addition of extra oxidant; 3) photo-aging with addition of 100  $\mu\text{M}$  of  $\text{H}_2\text{O}_2$ ; and 4) photo-aging with addition of 5  $\mu\text{M}$  of 3,4-DMB. Small aliquots of the solutions were then periodically taken from each tube to measure chemical composition and optical properties.

### 3.3.2 Chemical and Optical Analyses

Concentrations of GA and 3,4-DMB were measured by HPLC-PDA (Agilent Technologies Inc.). Light absorbance was measured using a UV-Vis spectrophotometer (UV-2501PC, Shimadzu). The mass concentration and chemical composition of the aqSOA products were characterized using HR-AMS (Aerodyne Res. Inc) after atomizing the liquid samples in argon (Ar, industrial grade, 99.997 %) followed by diffusion drying (Jiang et al., 2021).

AMS data were processed using standard toolkits (SQUIRREL v1.56D and PIKA 1.15D). Since Ar was used as the carrier gas, we were able to quantify the  $\text{CO}^+$  signal of aqSOA directly (Yu et al., 2016). The organic  $\text{H}_2\text{O}^+$  signal ( $\text{org-H}_2\text{O}^+$ ) can also be directly determined considering the low RH after the drier; however, to reduce noise,  $\text{org-H}_2\text{O}^+$  was parameterized as  $\text{org-H}_2\text{O}^+=0.4\times\text{CO}_2^+$  according to the correlation between the determined organic  $\text{H}_2\text{O}^+$  signal (= measured  $\text{H}_2\text{O}^+$  signal – sulfate-associated  $\text{H}_2\text{O}^+$  signal) and the measured organic  $\text{CO}_2^+$  signal (Jiang et al., 2021). The other  $\text{org-H}_2\text{O}^+$  related signals were parameterized as  $\text{org-OH}^+=0.25\times\text{org-H}_2\text{O}^+$  and  $\text{org-O}^+=0.04\times\text{org-H}_2\text{O}^+$  (Aiken et al., 2008). Atomic ratios of oxygen-to-carbon (O/C) and hydrogen-to-carbon (H/C), and organic mass-to-carbon ratio (OM/OC) ratios, were subsequently determined (Aiken et al., 2008), and the average oxidation state of carbon ( $\text{OS}_\text{C}$ ) of aqSOA was calculated as  $\text{OS}_\text{C}=2\times\text{O/C-H/C}$  (Kroll et al., 2011). The aqSOA mass concentration ( $[\text{Org}]_{\text{solution}}, \mu\text{g mL}^{-1}$ ) in the solution was calculated using sulfate as the internal standard:

$$[\text{Org}]_{\text{solution}} = [\text{Org}]_{\text{AMS}} \times \frac{[\text{Sulfate}]_{\text{solution}}}{[\text{Sulfate}]_{\text{AMS}}} \quad (\text{Eq. 1})$$

where  $[\text{Org}]_{\text{AMS}}$  and  $[\text{Sulfate}]_{\text{AMS}}$  are the AMS-measured concentrations ( $\mu\text{g m}^{-3}$ ) of aqSOA and sulfate in the aerosolized solution, and  $[\text{Sulfate}]_{\text{solution}}$  is the spiked concentration ( $\mu\text{g mL}^{-1}$ ) of sulfate in the solution. The aqSOA mass yield ( $Y_{\text{SOA}}$ ) after a given time of illumination ( $t$ ) was calculated as:

$$Y_{\text{SOA}} = \frac{[\text{Org}]_t}{[\text{GA}]_0 - [\text{GA}]_t} \quad (\text{Eq. 2})$$

where  $[\text{GA}]_0$  is the initial GA concentration ( $\mu\text{g mL}^{-1}$ ) in the solution, and  $[\text{Org}]_t$  and  $[\text{GA}]_t$  denote the concentrations of GA and aqSOA, respectively, in the solution after a period of irradiation.

Positive matrix factorization (PMF) was performed on the combined matrix of the high-resolution mass spectra ( $m/z$  12–360) and the UV-vis spectra (280–600 nm) of the  $\bullet\text{OH}$ -aqSOA and  $^3\text{C}^*$ -aqSOA separately. The PMF results were evaluated using the PMF Evaluation Toolkit (PET v3.08 downloaded from: [http://cires1.colorado.edu/jimenez-group/wiki/index.php/PMF-AMS\\_Analysis\\_Guide](http://cires1.colorado.edu/jimenez-group/wiki/index.php/PMF-AMS_Analysis_Guide)). A three-factor solution with  $f_{\text{Peak}} = 0$  was chosen based on the evaluation criteria (Ulbrich et al., 2009; Zhang et al., 2011) for both  $\bullet\text{OH}$ - and  $^3\text{C}^*$ -aqSOA. Figures S1 and S2 present the summary of diagnostic plots for the 3-factor PMF solution for  $^3\text{C}^*$ - and  $\bullet\text{OH}$ -aqSOA, respectively.

The light absorption coefficient ( $\alpha_\lambda, \text{cm}^{-1}$ ) of the aqSOA was calculated as:

$$\alpha_\lambda = \frac{A_{\text{total},\lambda} - A_{\text{GA},\lambda} - A_{\text{DMB},\lambda}}{l} \quad (\text{Eq. 3})$$



where  $A_{\text{total},\lambda}$  is the total measured base-10 light absorbance of the solution at wavelength  $\lambda$ ,  $A_{\text{GA},\lambda}$  and  $A_{\text{DMB},\lambda}$  denote the absorbance contributed by GA and 3,4-DMB, and  $l$  is the pathlength of the cuvette (1 cm). The mass absorption coefficient ( $\text{MAC}_\lambda$ ,  $\text{m}^2 \text{g}^{-1}$ ) of the aqSOA was calculated as:

$$\text{MAC}_\lambda = \frac{2.303 \times \alpha_\lambda}{[\text{Org}]_{\text{solution}}} \times 100 \quad (\text{Eq. 4})$$

where  $[\text{Org}]_{\text{solution}}$  is the aqSOA mass concentration ( $\mu\text{g mL}^{-1}$ ) in the solution, 2.303 is a conversion factor between  $\log_{10}$  and natural log, and 100 is for unit conversion. The absorption Ångström exponent (AAE) of the aqSOA was calculated as:

$$\text{AAE}_{\lambda_1-\lambda_2} = - \frac{\ln \frac{\alpha_{\lambda_1}}{\alpha_{\lambda_2}}}{\ln \frac{\lambda_1}{\lambda_2}} \quad (\text{Eq. 5})$$

where  $\alpha_{\lambda_1}$  and  $\alpha_{\lambda_2}$  denote the light absorption coefficients at wavelengths  $\lambda_1$  and  $\lambda_2$ . The rate of sunlight absorption of the PM extracts ( $R_{\text{abs}}$ ,  $\text{mol photons L}^{-1} \text{s}^{-1}$ ) was calculated as:

$$R_{\text{abs}} = 2.303 \times \frac{10^3}{N_A} \times \sum_{290 \text{ nm}}^{500 \text{ nm}} (\alpha_\lambda \times I_\lambda \times \Delta\lambda) \quad (\text{Eq. 6})$$

where  $I_\lambda$  is the midday, winter-solstice actinic flux in Davis ( $\text{photons cm}^{-2} \text{s}^{-1} \text{nm}^{-1}$ ) from the Tropospheric Ultraviolet and Visible (TUV) Radiation Model version 5.3 ([https://www.acom.ucar.edu/Models/TUV/Interactive\\_TUV/](https://www.acom.ucar.edu/Models/TUV/Interactive_TUV/)),  $\Delta\lambda$  is the interval between adjacent wavelengths in the TUV output, 2.303 is for base conversion between  $\log_{10}$  and natural log,  $10^3$  is for unit conversion, and  $N_A$  is Avogadro's number.

### 3.4 Results and Discussion

#### 3.4.1 AqSOA Formation in •OH- and <sup>3</sup>C\*-Initiated Photoreactions of Guaiacyl Acetone

As shown in Figures 1a and 1h, in both  $\bullet\text{OH}$ - and  $^3\text{C}^*$ -initiated photoreactions, GA loss followed first-order kinetics, with fitted rate constants of 0.14 and 0.73  $\text{h}^{-1}$ , respectively. For our oxidant concentrations and illumination conditions, the reaction rate of GA with  $^3\text{C}^*$  is 5.2 times faster than that with  $\bullet\text{OH}$ , consistent with previously reported kinetics for other phenols (Smith et al., 2014; Yu et al., 2016). The second-order rate constant for GA reacting with  $\bullet\text{OH}$  and  $^3\text{C}^*$  are  $1.5 \times 10^{10}$  and  $1.8 \times 10^9 \text{ M}^{-1} \text{ s}^{-1}$ , respectively (Arciva et al., 2022; Ma et al., 2021). The faster GA decay rate in the  $^3\text{C}^*$  reaction in this study reflects higher oxidant concentration in the  $^3\text{C}^*$  reaction ( $[\bullet\text{OH}]_{\text{ss}} \approx 2.6 \times 10^{-15} \text{ M}$  in the OH reaction vs.  $[^3\text{C}^*]_{\text{ss}} \approx 1.1 \times 10^{-13} \text{ M}$  in the  $^3\text{C}^*$  reaction). The aqSOA mass increased while GA is transformed (Figures 1c and 1j). Initially, the aqSOA formation rate relative to the GA decay rate is similar for both  $\bullet\text{OH}$ - and  $^3\text{C}^*$ -photoreactions, with a mass yield of  $\sim 80\%$  at one GA half-life ( $t_{1/2}$ , which is 4.8 h for  $\bullet\text{OH}$  reaction and 0.95 h for  $^3\text{C}^*$  reaction). However, in  $\bullet\text{OH}$ -mediated reactions, aqSOA formation slowed down after  $t_{1/2}$ , resulting in a decreased SOA yield of  $\sim 50\%$  at  $2 t_{1/2}$  (i.e., when  $3/4$  of the initial GA had reacted), while in  $^3\text{C}^*$ -mediated reaction, aqSOA yield stabilized around 80% even when GA had reacted completely (Figures 1d and 1k). This result suggests that  $^3\text{C}^*$  oxidation of GA produces higher amounts of low-volatility products, while  $\bullet\text{OH}$  reactions have a greater tendency to form volatile and semi-volatile compounds that evaporate from the condensed phase.

The chemical composition of GA aqSOA evolved continuously over the course of photoreactions. The atomic oxygen-to-carbon (O/C) ratio, organic-mass-to-organic-carbon (OM/OC) ratio, and oxidation state of carbon ( $\text{OS}_\text{C}$ ) of the aqSOA increased, while the hydrogen-to-carbon (H/C) ratio slightly decreased until GA reacted out in both  $\bullet\text{OH}$ - and  $^3\text{C}^*$ -initiated reactions (Figures 1e-g and 1-n). Figures 2a-b show the AMS spectra of  $\bullet\text{OH}$ - and  $^3\text{C}^*$ -aqSOA when  $\sim 95\%$  of the initial GA reacted (at 24 h for  $\bullet\text{OH}$  reaction and 3.5 h for  $^3\text{C}^*$  reaction). The

•OH-aqSOA ( $O/C = 0.64$  and  $OS_C = -0.10$ ) was more oxidized and oxygenated than  $^3C^*$ -aqSOA ( $O/C = 0.56$  and  $OS_C = -0.29$ ). In addition, compared with •OH-aqSOA, the AMS spectrum of  $^3C^*$ -aqSOA showed significantly more enhanced high  $m/z$  signals including the AMS tracer ions of GA oligomers,  $C_{18}H_{19}O_5^+$  and  $C_{20}H_{22}O_6^+$  ( $m/z = 315$  and  $m/z = 358$ ; Figure 2) (Jiang et al., 2021), suggesting higher production of oligomers in  $^3C^*$ -initiated photoreactions. This observation agrees with our previous study on the oxidation of phenol, guaiacol, and syringol, where more oligomerization occurred in photoreactions initiated by  $^3C^*$ , while •OH-initiated reactions promoted the formation of organic acids and other ring-opening species (Sun et al., 2010; Yu et al., 2014). The compositional differences between •OH-aqSOA and  $^3C^*$ -aqSOA may partly be explained by the differences in oxidant concentration and GA decay rate. Although the second-order rate constant for GA reacting with •OH is  $\sim 8$  times higher than that with  $^3C^*$ , the initial steady state concentration of  $^3C^*$  is  $\sim 40$  times higher than •OH and it results in a much faster GA decay in the  $^3C^*$  reactions. Higher concentration of  $^3C^*$  may facilitate oligomerization. On the other hand, the slower GA decay in •OH reaction may suggest longer irradiation time for a given amount of GA compared with that in  $^3C^*$  reaction, which allows further oxidation and fragmentation to occur and results in the production of smaller molecules.

Figures 3d-f and j-l (and Figures S3 and S4) show the mass absorption coefficient spectra of •OH- and  $^3C^*$ -aqSOA. The initially formed aqSOA is more light-absorbing than the parent GA, likely due to the formation of GA oligomers and functionalized products which contain conjugated structures. Phenolic dimers and higher oligomers formed through coupling of phenoxyl radicals, and monomeric phenol derivatives formed through •OH and carbonyl addition to the aromatic ring, are effective light absorbers (Misovich et al., 2021; Yu et al., 2014). In addition,  $^3C^*$ -aqSOA is more light-absorbing than •OH-aqSOA, consistent with the observation that  $^3C^*$ -aqSOA contains

more oligomers and other high molecular-weight species while •OH-aqSOA is more enriched in small, highly oxidized compounds.

### 3.4.2 Evolution of SOA Yield and AqSOA Composition during Prolonged Aging

After ~95% of the initial GA reacted, the aqSOA was further aged under different conditions: 1) dark aging; 2) continued illumination without additional oxidant; and 3) illumination with added oxidant (•OH or <sup>3</sup>C\*). As shown in Figure 1, the mass concentration and elemental ratios of aqSOA display negligible change in the dark, suggesting dark aging did not lead to significant chemical evolution of the aqSOA. On the contrary, exposure to light led to 47% and 39% loss in •OH- and <sup>3</sup>C\*-aqSOA mass, respectively, over the 48 h and 11.5 h prolonged aging period (Figures 1c and 1j), indicating the importance of fragmentation and evaporation of volatile compounds during photo-aging. Here, we focus on photo-aging without addition of extra oxidant, while the effects of elevated oxidant concentrations will be discussed in Section 3.4.4. As shown in Figures 1, 4 and 5, the chemical composition of <sup>3</sup>C\*-aqSOA evolved continuously during photo-aging, with the O/C ratio increasing from 0.59 to 0.77, consistent with previous findings that SOA becomes more oxygenated and oxidized during chemical aging (Kroll et al., 2015; Yu et al., 2016). On the other hand, the O/C and H/C ratios of •OH-aqSOA show negligible change (O/C=0.67±0.008 and H/C=1.36±0.008) during prolonged photo-aging, although the aqSOA mass decreased significantly. This is likely explained by evaporation of highly oxidized volatile compounds occurring simultaneously with the transformation of less oxidized species to more oxidized low-volatility products, in which the changes of the bulk elemental ratios can be counterbalanced.

To further elucidate the chemical evolution of GA aqSOA, we performed PMF analysis on the combined AMS and UV–vis absorption data. For both •OH-aqSOA and <sup>3</sup>C\*-aqSOA, three factors with distinct temporal profiles and corresponding mass and absorption spectra were resolved,

representing different generations of aqSOA products. Figure 6 displays the temporal and mass spectral profiles of  $^{13}\text{C}^*$ -aqSOA factors. The first-generation  $^{13}\text{C}^*$ -aqSOA, which is the least-oxidized ( $\text{O}/\text{C}=0.49$  and  $\text{H}/\text{C}=1.48$ ) shows enhanced signals of GA oligomer tracers such as  $\text{C}_{18}\text{H}_{19}\text{O}_5^+$  and  $\text{C}_{20}\text{H}_{22}\text{O}_6^+$  (Figure 6j-k and Figure S5). These products grow rapidly initially and peak in the first hour of irradiation, but subsequently decrease quickly and decay completely when GA has reacted away. The second-generation factor ( $\text{O}/\text{C}=0.59$  and  $\text{H}/\text{C}=1.42$ ), in which oligomer tracers are substantially reduced but tracers of functionalized GA monomers such as  $\text{C}_9\text{H}_7\text{O}_3^+$  and  $\text{C}_{15}\text{H}_{11}\text{O}_4^+$  are enriched (Figure 6j-k and Figure S5), builds up slowly during irradiation, peaks later than the 1st-generation factor, and then decays with a slower rate. Both the 1st- and 2nd-generation  $^{13}\text{C}^*$ -aqSOA factors disappear by the end of the photo-aging. The third-generation  $^{13}\text{C}^*$ -aqSOA factor is the most oxidized ( $\text{O}/\text{C}=0.86$  and  $\text{H}/\text{C}=1.36$ ), shows negligible high  $m/z$  signals in the mass spectra but is enriched of small, oxygenated ions such as  $\text{CHO}_2^+$ ,  $\text{CH}_2\text{O}_2^+$ ,  $\text{C}_2\text{H}_2\text{O}_2^+$ , and  $\text{C}_2\text{H}_4\text{O}_2^+$  (Figure 6j-k and Figure S5). This third factor starts to increase when the 1st-generation factor decays and shows a slight decrease by the end of the prolonged photo-aging. This agrees with our previous findings that oligomerization and functionalization dominate the initial formation of phenolic aqSOA whereas fragmentation and ring-opening reactions to make more oxidized compounds become more important later (Jiang et al., 2021; Yu et al., 2016). The mass spectral profiles of the 1st- and 2nd-generation  $^{13}\text{C}^*$ -aqSOA obtained in this study are similar to those reported in our previous work on aqSOA formation from  $\text{GA} + ^{13}\text{C}^*$  photoreactions (Jiang et al., 2021). However, the 3rd-generation factor in this study - which used longer aging times than our previous work - is significantly more oxidized than previously reported, suggesting that prolonged aging significantly increases the oxidation state of aqSOA, and that the highly oxidized species after long periods of aging are mainly fragmentation products. In addition, in contrast to

the previous study on GA aqSOA formation, in this work decay of the 3rd-generation aqSOA is observed, indicating that extensive aging forms volatile compounds that evaporate from the condensed phase and result in mass loss of aqSOA. It also implies that photochemical aging may serve as an efficient removal process for aqSOA in the atmosphere, in addition to wet and dry deposition (Hodzic et al., 2016).

As shown in Figures 6a-c and 7a--c, the  $^3\text{C}^*$ -aqSOA and  $\bullet\text{OH}$ -aqSOA factors generally display similar mass spectral features. However, in  $\bullet\text{OH}$ -aqSOA, the 2nd-generation factor (O/C=0.73 and H/C=1.36) is slightly more oxidized than the 3rd-generation (O/C=0.68 and H/C=1.41). Also, the contribution of the 2nd-generation factor to the total aqSOA mass is higher in  $\bullet\text{OH}$ -initiated reaction than in  $^3\text{C}^*$ -initiated reaction (52% vs. 34%; Figure 6e and Figure 7e). These results suggest that  $\bullet\text{OH}$  reactions form highly oxidized products that gradually decay at long aging times, while  $^3\text{C}^*$  reactions form more recalcitrant highly oxidized products that remain in the particle phase. This is likely due to although both  $\bullet\text{OH}$  and  $^3\text{C}^*$  can react rapidly with GA, the aqSOA products (especially the non-phenolic products) may react slowly with  $^3\text{C}^*$ , which results in the more recalcitrant characteristic of  $^3\text{C}^*$ -aqSOA. Note that the reactions of  $^3\text{C}^*$  with GA can produce  $\text{H}_2\text{O}_2$  which generates  $\bullet\text{OH}$ , leading to increased  $\bullet\text{OH}$  concentration in the  $^3\text{C}^*$  reactions, especially in the extended aging periods. However, the amount of  $\text{H}_2\text{O}_2$  produced may be much smaller than that present in the  $\bullet\text{OH}$  reactions and the influence may not be significant. Another possible explanation is that GA reacts much more slowly in the  $\bullet\text{OH}$  solution than in the  $^3\text{C}^*$  system, and thus the newly-formed  $\bullet\text{OH}$  aqSOA has a great chance to go rapid further oxidation, while the newly-formed  $^3\text{C}^*$  aqSOA need to compete with GA for light and oxidant exposure. This hypothesis can also be supported by the behaviors of a group of highly oxygenated small ions (e.g.,

CHO<sub>2</sub><sup>+</sup> and CH<sub>2</sub>O<sub>2</sub><sup>+</sup>) which show high correlation with the 2nd-generation in •OH aqSOA but correlate with the 3rd-generation in <sup>3</sup>C\* aqSOA (Figure 6j-k and Figure 7j-k).

### 3.4.3 Evolution of AqSOA Optical Properties during Prolonged Aging

Figures 3c-f, 3i-l, S3 and S4 show the change of mass absorption coefficient of •OH- and <sup>3</sup>C\*-aqSOA. Photobleaching occurs during prolonged aging, with the MAC<sub>365nm</sub> of •OH-aqSOA decreasing from 0.41 (the maximum) to 0.21 m<sup>2</sup> g<sup>-1</sup>, and the MAC<sub>365nm</sub> of <sup>3</sup>C\*-aqSOA decreasing from 0.64 (the maximum) to 0.19 m<sup>2</sup> g<sup>-1</sup>. The rates of sunlight absorption, with and without normalization by aqSOA mass, also decrease in prolonged aging (Figure 3a-b and 3g-h). Figure 8 displays the AAE of aqSOA as a function of log<sub>10</sub>(MAC<sub>405</sub>) and an optical-based classification of BrC (Saleh, 2020; Zhai et al., 2022). During prolonged photo-aging, GA aqSOA evolves from weak BrC to the very weak BrC class. The evolution of light absorption properties of GA aqSOA is also influenced by elevated oxidant concentrations, as discussed in Section 3.4.4.

Figure 9 shows the PMF-resolved mass absorption coefficient spectra of the three generations of GA aqSOA factors from the •OH- and <sup>3</sup>C\*-initiated reactions. In general, <sup>3</sup>C\*-aqSOA factors are more light absorbing than •OH-aqSOA factors, consistent with the higher fraction of oligomers and conjugated high molecular weight products in the triplet solutions. The 1st-generation aqSOA factors show a hump after 340 nm in the MAC spectra. This MAC enhancement in 340-400 nm has been observed previously in phenolic aqSOA (Smith et al., 2016), and it agrees with the high conjugation in oligomeric products. The 2nd-generation aqSOA factors are the most absorbing (MAC<sub>365nm</sub>=0.21 m<sup>2</sup> g<sup>-1</sup> for •OH aqSOA and 0.40 m<sup>2</sup> g<sup>-1</sup> for <sup>3</sup>C\* aqSOA). Compared with the 2nd-generation <sup>3</sup>C\*-aqSOA, relatively lower MAC was observed for the 2nd-generation •OH-aqSOA, likely due to its higher oxidation degree, which leads to the destruction of chromophores. The 3rd-generation aqSOA factors are the least absorbing (MAC<sub>365nm</sub>=0.04 m<sup>2</sup> g<sup>-1</sup> for •OH aqSOA and 0.01

$\text{m}^2 \text{g}^{-1}$  for  $^3\text{C}^*$  aqSOA), consistent with the dominance of fragmentation and ring-opening products in the factors.

### 3.4.4 Effects of Additional Oxidant Exposure on AqSOA Aging

To gain insights into how condensed-phase oxidants can influence the photo-aging of phenolic aqSOA, we added either  $100 \mu\text{M}$  of  $\text{H}_2\text{O}_2$  or  $5 \mu\text{M}$  3,4-DMB into the solution once the majority (~95 %) of GA had reacted. Since GA decay followed first-order kinetics, we assume the oxidant concentration did not change significantly during the initial aqSOA formation, and this assumption can also be partly supported by the relatively stable 3,4-DMB concentration in the first 3.5 hours in the  $^3\text{C}^*$ -initiated reaction (Figure 1i). In this context, adding extra  $\text{H}_2\text{O}_2$  or 3,4-DMB would provide higher  $\bullet\text{OH}$  or  $^3\text{C}^*$  concentration as well as higher total oxidant concentration during prolonged photo-aging.

Figure 1c shows that the decay of  $\bullet\text{OH}$ -aqSOA accelerated under conditions of elevated  $\bullet\text{OH}$  or  $^3\text{C}^*$  during photo-aging. As shown in Figure 7f and 7h, the decay of 1st- and 2nd-generation  $\bullet\text{OH}$ -aqSOA was increased when extra oxidants were introduced, and concurrently, the formation of the 3rd-generation factor was faster, suggesting a promoted transformation from 1st- and 2nd-generation  $\bullet\text{OH}$ -aqSOA to the 3rd-generation. In addition, in the later period, faster decay of 3rd-generation  $\bullet\text{OH}$ -aqSOA was observed in experiments with extra oxidant, suggesting that higher oxidant concentration also facilitates the breakdown of the 3rd-generation  $\bullet\text{OH}$ -aqSOA in later period. Figure 1e-g shows the evolution of elemental ratios of  $\bullet\text{OH}$ -aqSOA under conditions of elevated oxidant concentration. Increased  $\bullet\text{OH}$  or  $^3\text{C}^*$  initially increases the O/C and OM/OC of  $\bullet\text{OH}$ -aqSOA, but eventually leads to a decrease in both by the end of the photo-aging, likely due to formation and evaporation of volatile highly oxidized species. Furthermore, faster photobleaching of  $\bullet\text{OH}$  aqSOA was observed under conditions of increased oxidant concentration.



As shown in Figure 3c-f, the UVA and visible MAC values of the aqSOA decrease faster when extra oxidants were added, indicating faster degradation of BrC chromophores. It is worth mentioning that adding 100  $\mu\text{M}$  of  $\text{H}_2\text{O}_2$  (an  $\bullet\text{OH}$  source) during aging shows a greater impact on the decay of  $\bullet\text{OH}$  aqSOA mass and absorption than adding 5  $\mu\text{M}$  of 3,4-DMB ( $^3\text{C}^*$  source), although the GA reaction with  $^3\text{C}^*$  is much faster than with  $\bullet\text{OH}$  in this study. This suggests that addition of  $^3\text{C}^*$  during aging produces low-volatility, light-absorbing products that counterbalance part of the mass and absorption loss due to fragmentation and evaporation.

Elevated oxidant concentrations also affect the aging of  $^3\text{C}^*$  aqSOA. Different from  $\bullet\text{OH}$ -aqSOA,  $^3\text{C}^*$ -aqSOA only shows slightly accelerated mass and absorption decay when  $\bullet\text{OH}$  is added prior to prolonged aging (Figure 1j-k and Figure 3g-l). A possible explanation is that, compared with the preexisting  $^3\text{C}^*$  in the solution, the added  $\bullet\text{OH}$  only accounts for a small fraction of the total oxidant exposure (considering the much slower  $\bullet\text{OH}$  reaction compared with the  $^3\text{C}^*$  reaction), and thus exhibits little impact. Another possible reason may be that  $\bullet\text{OH}$  can react with 3,4-DMB in the solution to produce low-volatility products which balance out the increased decay of  $^3\text{C}^*$  aqSOA; this is consistent with the fast decay of 3,4-DMB after the addition of  $\bullet\text{OH}$  (Figure 1i). On the other hand, adding extra  $^3\text{C}^*$  (or 3,4-DMB) into the  $^3\text{C}^*$ -initiated reaction during aging inhibits the decay of  $^3\text{C}^*$ -aqSOA mass and light absorption, due to enhanced formation of 2nd-generation products (Figure 6h). This enhancement suggests that increased  $^3\text{C}^*$  concentration during aging promotes the formation of low-volatility functionalized products.

### 3.5 Conclusions

This study presents the evolution of composition and optical properties of phenolic aqSOA during prolonged photo-aging, including the effects of increased oxidant concentration. AqSOA

is produced rapidly from the photoreactions of GA with  $^3\text{C}^*$  and  $\bullet\text{OH}$ . The  $^3\text{C}^*$  reaction is significantly faster than the  $\bullet\text{OH}$  reaction, shows higher aqSOA mass yield and produces higher amounts of oligomers and high molecular-weight species at the time when the majority of GA has reacted, whereas the  $\bullet\text{OH}$  reaction produces more oxidized aqSOA enriched in small, highly oxygenated species. Consistent with the compositional difference, the initial  $^3\text{C}^*$ -aqSOA is more light-absorbing than the  $\bullet\text{OH}$ -aqSOA.

Fragmentation and formation of volatile products become increasingly more important during prolonged photo-aging, leading to 39% and 47% mass loss of  $\bullet\text{OH}$ -aqSOA and  $^3\text{C}^*$ -aqSOA, respectively. These results suggest that photochemical aging can be an efficient removal process for atmospheric aqSOA in addition to wet and dry deposition. The chemical composition of aqSOA evolves, with oligomerization and functionalization dominating the initial aqSOA formation and fragmentation becoming more important during prolonged aging.  $^3\text{C}^*$ -aqSOA becomes increasingly more oxidized during aging, while  $\bullet\text{OH}$ -aqSOA exhibits a slight decrease in oxidation degree by the end of photo-aging when additional oxidant exposure was introduced; this is likely due to the formation and evaporation of highly oxidized volatile products. This suggests that photo-aging does not necessarily increase the average oxidation degree of condensed-phase organics, since evaporation of highly oxidized products can decrease the oxidation degree of aqSOA. Prolonged photo-aging causes more pronounced photobleaching, and as a result, shifting the phenolic aqSOA from weakly absorbing BrC to very weak BrC. PMF analysis shows that the 2nd-generation aqSOA is enriched in functionalized phenolic compounds and is the most light-absorbing in the near UV and visible wavelengths. Elevated oxidant concentrations during photo-aging accelerate the relative importance of fragmentation reactions over oligomerization and

functionalization, which eventually promote the breakdown and evaporation of fragmentation products, leading to faster mass and absorption decay.

### **Acknowledgements**

This research was supported by grants from the U.S. Department of Energy (DOE) Atmospheric System Research Program (Grant #DESC0022140), the National Science Foundation (NSF) (Grant #AGS-2220307), and the California Agricultural Experiment Station (Projects CA-D-ETX-2102-H and CA-D-LAW-6403-RR). W.J. also acknowledges funding from the Matsumura Memorial Fellowship from the University of California at Davis.

# Figures

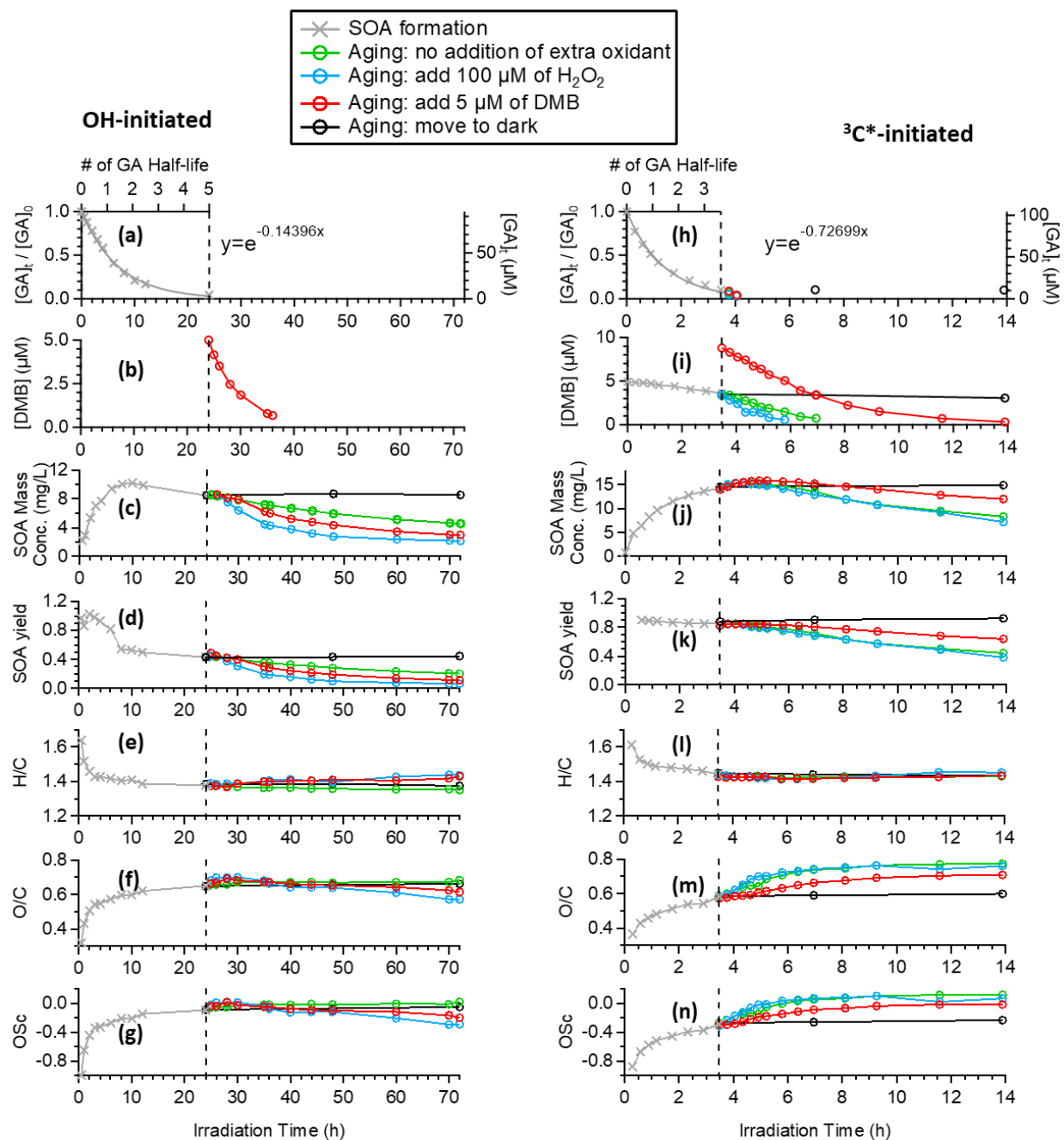


**Figure 1.** Overview of aqSOA formation and aging in  $\bullet\text{OH}$ - and  $^3\text{C}^*$ -initiated photoreactions of GA. Decay of (a & h) GA and (b & i) 3,4-DMB in the solution. Trends of aqSOA (c & j) mass concentration and (d & k) mass yield and (e & l) H/C, (f & m) O/C and (g & n)  $\text{OSC}$  determined by HR-ToF-AMS.

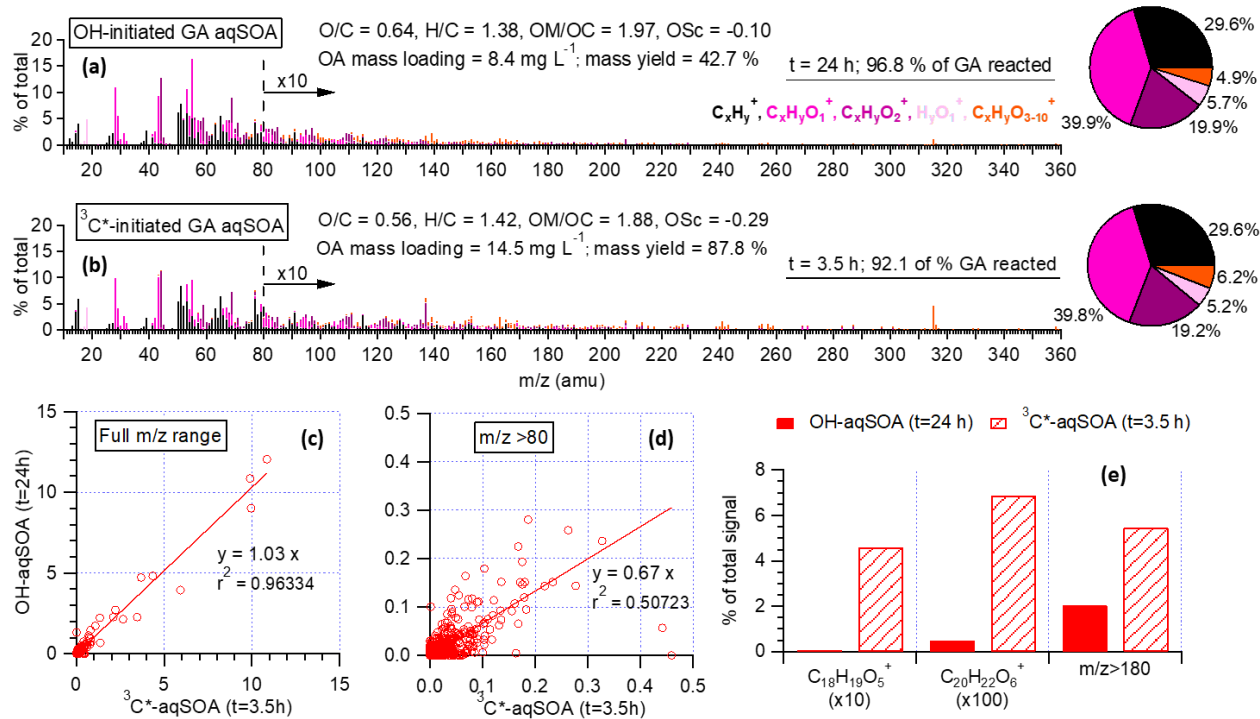


**Figure 2.** HRMS of (a) •OH-initiated aqSOA and (b) <sup>3</sup>C\*-initiated aqSOA determined by AMS after ~95% of the initial GA has reacted. Scatter plots that compare the mass spectra of OH-aqSOA with <sup>3</sup>C\*-aqSOA for (c) all ions and for (d) ions with m/z > 80. (e) Relative abundances of GA oligomer tracers and large ions (m/z > 180) in the AMS spectra of OH- and <sup>3</sup>C\*-aqSOA.

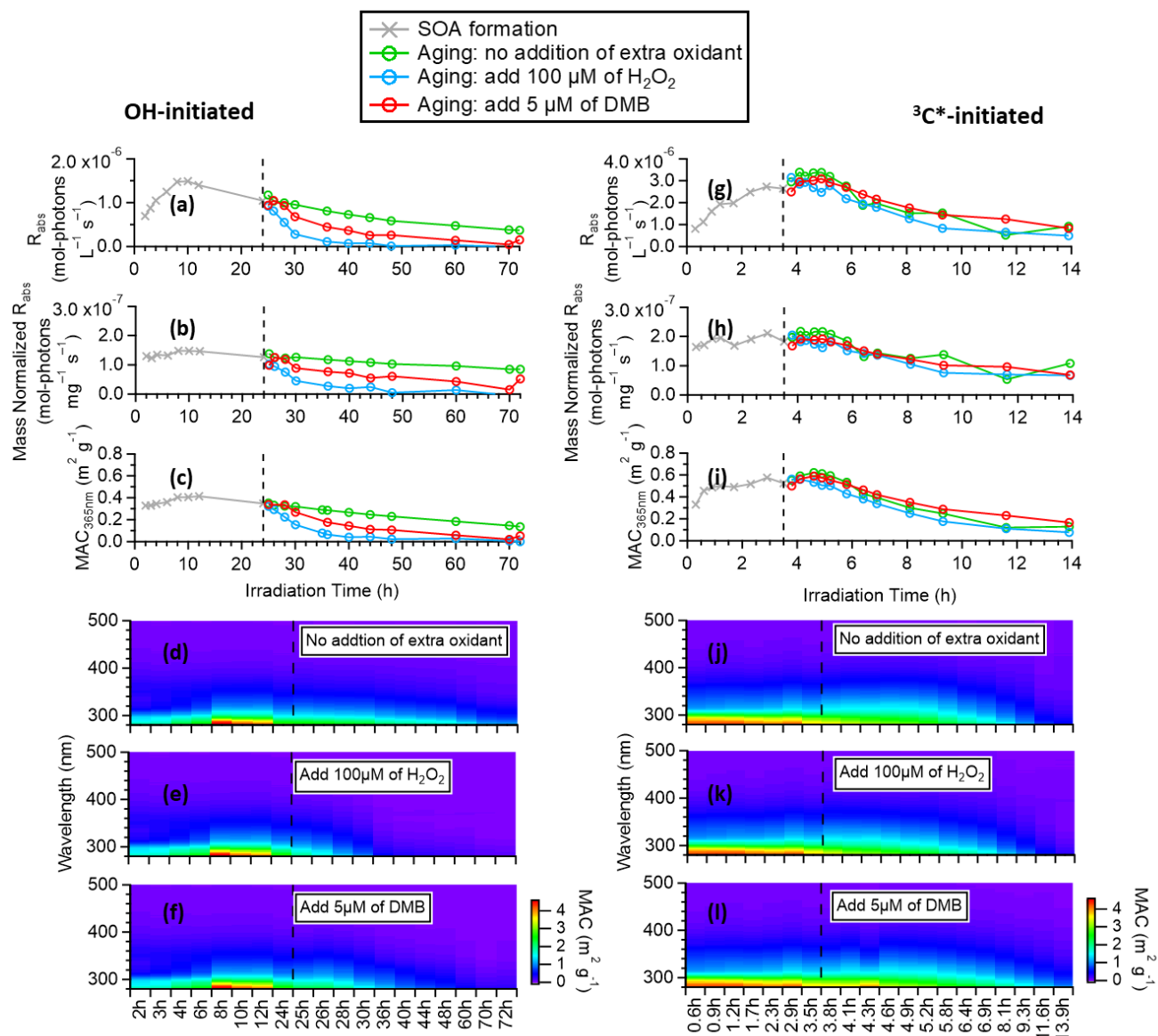


**Figure 3.** Evolution of optical properties of the  $\bullet\text{OH}$ - and  $^3\text{C}^*$ -initiated aqSOA: (a & g) rate of sunlight absorption; (b & h) SOA mass-normalized rate of sunlight absorption; (c & i) mass absorption coefficients at 365 nm; and (d-f & j-l) mass absorption coefficient spectra in the wavelength range of 280-500 nm.

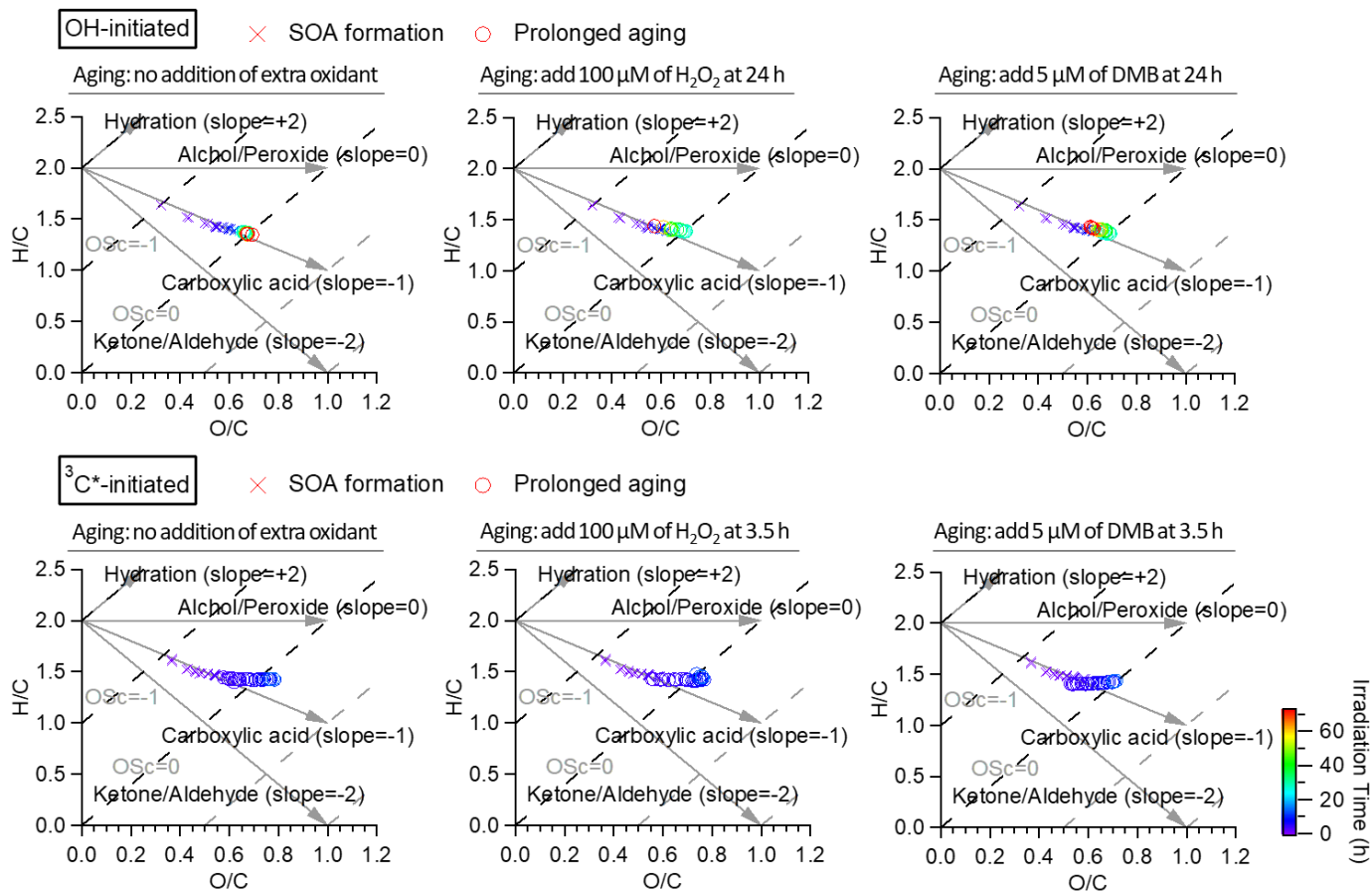


**Figure 4.** Evolution of  $\bullet\text{OH}$  and  $^3\text{C}^*$ -initiated aqSOA in Van Krevelen diagram under different aging conditions.

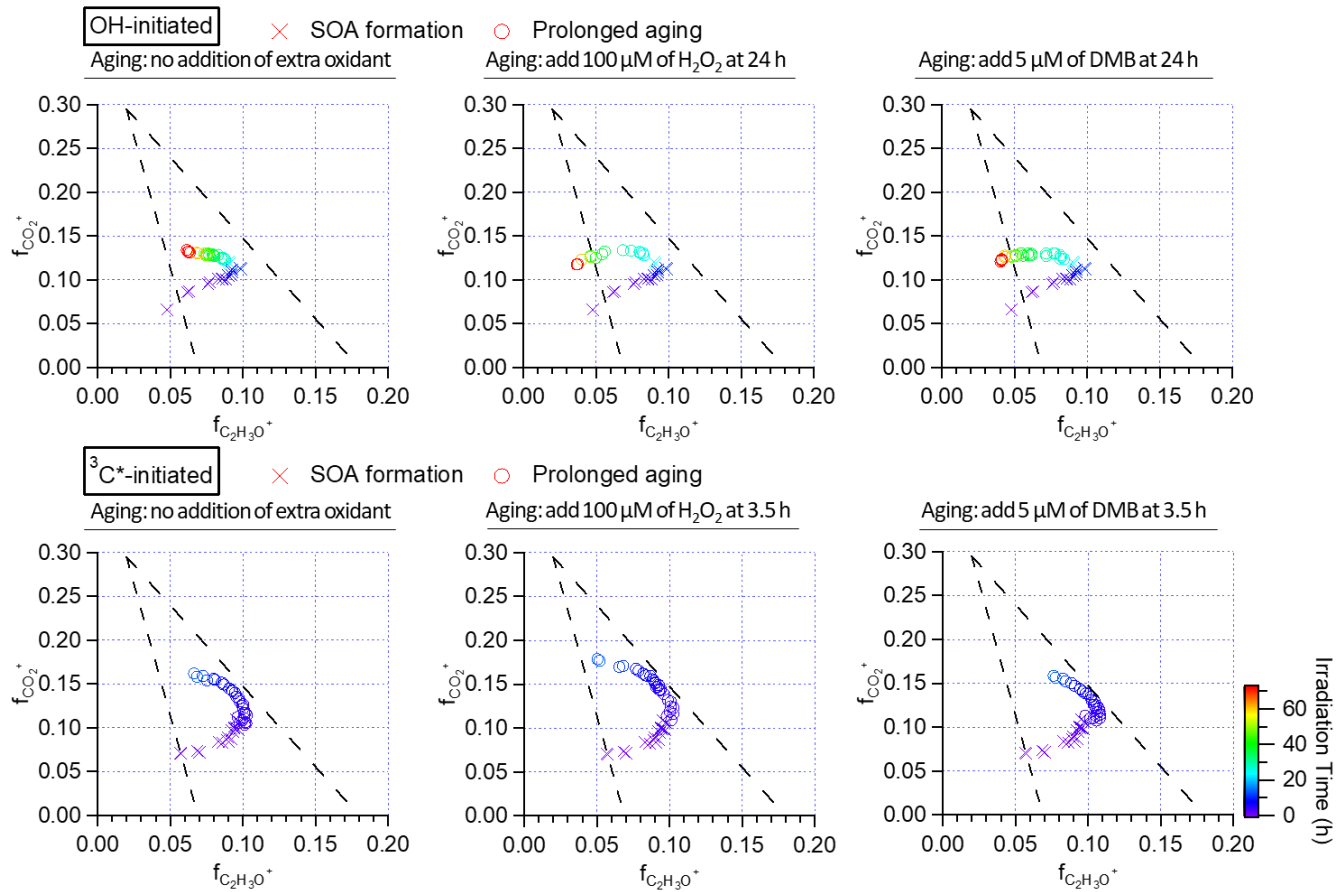


**Figure 5.** Evolution of OH and  $^3\text{C}^*$ -initiated aqSOA in triangle plot ( $f_{\text{CO}_2^+}$  vs  $f_{\text{C}_2\text{H}_3\text{O}^+}$ ) under different aging conditions.



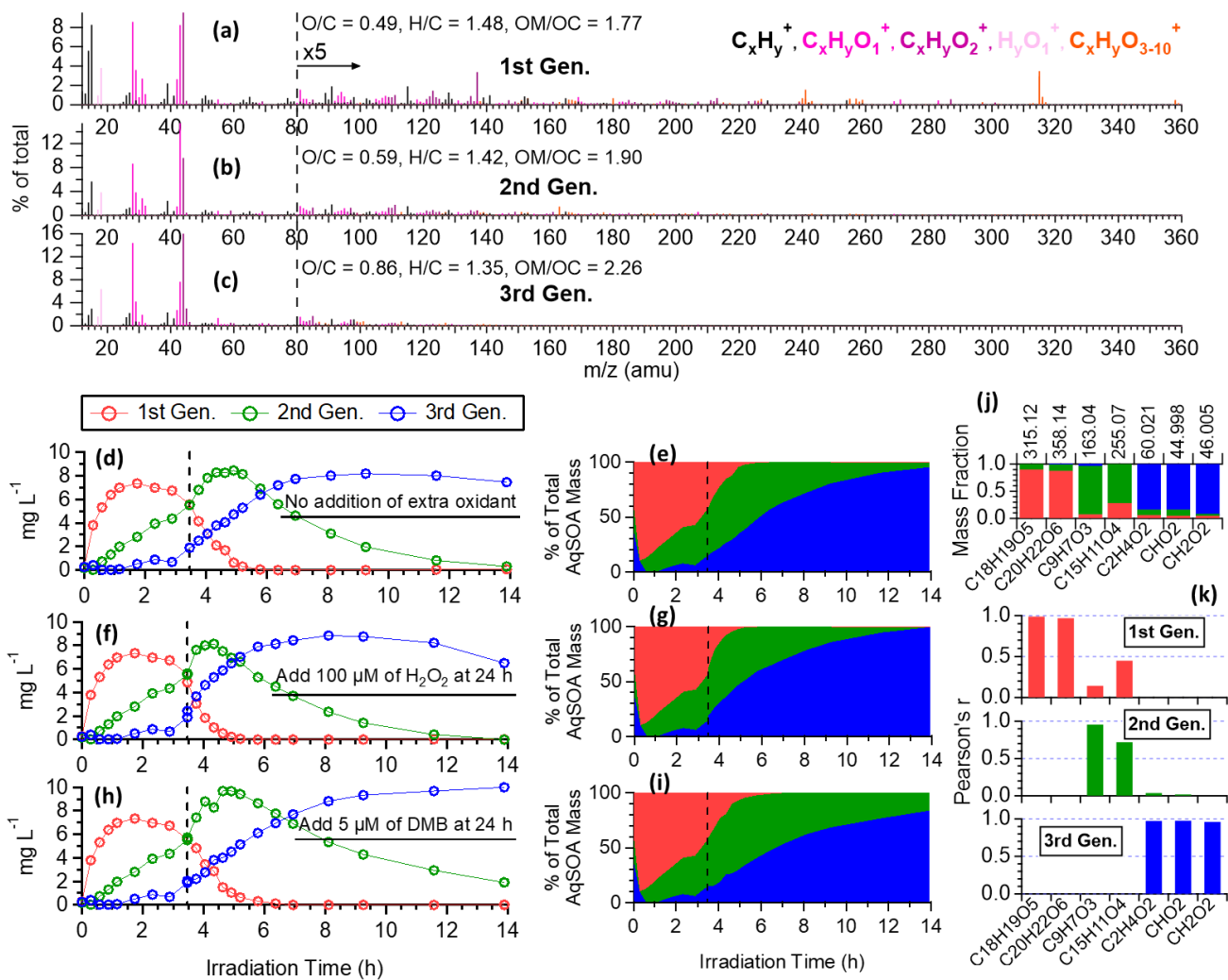


**Figure 6.** PMF-resolved three generations of aqSOA products in <sup>3</sup>C\*-initiated reactions: (a-c) MS profiles; (d-h) mass concentration time series; and (e-i) fractional contribution time series of the PMF factors. (j) Mass fraction of selected AMS tracer ions attributed to each PMF factor. (k) Correlation between PMF factors and selected AMS tracer ions.

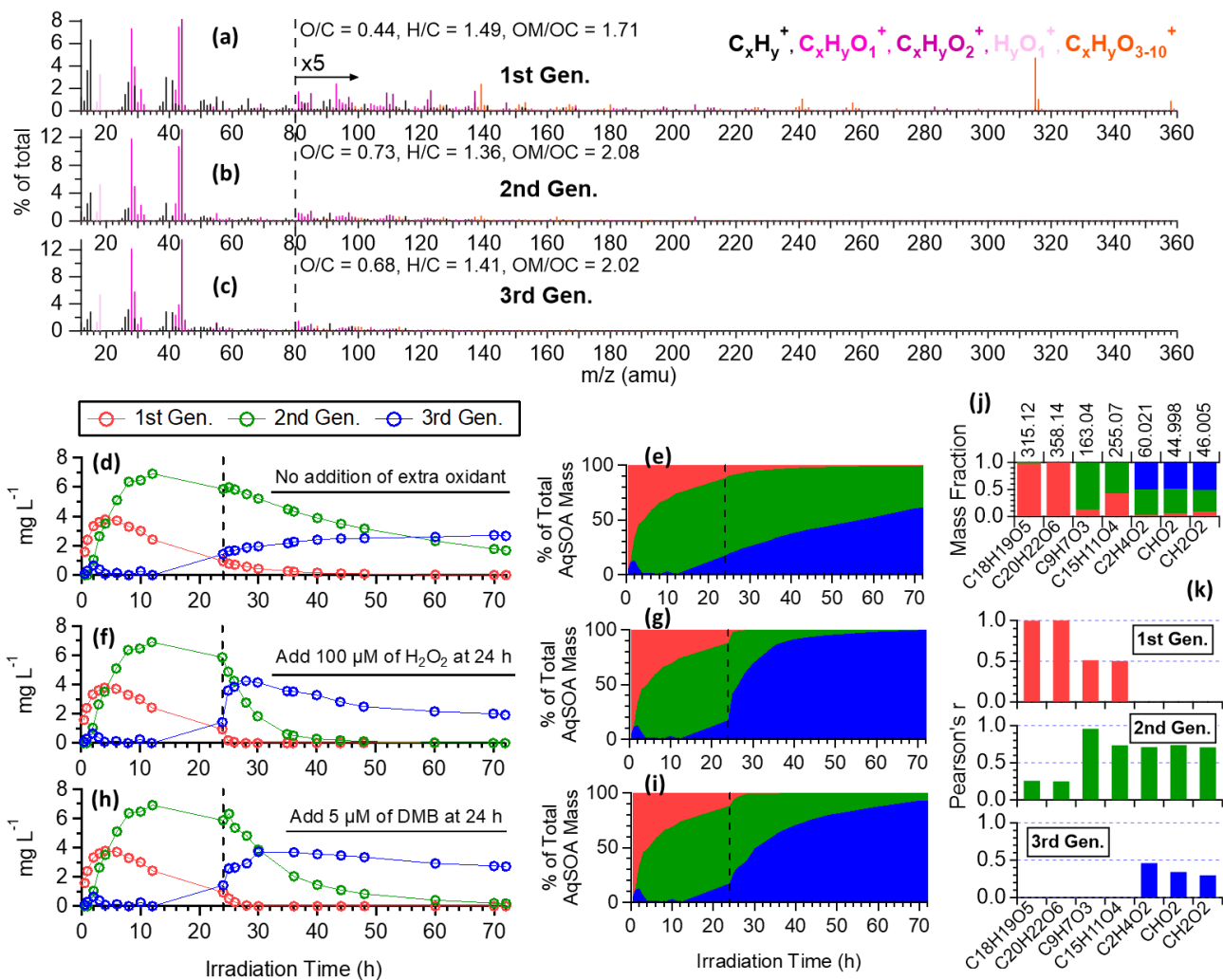


**Figure 7.** PMF resolved three generations of aqSOA products in OH-initiated reactions: (a-c) MS profiles; (d-h) mass concentration time series; and (e-i) fractional contribution time series of the PMF factors. (j) Mass fraction of selected AMS tracer ions attributed to each PMF factor. (k) Correlation between PMF factors and selected AMS tracer ions.

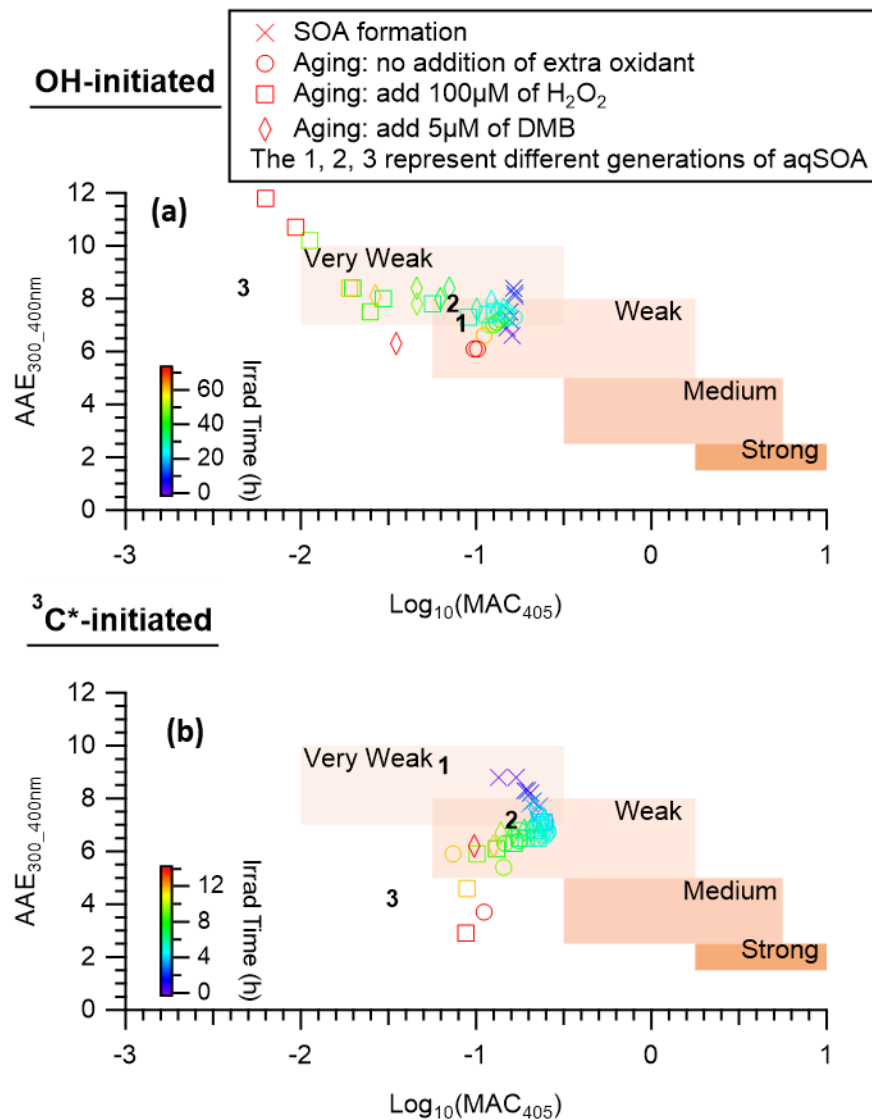


**Figure 8.** Plots of the light absorption properties of (a) OH-initiated aqSOA and (b) <sup>3</sup>C\*-initiated aqSOA in the AAE vs. log<sub>10</sub>(MAC<sub>405</sub>) space which displays the optical-based BrC classification scheme (Saleh, 2020). The shaded areas in the plot from top to bottom represent very weakly, weakly, moderately, and strongly absorbing BrC. The numbers 1, 2, and 3 represent the different generations of aqSOA obtained from PMF.



## Reference

- Aiken, A. C., DeCarlo, P. F., Kroll, J. H., Worsnop, D. R., Huffman, J. A., Docherty, K. S., Ulbrich, I. M., Mohr, C., Kimmel, J. R., Sueper, D., Sun, Y., Zhang, Q., Trimborn, A., Northway, M., Ziemann, P. J., Canagaratna, M. R., Onasch, T. B., Alfarra, M. R., Prevot, A. S. H., Dommen, J., Duplissy, J., Metzger, A., Baltensperger, U. and Jimenez, J. L.: O/C and OM/OC Ratios of Primary, Secondary, and Ambient Organic Aerosols with High-Resolution Time-of-Flight Aerosol Mass Spectrometry, *Environ. Sci. Technol.*, 42(12), 4478–4485, doi:10.1021/es703009q, 2008.
- Anastasio, C., Faust, B. C. and Rao, C. J.: Aromatic Carbonyl Compounds as Aqueous-Phase Photochemical Sources of Hydrogen Peroxide in Acidic Sulfate Aerosols, Fogs, and Clouds. 1. Non-Phenolic Methoxybenzaldehydes and Methoxyacetophenones with Reductants (Phenols), *Environ. Sci. Technol.*, 31(1), 218–232, doi:10.1021/es960359g, 1997.
- Arakaki, T., Anastasio, C., Kuroki, Y., Nakajima, H., Okada, K., Kotani, Y., Handa, D., Azechi, S., Kimura, T., Tshukako, A. and Miyagi, Y.: A General Scavenging Rate Constant for Reaction of Hydroxyl Radical with Organic Carbon in Atmospheric Waters, *Environ. Sci. Technol.*, 47(15), 8196–8203, doi:10.1021/es401927b, 2013.
- Berndt, T. and Böge, O.: Formation of phenol and carbonyls from the atmospheric reaction of OH radicals with benzene, *Phys. Chem. Chem. Phys.*, 8(10), 1205–1214, doi:10.1039/B514148F, 2006.
- Bones, D. L., Henricksen, D. K., Mang, S. A., Gonsior, M., Bateman, A. P., Nguyen, T. B., Cooper, W. J. and Nizkorodov, S. A.: Appearance of strong absorbers and fluorophores in limonene-O<sub>3</sub> secondary organic aerosol due to NH<sub>4</sub><sup>+</sup>-mediated chemical aging over long time scales, *J. Geophys. Res. Atmos.*, 115(D5), doi:https://doi.org/10.1029/2009JD012864, 2010.
- Bruns, E. A., El Haddad, I., Slowik, J. G., Kilic, D., Klein, F., Baltensperger, U. and Prévôt, A. S. H.: Identification of significant precursor gases of secondary organic aerosols from residential wood combustion, , 6, 27881, doi:10.1038/srep27881, 2016.
- Chang, J. L. and Thompson, J. E.: Characterization of colored products formed during irradiation of aqueous solutions containing H<sub>2</sub>O<sub>2</sub> and phenolic compounds, *Atmos. Environ.*, 44(4), 541–551, doi:https://doi.org/10.1016/j.atmosenv.2009.10.042, 2010.
- Collett, J. L., Hoag, K. J., Sherman, D. E., Bator, A. and Richards, L. W.: Spatial and temporal variations in San Joaquin Valley fog chemistry, *Atmos. Environ.*, 33(1), 129–140, doi:https://doi.org/10.1016/S1352-2310(98)00136-8, 1998.
- Corral Arroyo, P., Bartels-Rausch, T., Alpert, P. A., Dumas, S., Perrier, S., George, C. and Ammann, M.: Particle-Phase Photosensitized Radical Production and Aerosol Aging, *Environ. Sci. Technol.*, 52(14), 7680–7688, doi:10.1021/acs.est.8b00329, 2018.
- Daumit, K. E., Carrasquillo, A. J., Sugrue, R. A. and Kroll, J. H.: Effects of Condensed-Phase Oxidants on Secondary Organic Aerosol Formation, *J. Phys. Chem. A*, 120(9), 1386–1394, doi:10.1021/acs.jpca.5b06160, 2016.
- Farley, R., Bernays, N., Jaffe, D. A., Ketcherside, D., Hu, L., Zhou, S., Collier, S. and Zhang, Q.:

- Persistent Influence of Wildfire Emissions in the Western United States and Characteristics of Aged Biomass Burning Organic Aerosols under Clean Air Conditions, *Environ. Sci. Technol.*, 56(6), 3645–3657, doi:10.1021/acs.est.1c07301, 2022.
- Fredrickson, C. D., Palm, B. B., Lee, B. H., Zhang, X., Orlando, J. J., Tyndall, G. S., Garofalo, L. A., Pothier, M. A., Farmer, D. K., Decker, Z. C. J., Robinson, M. A., Brown, S. S., Murphy, S. M., Shen, Y., Sullivan, A. P., Schobesberger, S. and Thornton, J. A.: Formation and Evolution of Catechol-Derived SOA Mass, Composition, Volatility, and Light Absorption, *ACS Earth Sp. Chem.*, 6(4), 1067–1079, doi:10.1021/acsearthspacechem.2c00007, 2022.
- George, C., Ammann, M., D’Anna, B., Donaldson, D. J. and Nizkorodov, S. A.: Heterogeneous Photochemistry in the Atmosphere, *Chem. Rev.*, 115(10), 4218–4258, doi:10.1021/cr500648z, 2015a.
- George, K. M., Ruthenburg, T. C., Smith, J., Yu, L., Zhang, Q., Anastasio, C. and Dillner, A. M.: FT-IR quantification of the carbonyl functional group in aqueous-phase secondary organic aerosol from phenols, *Atmos. Environ.*, 100, 230–237, doi:10.1016/j.atmosenv.2014.11.011, 2015b.
- Gilardoni, S., Massoli, P., Paglione, M., Giulianelli, L., Carbone, C., Rinaldi, M., Decesari, S., Sandrini, S., Costabile, F., Gobbi, G. P., Pietrogrande, M. C., Visentin, M., Scotto, F., Fuzzi, S. and Facchini, M. C.: Direct observation of aqueous secondary organic aerosol from biomass-burning emissions, *Proc. Natl. Acad. Sci.*, 113(36), 10013–10018, doi:10.1073/pnas.1602212113, 2016.
- Hawthorne, S. B., Krieger, M. S., Miller, D. J. and Mathiason, M. B.: Collection and quantitation of methoxylated phenol tracers for atmospheric pollution from residential wood stoves, *Environ. Sci. Technol.*, 23(4), 470–475, doi:10.1021/es00181a013, 1989.
- Hems, R. F. and Abbatt, J. P. D.: Aqueous Phase Photo-oxidation of Brown Carbon Nitrophenols: Reaction Kinetics, Mechanism, and Evolution of Light Absorption, *ACS Earth Sp. Chem.*, doi:10.1021/acsearthspacechem.7b00123, 2018.
- Hems, R. F., Schnitzler, E. G., Liu-Kang, C., Cappa, C. D. and Abbatt, J. P. D.: Aging of Atmospheric Brown Carbon Aerosol, *ACS Earth Sp. Chem.*, 5(4), 722–748, doi:10.1021/acsearthspacechem.0c00346, 2021.
- Henry, K. M. and Donahue, N. M.: Photochemical Aging of  $\alpha$ -Pinene Secondary Organic Aerosol: Effects of OH Radical Sources and Photolysis, *J. Phys. Chem. A*, 116(24), 5932–5940, doi:10.1021/jp210288s, 2012.
- Herrmann, H., Hoffmann, D., Schaefer, T., Bräuer, P. and Tilgner, A.: Tropospheric Aqueous-Phase Free-Radical Chemistry: Radical Sources, Spectra, Reaction Kinetics and Prediction Tools, *ChemPhysChem*, 11(18), 3796–3822, doi:https://doi.org/10.1002/cphc.201000533, 2010.
- Herrmann, H., Schaefer, T., Tilgner, A., Styler, S. A., Weller, C., Teich, M. and Otto, T.: Tropospheric Aqueous-Phase Chemistry: Kinetics, Mechanisms, and Its Coupling to a Changing Gas Phase, *Chem. Rev.*, 115(10), 4259–4334, doi:10.1021/cr500447k, 2015.
- Hodzic, A., Kasibhatla, P. S., Jo, D. S., Cappa, C. D., Jimenez, J. L., Madronich, S. and Park, R.

- J.: Rethinking the global secondary organic aerosol (SOA) budget: stronger production, faster removal, shorter lifetime, *Atmos. Chem. Phys.*, 16(12), 7917–7941, doi:10.5194/acp-16-7917-2016, 2016.
- Huang, D. D., Zhang, Q., Cheung, H. H. Y., Yu, L., Zhou, S., Anastasio, C., Smith, J. D. and Chan, C. K.: Formation and Evolution of aqSOA from Aqueous-Phase Reactions of Phenolic Carbonyls: Comparison between Ammonium Sulfate and Ammonium Nitrate Solutions, *Environ. Sci. Technol.*, doi:10.1021/acs.est.8b03441, 2018.
- Jiang, W., Misovich, M. V, Hettiyadura, A. P. S., Laskin, A., McFall, A. S., Anastasio, C. and Zhang, Q.: Photosensitized Reactions of a Phenolic Carbonyl from Wood Combustion in the Aqueous Phase—Chemical Evolution and Light Absorption Properties of AqSOA, *Environ. Sci. Technol.*, 55(8), 5199–5211, doi:10.1021/acs.est.0c07581, 2021.
- Jimenez, J. L., Canagaratna, M. R., Donahue, N. M., Prevot, A. S. H., Zhang, Q., Kroll, J. H., DeCarlo, P. F., Allan, J. D., Coe, H., Ng, N. L., Aiken, A. C., Docherty, K. S., Ulbrich, I. M., Grieshop, A. P., Robinson, A. L., Duplissy, J., Smith, J. D., Wilson, K. R., Lanz, V. A., Hueglin, C., Sun, Y. L., Tian, J., Laaksonen, A., Raatikainen, T., Rautiainen, J., Vaattovaara, P., Ehn, M., Kulmala, M., Tomlinson, J. M., Collins, D. R., Cubison, M. J., Dunlea, J., Huffman, J. A., Onasch, T. B., Alfarra, M. R., Williams, P. I., Bower, K., Kondo, Y., Schneider, J., Drewnick, F., Borrmann, S., Weimer, S., Demerjian, K., Salcedo, D., Cottrell, L., Griffin, R., Takami, A., Miyoshi, T., Hatakeyama, S., Shimono, A., Sun, J. Y., Zhang, Y. M., Dzepina, K., Kimmel, J. R., Sueper, D., Jayne, J. T., Herndon, S. C., Trimborn, A. M., Williams, L. R., Wood, E. C., Middlebrook, A. M., Kolb, C. E., Baltensperger, U. and Worsnop, D. R.: Evolution of Organic Aerosols in the Atmosphere, *Science* (80-. ), 326(5959), 1525–1529, doi:10.1126/science.1180353, 2009.
- Kang, E., Toohey, D. W. and Brune, W. H.: Dependence of SOA oxidation on organic aerosol mass concentration and OH exposure: experimental PAM chamber studies, *Atmos. Chem. Phys.*, 11(4), 1837–1852, doi:10.5194/acp-11-1837-2011, 2011.
- Kaur, R. and Anastasio, C.: First Measurements of Organic Triplet Excited States in Atmospheric Waters, *Environ. Sci. Technol.*, 52(9), 5218–5226, doi:10.1021/acs.est.7b06699, 2018.
- Kaur, R., Labins, J. R., Helbock, S. S., Jiang, W., Bein, K. J., Zhang, Q. and Anastasio, C.: Photooxidants from brown carbon and other chromophores in illuminated particle extracts, *Atmos. Chem. Phys.*, 19(9), 6579–6594, doi:10.5194/acp-19-6579-2019, 2019.
- Kroll, J. H., Donahue, N. M., Jimenez, J. L., Kessler, S. H., Canagaratna, M. R., Wilson, K. R., Altieri, K. E., Mazzoleni, L. R., Wozniak, A. S., Bluhm, H., Mysak, E. R., Smith, J. D., Kolb, C. E. and Worsnop, D. R.: Carbon oxidation state as a metric for describing the chemistry of atmospheric organic aerosol, *Nat Chem*, 3(2), 133–139, doi:10.1038/nchem.948, 2011.
- Kroll, J. H., Lim, C. Y., Kessler, S. H. and Wilson, K. R.: Heterogeneous Oxidation of Atmospheric Organic Aerosol: Kinetics of Changes to the Amount and Oxidation State of Particle-Phase Organic Carbon, *J. Phys. Chem. A*, 119(44), 10767–10783, doi:10.1021/acs.jpca.5b06946, 2015.
- Lambe, A. T., Onasch, T. B., Croasdale, D. R., Wright, J. P., Martin, A. T., Franklin, J. P., Massoli, P., Kroll, J. H., Canagaratna, M. R., Brune, W. H., Worsnop, D. R. and Davidovits, P.:

- Transitions from Functionalization to Fragmentation Reactions of Laboratory Secondary Organic Aerosol (SOA) Generated from the OH Oxidation of Alkane Precursors, *Environ. Sci. Technol.*, 46(10), 5430–5437, doi:10.1021/es300274t, 2012.
- Lambe, A. T., Cappa, C. D., Massoli, P., Onasch, T. B., Forestieri, S. D., Martin, A. T., Cummings, M. J., Croasdale, D. R., Brune, W. H., Worsnop, D. R. and Davidovits, P.: Relationship between Oxidation Level and Optical Properties of Secondary Organic Aerosol, *Environ. Sci. Technol.*, 47(12), 6349–6357, doi:10.1021/es401043j, 2013.
- Lambe, A. T., Chhabra, P. S., Onasch, T. B., Brune, W. H., Hunter, J. F., Kroll, J. H., Cummings, M. J., Brogan, J. F., Parmar, Y., Worsnop, D. R., Kolb, C. E. and Davidovits, P.: Effect of oxidant concentration, exposure time, and seed particles on secondary organic aerosol chemical composition and yield, *Atmos. Chem. Phys.*, 15(6), 3063–3075, doi:10.5194/acp-15-3063-2015, 2015.
- Li, X., Tao, Y., Zhu, L., Ma, S., Luo, S., Zhao, Z., Sun, N., Ge, X. and Ye, Z.: Optical and chemical properties and oxidative potential of aqueous-phase products from OH and 3C\*-initiated photooxidation of eugenol, *Atmos. Chem. Phys.*, 22(11), 7793–7814, doi:10.5194/acp-22-7793-2022, 2022.
- Liu, J., Lin, P., Laskin, A., Laskin, J., Kathmann, S. M., Wise, M., Caylor, R., Imholt, F., Selimovic, V. and Shilling, J. E.: Optical properties and aging of light-absorbing secondary organic aerosol, *Atmos. Chem. Phys.*, 16(19), 12815–12827, doi:10.5194/acp-16-12815-2016, 2016.
- McWhinney, R. D., Zhou, S. and Abbatt, J. P. D.: Naphthalene SOA: redox activity and naphthoquinone gas–particle partitioning, *Atmos. Chem. Phys.*, 13(19), 9731–9744, doi:10.5194/acp-13-9731-2013, 2013.
- Misovich, M. V., Hettiyadura, A. P. S., Jiang, W., Zhang, Q. and Laskin, A.: Molecular-Level Study of the Photo-Oxidation of Aqueous-Phase Guaiacyl Acetone in the Presence of 3C\*: Formation of Brown Carbon Products, *ACS Earth Sp. Chem.*, 5(8), 1983–1996, doi:10.1021/acsearthspacechem.1c00103, 2021.
- Morgan, W. T., Allan, J. D., Bower, K. N., Highwood, E. J., Liu, D., McMeeking, G. R., Northway, M. J., Williams, P. I., Krejci, R. and Coe, H.: Airborne measurements of the spatial distribution of aerosol chemical composition across Europe and evolution of the organic fraction, *Atmos. Chem. Phys.*, 10(8), 4065–4083, doi:10.5194/acp-10-4065-2010, 2010.
- Ng, N. L., Canagaratna, M. R., Zhang, Q., Jimenez, J. L., Tian, J., Ulbrich, I. M., Kroll, J. H., Docherty, K. S., Chhabra, P. S., Bahreini, R., Murphy, S. M., Seinfeld, J. H., Hildebrandt, L., Donahue, N. M., DeCarlo, P. F., Lanz, V. A., Prévôt, A. S. H., Dinar, E., Rudich, Y. and Worsnop, D. R.: Organic aerosol components observed in Northern Hemispheric datasets from Aerosol Mass Spectrometry, *Atmos. Chem. Phys.*, 10(10), 4625–4641, doi:10.5194/acp-10-4625-2010, 2010.
- Ng, N. L., Canagaratna, M. R., Jimenez, J. L., Chhabra, P. S., Seinfeld, J. H. and Worsnop, D. R.: Changes in organic aerosol composition with aging inferred from aerosol mass spectra, *Atmos. Chem. Phys.*, 11(13), 6465–6474, doi:10.5194/acp-11-6465-2011, 2011.
- Nolte, C. G., Schauer, J. J., Cass, G. R. and Simoneit, B. R. T.: Highly Polar Organic Compounds



- Present in Wood Smoke and in the Ambient Atmosphere, *Environ. Sci. Technol.*, 35(10), 1912–1919, doi:10.1021/es001420r, 2001.
- O'Brien, R. E. and Kroll, J. H.: Photolytic Aging of Secondary Organic Aerosol: Evidence for a Substantial Photo-Recalcitrant Fraction, *J. Phys. Chem. Lett.*, 10(14), 4003–4009, doi:10.1021/acs.jpcclett.9b01417, 2019.
- Palm, B. B., Peng, Q., Fredrickson, C. D., Lee, B. H., Garofalo, L. A., Pothier, M. A., Kreidenweis, S. M., Farmer, D. K., Pokhrel, R. P., Shen, Y., Murphy, S. M., Permar, W., Hu, L., Campos, T. L., Hall, S. R., Ullmann, K., Zhang, X., Flocke, F., Fischer, E. V and Thornton, J. A.: Quantification of organic aerosol and brown carbon evolution in fresh wildfire plumes, *Proc. Natl. Acad. Sci.*, 117(47), 29469–29477, doi:10.1073/pnas.2012218117, 2020.
- Pang, H., Zhang, Q., Lu, X., Li, K., Chen, H., Chen, J., Yang, X., Ma, Y., Ma, J. and Huang, C.: Nitrite-Mediated Photooxidation of Vanillin in the Atmospheric Aqueous Phase, *Environ. Sci. Technol.*, 53(24), 14253–14263, doi:10.1021/acs.est.9b03649, 2019.
- Raja, S., Raghunathan, R., Yu, X.-Y., Lee, T., Chen, J., Kommalapati, R. R., Murugesan, K., Shen, X., Qingzhong, Y., Valsaraj, K. T. and Collett, J. L.: Fog chemistry in the Texas–Louisiana Gulf Coast corridor, *Atmos. Environ.*, 42(9), 2048–2061, doi:https://doi.org/10.1016/j.atmosenv.2007.12.004, 2008.
- Saleh, R.: From Measurements to Models: Toward Accurate Representation of Brown Carbon in Climate Calculations, *Curr. Pollut. Reports*, 6(2), 90–104, doi:10.1007/s40726-020-00139-3, 2020.
- Sareen, N., Moussa, S. G. and McNeill, V. F.: Photochemical Aging of Light-Absorbing Secondary Organic Aerosol Material, *J. Phys. Chem. A*, 117(14), 2987–2996, doi:10.1021/jp309413j, 2013.
- Schauer, J. J., Kleeman, M. J., Cass, G. R. and Simoneit, B. R. T.: Measurement of Emissions from Air Pollution Sources. 3. C1–C29 Organic Compounds from Fireplace Combustion of Wood, *Environ. Sci. Technol.*, 35(9), 1716–1728, doi:10.1021/es001331e, 2001.
- Sedlacek, A. J. I. I., Lewis, E. R., Onasch, T. B., Zuidema, P., Redemann, J., Jaffe, D. and Kleinman, L. I.: Using the Black Carbon Particle Mixing State to Characterize the Lifecycle of Biomass Burning Aerosols, *Environ. Sci. Technol.*, 56(20), 14315–14325, doi:10.1021/acs.est.2c03851, 2022.
- Simpson, C. D. and Naeher, L. P.: Biological monitoring of wood-smoke exposure, *Inhal. Toxicol.*, 22(2), 99–103, doi:10.3109/08958370903008862, 2010.
- Smith, J. D., Sio, V., Yu, L., Zhang, Q. and Anastasio, C.: Secondary Organic Aerosol Production from Aqueous Reactions of Atmospheric Phenols with an Organic Triplet Excited State, *Environ. Sci. Technol.*, 48(2), 1049–1057, doi:10.1021/es4045715, 2014.
- Smith, J. D., Kinney, H. and Anastasio, C.: Phenolic carbonyls undergo rapid aqueous photodegradation to form low-volatility, light-absorbing products, *Atmos. Environ.*, 126, 36–44, doi:http://dx.doi.org/10.1016/j.atmosenv.2015.11.035, 2016.
- Sun, Y. L., Zhang, Q., Anastasio, C. and Sun, J.: Insights into secondary organic aerosol formed via aqueous-phase reactions of phenolic compounds based on high resolution mass

- spectrometry, *Atmos. Chem. Phys.*, 10(10), 4809–4822, doi:10.5194/acp-10-4809-2010, 2010.
- Tsigaridis, K., Daskalakis, N., Kanakidou, M., Adams, P. J., Artaxo, P., Bahadur, R., Balkanski, Y., Bauer, S. E., Bellouin, N., Benedetti, A., Bergman, T., Berntsen, T. K., Beukes, J. P., Bian, H., Carslaw, K. S., Chin, M., Curci, G., Diehl, T., Easter, R. C., Ghan, S. J., Gong, S. L., Hodzic, A., Hoyle, C. R., Iversen, T., Jathar, S., Jimenez, J. L., Kaiser, J. W., Kirkevåg, A., Koch, D., Kokkola, H., Lee, Y. H., Lin, G., Liu, X., Luo, G., Ma, X., Mann, G. W., Mihalopoulos, N., Morcrette, J.-J., Müller, J.-F., Myhre, G., Myriokefalitakis, S., Ng, N. L., O'Donnell, D., Penner, J. E., Pozzoli, L., Pringle, K. J., Russell, L. M., Schulz, M., Sciare, J., Seland, Ø., Shindell, D. T., Sillman, S., Skeie, R. B., Spracklen, D., Stavrou, T., Steenrod, S. D., Takemura, T., Tiitta, P., Tilmes, S., Tost, H., van Noije, T., van Zyl, P. G., von Salzen, K., Yu, F., Wang, Z., Wang, Z., Zaveri, R. A., Zhang, H., Zhang, K., Zhang, Q. and Zhang, X.: The AeroCom evaluation and intercomparison of organic aerosol in global models, *Atmos. Chem. Phys.*, 14(19), 10845–10895, doi:10.5194/acp-14-10845-2014, 2014.
- Ulbrich, I. M., Canagaratna, M. R., Zhang, Q., Worsnop, D. R. and Jimenez, J. L.: Interpretation of organic components from Positive Matrix Factorization of aerosol mass spectrometric data, *Atmos. Chem. Phys.*, 9(9), 2891–2918, doi:10.5194/acp-9-2891-2009, 2009.
- Volkamer, R., Klotz, B., Barnes, I., Imamura, T., Wirtz, K., Washida, N., Becker, K. H. and Platt, U.: OH-initiated oxidation of benzene Part I. Phenol formation under atmospheric conditions, *Phys. Chem. Chem. Phys.*, 4(9), 1598–1610, doi:10.1039/B108747A, 2002.
- Wagstrom, K. M. and Pandis, S. N.: Determination of the age distribution of primary and secondary aerosol species using a chemical transport model, *J. Geophys. Res. Atmos.*, 114(D14), doi:https://doi.org/10.1029/2009JD011784, 2009.
- Yang, J., Au, W. C., Law, H., Lam, C. H. and Nah, T.: Formation and evolution of brown carbon during aqueous-phase nitrate-mediated photooxidation of guaiacol and 5-nitroguaiacol, *Atmos. Environ.*, 254, 118401, doi:https://doi.org/10.1016/j.atmosenv.2021.118401, 2021.
- Yee, L. D., Kautzman, K. E., Loza, C. L., Schilling, K. A., Coggon, M. M., Chhabra, P. S., Chan, M. N., Chan, A. W. H., Hersey, S. P., Crouse, J. D., Wennberg, P. O., Flagan, R. C. and Seinfeld, J. H.: Secondary organic aerosol formation from biomass burning intermediates: phenol and methoxyphenols, *Atmos. Chem. Phys.*, 13(16), 8019–8043, doi:10.5194/acp-13-8019-2013, 2013.
- Yu, L., Smith, J., Laskin, A., Anastasio, C., Laskin, J. and Zhang, Q.: Chemical characterization of SOA formed from aqueous-phase reactions of phenols with the triplet excited state of carbonyl and hydroxyl radical, *Atmos. Chem. Phys.*, 14(24), 13801–13816, doi:10.5194/acp-14-13801-2014, 2014.
- Yu, L., Smith, J., Laskin, A., George, K. M., Anastasio, C., Laskin, J., Dillner, A. M. and Zhang, Q.: Molecular transformations of phenolic SOA during photochemical aging in the aqueous phase: competition among oligomerization, functionalization, and fragmentation, *Atmos. Chem. Phys.*, 16(7), 4511–4527, doi:10.5194/acp-16-4511-2016, 2016.
- Zhai, L., An, Y., Feng, L., Qin, X. and Xu, J.: Contrasting the physical and chemical characteristics of dissolved organic matter between glacier and glacial runoff from a mountain glacier on the Tibetan Plateau, *Sci. Total Environ.*, 848, 157784,

doi:<https://doi.org/10.1016/j.scitotenv.2022.157784>, 2022.

Zhang, Q., Jimenez, J. L., Canagaratna, M. R., Ulbrich, I. M., Ng, N. L., Worsnop, D. R. and Sun, Y.: Understanding atmospheric organic aerosols via factor analysis of aerosol mass spectrometry: a review, *Anal. Bioanal. Chem.*, 401(10), 3045–3067, doi:10.1007/s00216-011-5355-y, 2011.

Zhou, S., Collier, S., Jaffe, D. A., Briggs, N. L., Hee, J., Sedlacek III, A. J., Kleinman, L., Onasch, T. B. and Zhang, Q.: Regional influence of wildfires on aerosol chemistry in the western US and insights into atmospheric aging of biomass burning organic aerosol, *Atmos. Chem. Phys.*, 17(3), 2477–2493, doi:10.5194/acp-17-2477-2017, 2017.

Zhou, S., Collier, S., Jaffe, D. A. and Zhang, Q.: Free tropospheric aerosols at the Mt. Bachelor Observatory: more oxidized and higher sulfate content compared to boundary layer aerosols, *Atmos. Chem. Phys.*, 19(3), 1571–1585, doi:10.5194/acp-19-1571-2019, 2019.

## Supporting Information

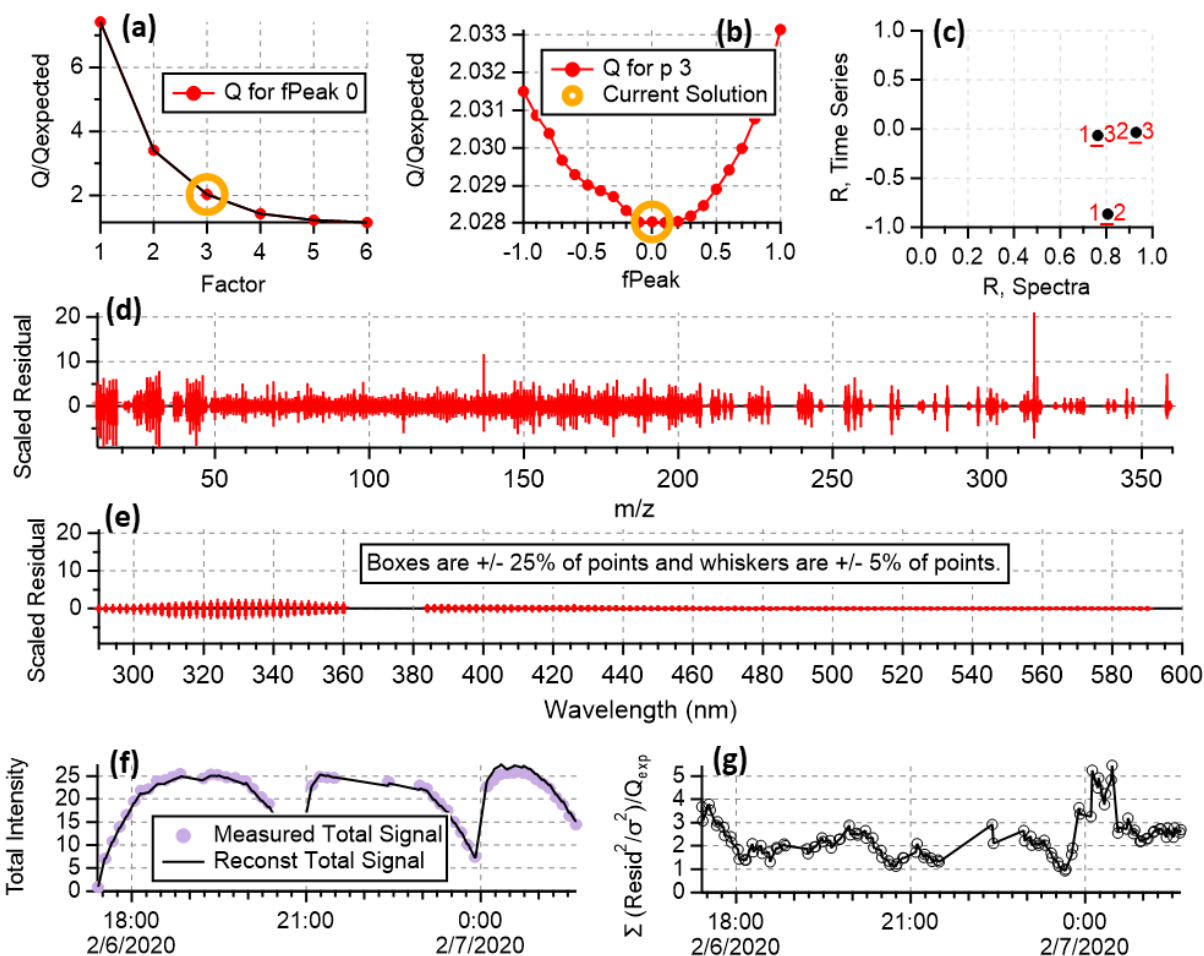


**Figure S1.** Summary of diagnostic plots for the three-factor solution for PMF analysis of  $^{13}\text{C}^*$ -initiated reactions: (a)  $Q/Q_{\text{exp}}$  as a function of number of factors selected for PMF modeling. (b)  $Q/Q_{\text{exp}}$  as a function of  $f_{\text{Peak}}$ . (c) Correlations among PMF factors. (d) Box and whisker plot showing the distributions of scaled residuals for each AMS ion. (e) Box and whisker plot showing the distributions of scaled residuals for each light absorption wavelength. (f) Reconstructed and measured total signal for each sample. (g)  $Q/Q_{\text{exp}}$  for each sample.

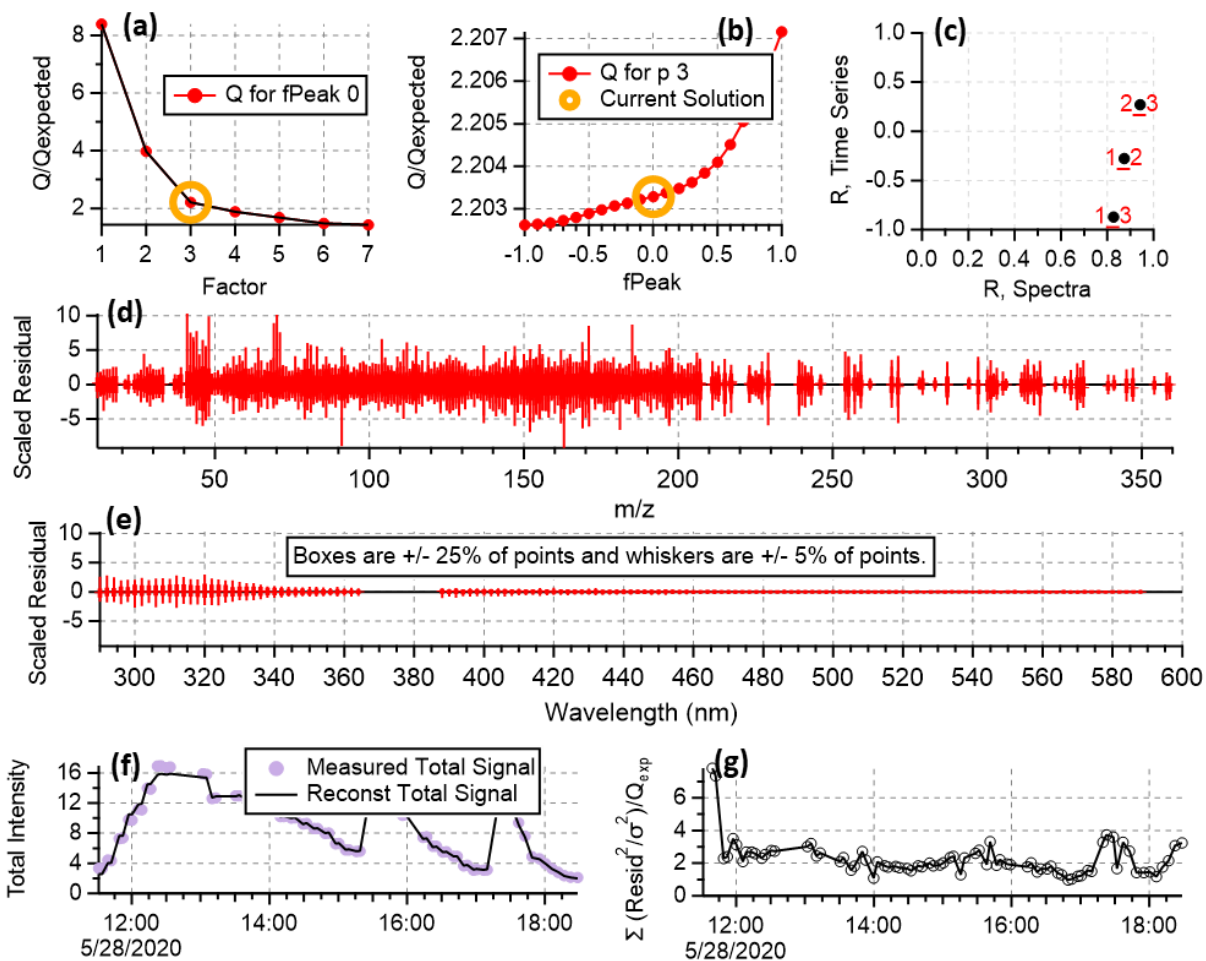


**Figure S2.** Summary of diagnostic plots for the three-factor solution for PMF analysis of OH-initiated reactions : (a)  $Q/Q_{\text{exp}}$  as a function of number of factors selected for PMF modeling. (b)  $Q/Q_{\text{exp}}$  as a function of  $f_{\text{Peak}}$ . (c) Correlations among PMF factors. (d) Box and whisker plot showing the distributions of scaled residuals for each AMS ion. (e) Box and whisker plot showing the distributions of scaled residuals for each light absorption wavelength. (f) Reconstructed and measured total signal for each sample. (g)  $Q/Q_{\text{exp}}$  for each sample.

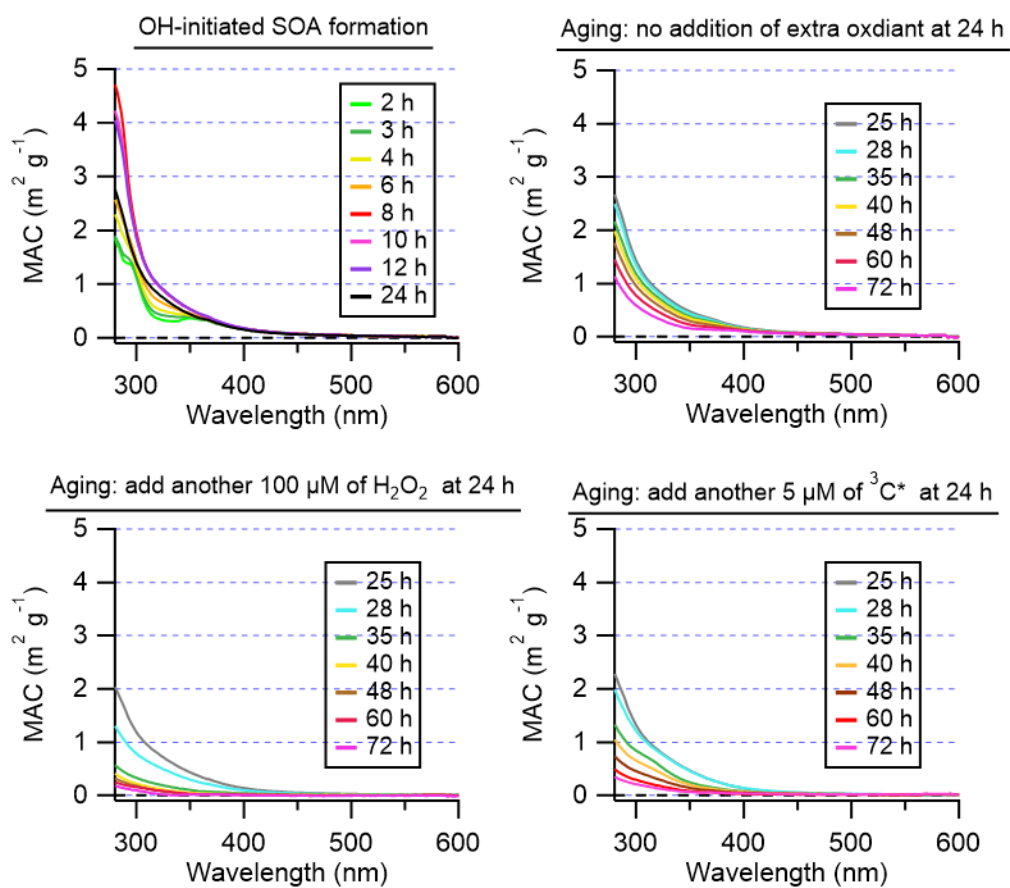


**Figure S3.** Evolution of mass absorption coefficient spectra of aqSOA in OH-initiated reactions.

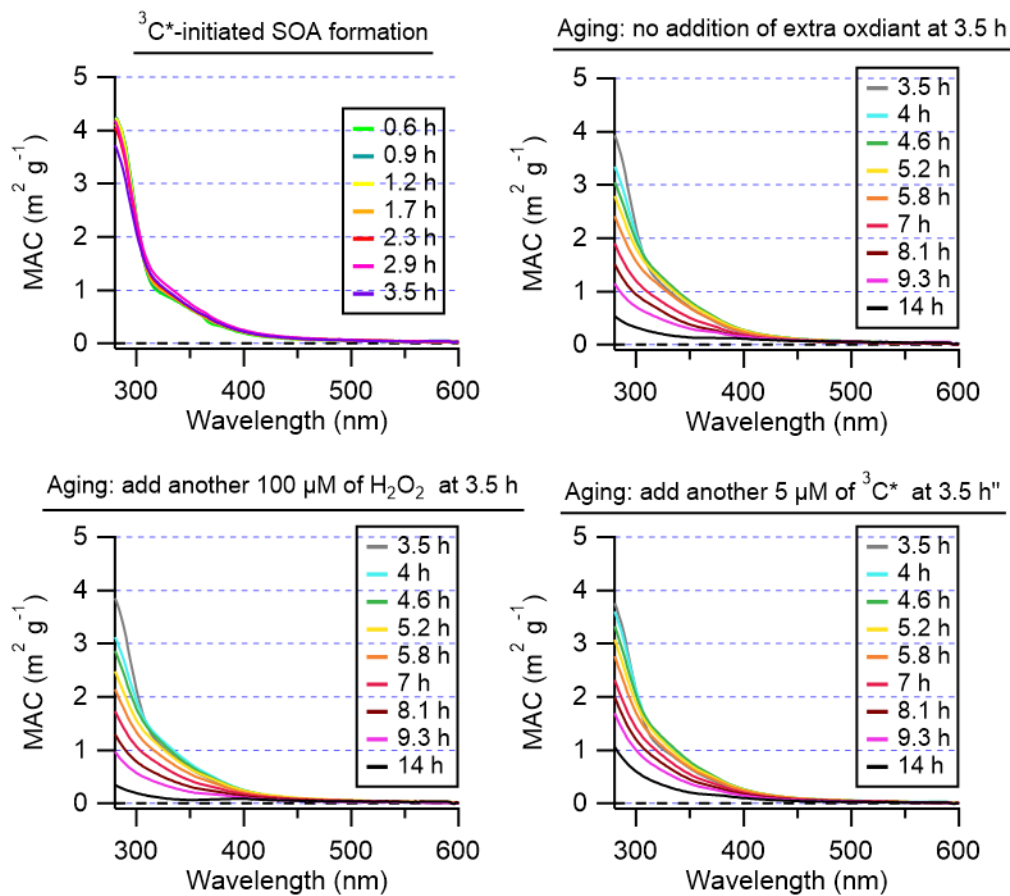


**Figure S4.** Evolution of mass absorption coefficient spectra of aqSOA in  $^3\text{C}^*$ -initiated reactions.

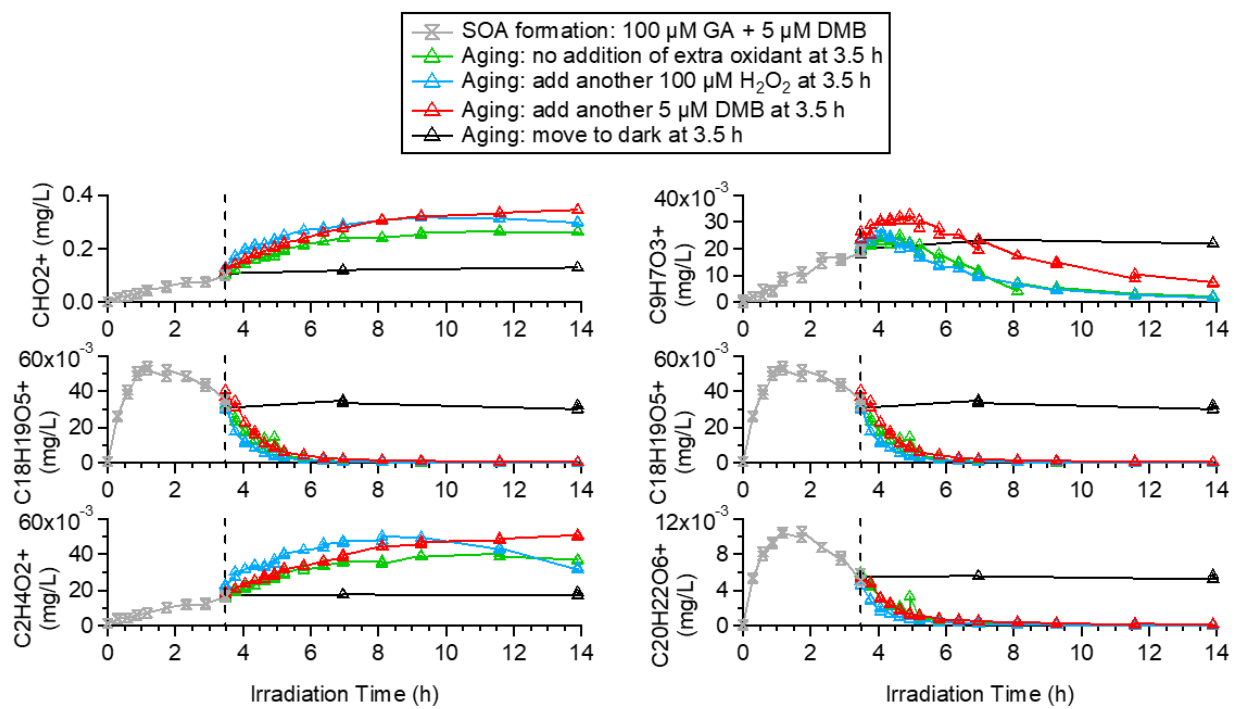


**Figure S5.** Trend of selected AMS tracer ions in  $^{13}\text{C}^*$ -initiated reactions.



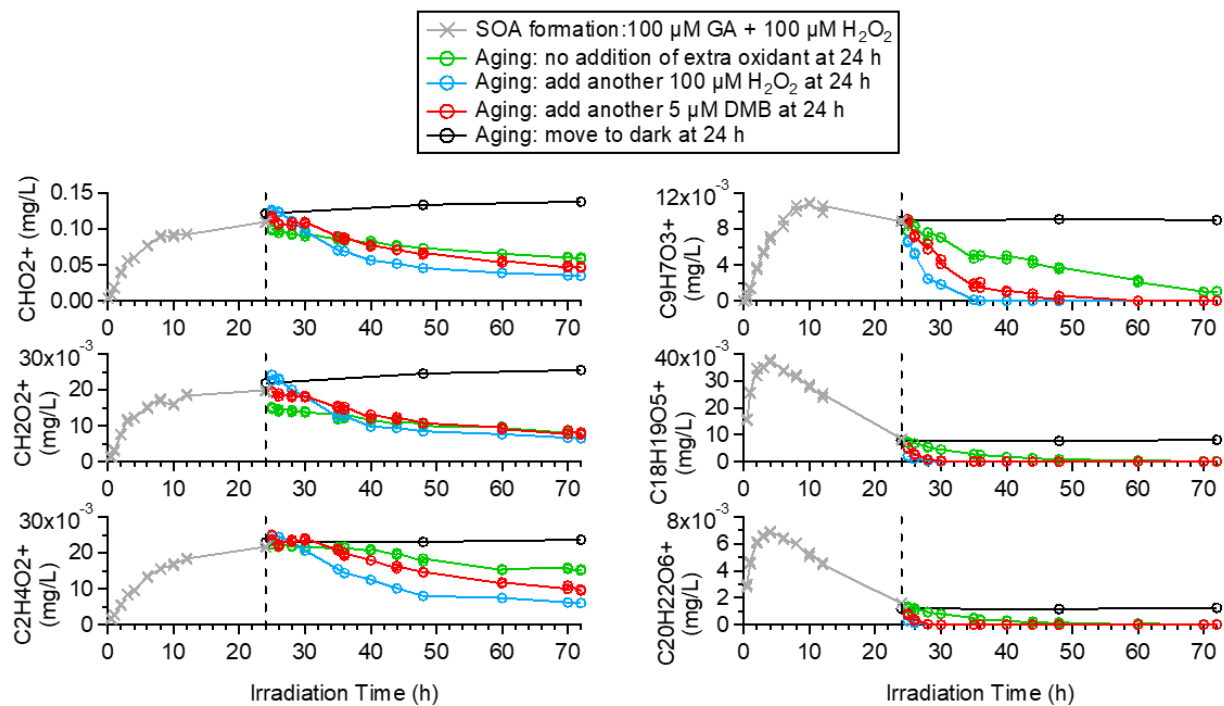


**Figure S6.** Trend of selected AMS tracer ions in OH-initiated reactions.

## **Chapter 4: Chemical Differences between Phenolic Secondary Organic Aerosol Formed through Gas-phase and Aqueous-phase Reactions**

### **4.1 Abstract**

Phenols, emitted in significant quantities from biomass burning (BB) through the pyrolysis of lignin, can undergo rapid photochemical reactions in both the gas and aqueous phase to form secondary organic aerosol (SOA). In this study, we investigate the compositional differences between the SOA formed from gas-phase reactions (gasSOA) and aqueous-phase reactions (aqSOA) of guaiacol ( $C_7H_8O_2$ ; 2-methoxyphenol), a basic structure of BB-emitted phenols. Significant chemical differences are observed between the gasSOA and aqSOA, indicating major mechanistic differences between reactions in these phases in the atmosphere. While gas-phase reactions of guaiacol quickly produce highly oxidized gasSOA ( $O/C > 0.8$ ), aqueous-phase reactions initially produce significantly less oxidized aqSOA. However, continued aqueous-phase reactions increase the oxidation degree of aqSOA and thus at later periods the aqSOA and gasSOA show more similar bulk chemical compositions. A major distinction between aqSOA and gasSOA is the relative abundance of oligomers and other high molecular weight products: these are much more abundantly produced via aqueous-phase reactions. Additionally, carboxylic acid formation is more significant in aqSOA than in gasSOA over the course of the reactions. Furthermore, molecular-level analysis identified some common SOA products - mainly functionalized monomers - in both gas- and aqueous-phase reactions. These results highlight the chemical differences between guaiacol gasSOA and aqSOA which suggest important differences in their

implications, indicating the importance of incorporating both gas- and aqueous-phase reaction pathways for SOA formation in models.

## 4.2 Introduction

Secondary organic aerosol (SOA) makes up a substantial fraction of tropospheric aerosol mass (Zhang et al., 2007). Given the wide range of emission sources, as well as physical and chemical processes in the atmosphere, the chemical composition of SOA is extremely complex, which makes the characterization of SOA formation a challenge. Traditionally, SOA was thought to be formed only through gas-phase oxidation of volatile organic compounds (VOCs) followed by partitioning of low-volatility products into the particle phase. However, recent studies have shown that SOA can also be formed effectively through aqueous-phase reactions in cloud and fog drops as well as in particle water. This formation of aqueous SOA (aqSOA) occurs when water-soluble organic gases partition to atmospheric water and are then oxidized to form low volatility species that remain in the condensed phase (Saffari et al., 2016; Youn et al., 2013). Considering the large amount of cloud, fog and aerosol water in the atmosphere, aqSOA is estimated to contribute nearly as much mass as SOA formed through gas-phase reactions (gasSOA) (Ervens et al., 2011).

GasSOA and aqSOA can show quite different chemical compositions and properties. As functionalization and accretion (e.g., acid formation and oligomerization) play important roles in aqSOA formation, while fragmentation is a dominant pathway in gasSOA formation mechanisms, aqSOA tends to be more oxygenated than gasSOA (Aiken et al., 2008; Lim et al., 2010; Ng et al., 2010b). Furthermore, highly-oxygenated aqSOA tends to be more hygroscopic and more capable of forming cloud and fog droplets than gasSOA, and thus can impact climate differently. AqSOA

can comprise colored organic species and is a significant source of brown carbon (BrC) aerosol (Woo et al., 2013). Moreover, since aqSOA is more oxygenated and water-soluble than gasSOA, it can be removed by wet deposition more easily, and thus typically has shorter atmospheric lifetimes than gasSOA (Fu et al., 2008, 2009).

An important precursor of SOA in both phases are phenols, a family of aromatic compounds emitted in large quantities from biomass burning through the pyrolysis of lignin. Phenols are abundant, accounting for 45% of the primary particulate mass emitted from wood combustion (Hawthorne et al., 1989). Guaiacol is a common methoxyphenol that is emitted from both hard and soft woods (Simpson and Naeher, 2010). Gas-phase  $\cdot\text{OH}$  photooxidation of guaiacol under low  $\text{NO}_x$  conditions produces gasSOA with mass yields in the range of 44-50% (Yee et al., 2013). The gas-phase reaction initiates with H-abstraction from the hydroxyl substituent to form a phenoxy radical, or OH addition to the aromatic ring to form an organic peroxy radical, followed by hydroxylation, fragmentation (ring-opening reactions), and demethoxylation reactions. Additionally, nitrophenols are formed from gas-phase reactions of phenols under high  $\text{NO}_x$  conditions (Lauraguais et al., 2014). Besides gas-phase reactions, due to guaiacol's moderate Henry's law constant, it appreciably partitions to fog and cloud drops, where it reacts quickly with oxidants (e.g., hydroxyl radicals ( $\cdot\text{OH}$ ) and triplet excited states of organic carbon ( $^3\text{C}^*$ )) to generate aqSOA with mass yields close to 100% (Sun et al., 2010; Yu et al., 2014). Oligomerization, functionalization, and fragmentation are important pathways for guaiacol aqSOA formation (Sun et al., 2010; Yu et al., 2014).

In this work we compare the bulk chemical compositions of guaiacol gasSOA and aqSOA analyzed by high resolution time-of-flight aerosol mass spectrometry (HR-ToF-AMS). We investigate the bulk chemistry evolution, oligomer formation and carboxylic acid formation in

guaiacol gasSOA and aqSOA and aim to demonstrate major differences in formation mechanisms between the gasSOA and aqSOA.

## 4.3 Experimental Methods

### 4.3.1 Overview of Photooxidation Experiments

Gas-phase photoreaction experiment data were obtained from Yee et al. (2013), which describes the experimental procedures. Briefly, experiments were conducted in the Caltech dual 28m<sup>3</sup> Teflon laboratory chambers under low NO<sub>x</sub> and high NO<sub>x</sub> conditions using ·OH to oxidize guaiacol. In the low-NO<sub>x</sub> experiments (initial NO<sub>x</sub> < 5 ppb), H<sub>2</sub>O<sub>2</sub> was the ·OH source, while in the high-NO<sub>x</sub> experiments (initial NO<sub>x</sub> ~ hundreds of ppb), HONO was the ·OH source. H<sub>2</sub>O<sub>2</sub> or HONO was vaporized in a glass trap and introduced into the chamber by purified air flow. Ammonium sulfate seed aerosol was used to promote condensation of the oxidation products. Guaiacol was vaporized in a glass bulb and introduced into the chamber by purified air stream. Three hundred 40 W black lights with an emission spectrum that peaks between 340 – 350 nm were used for irradiation.

Aqueous-phase experiments were performed under simulated sunlight inside a RPR-200 photoreactor system (George et al., 2015b) through the reaction of guaiacol with ·OH or <sup>3</sup>C\*. The detailed experiment procedure is described in previous work (Yu et al., 2016), and a brief summary is given here. The initial reaction solution was prepared by dissolving 100 μM of guaiacol in air-saturated Milli-Q water with pH adjusted to 5 with sulfuric acid. In the ·OH reaction experiments, 100 μM of H<sub>2</sub>O<sub>2</sub> was added to the solution as the source of ·OH, and in the <sup>3</sup>C\* reaction

experiments, 5  $\mu\text{M}$  of 3,4-dimethoxybenzaldehyde (3,4-DMB) was added to as the source of  $^{13}\text{C}^*$ . The experimental conditions for each photo-oxidation system are summarized in Table S1.

### 4.3.2 Chemical Analysis

High-resolution time-of-flight aerosol mass spectrometer (Aerodyne Res. Inc., Billerica, MA) was used to characterize the chemical composition of the gasSOA and aqSOA. The “V-mode” data were analyzed to determine the elemental ratios (atomic oxygen-to-carbon ratio, O/C and hydrogen-to-carbon ratio, H/C) of the SOA and the behaviors of fragment ions in the mass spectra of SOA. The AMS data were analyzed using the AMS data analysis software (SQUIRREL and PIKA). For gasSOA, the signal of  $\text{CO}^+$  and the  $\text{H}_2\text{O}$ -related ions (e.g.  $\text{H}_2\text{O}^+$ ,  $\text{HO}^+$ , and  $\text{O}^+$ ) were estimated as described in Aiken et al. (2008). For aqSOA, since argon was used as the carrier gas and the physically bonded water molecules were removed from the particles,  $\text{CO}^+$  and the  $\text{H}_2\text{O}$ -related ions were determined directly in the spectra of aqSOA. The average oxidation state of carbon (OS<sub>C</sub>) was determined as  $\text{OS}_C = 2 \times \text{O/C} - \text{H/C}$ , as the SOA we investigate in this study mainly consists of C, H, and O atoms and the amount of peroxide groups is negligible (Kroll et al., 2011).

## 4.4 Results and Discussion

### 4.4.1 Comparison of chemical composition between gasSOA and aqSOA at $t_{0.5}$ and $t_{0.25}$

Figure 1 shows the elemental ratios, average oxidation states of carbon (OS<sub>C</sub>), and mass spectra of gasSOA and aqSOA at two time points. As shown in Fig. 1a, when 50% of the guaiacol has reacted (i.e. at one half-life of guaiacol,  $t_{0.5}$ ), aqSOA compared to gasSOA shows lower O/C ratios (0.63 – 0.88 vs. 0.85 – 0.90), higher H/C ratios (1.46 – 1.70 vs. 1.17 – 1.23) and lower OS<sub>C</sub>

( $-0.20 - 0.07$  vs.  $0.47 - 0.64$ ). At the time when 75% of the initial guaiacol has reacted (i.e. two half-lives of guaiacol or  $t_{0.25}$ ), O/C and OSc of gasSOA and aqSOA both increase, with a more significant trend for aqSOA (Fig. 1d). These results suggest that, in comparison to aqueous-phase reactions, gas-phase reactions of guaiacol produce more oxidized SOA initially. However, at longer reaction times the oxidation degree of aqSOA increases significantly, while that of gasSOA barely changes. Fig. 1b and Fig. 1e show the mass fractions of high  $m/z$  fragments in the AMS spectra:  $m/z > 124$  and  $m/z > 246$ , cutpoints that represent the molecular weights of guaiacol and guaiacol dimer, respectively. Since electron impact ionization produces ions no larger than the molecular ion, the higher fraction of high  $m/z$  fragments in the mass spectra of aqSOA indicates that aqueous-phase reactions produce more large molecules than do gas-phase reactions. The higher fraction of fragments with  $m/z > 246$  in aqSOA compared to gasSOA indicate that oligomer formation is much more abundant in aqueous-phase reactions. On the other hand, at  $t_{0.25}$ , the fraction of high  $m/z$  fragments in aqSOA decreases compared with that at  $t_{0.5}$ , especially in the  $\cdot\text{OH}$ -initiated aqueous reaction system, indicating the oligomers formed in the initial stage of aqueous-phase reactions can be destroyed in later periods.

Figure 2 shows the AMS spectra of guaiacol gasSOA and aqSOA at  $t_{0.5}$ . The fragments in the mass spectra are separated into five ion categories ( $\text{C}_x\text{H}_y^+$ ,  $\text{H}_y\text{O}_1^+$ ,  $\text{C}_x\text{H}_y\text{O}_1^+$ ,  $\text{C}_x\text{H}_y\text{O}_2^+$ , and  $\text{C}_x\text{H}_y\text{O}_{\text{gt}2}^+$ ), and the contribution of each ion category to the total AMS signal is summarized in Fig 1e and Fig 1f. In all the SOA mass spectra, intense signals are observed at  $m/z$  44 ( $\text{CO}_2^+$ ),  $m/z$  18 ( $\text{H}_2\text{O}^+$ ), and  $m/z$  28 ( $\text{CO}^+$ ). The  $\text{C}_x\text{H}_y^+$ ,  $\text{C}_x\text{H}_y\text{O}_1^+$ , and  $\text{C}_x\text{H}_y\text{O}_2^+$  groups are the dominant ion categories, which together account for more than 90% and 75% of the total signal in the mass spectra of the gasSOA and aqSOA, respectively. This mass spectral pattern is similar to the previously reported spectrum of fulvic acid, which is a model representative of oxidized OA

(OOA) (Zhang et al., 2005). On the other hand, in comparison to gasSOA, the mass spectra of aqSOA show lower fractions of  $C_xH_yO_1^+$  and higher fractions of  $C_xH_yO_{gt2}^+$ . The fraction of  $C_xH_yO_1^+$  is mainly controlled by the contribution of  $m/z$  28 ( $CO^+$ ), while the higher fraction of  $C_xH_yO_{gt2}^+$  in aqSOA is mainly due to the contribution of high  $m/z$  multiple-oxygenated ions. In addition, the fraction of the  $C_xH_y^+$  ion category shows a significant decrease from  $t_{0.5}$  to  $t_{0.25}$  in the aqSOA, but shows no change in gasSOA formation. These observations suggest that further oxidation occurs in prolonged aqueous-phase reactions, but perhaps not in prolonged gas-phase reactions.

#### 4.4.2 Chemical evolution of gasSOA and aqSOA

Figure 3a shows the “triangle plot” (i.e., a scatter plot of  $f_{44}$  vs.  $f_{43}$  where  $f_{44}$  and  $f_{43}$  are the ratios of the organic signals at  $m/z$  44 and 43 to the total organic signal in AMS spectra) and the Van Krevelen diagram of gasSOA and aqSOA throughout the course of each reaction. In the triangle plot, the gasSOA and the aqSOA data are to the left of the “triangle” and migrate upwards during irradiation, suggesting that both gas- and aqueous-phase reactions of guaiacol produce oxidized species with  $f_{44}$  values similar to ambient low-volatility oxygenated organic aerosol (LV-OOA). The upward motion during aging shows that the SOA generally gets more oxidized during irradiation. In the Van Krevelen diagram of Figure 3c, the O/C ratios of the gasSOA and the aqSOA fall within the range of ambient LV-OOA (Jimenez et al., 2009). Over the course of each reaction, both gasSOA and aqSOA show increasing O/C and slightly decreased H/C ratios. However, the increase of oxidation degree is more significant for the aqSOA, indicating that further oxidation occurs in the prolonged aqueous-phase reactions but barely occurs in the prolonged gas-phase reactions. This result is consistent with the larger increase of  $f_{CO_2^+}$  during aqSOA aging compared to gasSOA (Figure 3b). In the Van Krevelen diagram, the slopes of the



gasSOA data are  $-0.39$  and  $-0.68$  for low and high  $\text{NO}_x$  reactions, respectively, while the slopes of the aqSOA data are  $-0.65$  and  $-0.15$  for  $^3\text{C}^*$ -initiated and OH-initiated reactions, respectively. The slopes in Van Krevelen space can be an indicator of reactions and processes involved in aerosol aging (Heald et al., 2010). According to the relationships between the slope and the reaction type (Table S3), our results imply that the oxidation of guaiacol SOA involves the substitution of aliphatic functionality with alcohol, peroxide, or carboxylic acid.

#### 4.4.3 Formation of oligomers and high molecular weight species

Previous studies on aqSOA formation have demonstrated that phenolic compounds can undergo quick aqueous-phase photooxidation to form dimers and higher oligomers via C-C or C-O coupling of phenoxy radicals (Kobayashi and Higashimura, 2003; Sun et al., 2010; Yu et al., 2014). In this study, oligomerization is observed in aqSOA but not gasSOA. Figure 4 and Figure S1 show the mass fraction trend of a group of AMS tracer ions for guaiacol oligomers (e.g.  $\text{C}_{11}\text{H}_7\text{O}_2^+$ ,  $\text{C}_{12}\text{H}_{11}\text{O}_3^+$ ,  $\text{C}_{13}\text{H}_{11}\text{O}_4^+$ ,  $\text{C}_{14}\text{H}_{14}\text{O}_4^+$ ,  $\text{C}_{14}\text{H}_{14}\text{O}_5^+$  and  $\text{C}_{21}\text{H}_{20}\text{O}_6^+$ ) throughout the course of each reaction. For aqSOA, the oligomer ions show significant enhancements early in the reactions and decreases with continued reaction time. This suggests oligomers are produced in the initial period of aqueous-phase reactions, but are decomposed and transformed to smaller molecules via functionalization and fragmentation in later periods, consistent with previous findings (Yu et al., 2016). In addition, C-C coupling, rather than C-O coupling, tends to be the main oligomerization mechanism in guaiacol aqSOA formation. The major fragment ions of guaiacol C-C dimers are  $m/z$  246, 231, and 203, while  $m/z$  108 and 137 are the prominent fragments of guaiacol C-O dimers in electron ionization mass spectra (Braga et al., 2005). In our observation,  $m/z$  246 ( $\text{C}_{14}\text{H}_{14}\text{O}_4^+$ ),  $m/z$  231 ( $\text{C}_{13}\text{H}_{11}\text{O}_4^+$ ), and  $m/z$  203 ( $\text{C}_{12}\text{H}_{11}\text{O}_3^+$ ) are present in the AMS spectra of guaiacol aqSOA, while no significant signal appears at  $m/z$  108 or 137. On the other hand, in the gasSOA, none of

the proposed oligomer ions are observed. One possible reason could be efficient loss of oligomers to chamber walls prior to gas-particle partitioning due to their semi-volatile to low-volatile properties (Kroll et al., 2005, 2007; Yu et al., 2016). The other possible reason could be that oligomers are not formed in the gas-phase reactions. This could be because the ratio of oxidant to guaiacol in the gas-phase experiments is much higher than in the aqueous phase, which could favor functionalization and fragmentation pathways and suppress oligomerization in the gas phase.

Besides the previously proposed AMS tracer ions for guaiacol oligomers, several other ions (e.g.,  $C_9H_7O^+$ ,  $C_8H_7O_3^+$ ,  $C_{12}H_9O_2^+$ ,  $C_{11}H_9O_3^+$ ,  $C_{12}H_9O_3^+$  and  $C_{13}H_9O_3^+$ ) are significantly enhanced in aqSOA but are not present in gasSOA (Figure 5 and Figure S2). Most of these ions show trends similar to the previously proposed oligomer ions – significant enhancement at the beginning of the aqueous-phase reactions followed by decrease in the later periods. Considering the stable contribution of these ions in the mass spectra of guaiacol aqSOA, they can potentially be used as AMS tracer ions to identify guaiacol aqSOA.

#### **4.4.4 Formation of organic acids**

Organic acids are an important component in SOA, especially in aged SOA (Heald et al., 2010; Levin et al., 2014). Both gas- and aqueous-phase reactions can generate organic acids during SOA formation. The AMS signal at  $m/z$  44 (mainly  $CO_2^+$ ) shows a good correlation with organic acid concentrations and is commonly used as an AMS marker for organic acids in field and laboratory studies (Canagaratna et al., 2015; Duplissy et al., 2011; Sorooshian et al., 2010; Takegawa et al., 2007). Here, we find  $HCO_2^+$  may be a better indicator of organic acid formation. Figure S3 shows the National Institute of Standards and Technology (NIST) mass spectra of eight common small organic acids that may appear in the SOA. The mass spectra of these organic acids all show more significant signals at  $m/z$  45 ( $CHO_2^+$ ) compared to  $m/z$  44. Also, Figure S4 shows

the time series of  $f_{\text{CHO}_2^+}$  (the ratios of the  $\text{CHO}_2^+$  signal to the total organic signal in the AMS spectra) and the concentration of eight small organic acids measured by IC in the aqSOA. Good correlation is obtained between  $f_{\text{CHO}_2^+}$  and the total small acid concentration, suggesting  $f_{\text{CHO}_2^+}$  can be a good marker for organic acid formation. Another reason for using  $\text{CHO}_2^+$  rather than  $\text{CO}_2^+$  as a proxy of organic acids is that oxidized species other than acids, e.g., esters and peroxides, also contribute to the  $\text{CO}_2^+$  signal, thus  $\text{HCO}_2^+$  might be more specific. Figure 6 shows the time series of  $f_{\text{CHO}_2^+}$  in gasSOA and aqSOA throughout the course of each reaction. In the initial stage of the reactions, gasSOA contains more acid than aqSOA, but the fraction of organic acids in the gasSOA increases very little during continued illumination, whereas the contribution of organic acids in the aqSOA increases significantly. In the later periods, the organic acid fractions in aqSOA are higher than in gasSOA, suggesting that prolonged aqueous reactions of phenols might be an important source of organic acids in aerosol.

#### 4.4.5 Molecular level comparison

To gain insights into its molecular composition, Yu et al. (2014) performed nano-DESI measurements on the guaiacol aqSOA formed from  $^3\text{C}^*$ - and OH-initiated reactions (Figure 7). According to the assigned molecular formulas in the nano-DESI MS,  $\text{C}_{14}\text{H}_{14}\text{O}_4$  and  $\text{C}_{14}\text{H}_{14}\text{O}_6$  are the two most abundant products in the guaiacol aqSOA formed from both the  $^3\text{C}^*$ -initiated and the OH-initiated reactions. Tables S4 and S5 show the formulas and proposed structures of the top 10 most abundant products identified in the guaiacol aqSOA, which are dominated by guaiacol dimers and trimers and derivatives. These results clearly indicate the important role of oligomerization in guaiacol aqSOA formation. In contrast, no oligomer species were identified in the guaiacol gasSOA.

Proposed oxidation pathways of guaiacol in the gas phase (Yee et al., 2013) start with OH addition to the aromatic ring, followed by reaction with oxygen to form an organic peroxy radical (Figure 8). The organic peroxy radical can subsequently produce a guaiacol-OH adduct ( $C_7H_8O_3$ ) by eliminating  $HO_2$ . Successive OH addition products of guaiacol (e.g.  $C_7H_8O_4$  and  $C_7H_8O_5$ .) can then be produced through continuous OH addition and  $HO_2$  elimination. In addition, the isomerization of the organic peroxy radical can lead to the formation of a bicyclic radical that can rearrange, breaking the oxygen bridge to form an epoxide ( $C_7H_8O_5$ ). The bicyclic peroxy radical can also decompose to several ring-opening fragments (e.g.  $C_4H_6O_3$ ,  $C_3H_4O_4$ ,  $C_5H_6O_3$  and  $C_5H_6O_4$ ). Moreover, demethoxylation of guaiacol to form catechol ( $C_6H_6O_2$ ) also occurs in the gas phase. The proposed gasSOA products from guaiacol are identified in the guaiacol aqSOA (Figure 7 and Figure S5). These results suggest that hydroxylation, demethoxylation, and ring-opening reactions can occur in both gas-phase and aqueous-phase reactions of guaiacol, while oligomerization is favored in the aqueous phase (Figure 8).

This study investigates the chemical differences between guaiacol gasSOA and aqSOA over the courses of the photochemical reactions. The gasSOA is more oxidized and shows more acid formation than aqSOA at the initial stages of the reactions. However, in the prolonged gas-phase reactions, the oxidation degree and acid formation of gasSOA show negligible change, while in the prolonged aqueous-phase reactions, aqSOA shows evident increase in oxidation degree and acid formation. The more significant chemistry change in aqSOA over the course of the reaction suggests that aqueous-phase reactions tend to include more complex reaction mechanisms and tend to produce multiple generations of SOA products. In addition, oligomers are observed in aqSOA but not in gasSOA, suggesting oligomerization plays an important role in aqueous-phase reactions, but may not occur in gas-phase reactions.

## **Acknowledgements**

This work was supported by the US Department of Energy (DE-SC0014620), National Science Foundation (AGS-1036675) and the California Agricultural Experiment Station (CA-D-ETX-2102-H).

## Reference

- Aiken, A. C., DeCarlo, P. F., Kroll, J. H., Worsnop, D. R., Huffman, J. A., Docherty, K. S., Ulbrich, I. M., Mohr, C., Kimmel, J. R., Sueper, D., Sun, Y., Zhang, Q., Trimborn, A., Northway, M., Ziemann, P. J., Canagaratna, M. R., Onasch, T. B., Alfarra, M. R., Prevot, A. S. H., Dommen, J., Duplissy, J., Metzger, A., Baltensperger, U. and Jimenez, J. L.: O/C and OM/OC Ratios of Primary, Secondary, and Ambient Organic Aerosols with High-Resolution Time-of-Flight Aerosol Mass Spectrometry, *Environ. Sci. Technol.*, 42(12), 4478–4485, doi:10.1021/es703009q, 2008.
- Braga, D., Christophis, C., Noll, S. and Hampp, N.: Selective photochemical synthesis of 3,3'-dimethoxy-4,2'-dihydroxybiphenyl, *J. Photochem. Photobiol. A Chem.*, 172(2), 115–120, doi:http://dx.doi.org/10.1016/j.jphotochem.2004.11.014, 2005.
- Canagaratna, M. R., Jimenez, J. L., Kroll, J. H., Chen, Q., Kessler, S. H., Massoli, P., Hildebrandt Ruiz, L., Fortner, E., Williams, L. R., Wilson, K. R., Surratt, J. D., Donahue, N. M., Jayne, J. T. and Worsnop, D. R.: Elemental ratio measurements of organic compounds using aerosol mass spectrometry: characterization, improved calibration, and implications, *Atmos. Chem. Phys.*, 15(1), 253–272, doi:10.5194/acp-15-253-2015, 2015.
- Duplissy, J., DeCarlo, P. F., Dommen, J., Alfarra, M. R., Metzger, A., Barmapadimos, I., Prevot, A. S. H., Weingartner, E., Tritscher, T., Gysel, M., Aiken, A. C., Jimenez, J. L., Canagaratna, M. R., Worsnop, D. R., Collins, D. R., Tomlinson, J. and Baltensperger, U.: Relating hygroscopicity and composition of organic aerosol particulate matter, *Atmos. Chem. Phys.*, 11(3), 1155–1165, doi:10.5194/acp-11-1155-2011, 2011.
- Ervens, B., Turpin, B. J. and Weber, R. J.: Secondary organic aerosol formation in cloud droplets and aqueous particles (aqSOA): a review of laboratory, field and model studies, *Atmos. Chem. Phys.*, 11(21), 11069–11102, doi:10.5194/acp-11-11069-2011, 2011.
- Fu, T.-M., Jacob, D. J., Wittrock, F., Burrows, J. P., Vrekoussis, M. and Henze, D. K.: Global budgets of atmospheric glyoxal and methylglyoxal, and implications for formation of secondary organic aerosols, *J. Geophys. Res. Atmos.*, 113(D15), n/a-n/a, doi:10.1029/2007JD009505, 2008.
- Fu, T.-M., Jacob, D. J. and Heald, C. L.: Aqueous-phase reactive uptake of dicarbonyls as a source of organic aerosol over eastern North America, *Atmos. Environ.*, 43(10), 1814–1822, doi:http://dx.doi.org/10.1016/j.atmosenv.2008.12.029, 2009.
- George, K. M., Ruthenburg, T. C., Smith, J., Yu, L., Zhang, Q., Anastasio, C. and Dillner, A. M.: FT-IR quantification of the carbonyl functional group in aqueous-phase secondary organic aerosol from phenols, *Atmos. Environ.*, 100, 230–237, doi:10.1016/j.atmosenv.2014.11.011, 2015.
- Hawthorne, S. B., Krieger, M. S., Miller, D. J. and Mathiason, M. B.: Collection and quantitation of methoxylated phenol tracers for atmospheric pollution from residential wood stoves, *Environ. Sci. Technol.*, 23(4), 470–475, doi:10.1021/es00181a013, 1989.
- Heald, C. L., Kroll, J. H., Jimenez, J. L., Docherty, K. S., DeCarlo, P. F., Aiken, A. C., Chen, Q.,

- Martin, S. T., Farmer, D. K. and Artaxo, P.: A simplified description of the evolution of organic aerosol composition in the atmosphere, *Geophys. Res. Lett.*, 37(8), L08803, doi:10.1029/2010GL042737, 2010.
- Jimenez, J. L., Canagaratna, M. R., Donahue, N. M., Prevot, A. S. H., Zhang, Q., Kroll, J. H., DeCarlo, P. F., Allan, J. D., Coe, H., Ng, N. L., Aiken, A. C., Docherty, K. S., Ulbrich, I. M., Grieshop, A. P., Robinson, A. L., Duplissy, J., Smith, J. D., Wilson, K. R., Lanz, V. A., Hueglin, C., Sun, Y. L., Tian, J., Laaksonen, A., Raatikainen, T., Rautiainen, J., Vaattovaara, P., Ehn, M., Kulmala, M., Tomlinson, J. M., Collins, D. R., Cubison, M. J., Dunlea, J., Huffman, J. A., Onasch, T. B., Alfarra, M. R., Williams, P. I., Bower, K., Kondo, Y., Schneider, J., Drewnick, F., Borrmann, S., Weimer, S., Demerjian, K., Salcedo, D., Cottrell, L., Griffin, R., Takami, A., Miyoshi, T., Hatakeyama, S., Shimono, A., Sun, J. Y., Zhang, Y. M., Dzepina, K., Kimmel, J. R., Sueper, D., Jayne, J. T., Herndon, S. C., Trimborn, A. M., Williams, L. R., Wood, E. C., Middlebrook, A. M., Kolb, C. E., Baltensperger, U. and Worsnop, D. R.: Evolution of Organic Aerosols in the Atmosphere, *Science* (80-. ), 326(5959), 1525–1529, doi:10.1126/science.1180353, 2009.
- Kobayashi, S. and Higashimura, H.: Oxidative polymerization of phenols revisited, *Prog. Polym. Sci.*, 28(6), 1015–1048, doi:10.1016/S0079-6700(03)00014-5, 2003.
- Kroll, J. H., Ng, N. L., Murphy, S. M., Varutbangkul, V., Flagan, R. C. and Seinfeld, J. H.: Chamber studies of secondary organic aerosol growth by reactive uptake of simple carbonyl compounds, *J. Geophys. Res. Atmos.*, 110(D23), D23207, doi:10.1029/2005JD006004, 2005.
- Kroll, J. H., Chan, A. W. H., Ng, N. L., Flagan, R. C. and Seinfeld, J. H.: Reactions of Semivolatile Organics and Their Effects on Secondary Organic Aerosol Formation, *Environ. Sci. Technol.*, 41(10), 3545–3550, doi:10.1021/es062059x, 2007.
- Kroll, J. H., Donahue, N. M., Jimenez, J. L., Kessler, S. H., Canagaratna, M. R., Wilson, K. R., Altieri, K. E., Mazzoleni, L. R., Wozniak, A. S., Bluhm, H., Mysak, E. R., Smith, J. D., Kolb, C. E. and Worsnop, D. R.: Carbon oxidation state as a metric for describing the chemistry of atmospheric organic aerosol, *Nat Chem*, 3(2), 133–139, doi:10.1038/nchem.948, 2011.
- Lauraguais, A., Coeur-Tourneur, C., Cassez, A., Deboudt, K., Fourmentin, M. and Choël, M.: Atmospheric reactivity of hydroxyl radicals with guaiacol (2-methoxyphenol), a biomass burning emitted compound: Secondary organic aerosol formation and gas-phase oxidation products, *Atmos. Environ.*, 86, 155–163, doi:http://dx.doi.org/10.1016/j.atmosenv.2013.11.074, 2014.
- Levin, E. J. T., Prenni, A. J., Palm, B. B., Day, D. A., Campuzano-Jost, P., Winkler, P. M., Kreidenweis, S. M., DeMott, P. J., Jimenez, J. L. and Smith, J. N.: Size-resolved aerosol composition and its link to hygroscopicity at a forested site in Colorado, *Atmos. Chem. Phys.*, 14(5), 2657–2667, doi:10.5194/acp-14-2657-2014, 2014.
- Lim, Y. B., Tan, Y., Perri, M. J., Seitzinger, S. P. and Turpin, B. J.: Aqueous chemistry and its role in secondary organic aerosol (SOA) formation, *Atmos. Chem. Phys.*, 10(21), 10521–10539, doi:10.5194/acp-10-10521-2010, 2010.

- Ng, N. L., Canagaratna, M. R., Zhang, Q., Jimenez, J. L., Tian, J., Ulbrich, I. M., Kroll, J. H., Docherty, K. S., Chhabra, P. S., Bahreini, R., Murphy, S. M., Seinfeld, J. H., Hildebrandt, L., Donahue, N. M., DeCarlo, P. F., Lanz, V. A., Prévôt, A. S. H., Dinar, E., Rudich, Y. and Worsnop, D. R.: Organic aerosol components observed in Northern Hemispheric datasets from Aerosol Mass Spectrometry, *Atmos. Chem. Phys.*, 10(10), 4625–4641, doi:10.5194/acp-10-4625-2010, 2010.
- Saffari, A., Hasheminassab, S., Shafer, M. M., Schauer, J. J., Chatila, T. A. and Sioutas, C.: Nighttime aqueous-phase secondary organic aerosols in Los Angeles and its implication for fine particulate matter composition and oxidative potential, *Atmos. Environ.*, 133, 112–122, doi:http://dx.doi.org/10.1016/j.atmosenv.2016.03.022, 2016.
- Simpson, C. D. and Naeher, L. P.: Biological monitoring of wood-smoke exposure, *Inhal. Toxicol.*, 22(2), 99–103, doi:10.3109/08958370903008862, 2010.
- Sorooshian, A., Murphy, S. M., Hersey, S., Bahreini, R., Jonsson, H., Flagan, R. C. and Seinfeld, J. H.: Constraining the contribution of organic acids and AMS m/z 44 to the organic aerosol budget: On the importance of meteorology, aerosol hygroscopicity, and region, *Geophys. Res. Lett.*, 37(21), n/a-n/a, doi:10.1029/2010GL044951, 2010.
- Sun, Y. L., Zhang, Q., Anastasio, C. and Sun, J.: Insights into secondary organic aerosol formed via aqueous-phase reactions of phenolic compounds based on high resolution mass spectrometry, *Atmos. Chem. Phys.*, 10(10), 4809–4822, doi:10.5194/acp-10-4809-2010, 2010.
- Takegawa, N., Miyakawa, T., Kawamura, K. and Kondo, Y.: Contribution of Selected Dicarboxylic and  $\omega$ -Oxocarboxylic Acids in Ambient Aerosol to the m/z 44 Signal of an Aerodyne Aerosol Mass Spectrometer, *Aerosol Sci. Technol.*, 41(4), 418–437, doi:10.1080/02786820701203215, 2007.
- Woo, J. L., Kim, D. D., Schwier, A. N., Li, R. and McNeill, V. F.: Aqueous aerosol SOA formation: impact on aerosol physical properties, *Faraday Discuss.*, 165(0), 357–367, doi:10.1039/C3FD00032J, 2013.
- Yee, L. D., Kautzman, K. E., Loza, C. L., Schilling, K. A., Coggon, M. M., Chhabra, P. S., Chan, M. N., Chan, A. W. H., Hersey, S. P., Crounse, J. D., Wennberg, P. O., Flagan, R. C. and Seinfeld, J. H.: Secondary organic aerosol formation from biomass burning intermediates: phenol and methoxyphenols, *Atmos. Chem. Phys.*, 13(16), 8019–8043, doi:10.5194/acp-13-8019-2013, 2013.
- Youn, J.-S., Wang, Z., Wonaschütz, A., Arellano, A., Betterton, E. A. and Sorooshian, A.: Evidence of aqueous secondary organic aerosol formation from biogenic emissions in the North American Sonoran Desert, *Geophys. Res. Lett.*, 40(13), 3468–3472, doi:10.1002/grl.50644, 2013.
- Yu, L., Smith, J., Laskin, A., Anastasio, C., Laskin, J. and Zhang, Q.: Chemical characterization of SOA formed from aqueous-phase reactions of phenols with the triplet excited state of carbonyl and hydroxyl radical, *Atmos. Chem. Phys.*, 14(24), 13801–13816, doi:10.5194/acp-14-13801-2014, 2014.
- Yu, L., Smith, J., Laskin, A., George, K. M., Anastasio, C., Laskin, J., Dillner, A. M. and Zhang,



Q.: Molecular transformations of phenolic SOA during photochemical aging in the aqueous phase: competition among oligomerization, functionalization, and fragmentation, *Atmos. Chem. Phys.*, 16(7), 4511–4527, doi:10.5194/acp-16-4511-2016, 2016.

Zhang, Q., Alfarra, M. R., Worsnop, D. R., Allan, J. D., Coe, H., Canagaratna, M. R. and Jimenez, J. L.: Deconvolution and Quantification of Hydrocarbon-like and Oxygenated Organic Aerosols Based on Aerosol Mass Spectrometry, *Environ. Sci. Technol.*, 39(13), 4938–4952, doi:10.1021/es048568l, 2005.

Zhang, Q., Jimenez, J. L., Canagaratna, M. R., Allan, J. D., Coe, H., Ulbrich, I., Alfarra, M. R., Takami, A., Middlebrook, A. M., Sun, Y. L., Dzepina, K., Dunlea, E., Docherty, K., DeCarlo, P. F., Salcedo, D., Onasch, T., Jayne, J. T., Miyoshi, T., Shimono, A., Hatakeyama, S., Takegawa, N., Kondo, Y., Schneider, J., Drewnick, F., Borrmann, S., Weimer, S., Demerjian, K., Williams, P., Bower, K., Bahreini, R., Cottrell, L., Griffin, R. J., Rautiainen, J., Sun, J. Y., Zhang, Y. M. and Worsnop, D. R.: Ubiquity and dominance of oxygenated species in organic aerosols in anthropogenically-influenced Northern Hemisphere midlatitudes, *Geophys. Res. Lett.*, 34(13), n/a-n/a, doi:10.1029/2007GL029979, 2007.

## Figures

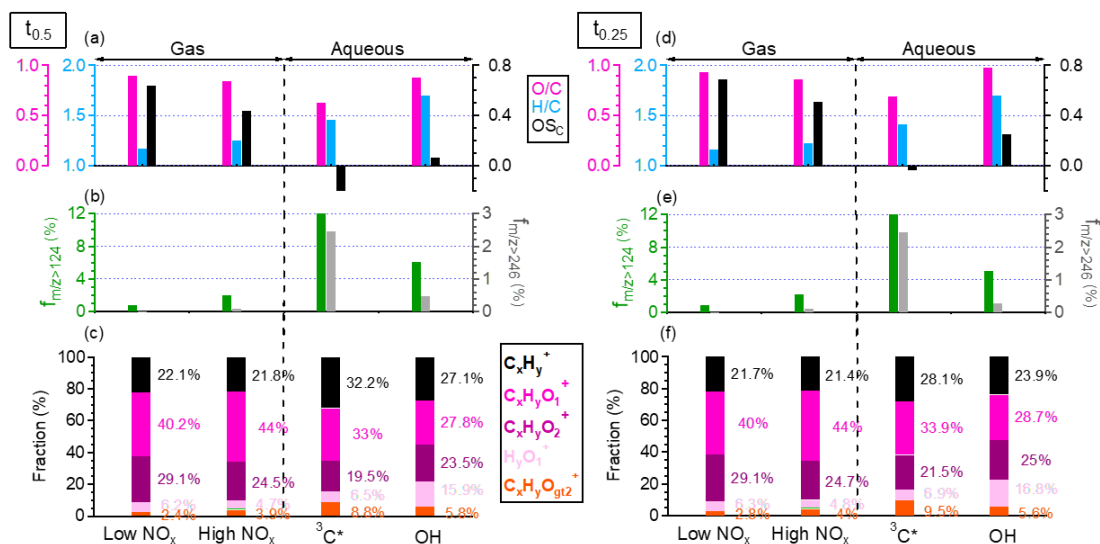


Figure 1. Elemental ratios and OSc (a and d), mass fractions of large ions ( $m/z > 124$  and  $m/z > 246$ ) in the AMS spectra (b and e), and ion categories in the AMS spectra (c and f) of SOA formed in gas- and aqueous-phase reactions at  $t_{0.5}$  and  $t_{0.25}$ . Half-lives of guaiacol are 2.35, 1.27, 0.92, and 3.17 hours in the low- $NO_x$ , high- $NO_x$ ,  $3C^*$ , and OH conditions, respectively. Times for GUA to decay to 25% of its initial concentration in these four reaction systems are 4.68, 2.48, 1.82, and 6.32 hours, respectively.

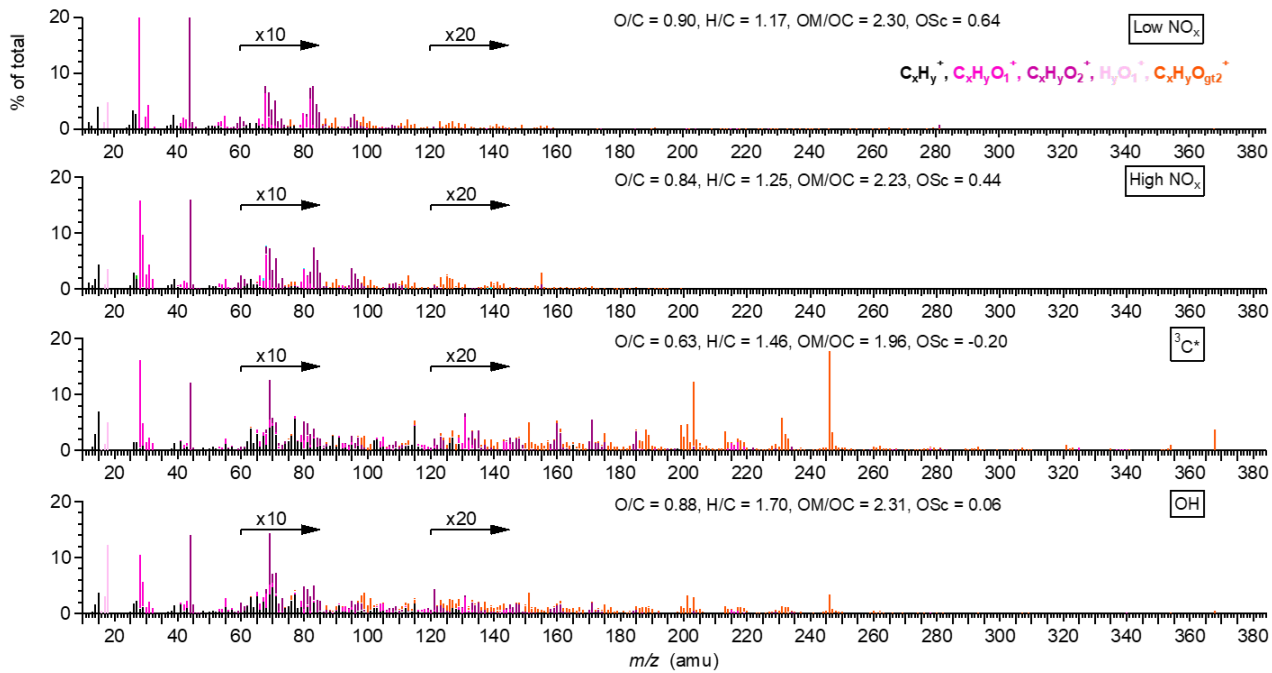


Figure 2. AMS spectra of SOA formed in the gas- and aqueous-phase reactions at  $t_{0.5}$ .

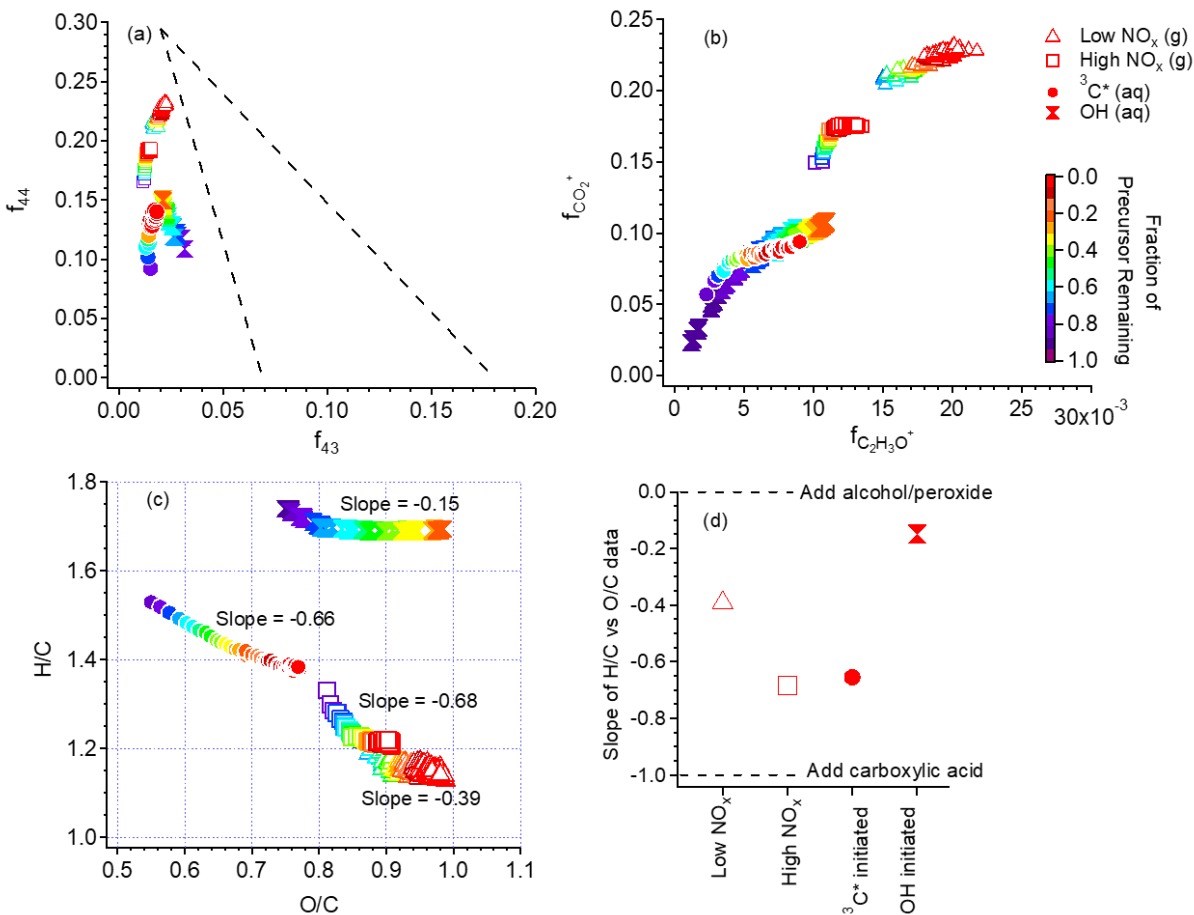


Figure 3. Evolution profiles of gasSOA and aqSOA in the (a)  $f_{44}$  vs.  $f_{43}$  space, (b)  $f_{CO_2^+}$  vs.  $f_{C_2H_3O^+}$  space, and (c) Van Krevelen diagram based on AMS measurements, and (d) summarized slopes of the SOA data from the Van Krevelen diagram

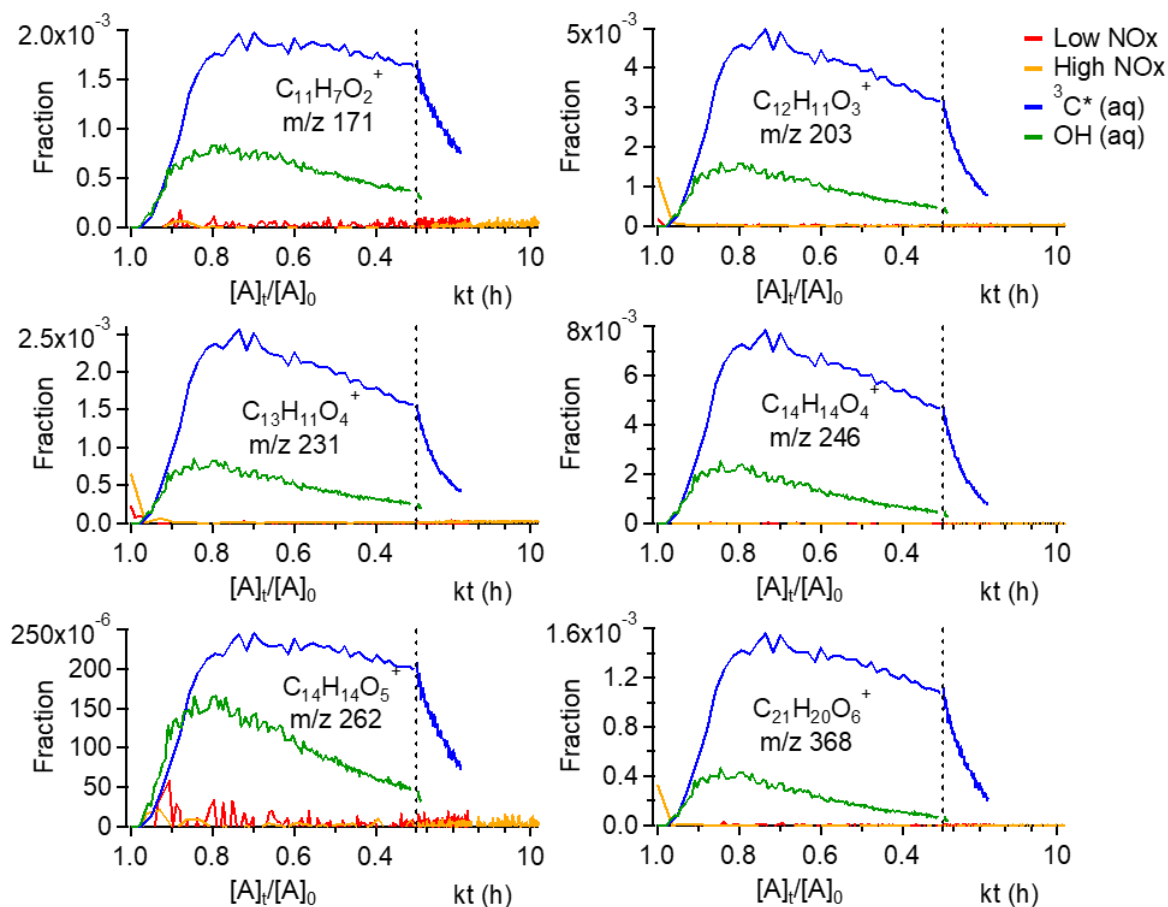


Figure 4. Mass fraction of previously proposed guaiacol oligomer MS fragments over the course of the gas- and aqueous-phase reactions. The fraction of guaiacol remaining in the reaction system at time  $t$  (i.e.,  $[A]_t/[A]_0$ ) indicates reaction progress up to the point that 75% of guaiacol has reacted, while  $kt$  (the product of the measured first-order rate constant for GUA loss and the reaction time) indicates reaction progress after 75% of GUA has reacted.

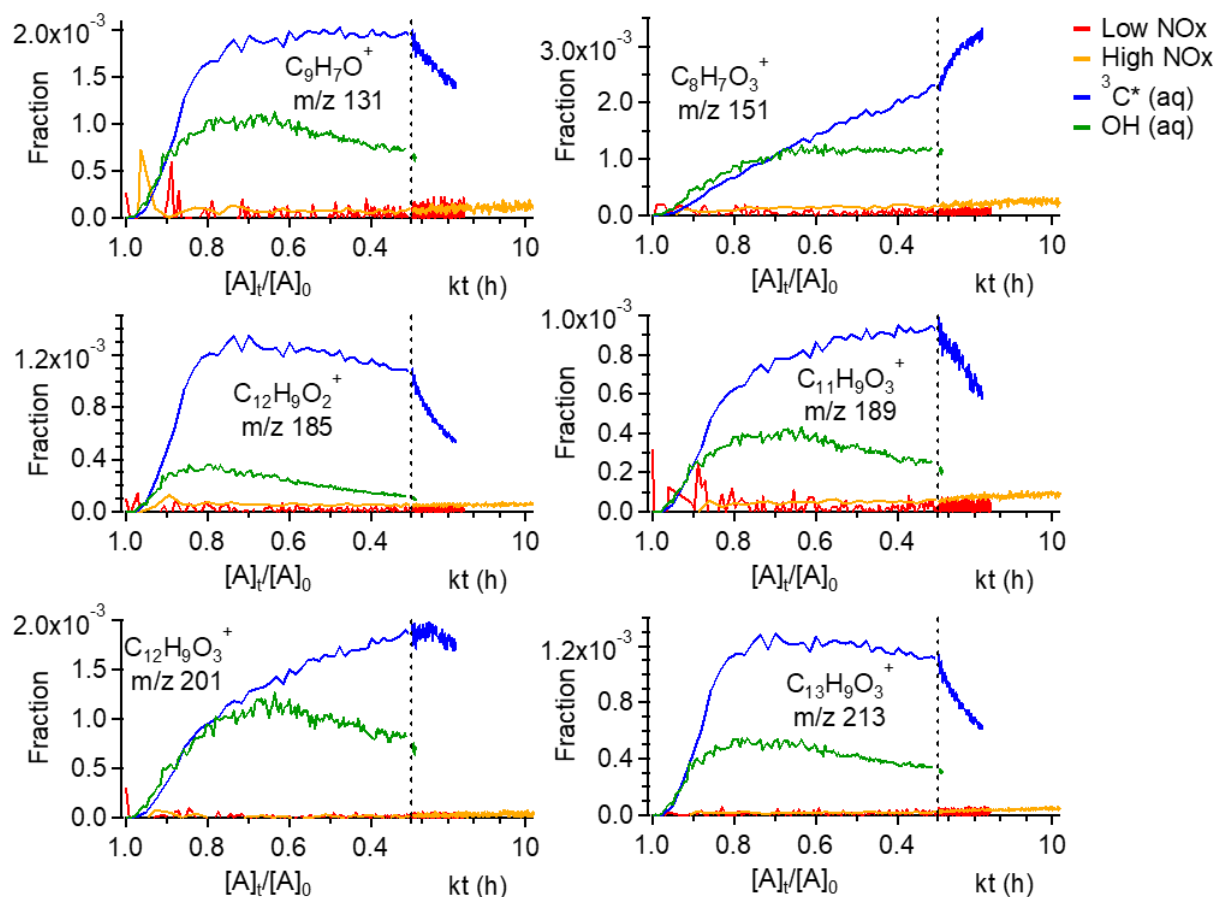


Figure 5. Mass fraction of six possible AMS tracer ions for guaiacol aqSOA over the courses of gas- and aqueous-phase reactions. The fraction of guaiacol remaining in the reaction system at time  $t$  ( $[A]_t/[A]_0$ ) is used as an indicator of reaction progress before 75% of the guaiacol has reacted. The  $kt$  (where  $k$  is the measured first-order rate constant for guaiacol loss and  $t$  is the reaction time) is used as an indicator of reaction progress after 75% of the guaiacol has reacted.

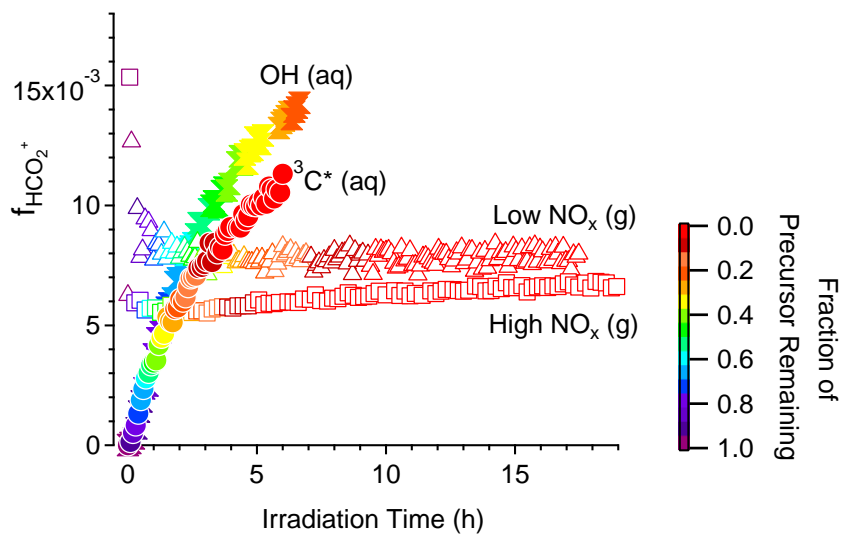


Figure 6. Mass fraction of  $\text{HCO}_2^+$  in the AMS spectra of gasSOA and aqSOA throughout the course of the reactions

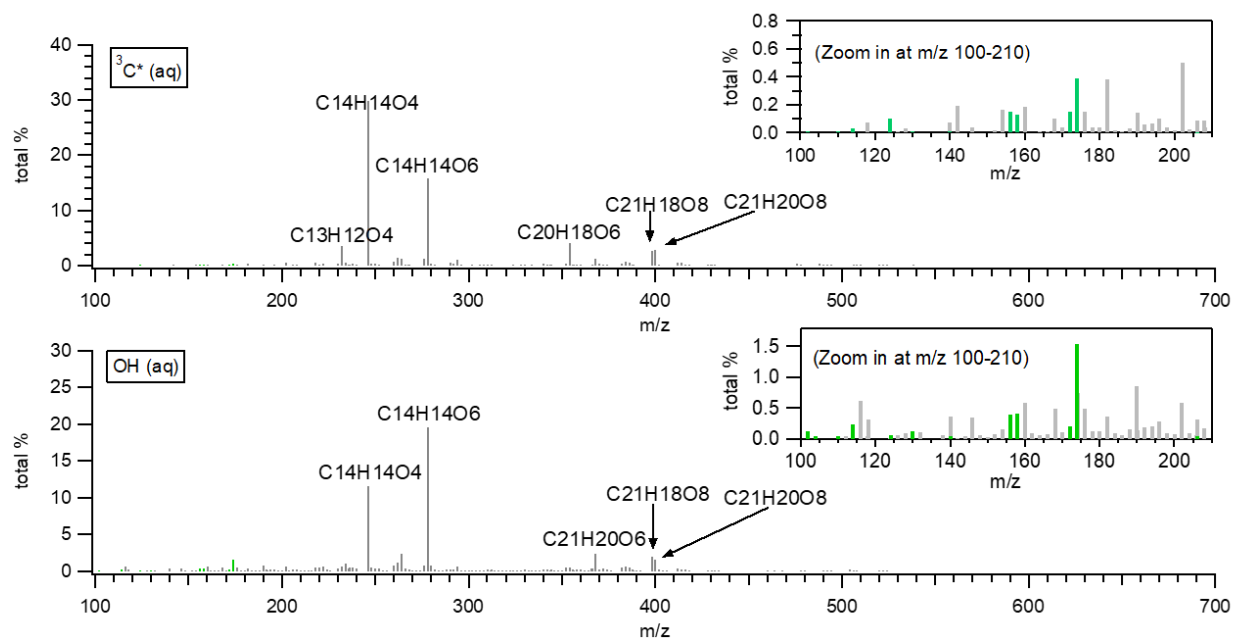


Figure 7. Nano-DESI MS of aqSOA produced from guaiacol reaction with  $^3\text{C}^*$  and OH at  $t_{0.5}$ . The green sticks represent the common products that have been identified in both aqSOA and gasSOA.



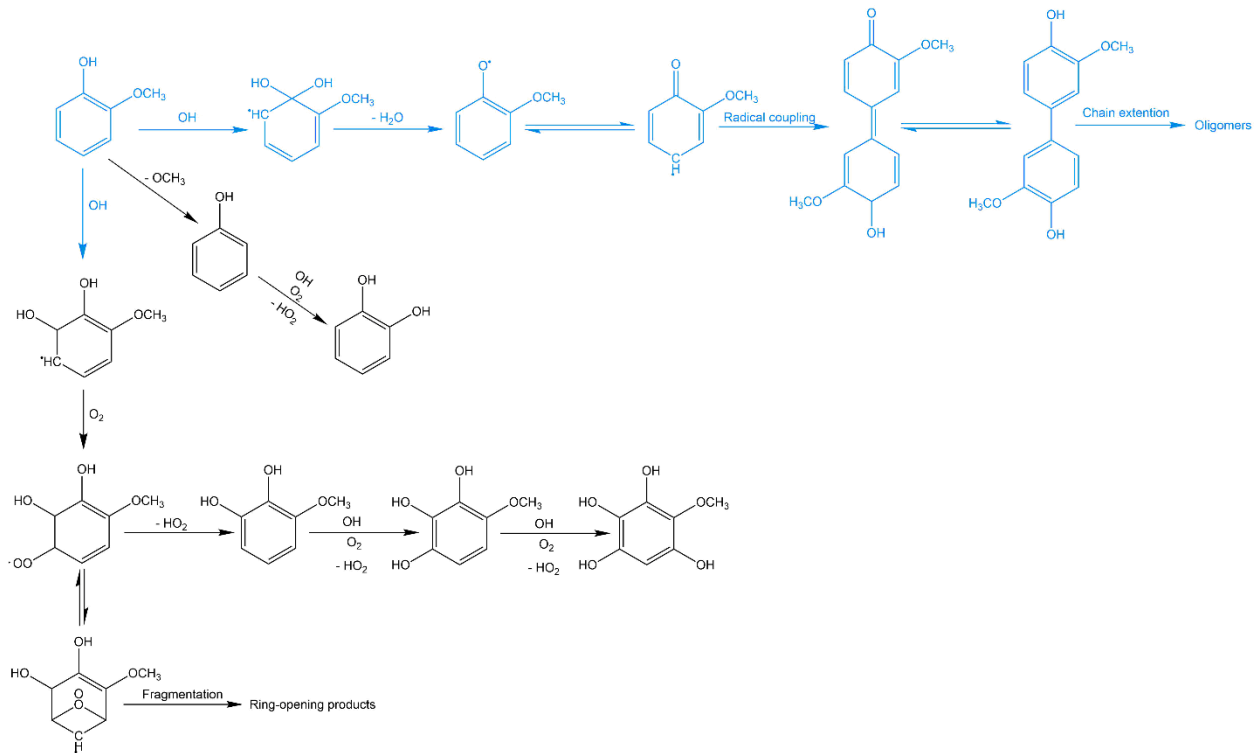


Figure 8. Proposed mechanisms for guaiacol photo-oxidation including hydroxylation, demethoxylation, oligomerization, and fragmentation. The black pathways occur in both gas and aqueous phases, while the blue pathways occur only in the aqueous phase.

## Supporting Information

Table S1. Experimental conditions of gas- and aqueous-phase photochemical experiments

Gas-phase	[Guaiacol] <sub>0</sub> (ppb)	Oxidant source	[NO <sub>2</sub> ] (ppb)	[NO] (ppb)	RH	Seed aerosol	Temp. (°C)	Light source
Low NO <sub>x</sub>	5.9	H <sub>2</sub> O <sub>2</sub>	< 5	< 5	< 10 %	Ammonium sulfate	20-26	Simulated sunlight peaks at 340–350 nm
High NO <sub>x</sub>	55.3	HONO	518	330				
Aqueous- phase	[Guaiacol] <sub>0</sub> (μM)	Oxidant source		Solution pH		Temp. (°C)	Light source	
3C* initiated	100	3,4- dimethoxybenzaldehyde		5		20	Simulated sunlight using 300, 350, and 419 nm bulbs	
OH initiated		H <sub>2</sub> O <sub>2</sub>						

Table S2. Elemental ratios, mass fractions of large ions ( $m/z > 124$  and  $m/z > 246$ ) in the AMS spectra, and the contribution of ion categories in the AMS spectra of gasSOA and aqSOA at  $t_{0.5}$  and  $t_{0.25}$

	$t_{0.5}$				$t_{0.25}$			
	Irradiation Time (h)	H/C	O/C	OSc	Irradiation Time (h)	H/C	O/C	OSc
Low NOx	2.35	1.17	0.9	0.64	4.68	1.16	0.93	0.69
High NOx	1.27	1.23	0.85	0.47	2.48	1.22	0.88	0.54
$^3C^*$	0.92	1.46	0.63	-0.2	1.82	1.41	0.69	-0.04
OH	3.17	1.7	0.88	0.07	6.32	1.7	0.98	0.27

Table S3. Effects of functionalization reactions on the H/C and O/C of SOA (Heald et al. 2010)

Reaction	Slop of H/C vs. O/C
+ water (Hydration)	2
+ alcohol/peroxide	0
+ carboxylic acid	-1
+ ketone/aldehyde	-2

Table S4. Top 10 most abundant products identified in the guaiacol aqSOA from  $^{13}\text{C}^*$  reaction at  $t_{0.5}$  by nano-DESI MS

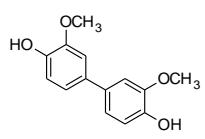
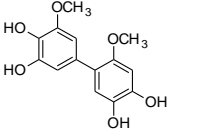
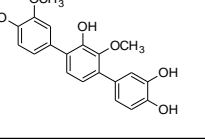
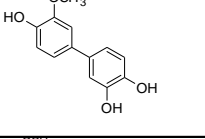
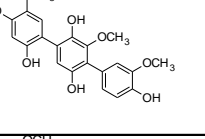
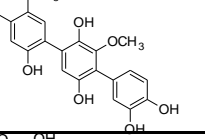
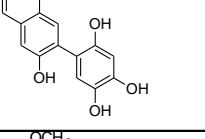
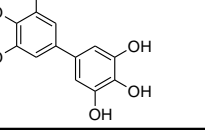
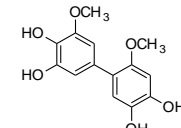
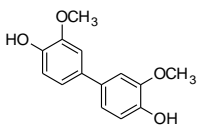
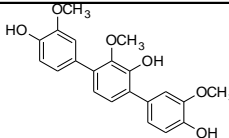
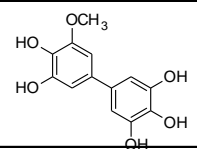
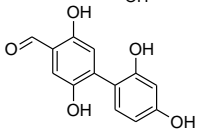
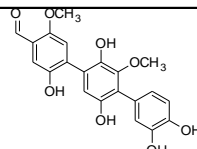
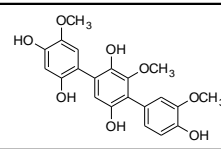
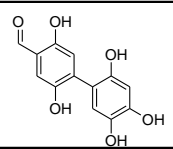
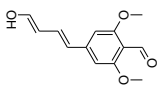
Intensity	Mass	Formula	Proposed Structure
29.8396	246.089	C14H14O4	
15.7181	278.079	C14H14O6	
4.07175	354.11	C20H18O6	
3.55069	232.074	C13H12O4	
2.7784	400.116	C21H20O8	
2.64177	398.1	C21H18O8	
1.34194	262.048	C13H10O6	
1.27556	264.063	C13H12O6	
1.23201	276.063	C14H12O6	
1.19055	246.053	C13H10O5	

Table S5. Top 10 most abundant products identified in the guaiacol aqSOA at  $t_{0.5}$  from OH reaction by nano-DESI MS

Intensity	Mass	Formula	Proposed Structure
19.6304	278.079	C <sub>14</sub> H <sub>14</sub> O <sub>6</sub>	
11.5625	246.089	C <sub>14</sub> H <sub>14</sub> O <sub>4</sub>	
2.36356	368.126	C <sub>21</sub> H <sub>20</sub> O <sub>6</sub>	
2.35575	264.063	C <sub>13</sub> H <sub>12</sub> O <sub>6</sub>	
2.30941	246.053	C <sub>13</sub> H <sub>10</sub> O <sub>5</sub>	
1.97805	398.1	C <sub>21</sub> H <sub>18</sub> O <sub>8</sub>	
1.53479	174.053	C <sub>7</sub> H <sub>10</sub> O <sub>5</sub>	
1.52664	400.116	C <sub>21</sub> H <sub>20</sub> O <sub>8</sub>	
1.24117	262.048	C <sub>13</sub> H <sub>10</sub> O <sub>6</sub>	
1.11124	234.089	C <sub>13</sub> H <sub>14</sub> O <sub>4</sub>	

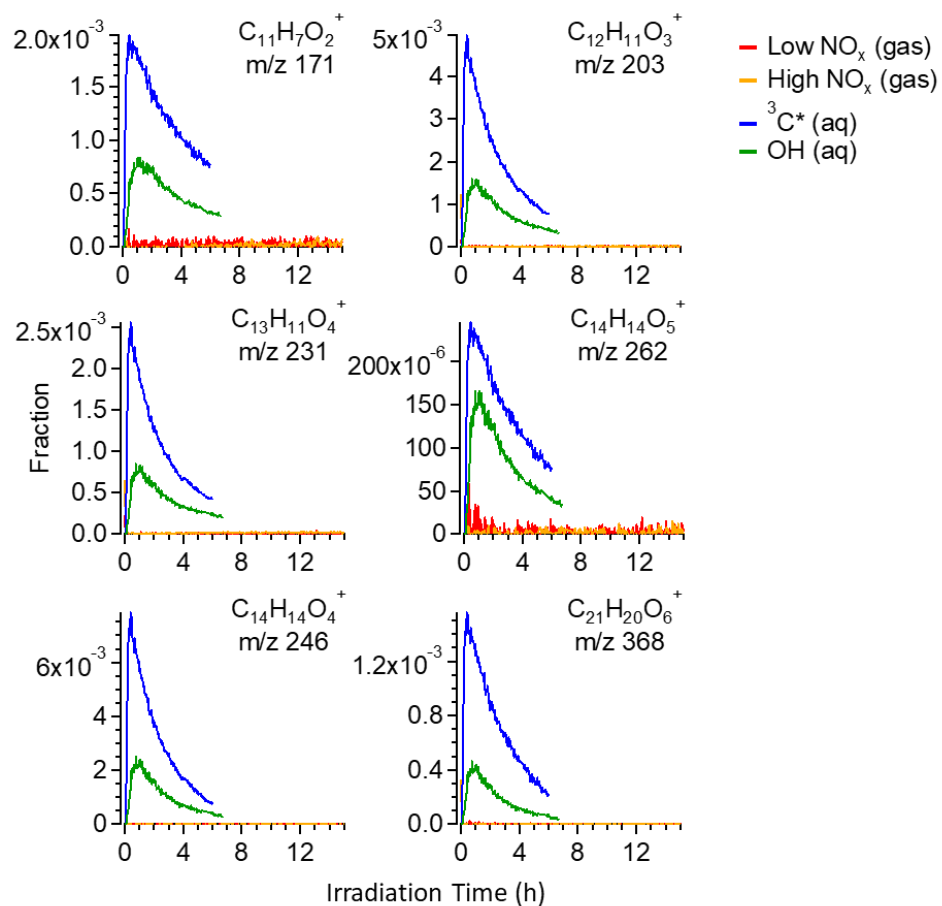


Figure S1. Mass fraction of previous proposed guaiacol oligomer MS fragments over the courses of gas- and aqueous-phase reactions

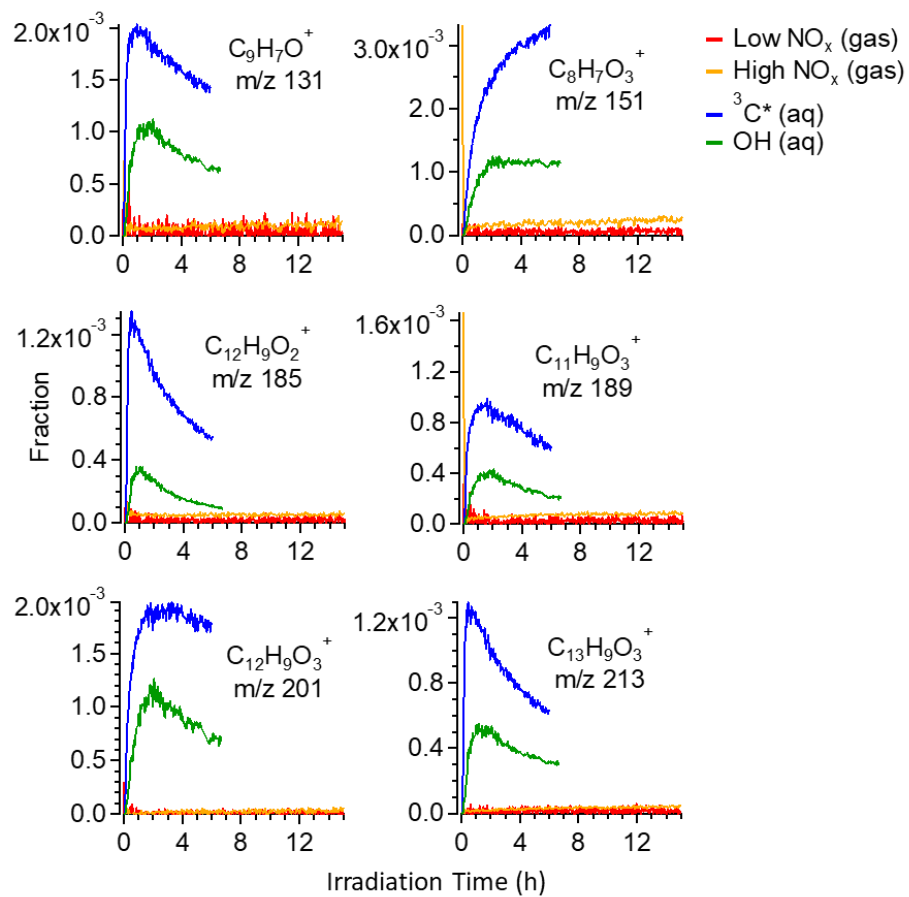


Figure S2. Mass fraction of possible AMS tracer ions for guaiacol aqSOA over the courses of gas- and aqueous-phase reactions



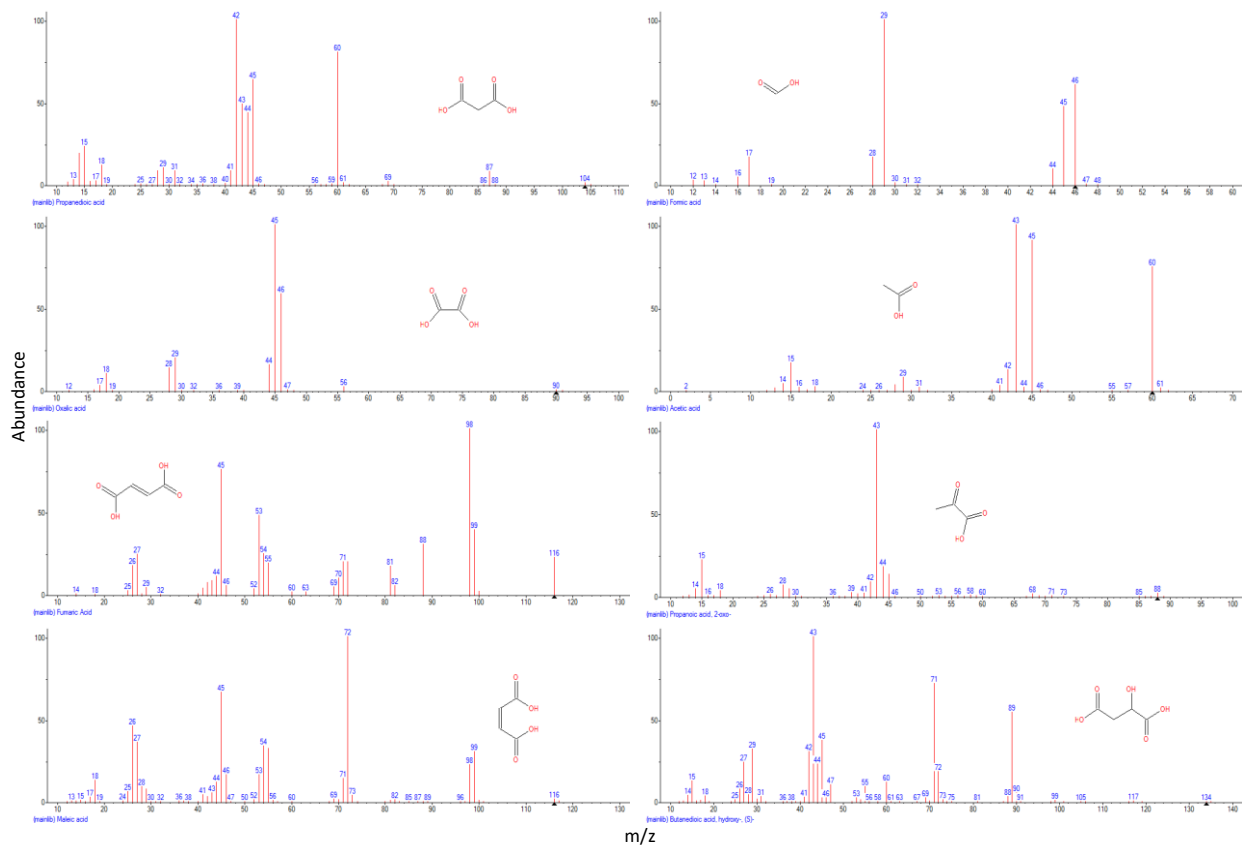


Figure S3. NIST MS spectra of eight common small organic acids in SOA

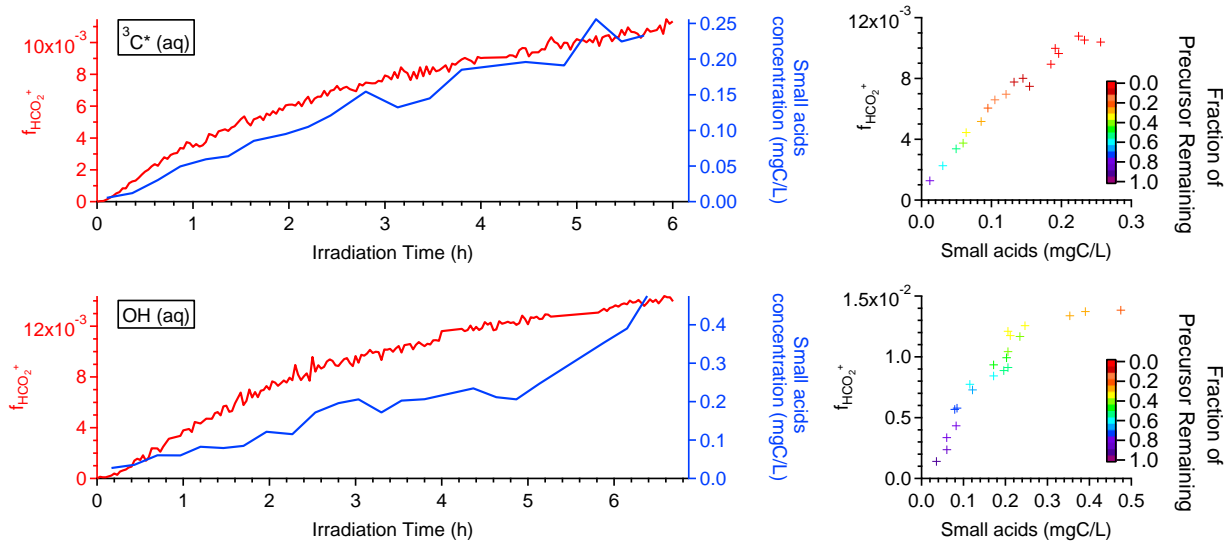


Figure S4. Time series of  $f_{\text{HCO}_2^+}$  and eight common small organic acids in aqSOA and the correlation between  $f_{\text{HCO}_2^+}$  and total small organic acid concentration

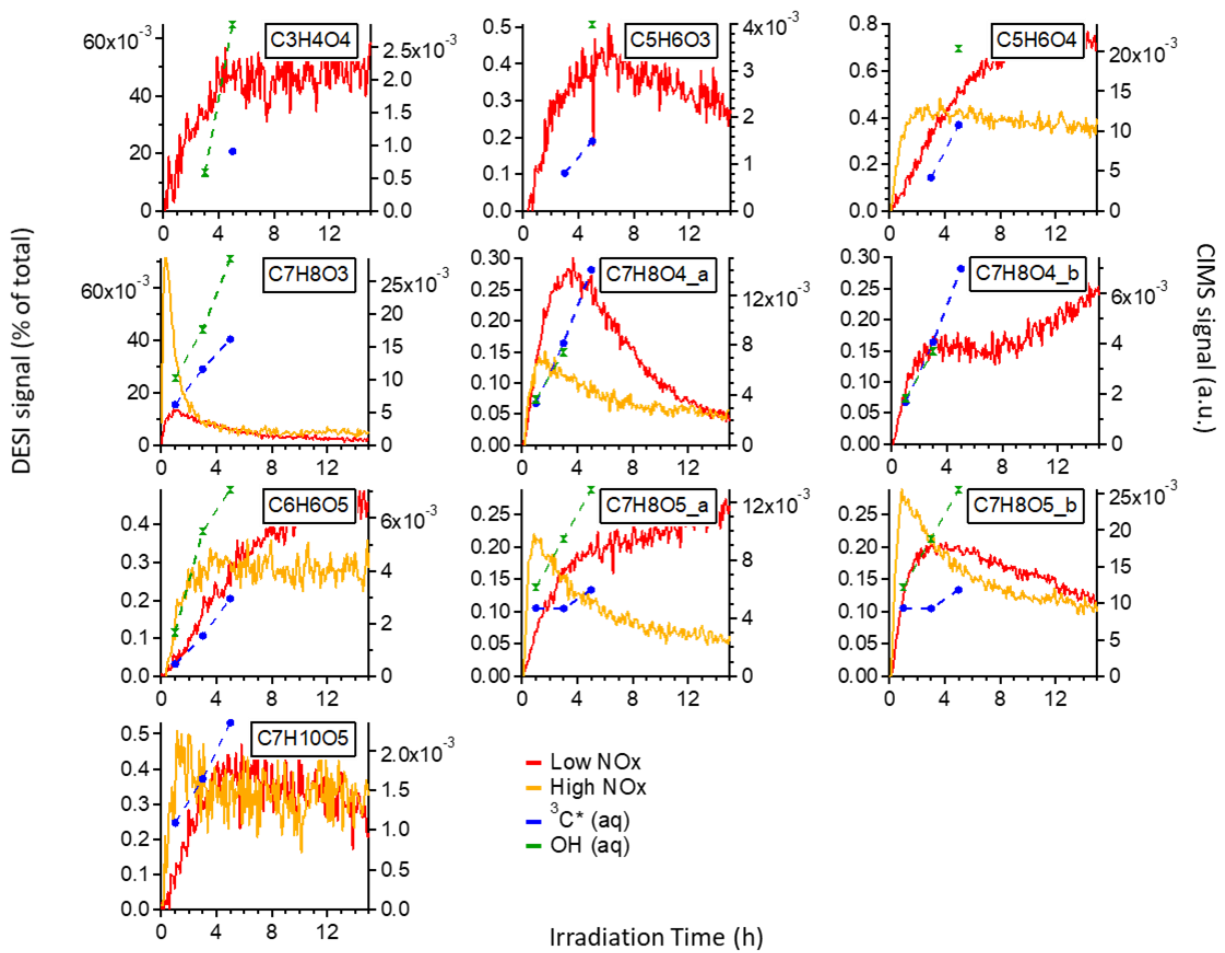


Figure S5. Time series of common products formed both in gasSOA and aqSOA

# Chapter 5: Chemical and Light-Absorption Properties of Water-Soluble Organic Aerosols in Northern California and Photooxidant Production by Brown Carbon Components

## 5.1 Abstract

Atmospheric brown carbon (BrC), which absorbs sunlight efficiently in the near-UV and visible ranges, can impact the radiative balance of the earth and initiate photoreactions that form oxidants. However, the light absorption and photochemical properties of BrC from different sources remain poorly understood. To address this gap, particulate matter (PM) samples were collected at Davis, CA from Nov 2019 to Oct 2020 and the water-soluble components were analyzed using high resolution aerosol mass spectrometry (HR-AMS), ion chromatography (IC), total organic carbon (TOC) analyzer, and ultraviolet–visible spectroscopy (UV-vis). In addition, the concentrations of three major aqueous-phase photooxidants, i.e., hydroxyl radical ( $\bullet\text{OH}$ ), singlet molecular oxygen ( $^1\text{O}_2^*$ ), and oxidizing triplet excited states of organic carbon ( $^3\text{C}^*$ ), were measured in dilute PM extracts during illumination with simulated sunlight.

Positive matrix factorization (PMF) applied to the combined HR-AMS and UV-vis data resolved five water-soluble organic aerosol (WSOA) factors with distinct mass spectra and UV-vis spectra profiles: a fresh and an aged water-soluble biomass burning organic aerosol ( $\text{wsBBOA}$ ) and three types of water-soluble oxygenated OA ( $\text{wsOOA}$ ) with different degrees of oxidation. The fresh  $\text{wsBBOA}$  is the most light-absorbing, with a mass absorption coefficient (MAC) of  $1.1 \text{ m}^2 \text{ g}^{-1}$  at 365 nm. The aged  $\text{wsBBOA}$  is significantly less absorbing ( $\text{MAC}_{365 \text{ nm}} = 0.25 \text{ m}^2 \text{ g}^{-1}$ ) while the  $\text{wsOOAs}$  are the least ( $\text{MAC}_{365 \text{ nm}} = 0.01 - 0.1 \text{ m}^2 \text{ g}^{-1}$ ). Absorption Ångström exponent

values of the fresh and aged  $w_s$ BBOA ( $AAE_{300-400nm} = 6.0$  and  $6.8$ , respectively) are lower than those of the  $w_s$ OOAs ( $7.2 - 14.7$ ). These results, together with the high abundance of  $w_s$ BBOA (average =  $51.9\%$  of the WSOA mass) in Davis, indicate that biomass burning activities, such as residential wood burning and wildfires, are an important source of BrC in northern California. Together, fresh and aged  $w_s$ BBOAs account for nearly  $90\%$  of the total rate of sunlight absorption by water-soluble  $PM_{2.5}$  in Davis. We also explored the relationships between WSOA composition and  $\bullet OH$ ,  $^1O_2^*$ , and  $^3C^*$  concentrations and estimated the oxidant production potentials of different WSOA factors. The photoexcitation of BrC chromophores from BB emissions and in highly aged OOA appears to be a potent source of  $^1O_2^*$  and  $^3C^*$ . Finally, based on applying our OA potentials to archived AMS data, we estimated concentrations of oxidants in clouds at dozens of sites in the northern hemisphere. The results suggest that oxygenated organic species play an important role in photooxidant formation in atmospheric waters.

## 5.2 Introduction

While atmospheric organic aerosols (OA) are typically considered to be light scattering (Seinfeld and Pandis, 2016), brown carbon (BrC) OA species absorb light in the visible and near-UV ranges (Andreae and Gelencsér, 2006). Unlike black carbon (BC), whose light absorption is only weakly wavelength dependent, BrC tends to absorb light much more efficiently at shorter wavelengths and thus has a larger absorption Ångström exponent (AAE) (Andreae and Gelencsér, 2006; Hecobian et al., 2010; Laskin et al., 2015). In field studies BrC contributed up to  $15\%$  of sunlight absorption by aerosols over the UV–vis spectrum and up to  $50\%$  at shorter wavelengths (Hoffer et al., 2006; Kirchstetter and Thatcher, 2012; Shamjad et al., 2016). In addition, according to model simulations, BrC accounts for  $21\%$  of the global mean surface OA concentration (Jo et al., 2016) and has a radiative forcing in the range of  $0.1-0.25\text{ W m}^{-2}$ , approximately  $25\%$  of the

radiative forcing by BC, enough to offset the cooling effect by non-absorbing OA (Chung et al., 2012; Feng et al., 2013).

By absorbing sunlight, BrC can also influence photochemical reactions and oxidant concentrations in the atmosphere. On the one hand, BrC absorption decreases surface actinic flux, especially in the UV range, thus leading to lower photolysis rates and lower production rates of ozone and radicals (e.g.,  $\bullet\text{OH}$ ,  $\text{HO}_2\bullet$ , and  $\text{RO}_2\bullet$ ) (Jo et al., 2016; Mok et al., 2016). For example, modeling has shown that BrC absorption can cause up to a 10% decrease of  $\bullet\text{OH}$  concentrations in the boundary layer over the Northern Hemisphere, and up to a 6% decrease of surface ozone concentration in Asia due to reductions in the  $\text{NO}_2$  photolysis rate (Jo et al., 2016). On the other hand, BrC compounds (such as aromatic carbonyls) can act as an important source of photochemically generated oxidants such as oxidizing triplet excited states of organic carbon ( $^3\text{C}^*$ ), singlet molecular oxygen ( $^1\text{O}_2^*$ ) and  $\bullet\text{OH}$  in aerosol water and cloud/fog droplets (González Palacios et al., 2016; Hawkins et al., 2018; Kaur et al., 2019; Kaur and Anastasio, 2017; Smith et al., 2016). Both  $^3\text{C}^*$  and  $^1\text{O}_2^*$  can be oxidants for electron-rich compounds, such as phenols (Canonica et al., 2000; Scully and Hoigné, 1987; Smith et al., 2014; Yu et al., 2014), isoprene and monoterpenes (Aregahegn et al., 2013), amino compounds (Canonica et al., 2006; Matheson and Lee, 1979), and aromatic hydrocarbons (Al-Nu'airat et al., 2021; Darmanyan et al., 1998).

The sources of BrC are complex, including both direct emissions from combustion processes and formation of light-absorbing compounds from reactions of biogenic and anthropogenic precursors (Bond et al., 2004; Laskin et al., 2015; Saleh et al., 2015). Global simulations estimate that burning of biomass and biofuel emits  $\sim 3.9$  and  $\sim 3.0$  Tg  $\text{yr}^{-1}$  of primary BrC, respectively, together accounting for 28% of BrC sources to surface air (Jo et al., 2016). Secondary BrC production is estimated at 5.7 Tg  $\text{yr}^{-1}$ , contributing to 23% of surface BrC (Jo et al., 2016). Field

studies also find that combustion emissions and secondary production are important sources of BrC (Hecobian et al., 2010; Laskin et al., 2015; Moschos et al., 2018). There are numerous formation pathways for secondary BrC, including reactions of ammonia or amines with carbonyls (Flores et al., 2014; Kampf et al., 2016; Laskin et al., 2014), oligomerization of glyoxal and methylglyoxal during cloud processing (Hawkins et al., 2014), aqueous formation of humic-like substances (HULIS) (Claeys et al., 2012; Gao et al., 2006), and aqueous oxidation of phenolic compounds (Jiang et al., 2021; Smith et al., 2016; Yu et al., 2014).

The chemical compositions of atmospheric BrC are complex and their optical and photochemical properties remain poorly characterized. A common approach for studying BrC is by performing solvent extractions of ambient PM samples and then measuring the UV-vis absorptivity and chemical characteristics of the PM extracts (Deng et al., 2022; Hecobian et al., 2010; Kirchstetter et al., 2004; Kirillova et al., 2014; Li et al., 2020; Liu et al., 2013; Moschos et al., 2018; Zhang et al., 2017). Aerosol mass spectrometry (AMS) is a particularly useful method for analyzing PM extracts and providing information about the sources and processes of BrC. For example, Moschos et al. (2018) estimated the sources and light absorption properties of several major BrC components in ambient PM by applying positive matrix factorization (PMF) on the combined dataset of AMS mass spectra and UV-vis spectra of the water-soluble fractions of ambient PM from Switzerland. Furthermore, Kaur et al. recently studied the photoactivity of atmospheric BrC by determining the concentrations of major condensed-phase oxidants (i.e.,  $\bullet\text{OH}$ ,  $^1\text{O}_2^*$  and  $^3\text{C}^*$ ) in dilute aqueous extracts of ambient PM and in fog waters during illumination (Kaur et al., 2019; Kaur and Anastasio, 2017, 2018).

In this study, we characterized the chemical composition and optical properties of water-soluble BrC species in  $\text{PM}_{2.5}$  samples collected at Davis, a small city in northern California, over

a period of one year. PMF was applied on the combined AMS and UV-vis spectral data to determine the bulk composition and mass absorption coefficient (MAC) spectra of major BrC components. Furthermore, concentrations of  $\bullet\text{OH}$ ,  $^1\text{O}_2^*$  and  $^3\text{C}^*$  were measured in dilute PM extracts illuminated by simulated sunlight and the relationships between WSOA composition and the photo-formation of aqueous-phase oxidants were explored. The oxidant production potentials of different BrC components were also estimated, and the results were used to estimate aqueous-phase concentrations of oxidants in clouds at dozens of sites worldwide.

## **5.3 Materials and Methods**

### **5.3.1 PM sample collection and extraction**

PM<sub>2.5</sub> samples were collected at Davis, CA (38.5449° N, 121.7405° W, ~ 15 miles to the southwest of Sacramento) from November 2019 to October 2020. Particles were collected on Teflon-coated quartz filters using a high-volume sampler with a PM<sub>2.5</sub> inlet. Each sample was collected for 24 h or one week continuously (Table S1). Immediately after sampling, a filter was wrapped in pre-baked aluminum foil, sealed in a Ziplock bag, and stored at -20 °C until extraction. The extraction procedure includes cutting a 2 cm × 2 cm piece off the filter, placing it in an amber glass vial with 1.0 mL of Milli-Q water, and shaking for 4 hours on a shaker (VWR OS-500) in the dark. Afterwards, the water extract was filtered by 0.22 μm PTFE filter, flash frozen using liquid N<sub>2</sub> and stored at -20 °C until use. The extraction procedure corresponds to an equivalent liquid water content (LWC) for the PM in the range of 9-66 mg-H<sub>2</sub>O m<sup>-3</sup>-air (Table S1), i.e., relatively concentrated cloud and fog drops.

### **5.3.2 Chemical and optical analyses of PM extracts**



PM extracts were analyzed for 1) major anions (i.e.,  $F^-$ ,  $Cl^-$ ,  $Br^-$ ,  $NO_3^-$ ,  $PO_4^{3-}$ ,  $SO_4^{2-}$  and formate) and cations (i.e.,  $Li^+$ ,  $Na^+$ ,  $NH_4^+$ ,  $K^+$ ,  $Ca^{2+}$  and  $Mg^{2+}$ ) using two ion chromatographs (881 Compact IC Pro, Metrohm) equipped with conductivity detectors; 2) water-soluble organic carbon (WSOC) using a total organic carbon analyzer (TOC-VPCH, Shimadzu); 3) light absorbance using a UV-Vis spectrophotometer (UV-2501PC, Shimadzu); and 4) mass concentrations and mass spectra of water-soluble organics, sulfate, nitrate, ammonium, and chloride using a high-resolution time-of-flight aerosol mass spectrometer (HR-AMS, Aerodyne Res. Inc). Prior to AMS analysis, PM extracts were spiked with isotopic  $^{34}S$  sulfate ( $^{34}SO_4^{2-}$ ) as an internal standard and nebulized in argon (Ar, industrial grade, 99.997%) using a micronebulization assembly (Niedek et al., 2022). The AMS was operated in the “V” mode (mass resolutions of  $\sim 3000$ ) to acquire mass spectra up to  $m/z = 425$  amu. AMS analyzes non-refractory aerosol species that evaporate at  $\sim 600$  °C under high vacuum via 70 eV EI mass spectrometry (Canagaratna et al., 2007; DeCarlo et al., 2006).

### 5.3.3 Measurements of photooxidants

The concentrations of three photooxidants -  $\bullet OH$ ,  $^1O_2^*$ , and  $^3C^*$  - were measured in the illuminated PM extracts using methods detailed in Kaur et al. (2019) and Ma et al. (In Preparation). Benzoic acid (BA) was used as the probe to quantify  $\bullet OH$  via BA loss and para-hydroxybenzoic acid formation, determined throughout illumination by a high-performance liquid chromatograph equipped with UV-vis detector (HPLC-UV). The  $^1O_2^*$  concentration was quantified using furfuryl alcohol (FFA) as the probe and deuterium oxide ( $D_2O$ ) as a diagnostic tool. For this analysis, two aliquots of the PM extract were taken: one was diluted 50% by  $H_2O$ , and the other was diluted 50% by  $D_2O$ . The diluted PM extracts were spiked with FFA and illuminated, and the loss of FFA was detected using HPLC-UV. The  $^3C^*$  concentration was measured using syringol (SYR) as the probe, and the loss of SYR was measured by HPLC-UV.

### 5.3.4 Data analysis

#### 5.3.4.1 UV-Vis absorption properties

The light absorption coefficient ( $\alpha_\lambda$ ,  $\text{cm}^{-1}$ ) of each PM extract was calculated as:

$$\alpha_\lambda = \frac{A_\lambda}{l} \quad (\text{Eq. 1})$$

where  $A_\lambda$  is the measured base-10 light absorbance of the PM extract at wavelength  $\lambda$ , and  $l$  is the pathlength of the cuvette (1 cm). The mass absorption efficiency ( $\text{MAC}_\lambda$ ,  $\text{m}^2 \text{g}^{-1}$ ) of the PM extract was calculated as:

$$\text{MAC}_\lambda = \frac{2.303 \times \alpha_\lambda}{C} \times 100 \quad (\text{Eq. 2})$$

where  $C$  is the WSOA mass concentration ( $\text{mg L}^{-1}$ ) in the PM extract measured by AMS, 2.303 is a conversion factor between  $\log_{10}$  and natural log, and 100 is for unit conversion. The rate of sunlight absorption of the PM extract ( $R_{\text{abs}}$ ,  $\text{mol photons L}^{-1} \text{s}^{-1}$ ) was calculated as:

$$R_{\text{abs}} = 2.303 \times \frac{10^3}{N_A} \times \sum_{290 \text{ nm}}^{500 \text{ nm}} (\alpha_\lambda \times I_\lambda \times \Delta\lambda) \quad (\text{Eq. 3})$$

where  $I_\lambda$  is the Davis winter-solstice actinic flux ( $\text{photons cm}^{-2} \text{s}^{-1} \text{nm}^{-1}$ ) from the Tropospheric Ultraviolet and Visible (TUV) Radiation Model version 5.3 ([https://www.acom.ucar.edu/Models/TUV/Interactive\\_TUV/](https://www.acom.ucar.edu/Models/TUV/Interactive_TUV/)),  $\Delta\lambda$  is the interval between adjacent wavelengths in the TUV output, 2.303 is for base conversion between  $\log_{10}$  and natural log,  $10^3$  is for unit conversion, and  $N_A$  is Avogadro's number. The absorption Ångström exponent (AAE) of the PM extract was fitted by Eq. 4:

$$\text{MAC}_\lambda = k \times \lambda^{-\text{AAE}} \quad (\text{Eq. 4})$$

where  $k$  is a wavelength-independent constant.

### 5.3.4.2 AMS data treatment and quantification of PM species

The AMS data were processed using the standard analysis toolkits (SQUIRREL v1.65C and PIKA 1.25C). The organic water signals were parameterized using the standard method for HR-AMS ambient data processing:  $\text{H}_2\text{O}^+ = 0.225 \times \text{CO}_2^+$ ,  $\text{HO}^+ = 0.25 \times \text{H}_2\text{O}^+$ , and  $\text{O}^+ = 0.04 \times \text{H}_2\text{O}^+$  (Aiken et al., 2008; Allan et al., 2004). Due to the use of Ar,  $\text{CO}^+$  signal was quantified directly (Yu et al., 2014). The atomic ratios of oxygen-to-carbon (O/C), hydrogen-to-carbon (H/C) and organic mass-to-carbon ratio (OM/OC) in the WSOA were calculated using the Aiken-Ambient method (Aiken et al., 2008).

By using the  $^{34}\text{S}$  sulfate internal standard, concentrations of water soluble PM components (i.e., sulfate, nitrate, organics, ammonium, and chloride) can be quantitatively determined via AMS analysis (Niedek et al., 2022). The concentration of species X in PM extract solution ( $[\text{X}]_{\text{solution}}$ ,  $\mu\text{g mL}^{-1}$ ) was calculated as:

$$[\text{X}]_{\text{solution}} = [\text{X}]_{\text{AMS}} \times \frac{[^{34}\text{sulfate}]_{\text{solution}}}{[^{34}\text{sulfate}]_{\text{AMS}}} \quad (\text{Eq. 5})$$

where  $[\text{X}]_{\text{AMS}}$  and  $[^{34}\text{sulfate}]_{\text{AMS}}$  are the AMS-measured concentrations ( $\mu\text{g m}^{-3}$ ) of X and the spiked  $^{34}\text{S}$  sulfate, respectively, in the aerosolized PM extract, and  $[^{34}\text{sulfate}]_{\text{solution}}$  is the known concentration ( $\mu\text{g mL}^{-1}$ ) of the  $^{34}\text{S}$  sulfate internal standard in the PM extract.

Next, the ambient concentration of X ( $[\text{X}]_{\text{ambient}}$ ,  $\mu\text{g m}^{-3}$ ) was calculated as:

$$[\text{X}]_{\text{ambient}} = \frac{[\text{X}]_{\text{solution}} \times V_{\text{extract}}}{V_{\text{air}}} \quad (\text{Eq. 6})$$

where  $V_{\text{extract}}$  is the volume (mL) of the PM extract solution, and  $V_{\text{air}}$  is the total volume ( $\text{m}^3$ ) of air sampled by a square cut of filter.

Figure S1 shows the comparisons of the AMS measured concentrations of water-soluble species versus those by IC measurements. AMS and IC agreed reasonably well for the measurements of sulfate concentration, while nitrate concentration was  $\sim 2$  times lower in AMS, which is likely due to evaporation of  $\text{NH}_4\text{NO}_3$  in the heated micronebulization spray chamber before AMS measurements. Thus, the IC-measured nitrate concentrations are reported in this study. In addition, as shown in Figure S2, the AMS measured organic carbon concentration agrees well with the TOC measurements.

#### 5.3.4.3 PMF analysis of combined AMS mass spectra and UV-Vis absorption spectra

To understand the chemical compositions and light absorption properties of WSOA components from different sources, positive matrix factorization (PMF) was performed on the combined matrix of the AMS spectra and the UV-vis spectra of the PM extracts. The AMS spectral matrix includes the high resolution mass spectra (HRMS) of organic ions between  $m/z$  12–120, selected phenolic tracer ions with  $m/z > 120$ , including  $\text{C}_7\text{H}_5\text{O}_2^+$ ,  $\text{C}_7\text{H}_8\text{O}_3^+$ ,  $\text{C}_8\text{H}_7\text{O}_3^+$ ,  $\text{C}_7\text{H}_8\text{O}_4^+$ ,  $\text{C}_8\text{H}_{10}\text{O}_4^+$ ,  $\text{C}_{10}\text{H}_{12}\text{O}_4^+$ ,  $\text{C}_{14}\text{H}_{11}\text{O}_3^+$ ,  $\text{C}_{14}\text{H}_{14}\text{O}_4^+$ ,  $\text{C}_{14}\text{H}_{14}\text{O}_5^+$ ,  $\text{C}_{18}\text{H}_{14}\text{O}_4^+$ ,  $\text{C}_{18}\text{H}_{17}\text{O}_5^+$ ,  $\text{C}_{16}\text{H}_{18}\text{O}_7^+$ ,  $\text{C}_{20}\text{H}_{22}\text{O}_6^+$ ,  $\text{C}_{21}\text{H}_{20}\text{O}_7^+$  (Jiang et al., 2021; Yu et al., 2014), and major inorganic ions, including  $\text{SO}_x^+$  ions (i.e.,  $\text{SO}^+$ ,  $\text{SO}_2^+$ ,  $\text{HSO}_2^+$ ,  $\text{SO}_3^+$ ,  $\text{HSO}_3^+$ ,  $\text{H}_2\text{SO}_4^+$ ) and  $\text{NO}_x^+$  ions (i.e.,  $\text{NO}^+$  and  $\text{NO}_2^+$ ) (Sun et al., 2012), and the unit mass solution (UMR) spectral signals at  $m/z$  121–425. The UV-vis spectral matrix includes the absorption spectra in the range of 290 – 500 nm. The PMF results were evaluated using the PMF Evaluation Toolkit (PET v3.08 downloaded from: [http://cires1.colorado.edu/jimenez-group/wiki/index.php/PMF-AMS\\_Analysis\\_Guide](http://cires1.colorado.edu/jimenez-group/wiki/index.php/PMF-AMS_Analysis_Guide)). The 5-factor solution with  $f_{\text{Peak}} = 0$  was chosen based on the evaluation criteria (Ulbrich et al., 2009; Zhang et al., 2011). A summary of the diagnostic plots for the 5-factor PMF solution is presented

in Figure S3. The calculations of organic and inorganic species concentrations and mass absorption coefficients for the PMF factors are presented in Section S1.

#### 5.3.4.4 Estimation of the oxidant formation potentials of the WSOA factors

In order to estimate the oxidant formation potentials of different WSOA factors, linear decomposition was performed on the concentration series of each one of the three oxidants measured in the illuminated PM extract (i.e., [ $\bullet$ OH], [ $^1$ O $_2^*$ ], or [ $^3$ C\*]; mol/L) as the linear combination of the concentration series of the 5 WSOA factors derived by PMF (i.e., [wsBBOA<sub>fresh</sub>], [wsBBOA<sub>aged</sub>], [wsOOA<sub>1</sub>], [wsOOA<sub>2</sub>], [wsOOA<sub>3</sub>]; mg/L):

$$[\text{Ox}]_{\text{mea}} = a \cdot [\text{wsBBOA}_{\text{fresh}}] + b \cdot [\text{wsBBOA}_{\text{aged}}] + c \cdot [\text{wsOOA}_1] + d \cdot [\text{wsOOA}_2] + e \cdot [\text{wsOOA}_3] + \epsilon_{\text{ox}}$$

(Eq. 7)

where [ $\text{Ox}$ ]<sub>mea</sub> is an array of the measured concentrations of a given oxidant, a – e are the least-squares fitting parameters, and  $\epsilon_{\text{ox}}$  is the residual vector. Here, a-e are in the units of mol-oxidant/mg-organic, representing the oxidant production potentials of the corresponding WSOA factors.  $\epsilon_{\text{ox}}$  (mol/L) represents the differences between the measured and the modeled oxidant concentrations.

## 5.4 Results and Discussions

### 5.4.1 Bulk composition and light absorption properties of WSOA in PM<sub>2.5</sub>

A total of 17 Davis PM<sub>2.5</sub> water extract samples were characterized, of which 7 were collected during summer, 7 during winter, one during spring and two during fall (Table S1). Four of the summer PM extracts were significantly impacted by wildfires. Figure 1 summarizes the chemical composition and light absorption properties of the water-soluble PM (WS-PM) components. The

WS-PM concentration is in the range of 1.0 – 16.3  $\mu\text{g m}^{-3}$  and represents 12% – 52% of the total ambient  $\text{PM}_{2.5}$  mass (Figure 1a). WSOA is a dominant component, accounting for 26% – 83% of the WS-PM mass, while nitrate contributes substantially (up to 50%) during winter (Figure 1b). The WSOA is moderately oxidized, with O/C ratios in the range of 0.43 – 0.71 and H/C ratios in the range of 1.25 – 1.45 (Figure 1c and Figure S5c). Figure 1d shows the mass fractions of three AMS tracer ions:  $\text{CHO}_2^+$  ( $m/z = 44.998$ ; a marker for carboxylic acids (Jiang et al., 2021)),  $\text{C}_2\text{H}_4\text{O}_2^+$  ( $m/z = 60.021$ ; a tracer for anhydrous sugars (e.g., levoglucosan) (Cubison et al., 2011)), and  $\text{C}_{14}\text{H}_{14}\text{O}_4^+$  ( $m/z = 246.089$ ; a tracer for phenolic aqueous secondary organic aerosol (aqSOA) (Yu et al., 2014)). The fractional contribution of  $\text{CHO}_2^+$  to the total WSOA signal ( $f_{\text{CHO}_2^+}$ ) ranges between 0.5 – 1.5% in the samples, suggesting a relatively stable content of carboxylic acids in the WSOA. However, both  $f_{\text{C}_2\text{H}_4\text{O}_2^+}$  and  $f_{\text{C}_{14}\text{H}_{14}\text{O}_4^+}$  increase significantly in the wildfire-influenced samples and in the winter samples (Figures 1d and S5b), indicating significant contributions of primary and secondary BBOAs by transported wildfire plumes as well as by winter-time residential wood combustion. In addition, as shown in Figure 1e and 1g, the wildfire-influenced samples are significantly more light absorbing, showing higher  $\text{MAC}_{365\text{nm}}$  (up to 1.1  $\text{m}^2 \text{g}^{-1}$ ) and lower  $\text{AAE}_{300-400\text{nm}}$  (down to 5.8), than the other samples whose  $\text{MAC}_{365\text{nm}}$  are in the range of 0.08 – 0.55 and the  $\text{AAE}_{300-400\text{nm}}$  are in the range of 6.8 – 9.9. These results are consistent with previous findings that biomass burning is an important source of BrC in the atmosphere (Laskin et al., 2015).

#### 5.4.2 Chemical compositions and light absorption of WSOA factors

To gain insights into the chemical and optical properties of different WSOA components, we performed PMF analysis on the combined AMS and UV–vis absorption data of the WS- $\text{PM}_{2.5}$  (see Sect. 5.3.4.3 for more details) and resolved five distinct WSOA factors. The first two factors are closely related to biomass burning: fresh water-soluble BBOA ( $\text{wsBBOA}_{\text{fresh}}$ ; O/C = 0.37,

MAC<sub>365nm</sub> = 1.1 m<sup>2</sup> g<sup>-1</sup>, AAE<sub>300-400nm</sub> = 6.0) and more aged wsBBOA<sub>aged</sub> (O/C = 0.58, MAC<sub>365nm</sub> = 0.25 m<sup>2</sup> g<sup>-1</sup>, AAE<sub>300-400nm</sub> = 6.8). The other three factors are oxygenated OA (OOA) termed as wsOOA1 (O/C = 0.52, MAC<sub>365nm</sub> = 0.10 m<sup>2</sup> g<sup>-1</sup>, AAE<sub>300-400nm</sub> = 7.2), wsOOA2 (O/C = 0.53, MAC<sub>365nm</sub> = 0.01 m<sup>2</sup> g<sup>-1</sup>, AAE<sub>300-400nm</sub> = 14.7) and wsOOA3 (O/C = 0.67, MAC<sub>365nm</sub> = 0.10 m<sup>2</sup> g<sup>-1</sup>, AAE<sub>300-400nm</sub> = 9.9).

The wsBBOAs are identified based on their mass spectral profiles, with enhanced signals of levoglucosan tracer ions (e.g., C<sub>2</sub>H<sub>4</sub>O<sub>2</sub><sup>+</sup> and C<sub>3</sub>H<sub>5</sub>O<sub>2</sub><sup>+</sup>) and phenolic tracer ions (e.g., C<sub>6</sub>H<sub>6</sub>O<sub>2</sub><sup>+</sup>, C<sub>8</sub>H<sub>10</sub>O<sub>4</sub><sup>+</sup>, C<sub>14</sub>H<sub>14</sub>O<sub>4</sub><sup>+</sup>) (Figure 2a). Correspondingly, the wsBBOAs contribute most to the time variation of the levoglucosan and the phenolic tracer ions (Figures 2c and S9). In contrast, the wsOOAs are less correlated with levoglucosan and phenolic tracers, but are characterized by oxygenated ions (e.g., CO<sub>2</sub><sup>+</sup> and CHO<sub>2</sub><sup>+</sup>) and different amounts of secondary inorganic ions (e.g., sulfate and nitrate) (Figures 2c and S9). wsOOA1 is associated with high amounts of both nitrate and sulfate in the PM, showing a nitrate-to-organic mass ratio (R<sub>NO<sub>3</sub>/Org</sub>) of 0.22 and a sulfate-to-organic mass ratio (R<sub>SO<sub>4</sub>/Org</sub>) of 0.11, whereas wsOOA2 is associated only with elevated nitrate signals (R<sub>NO<sub>3</sub>/Org</sub> = 0.80). The most oxidized wsOOA3, on the other hand, is associated only with a small amount of NO<sup>+</sup> ion, which is likely contributed by organonitrates. Note that the wsOOAs can also be influenced by biomass burning emissions to some degree. For example, wsOOA3, which is elevated in wildfire-influenced samples and shows more enhanced phenolic signals in the mass spectra than other wsOOAs, may contain some oxidation products of BB-emitted phenols.

Figure 2a-b presents the AMS mass spectral profiles of the WSOA factors and Figure 3 presents their mass absorption efficiency spectra. Among the five WSOA factors, wsBBOA<sub>fresh</sub> is the least oxidized and demonstrates mass spectral features observed for fresh BBOA in previous field studies (Young et al., 2016; Zhou et al., 2017). For example, as shown in Figure 2a, the

$w_{\text{SBBOA}_{\text{fresh}}}$  spectrum shows significantly enhanced contributions to the total organic signals by the levoglucosan tracer ions (i.e.,  $f_{\text{C}_2\text{H}_4\text{O}_2^+} = 2.9\%$  and  $f_{\text{C}_3\text{H}_5\text{O}_2^+} = 1.1\%$ ) and high mass ions (e.g.,  $f_{m/z > 120} = 10\%$ ), suggesting that  $w_{\text{SBBOA}_{\text{fresh}}}$  is enriched in anhydrous sugars and high molecular weight species. In addition, the association of  $w_{\text{SBBOA}_{\text{fresh}}}$  with moderately enhanced nitrate signals (Figure 2b) is consistent with the rapid conversion of  $\text{NO}_x$  to nitrate in fresh BB smoke (Zhou et al., 2017). Furthermore,  $w_{\text{SBBOA}_{\text{fresh}}}$  was elevated in the wildfire-influenced summer samples and in the winter samples (Figure 1f); this observation is consistent with the facts that the wildfire events were nearby (Figure S6) and that residential wood burning is common during winter in Davis.

$w_{\text{SBBOA}_{\text{fresh}}}$  is the most light-absorbing WSOA factor with the highest MAC ( $\text{MAC}_{365\text{nm}} = 1.1 \text{ m}^2 \text{ g}^{-1}$ ) and the lowest AAE ( $\text{AAE}_{300-400\text{nm}} = 6.0$ ) among the five WSOA factors (Figure 3). This agrees with previous findings that BBOA contains notable amounts of light-absorbing compounds such as particulate organic oxides of nitrogen (PONs; including nitro-organics (RNO2) and organic nitrates (RONO2)), polycyclic aromatic hydrocarbon (PAH) derivatives, and polyphenols (Lin et al., 2016; Reyes-Villegas et al., 2018). As summarized in Figure 3, the MAC values of  $w_{\text{SBBOA}_{\text{fresh}}}$  are comparable to those measured in ambient WSOA influenced by biomass burning (Du et al., 2014) and in lab-generated primary BBOA (Chen and Bond, 2010). Moschos et al. (2018) used the same WSOA source apportionment approach as done in this study, i.e., applying PMF on the combined AMS and UV-vis measurement data, for ambient PM samples collected in Switzerland and retrieved a  $w_{\text{SBBOA}}$  factor and two different  $w_{\text{SOOA}}$ s. Similarly, they found that the  $w_{\text{SBBOA}}$  factor is substantially more absorbing than the  $w_{\text{SOOA}}$ s. However, the Moschos  $w_{\text{SBBOA}}$  shows slightly higher MAC absorptivity than  $w_{\text{SBBOA}_{\text{fresh}}}$  in this study, especially in the visible light range, probably because the  $w_{\text{SBBOA}_{\text{fresh}}}$  in this study was more strongly



influenced by summer-time wildfires while the  $wsBBOA$  determined by Moschos et al. mainly represented wintertime residential wood combustion. Indeed, the light absorptivity of BBOA can be influenced by factors such as biomass types, burning conditions, and the aging of BBOA (Chen and Bond, 2010; Holder et al., 2016; Reisen et al., 2018). Another possible reason for the MAC difference may be black carbon absorption interference in Moschos' samples.  $wsBBOA_{fresh}$  accounts for a significant fraction of the total light absorption by WS-PM<sub>2.5</sub> in Davis, contributing an average of 61% of the total rate of sunlight absorption in all the PM<sub>2.5</sub> extracts and as high as 89% in wildfire-influenced samples (Figures 4 and 1g). Similar findings were reported previously in the southeastern U.S., where biomass burning dominates BrC absorption at both rural (Washenfelder et al., 2015) and urban sites (Hecobian et al., 2010).

The mass spectral profile of  $wsBBOA_{aged}$  is similar to those of the aged BBOA factors observed in previous studies (Farley et al., 2022; Young et al., 2016; Zhou et al., 2017). It is more oxidized and less absorbing than  $wsBBOA_{fresh}$  (Figures 2a and 3) and contains a lower level of anhydrous sugars ( $f_{C_2H_4O_2^+} = 0.64\%$  vs. 2.9% in  $wsBBOA_{fresh}$ ) but a higher content of carboxylates ( $f_{CHO_2^+} = 0.92\%$  vs. 0.13% in  $wsBBOA_{fresh}$ ). In addition,  $wsBBOA_{aged}$  shows high correlations with phenolic aqSOA tracer ions such as  $C_6H_6O_2^+$ ,  $C_7H_5O_2^+$ ,  $C_7H_8O_3^+$ ,  $C_7H_8O_4^+$ ,  $C_8H_7O_3^+$ ,  $C_{14}H_{14}O_4^+$ ,  $C_{14}H_{14}O_5^+$ ,  $C_{16}H_{18}O_7^+$ ,  $C_{18}H_{17}O_5^+$  and  $C_{20}H_{22}O_6^+$  (Figure S9 and Figure 2c). These results suggest that  $wsBBOA_{aged}$  represents more aged BB smoke and might contain aqSOA products formed from oxidation of BB-emitted phenols (Ervens et al., 2011; Jiang et al., 2021; Sun et al., 2010; Yu et al., 2014, 2016). The MAC of  $wsBBOA_{aged}$  is comparable to that of wintertime WSOA at a rural site in the southeast US, where biomass burning was identified as a major source of BrC (Hecobian et al., 2010).  $wsBBOA_{aged}$  on average accounts for 28% of the total sunlight absorption rate of the

PM extracts (Figure 1g). The lower light absorptivity of  $\text{wsBBOA}_{\text{aged}}$  compared to  $\text{wsBBOA}_{\text{fresh}}$  might indicate photobleaching during the aging of BBOA (Sumlin et al., 2017).

The three  $\text{wsOOA}$  factors comprise negligible amounts of BBOA tracers and phenolic SOA tracers (Figure 2c). In addition, the  $\text{wsOOA}$  factors are less light absorbing than the  $\text{wsBBOA}$  factors (Figure 3).  $\text{wsOOA1}$  and  $\text{wsOOA2}$  are more enhanced during wintertime, while the more oxidized  $\text{wsOOA3}$  is more abundant during summertime.  $\text{wsOOA1}$  is associated with high amounts of nitrate and sulfate in PM (Figure 2b). The signal ratio of  $\text{NO}^+$  to  $\text{NO}_2^+$  for OOA1 is 2.37, which is higher than that of pure ammonium nitrate ( $\text{NO}^+/\text{NO}_2^+ = 1.81$ ), indicating the possible presence of organonitrates. In addition,  $\text{CH}_3\text{SO}_2^+$  (a tracer ion for methanesulfonic acid (MSA) (Ge et al., 2012a)) is enriched in  $\text{wsOOA1}$ . Although MSA is commonly associated with oceanic sources, previous studies have found MSA in boundary layer OOA (Zhou et al., 2017) and it can be an aqueous-phase SOA product of S-containing VOCs from terrestrial sources (Ge et al., 2012a; Kim et al., 2019; Young et al., 2016). The enhanced sulfate and MSA concentrations in  $\text{wsOOA1}$  suggest that this factor is associated with aqSOA.  $\text{wsOOA2}$  is the least light-absorbing factor, and it shows significant association with nitrate in PM (Figure 2b). The signal ratio of  $\text{NO}^+$  to  $\text{NO}_2^+$  for  $\text{wsOOA2}$  is 1.58, similar to the value for pure ammonium nitrate, indicating the nitrate in  $\text{wsOOA2}$  is primarily in the form of  $\text{NH}_4\text{NO}_3$ .  $\text{wsOOA3}$  is the most oxidized ( $\text{O/C} = 0.67$ ) and most light-absorbing  $\text{wsOOA}$  factor. The mass spectra of the three  $\text{wsOOAs}$  show slightly enhanced relative abundance of the carboxylic acid tracer  $\text{CHO}_2^+$  (Figures 2a and 2c), suggesting the enrichment of organic acids in the  $\text{wsOOAs}$ .  $\text{wsOOA3}$  and  $\text{wsOOA1}$  have similar light absorptivity, with MAC values comparable to those of summertime ambient WSOA observed in rural Yorkville and in urban Columbus (Hecobian et al., 2010), as well as summertime  $\text{wsOOA}$  resolved from PMF analysis of samples from Switzerland (Moschos et al., 2018). The  $\text{wsOOAs}$

together account for only a small fraction of the total light absorption of the PM extracts in this study (Figures 4 and 1g).

### 5.4.3 Relationship between WSOA components and condensed-phase oxidants ( $\bullet\text{OH}$ , $^3\text{C}^*$ and $^1\text{O}_2^*$ )

Figure 5a displays the concentrations of  $\bullet\text{OH}$ ,  $^1\text{O}_2^*$  and  $^3\text{C}^*$  in the dilute PM extracts illuminated with simulated sunlight. The average steady state concentrations of  $\bullet\text{OH}$ ,  $^1\text{O}_2^*$  and  $^3\text{C}^*$  in the PM extracts are  $2 \times 10^{-15}$  M,  $2 \times 10^{-12}$  M and  $3 \times 10^{-13}$  M, respectively. These values are comparable with previously reported  $^1\text{O}_2^*$  and  $^3\text{C}^*$  concentrations in dilute particle extracts, but about 5 times higher for OH (Kaur et al., 2019). Since BrC is a potential source of  $^3\text{C}^*$ ,  $^1\text{O}_2^*$  and  $\bullet\text{OH}$ , whereas dissolved organic matter can be an important sink of condensed-phase oxidants (Arakaki et al., 2013; Herrmann et al., 2010), the oxidant concentrations may be highly dependent on the composition of the organic aerosol.

To explore the relationships between condensed-phase oxidants and OA composition, we performed linear regression analysis on the measured oxidant concentrations and modeled their linear dependence on the concentrations of the five WSOA factors (see Sect. 5.3.4.4 for more details). Figure 5a shows the modeled oxidant ( $\bullet\text{OH}$ ,  $^1\text{O}_2^*$  and  $^3\text{C}^*$ ) concentrations contributed by the five WSOA factors in each PM extract sample, and Figure 5b shows the correlation between the modeled and the measured oxidant concentrations. The concentrations of  $^1\text{O}_2^*$  and  $^3\text{C}^*$  can be properly modeled by the WSOA factors (Figure 5b), while  $\bullet\text{OH}$  is relatively poorly modeled with Pearson's  $r = 0.717$  for the correlation between modeled and measured  $\bullet\text{OH}$ . These results suggest that photoreactions of WSOA can be an important source of  $^1\text{O}_2^*$  and  $^3\text{C}^*$ , while  $\bullet\text{OH}$  may have other major sources, such as nitrite and nitrate photolysis (Anastasio and McGregor, 2001; Kaur

and Anastasio, 2017), photo-Fenton reactions (Arakaki and Faust, 1998) and peroxides (Lim and Turpin, 2015; Tong et al., 2016, 2017).

The least-squares fitting parameters derived from the linear decomposition analysis are in the unit of mol-oxidant/mg-organic, thus representing the oxidant production potentials of individual WSOA factors (Figure 6). Among the five WSOA factors,  $w_{\text{SBBOA}_{\text{fresh}}}$  demonstrates the highest  $^1\text{O}_2^*$  and  $^3\text{C}^*$  production potentials ( $1.85 \times 10^{-14}$  and  $2.52 \times 10^{-15}$  mol/mg-organic, respectively, equal to  $1.11 \times 10^7$  and  $1.52 \times 10^6$  molecules/ $\mu\text{g}$ -organic), which is consistent with the fact that  $w_{\text{SBBOA}_{\text{fresh}}}$  is the most light-absorbing WSOA factor and contains the highest abundance of BrC chromophores for  $^1\text{O}_2^*$  and  $^3\text{C}^*$  generation. For example, BB-emitted aromatic carbonyl BrC compounds absorb sunlight and are promoted to the excited singlet state, which undergoes intersystem crossing to produce  $^3\text{C}^*$  (Anastasio et al., 1997; Fleming et al., 2020; Kaur et al., 2019; Smith et al., 2016). Triplet states can undergo energy transfer reactions with ground state  $\text{O}_2$  to form  $^1\text{O}_2$  (Zepp et al., 1977). Although  $w_{\text{SBBOA}_{\text{fresh}}}$  is more light-absorbing than the other WSOA factors, with a  $\text{MAC}_{365\text{nm}}$  value 4–100 times higher than other WSOA factors, its potential to produce  $^1\text{O}_2^*$  and  $^3\text{C}^*$  production is only 1–4 times higher than the other factors. This result may suggest that the BrC chromophores in  $w_{\text{SBBOA}_{\text{fresh}}}$  are less efficient sources of  $^1\text{O}_2^*$  and  $^3\text{C}^*$ , i.e., have lower quantum yields (Ma et al., In Preparation). Figure S10 shows the modeled fractional contribution of individual WSOA factors to the total oxidant concentrations in the PM extracts. On average, fresh and aged  $w_{\text{SBBOA}}$  together account for 46%, 50% and 34%, respectively, of OH,  $^1\text{O}_2^*$  and  $^3\text{C}^*$  in illuminated PM extracts, suggesting that BB smoke is important sources of aqueous-phase oxidants.

Figure 7a shows the correlation coefficients between oxidant concentrations and AMS-measured WSOA ion families. While  $^1\text{O}_2^*$  and  $^3\text{C}^*$  correlate well with all the ion families ( $r$  in the

range of 0.91 – 0.98), •OH shows lower correlations (r in the range of 0.64 – 0.70). This is consistent with the fact that both  $^1\text{O}_2^*$  and  $^3\text{C}^*$  are formed from photoexcitation of chromophoric organics while •OH has more complex photochemical sources in the aqueous phase. In addition, both  $^1\text{O}_2^*$  and  $^3\text{C}^*$  show high correlations with N-containing ions; this is consistent with previous findings that N-containing compounds, such as nitrophenols (Desyaterik et al., 2013; Hems and Abbatt, 2018; Zhao et al., 2015) and imidazoles and pyrazines (Kim et al., 2019; Lin et al., 2015b) represent an important class of BrC species.

#### 5.4.4 Estimation of global aqueous-phase oxidant concentrations

Using the oxidant production potentials derived for different WSOA factors (Figure 6), we estimated the aqueous concentrations of •OH,  $^1\text{O}_2^*$  and  $^3\text{C}^*$  in ambient aerosols based on BBOA and OOA concentrations reported in previous studies. :

$$[\text{Ox}]_{\text{OA}} = \text{PP}_{\text{ox,OA}} \times \frac{[\text{OA}]}{100} \times f_{\text{ws,OA}} \quad (\text{Eq. 8})$$

In this equation,  $[\text{Ox}]_{\text{OA}}$  ( $\text{mol m}^{-3}$ ) is the estimated aqueous-phase oxidant concentration contributed by an WSOA factor,  $\text{PP}_{\text{ox,OA}}$  ( $\text{mol-oxidant/mg-organic}$ ) is the oxidant production potential of a WSOA factor,  $[\text{OA}]$  ( $\mu\text{g m}^{-3}$ ) is the ambient OA concentration, and  $f_{\text{ws,OA}}$  is the mass fraction of water-soluble components in an OA factor. To estimate the oxidant concentrations in different locations in the northern hemisphere, we used the oxidant production potential of  $\text{wsBBOA}_{\text{fresh}}$  to represent fresh  $\text{wsBBOA}$ ,  $\text{wsBBOA}_{\text{aged}}$  to represent oxidized  $\text{wsBBOA}$ , and the average value of  $\text{wsOOA1}$ ,  $\text{wsOOA2}$  and  $\text{wsOOA3}$  to represent  $\text{wsOOA}$ . Ambient OA concentration data were from previous studies (Farley et al., 2022; Ge et al., 2012b; Setyan et al., 2012; Young et al., 2016; Zhang et al., 2011; Zhou et al., 2016, 2017). The  $f_{\text{ws,OA}}$  values for BBOA and OOA used here were 37% and 49%, respectively, based on the results from Li et al. (2021).

Note that the modeled oxidant production potentials of wsBBOAs and wsOOAs in this study only represent the values under dilute conditions (e.g., cloud and fog). However, these values may not apply for concentrated aerosol particles, because the major sinks of the oxidants are different between dilute and concentrated conditions. For example, under dilute conditions, the dominant sink of  $^3\text{C}^*$  is  $\text{O}_2$ , whereas under concentrated conditions, organics are the major sink (Ma et al., In Preparation). The changed production-to-sink rate ratio of oxidants can influence the steady state concentration of oxidants, and results in changed oxidant production potential values.

Figure 8b-d present the estimated  $\bullet\text{OH}$ ,  $^1\text{O}_2^*$  and  $^3\text{C}^*$  concentrations contributed by wsBBOA and wsOOA at over 30 locations in northern hemisphere. The average estimated  $\bullet\text{OH}$ ,  $^1\text{O}_2^*$  and  $^3\text{C}^*$  concentrations at these locations are  $1.5 \times 10^{-20} \text{ mol m}^{-3}$ ,  $2.2 \times 10^{-17} \text{ mol m}^{-3}$  and  $4.2 \times 10^{-18} \text{ mol m}^{-3}$ , respectively. Although wsBBOA shows high oxidant production potentials (especially for  $^1\text{O}_2^*$  and  $^3\text{C}^*$ ), wsOOA appears to be a more important source of aqueous photooxidants due to the dominance of OOA at most ambient locations (Figure 8a). Note that there are several factors that may cause uncertainties in the oxidant estimation: 1) since the contributions from water-insoluble OA components are not considered, the oxidant concentrations may be underestimated; and 2) the oxidant production potentials we used here represent dilute conditions, nevertheless, for concentrated particle conditions, the oxidant production potentials could be lower due to increased sink rate, and thus the oxidant concentrations may be overestimated for concentrated particles.

## 5.5 Conclusions

In this study, PMF analysis was performed on the combined AMS and UV-Vis measurement data of the water extracts of  $\text{PM}_{2.5}$  samples collected from Davis over a period of one year to characterize the chemical composition and light absorption properties of water-soluble BrC aerosol

in Northern California. Five WSOA factors, including two  $wsBBOAs$  and three  $wsOOAs$ , were retrieved, each with distinct mass spectrum and MAC spectrum. The  $wsBBOA_{fresh}$  factor, which shows a similar MS profile as the fresh BBOAs reported in previous studies and has MAC values comparable to those of ambient aerosols influenced by BB emissions, is the most light-absorbing among the 5 factors.  $wsBBOA_{fresh}$  is estimated to account for 61% of the total sunlight absorption by the WS-PM<sub>2.5</sub>, indicating that freshly emitted biomass burning aerosol is a dominant source of BrC light absorption in northern California. The more oxidized and aged  $wsBBOA_{aged}$  is much less light-absorbing ( $MAC_{365\text{ nm}} = 0.25\text{ m}^2\text{ g}^{-1}$  vs.  $1.1\text{ m}^2\text{ g}^{-1}$ ), but nevertheless accounts for a significant portion (28%) of the total sunlight absorption by WS-PM<sub>2.5</sub>. The  $MAC_{365\text{ nm}}$  values of the three  $wsOOA$  factors are in the range of  $0.01 - 0.1\text{ m}^2\text{ g}^{-1}$  and the  $AAE_{300-400\text{ nm}}$  in the range of  $7.2 - 14.7$ . While the oxygenated organic species on average represent 48% of the total WSOA mass, they only account for 12 % of the total sunlight absorption by WS-PM<sub>2.5</sub> in Davis.

We applied a linear regression model to explore the relationships between the formation of oxidants ( $\bullet OH$ ,  $^1O_2^*$  and  $^3C^*$ ) in illuminated PM extracts and the composition of WSOA. While the concentrations of  $^1O_2^*$  and  $^3C^*$  can be predicted from linear combinations of the amounts of the five WSOA factors, the  $\bullet OH$  concentration is relatively poorly explained by the variation of the WSOA factors, reflecting more complicated sources and sinks of  $\bullet OH$ . The linear regression analysis allowed us to determine the oxidant production potentials of individual WSOA factors.  $wsBBOA_{fresh}$  appears to be the most potent at producing  $^1O_2^*$  whereas  $wsBBOA_{fresh}$  and  $wsOOAs$  show comparable production potentials for  $^3C^*$ . Using the oxidant production potentials determined in this study and the ambient OA measurements by AMS reported in previous studies, we then estimated the aqueous-phase oxidant concentrations under cloud and fog conditions at dozens of sites in northern hemisphere. The average estimated  $\bullet OH$ ,  $^1O_2^*$  and  $^3C^*$  concentrations

at these sites are  $1.5 \times 10^{-20}$  mol m<sup>-3</sup>,  $2.2 \times 10^{-17}$  mol m<sup>-3</sup> and  $4.2 \times 10^{-18}$  mol m<sup>-3</sup>, respectively. Furthermore, we found that due to the broad dominance of OOAs in ambient aerosol, oxygenated organic species are likely an important source of photo-oxidants in atmospheric condensed phases.

### **Acknowledgements**

This research was supported by grants from the U.S. Department of Energy (DOE) Atmospheric System Research Program (Grant #DESC0022140), the National Science Foundation (NSF) (Grant #AGS-2220307), and the California Agricultural Experiment Station (Projects CA-D-ETX-2102-H and CA-D-LAW-6403-RR). W.J. and L.M. also acknowledge additional funding from the Jastro-Shields Graduate Research Award and the Donald G. Crosby Fellowship at UC Davis.



## Figures

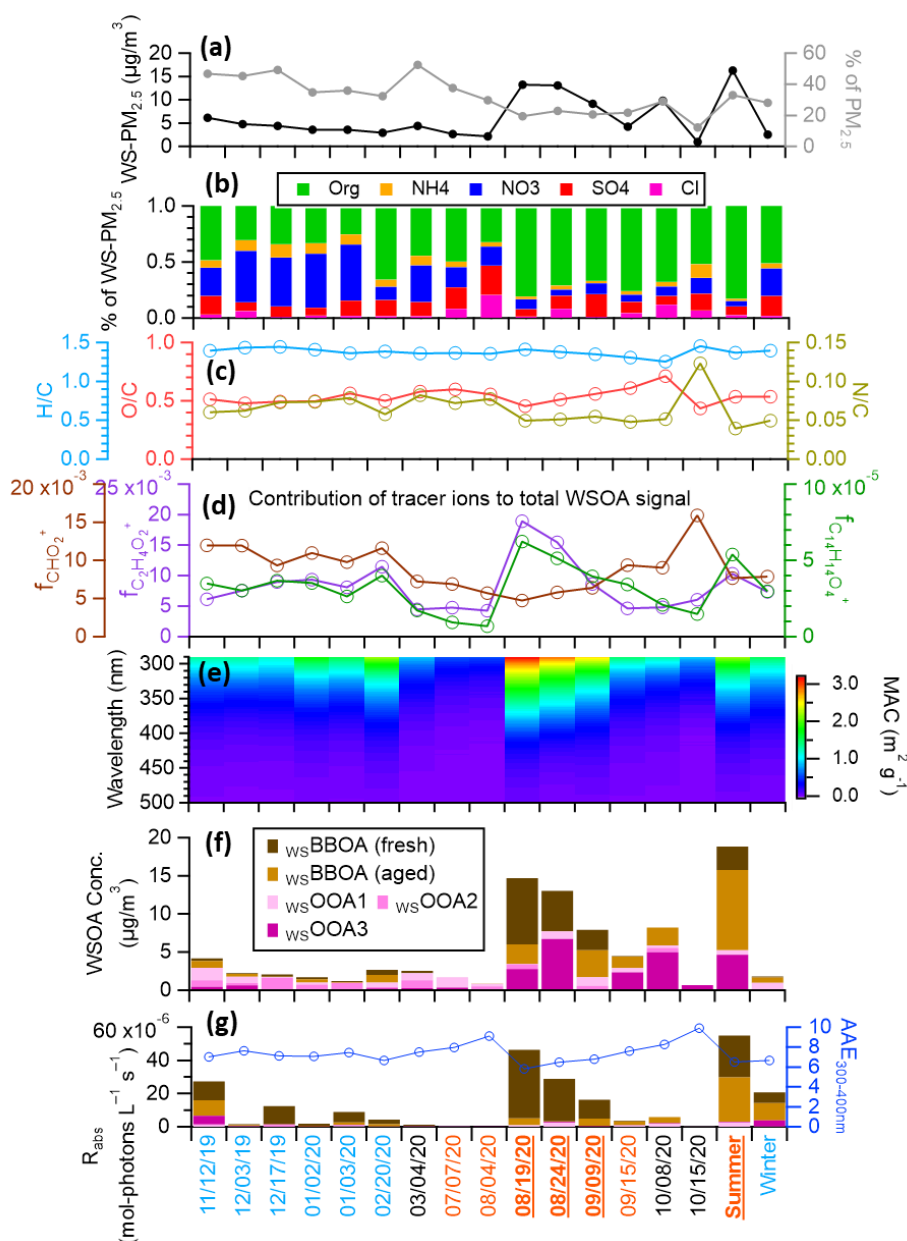


**Figure 1.** (a) Ambient mass concentration of water-soluble PM<sub>2.5</sub> (WS-PM<sub>2.5</sub>) and the mass fraction of WS-PM<sub>2.5</sub> in PM<sub>2.5</sub>. (b) Composition of WS-PM<sub>2.5</sub>. (c) Elemental ratios of the water-soluble OA (WSOA). (d) Contribution of selected AMS tracer ions to the total WSOA signal. (e) Mass absorption coefficient (MAC) of the WSOA. (f) Ambient concentrations of the five WSOA factors resolved from PMF. (g) Rate of sunlight absorption ( $R_{\text{abs}}$ ) contributed by each WSOA factor and AAE<sub>300-400nm</sub> of the WSOA. The x-axis labels show the PM sampling dates and the colors denote the seasons: winter (blue), summer (orange), and spring and fall (black). Samples significantly influenced by wildfire plumes are underlined. The last two samples are a composite summer sample and a composite winter sample, respectively. Details about the PM<sub>2.5</sub> samples are in Table S1.

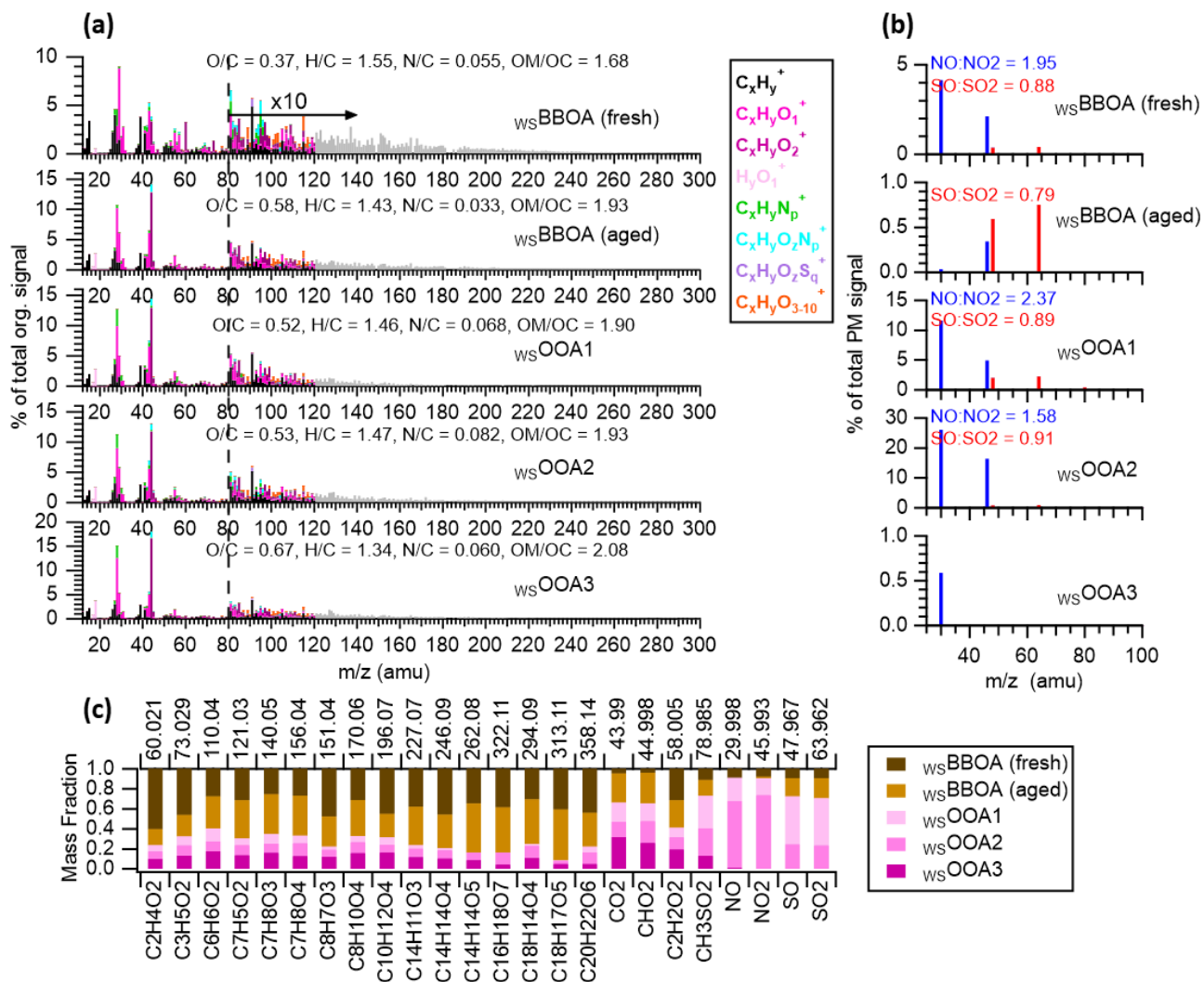


**Figure 2.** (a) Mass spectra of the five WSOA factors colored by ion families. HRMS ions are included for  $m/z < 120$ , and UMR ions for  $m/z > 120$ . (b) Signals of  $NO^+$ ,  $NO_2^+$ ,  $SO^+$ , and  $SO_2^+$  ions in the PMF-resolved WS-PM<sub>2.5</sub> factors. (c) Mass fraction of selected AMS tracer ions attributed to each WSOA factor.

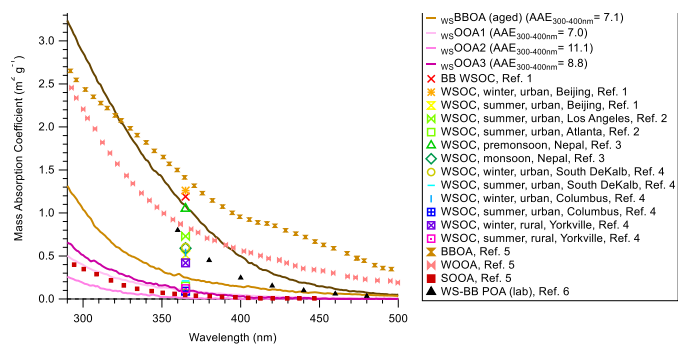


**Figure 3.** Comparisons of the mass absorption coefficients (MAC) of the five WSOA factors resolved in this study with previously reported values. Ref. 1: Du et al. (2014); Ref. 2: Zhang et al. (2011); Ref. 3: Wu et al. (2019); Ref. 4: Hecobian et al. (2010); Ref. 5: Moschos et al. (2018); Ref. 6: Chen and Bond (2010)

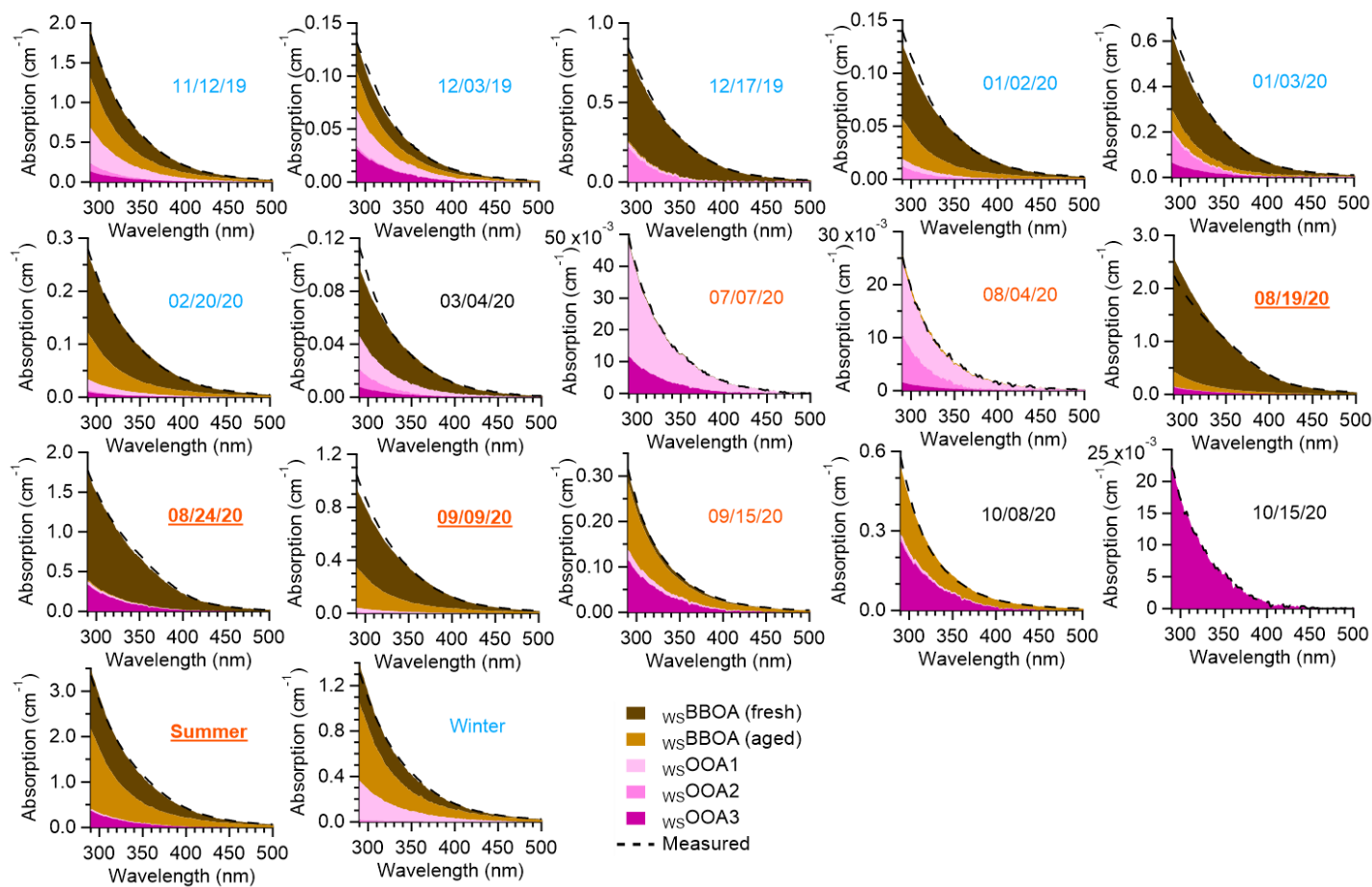


**Figure 4.** Contributions of the five WSOA factors to the total light absorption in each  $PM_{2.5}$  extract. Details about the samples are in Table S1.

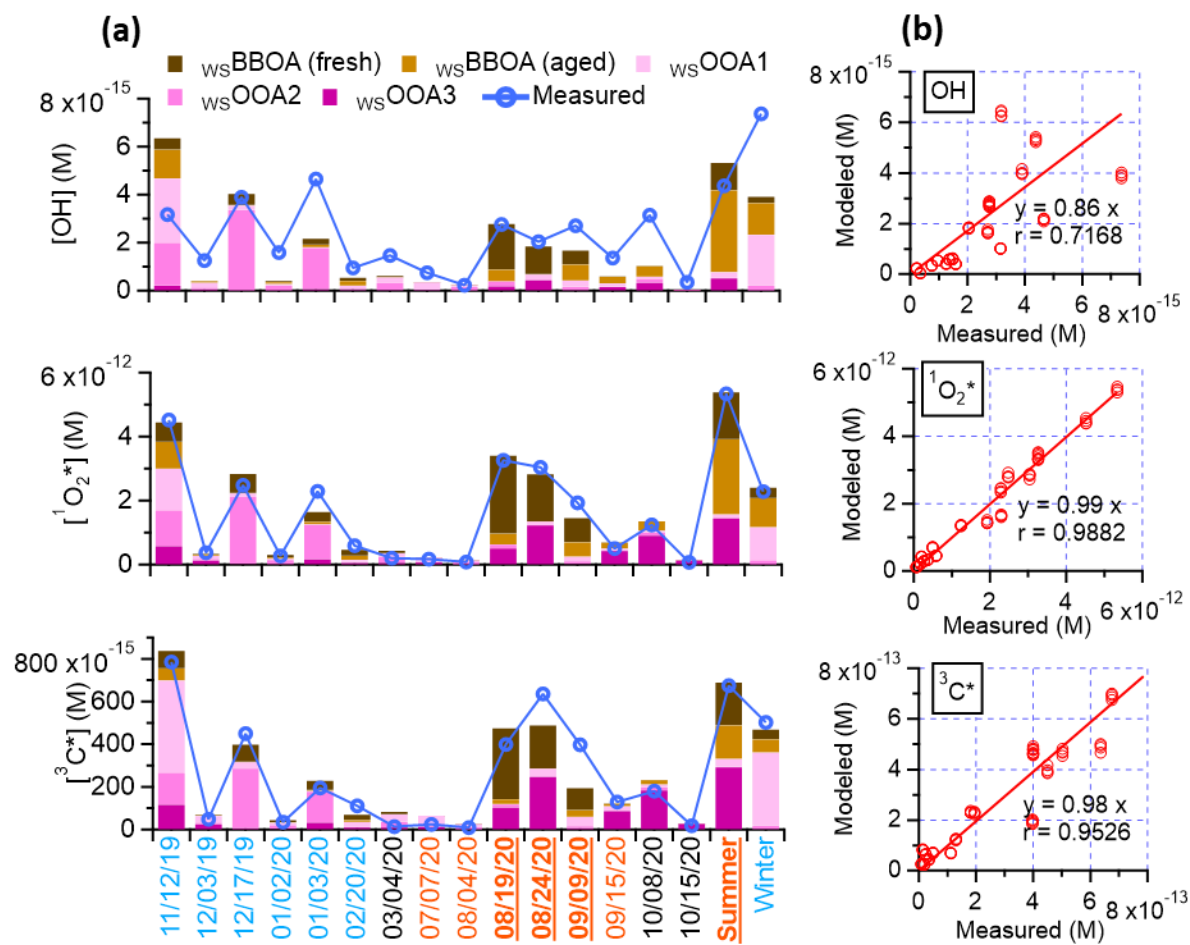
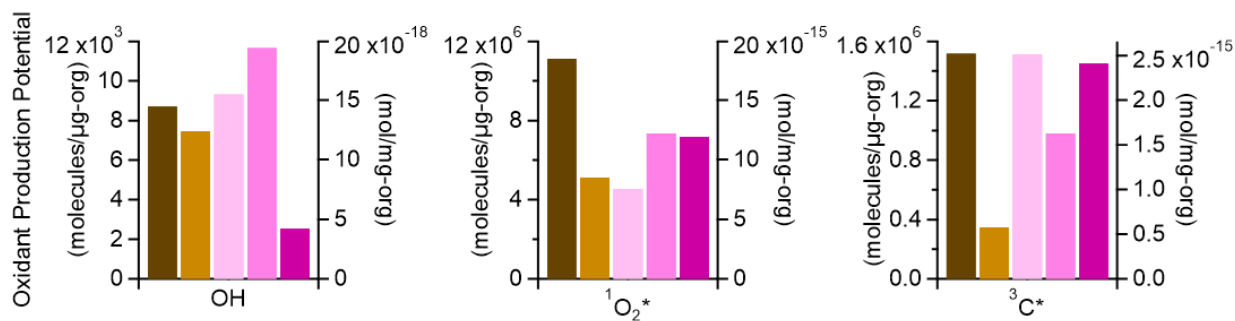


**Figure 5.** (a) Estimated concentrations of oxidants ( $\text{OH}$ ,  $^1\text{O}_2^*$  and  $^3\text{C}^*$ ) contributed by each WSOA factor, along with measured oxidant concentrations in illuminated  $\text{PM}_{2.5}$  extracts. (b) Scatter plots compare the modeled oxidant concentrations versus measured values. Details of each  $\text{PM}_{2.5}$  sample are in Table S1.



	Oxidant Production Potentials (molecules / μg-org)		
	OH	<sup>1</sup> O <sub>2</sub> *	<sup>3</sup> C*
wsBBOA (fresh)	8.71E+03	1.11E+07	1.52E+06
wsBBOA (aged)	7.45E+03	5.13E+06	3.47E+05
wsOOA1	9.33E+03	4.54E+06	1.51E+06
wsOOA2	1.17E+04	7.35E+06	9.80E+05
wsOOA3	2.54E+03	7.18E+06	1.45E+06

**Figure 6.** Estimated photo-production potentials of •OH, <sup>1</sup>O<sub>2</sub>\* and <sup>3</sup>C\* by each WSOA factor.

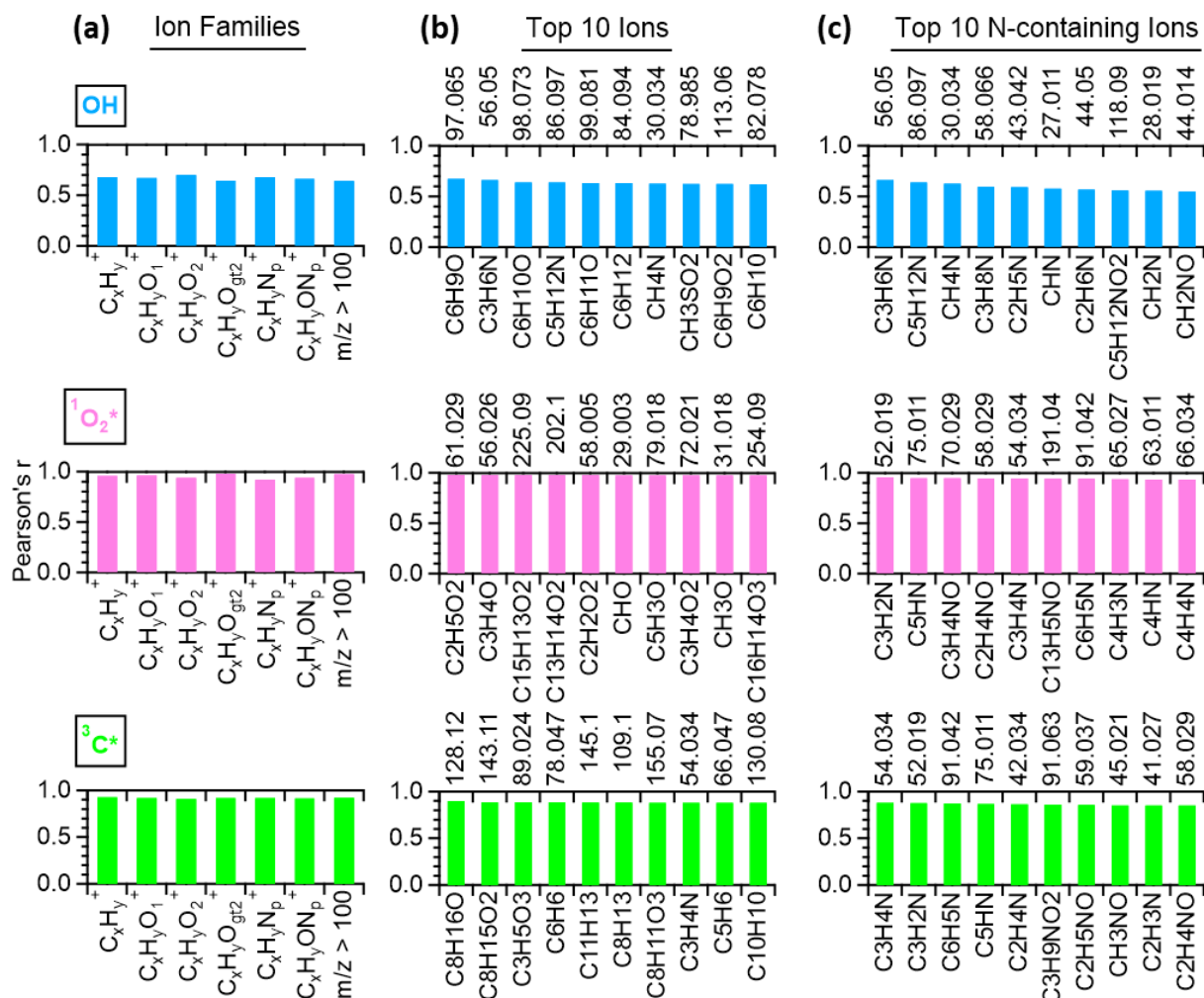


**Figure 7.** Pearson's  $r$  values for the correlations between concentrations of aqueous-phase oxidants (OH,  $^1O_2^*$ , or  $^3C^*$ ) measured in illuminated PM<sub>2.5</sub> extracts and AMS spectral signals for (a) WSOA ion families; (b) 10 best correlated WSOA ions; and (c) 10 best correlated N-containing WSOA ions. In (b) and (c), the bottom and top axes denote the elemental compositions and the exact masses of the corresponding ions.

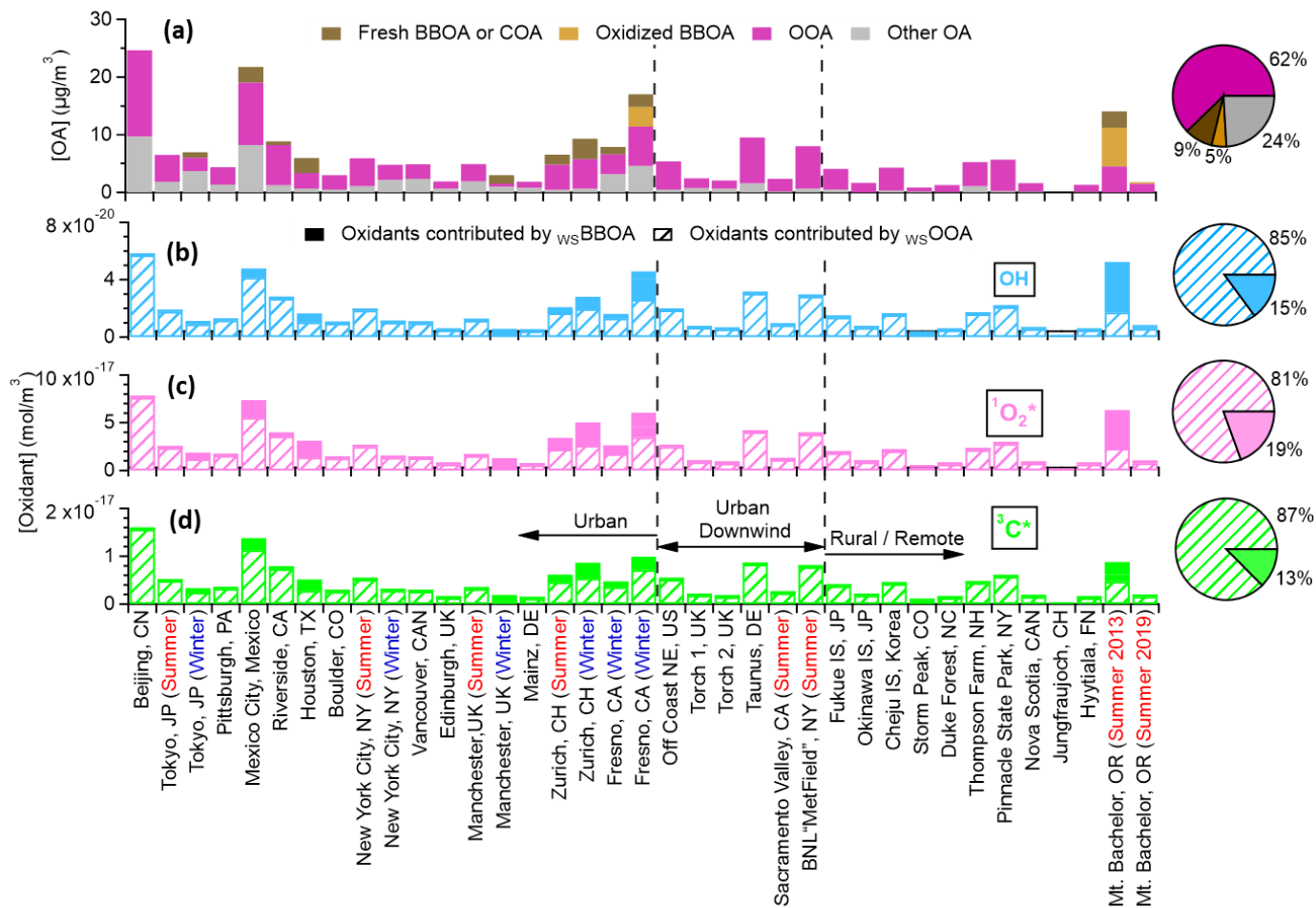


**Figure 8.** (a) Average concentrations of different OA factors at locations in northern hemisphere and (b-d) estimated condensed-phase concentrations of OH, <sup>1</sup>O<sub>2</sub>\* and <sup>3</sup>C\* contributed by water-soluble BBOA and OOA. Data in (a) were obtained from Zhang et al. (2011a), Ge et al. (2012b), Setyan et al. (2012), Zhou et al. (2016 and 2017), Young et al. (2016), and Farley et al. (2022).



## Reference

- Aiken, A. C., DeCarlo, P. F., Kroll, J. H., Worsnop, D. R., Huffman, J. A., Docherty, K. S., Ulbrich, I. M., Mohr, C., Kimmel, J. R., Sueper, D., Sun, Y., Zhang, Q., Trimborn, A., Northway, M., Ziemann, P. J., Canagaratna, M. R., Onasch, T. B., Alfarra, M. R., Prevot, A. S. H., Dommen, J., Duplissy, J., Metzger, A., Baltensperger, U. and Jimenez, J. L.: O/C and OM/OC Ratios of Primary, Secondary, and Ambient Organic Aerosols with High-Resolution Time-of-Flight Aerosol Mass Spectrometry, *Environ. Sci. Technol.*, 42(12), 4478–4485, doi:10.1021/es703009q, 2008.
- Al-Nu'airat, J., Oluwoye, I., Zeinali, N., Altarawneh, M. and Dlugogorski, B. Z.: Review of Chemical Reactivity of Singlet Oxygen with Organic Fuels and Contaminants, *Chem. Rec.*, 21(2), 315–342, doi:https://doi.org/10.1002/tcr.202000143, 2021.
- Allan, J. D., Delia, A. E., Coe, H., Bower, K. N., Alfarra, M. R., Jimenez, J. L., Middlebrook, A. M., Drewnick, F., Onasch, T. B., Canagaratna, M. R., Jayne, J. T. and Worsnop, D. R.: A generalised method for the extraction of chemically resolved mass spectra from Aerodyne aerosol mass spectrometer data, *J. Aerosol Sci.*, 35(7), 909–922, doi:http://dx.doi.org/10.1016/j.jaerosci.2004.02.007, 2004.
- Anastasio, C. and McGregor, K. G.: Chemistry of fog waters in California's Central Valley: 1. In situ photoformation of hydroxyl radical and singlet molecular oxygen, *Atmos. Environ.*, 35(6), 1079–1089, doi:https://doi.org/10.1016/S1352-2310(00)00281-8, 2001.
- Anastasio, C., Faust, B. C. and Rao, C. J.: Aromatic Carbonyl Compounds as Aqueous-Phase Photochemical Sources of Hydrogen Peroxide in Acidic Sulfate Aerosols, Fogs, and Clouds. 1. Non-Phenolic Methoxybenzaldehydes and Methoxyacetophenones with Reductants (Phenols), *Environ. Sci. Technol.*, 31(1), 218–232, doi:10.1021/es960359g, 1997.
- Andreae, M. O. and Gelencsér, A.: Black carbon or brown carbon? The nature of light-absorbing carbonaceous aerosols, *Atmos. Chem. Phys.*, 6(10), 3131–3148, doi:10.5194/acp-6-3131-2006, 2006.
- Arakaki, T. and Faust, B. C.: Sources, sinks, and mechanisms of hydroxyl radical ( $\bullet\text{OH}$ ) photoproduction and consumption in authentic acidic continental cloud waters from Whiteface Mountain, New York: The role of the Fe(r) ( $r = \text{II, III}$ ) photochemical cycle, *J. Geophys. Res. Atmos.*, 103(D3), 3487–3504, doi:https://doi.org/10.1029/97JD02795, 1998.
- Arakaki, T., Anastasio, C., Kuroki, Y., Nakajima, H., Okada, K., Kotani, Y., Handa, D., Azechi, S., Kimura, T., Tshuhako, A. and Miyagi, Y.: A General Scavenging Rate Constant for Reaction of Hydroxyl Radical with Organic Carbon in Atmospheric Waters, *Environ. Sci. Technol.*, 47(15), 8196–8203, doi:10.1021/es401927b, 2013.
- Aregahegn, K. Z., Nozière, B. and George, C.: Organic aerosol formation photo-enhanced by the formation of secondary photosensitizers in aerosols, *Faraday Discuss.*, 165(0), 123–134, doi:10.1039/C3FD00044C, 2013.
- Bond, T. C., Streets, D. G., Yarber, K. F., Nelson, S. M., Woo, J.-H. and Klimont, Z.: A technology-based global inventory of black and organic carbon emissions from combustion,

- J. Geophys. Res. Atmos., 109(D14), doi:<https://doi.org/10.1029/2003JD003697>, 2004.
- Canagaratna, M. R., Jayne, J. T., Jimenez, J. L., Allan, J. D., Alfarra, M. R., Zhang, Q., Onasch, T. B., Drewnick, F., Coe, H., Middlebrook, A., Delia, A., Williams, L. R., Trimborn, A. M., Northway, M. J., DeCarlo, P. F., Kolb, C. E., Davidovits, P. and Worsnop, D. R.: Chemical and microphysical characterization of ambient aerosols with the aerodyne aerosol mass spectrometer, *Mass Spectrom. Rev.*, 26(2), 185–222, doi:10.1002/mas.20115, 2007.
- Canonica, S., Hellrung, B. and Wirz, J.: Oxidation of Phenols by Triplet Aromatic Ketones in Aqueous Solution, *J. Phys. Chem. A*, 104(6), 1226–1232, doi:10.1021/jp9930550, 2000.
- Canonica, S., Hellrung, B., Müller, P. and Wirz, J.: Aqueous Oxidation of Phenylurea Herbicides by Triplet Aromatic Ketones, *Environ. Sci. Technol.*, 40(21), 6636–6641, doi:10.1021/es0611238, 2006.
- Chen, Y. and Bond, T. C.: Light absorption by organic carbon from wood combustion, *Atmos. Chem. Phys.*, 10(4), 1773–1787, doi:10.5194/acp-10-1773-2010, 2010.
- Chung, C. E., Ramanathan, V. and Decremer, D.: Observationally constrained estimates of carbonaceous aerosol radiative forcing, *Proc. Natl. Acad. Sci.*, 109(29), 11624–11629, doi:10.1073/pnas.1203707109, 2012.
- Claeys, M., Vermeulen, R., Yasmeeen, F., Gómez-González, Y., Chi, X., Maenhaut, W., Mészáros, T. and Salma, I.: Chemical characterisation of humic-like substances from urban, rural and tropical biomass burning environments using liquid chromatography with UV/vis photodiode array detection and electrospray ionisation mass spectrometry, *Environ. Chem.*, 9(3), 273–284 [online] Available from: <https://doi.org/10.1071/EN11163>, 2012.
- Cubison, M. J., Ortega, A. M., Hayes, P. L., Farmer, D. K., Day, D., Lechner, M. J., Brune, W. H., Apel, E., Diskin, G. S., Fisher, J. A., Fuelberg, H. E., Hecobian, A., Knapp, D. J., Mikoviny, T., Riemer, D., Sachse, G. W., Sessions, W., Weber, R. J., Weinheimer, A. J., Wisthaler, A. and Jimenez, J. L.: Effects of aging on organic aerosol from open biomass burning smoke in aircraft and laboratory studies, *Atmos. Chem. Phys.*, 11(23), 12049–12064, doi:10.5194/acp-11-12049-2011, 2011.
- Darmany, A. P., Jenks, W. S. and Jardon, P.: Charge-Transfer Quenching of Singlet Oxygen O<sub>2</sub>(<sup>1</sup>Δ<sub>g</sub>) by Amines and Aromatic Hydrocarbons, *J. Phys. Chem. A*, 102(38), 7420–7426, doi:10.1021/jp982326o, 1998.
- DeCarlo, P. F., Kimmel, J. R., Trimborn, A., Northway, M. J., Jayne, J. T., Aiken, A. C., Gonin, M., Fuhrer, K., Horvath, T., Docherty, K. S., Worsnop, D. R. and Jimenez, J. L.: Field-Deployable, High-Resolution, Time-of-Flight Aerosol Mass Spectrometer, *Anal. Chem.*, 78(24), 8281–8289, doi:10.1021/ac061249n, 2006.
- Deng, J., Ma, H., Wang, X., Zhong, S., Zhang, Z., Zhu, J., Fan, Y., Hu, W., Wu, L., Li, X., Ren, L., Pavuluri, C. M., Pan, X., Sun, Y., Wang, Z., Kawamura, K. and Fu, P.: Measurement report: Optical properties and sources of water-soluble brown carbon in Tianjin, North China – insights from organic molecular compositions, *Atmos. Chem. Phys.*, 22(10), 6449–6470, doi:10.5194/acp-22-6449-2022, 2022.
- Desyaterik, Y., Sun, Y., Shen, X., Lee, T., Wang, X., Wang, T. and Collett Jr., J. L.: Speciation

- of “brown” carbon in cloud water impacted by agricultural biomass burning in eastern China, *J. Geophys. Res. Atmos.*, 118(13), 7389–7399, doi:<https://doi.org/10.1002/jgrd.50561>, 2013.
- Du, Z., He, K., Cheng, Y., Duan, F., Ma, Y., Liu, J., Zhang, X., Zheng, M. and Weber, R.: A yearlong study of water-soluble organic carbon in Beijing II: Light absorption properties, *Atmos. Environ.*, 89, 235–241, doi:<https://doi.org/10.1016/j.atmosenv.2014.02.022>, 2014.
- Ervens, B., Turpin, B. J. and Weber, R. J.: Secondary organic aerosol formation in cloud droplets and aqueous particles (aqSOA): a review of laboratory, field and model studies, *Atmos. Chem. Phys.*, 11(21), 11069–11102, doi:10.5194/acp-11-11069-2011, 2011.
- Farley, R., Bernays, N., Jaffe, D. A., Ketcherside, D., Hu, L., Zhou, S., Collier, S. and Zhang, Q.: Persistent Influence of Wildfire Emissions in the Western United States and Characteristics of Aged Biomass Burning Organic Aerosols under Clean Air Conditions, *Environ. Sci. Technol.*, 56(6), 3645–3657, doi:10.1021/acs.est.1c07301, 2022.
- Feng, Y., Ramanathan, V. and Kotamarthi, V. R.: Brown carbon: a significant atmospheric absorber of solar radiation?, *Atmos. Chem. Phys.*, 13(17), 8607–8621, doi:10.5194/acp-13-8607-2013, 2013.
- Fleming, L. T., Lin, P., Roberts, J. M., Selimovic, V., Yokelson, R., Laskin, J., Laskin, A. and Nizkorodov, S. A.: Molecular composition and photochemical lifetimes of brown carbon chromophores in biomass burning organic aerosol, *Atmos. Chem. Phys.*, 20(2), 1105–1129, doi:10.5194/acp-20-1105-2020, 2020.
- Flores, J. M., Washenfelder, R. A., Adler, G., Lee, H. J., Segev, L., Laskin, J., Laskin, A., Nizkorodov, S. A., Brown, S. S. and Rudich, Y.: Complex refractive indices in the near-ultraviolet spectral region of biogenic secondary organic aerosol aged with ammonia, *Phys. Chem. Chem. Phys.*, 16(22), 10629–10642, doi:10.1039/C4CP01009D, 2014.
- Gao, S., Surratt, J. D., Knipping, E. M., Edgerton, E. S., Shahgholi, M. and Seinfeld, J. H.: Characterization of polar organic components in fine aerosols in the southeastern United States: Identity, origin, and evolution, *J. Geophys. Res. Atmos.*, 111(D14), doi:<https://doi.org/10.1029/2005JD006601>, 2006.
- Ge, X., Zhang, Q., Sun, Y., Ruehl, C. R. and Setyan, A.: Effect of aqueous-phase processing on aerosol chemistry and size distributions in Fresno, California, during wintertime, *Environ. Chem.*, 9(3), 221–235 [online] Available from: <https://doi.org/10.1071/EN11168>, 2012a.
- Ge, X., Setyan, A., Sun, Y. and Zhang, Q.: Primary and secondary organic aerosols in Fresno, California during wintertime: Results from high resolution aerosol mass spectrometry, *J. Geophys. Res. Atmos.*, 117(D19), doi:10.1029/2012JD018026, 2012b.
- González Palacios, L., Corral Arroyo, P., Aregahegn, K. Z., Steimer, S. S., Bartels-Rausch, T., Nozière, B., George, C., Ammann, M. and Volkamer, R.: Heterogeneous photochemistry of imidazole-2-carboxaldehyde: HO<sub>2</sub> radical formation and aerosol growth, *Atmos. Chem. Phys.*, 16(18), 11823–11836, doi:10.5194/acp-16-11823-2016, 2016.
- Hawkins, L. N., Baril, M. J., Sedehi, N., Galloway, M. M., De Haan, D. O., Schill, G. P. and Tolbert, M. A.: Formation of Semisolid, Oligomerized Aqueous SOA: Lab Simulations of Cloud Processing, *Environ. Sci. Technol.*, 48(4), 2273–2280, doi:10.1021/es4049626, 2014.

- Hawkins, L. N., Welsh, H. G. and Alexander, M. V: Evidence for pyrazine-based chromophores in cloud water mimics containing methylglyoxal and ammonium sulfate, *Atmos. Chem. Phys.*, 18(16), 12413–12431, doi:10.5194/acp-18-12413-2018, 2018.
- Hecobian, A., Zhang, X., Zheng, M., Frank, N., Edgerton, E. S. and Weber, R. J.: Water-Soluble Organic Aerosol material and the light-absorption characteristics of aqueous extracts measured over the Southeastern United States, *Atmos. Chem. Phys.*, 10(13), 5965–5977, doi:10.5194/acp-10-5965-2010, 2010.
- Hems, R. F. and Abbatt, J. P. D.: Aqueous Phase Photo-oxidation of Brown Carbon Nitrophenols: Reaction Kinetics, Mechanism, and Evolution of Light Absorption, *ACS Earth Sp. Chem.*, doi:10.1021/acsearthspacechem.7b00123, 2018.
- Herrmann, H., Hoffmann, D., Schaefer, T., Brüner, P. and Tilgner, A.: Tropospheric Aqueous-Phase Free-Radical Chemistry: Radical Sources, Spectra, Reaction Kinetics and Prediction Tools, *ChemPhysChem*, 11(18), 3796–3822, doi:https://doi.org/10.1002/cphc.201000533, 2010.
- Hoffer, A., Gelencsér, A., Guyon, P., Kiss, G., Schmid, O., Frank, G. P., Artaxo, P. and Andreae, M. O.: Optical properties of humic-like substances (HULIS) in biomass-burning aerosols, *Atmos. Chem. Phys.*, 6(11), 3563–3570, doi:10.5194/acp-6-3563-2006, 2006.
- Holder, A. L., Hagler, G. S. W., Aurell, J., Hays, M. D. and Gullett, B. K.: Particulate matter and black carbon optical properties and emission factors from prescribed fires in the southeastern United States, *J. Geophys. Res. Atmos.*, 121(7), 3465–3483, doi:https://doi.org/10.1002/2015JD024321, 2016.
- Jiang, W., Misovich, M. V, Hettiyadura, A. P. S., Laskin, A., McFall, A. S., Anastasio, C. and Zhang, Q.: Photosensitized Reactions of a Phenolic Carbonyl from Wood Combustion in the Aqueous Phase—Chemical Evolution and Light Absorption Properties of AqSOA, *Environ. Sci. Technol.*, 55(8), 5199–5211, doi:10.1021/acs.est.0c07581, 2021.
- Jo, D. S., Park, R. J., Lee, S., Kim, S.-W. and Zhang, X.: A global simulation of brown carbon: implications for photochemistry and direct radiative effect, *Atmos. Chem. Phys.*, 16(5), 3413–3432, doi:10.5194/acp-16-3413-2016, 2016.
- Kampf, C. J., Filippi, A., Zuth, C., Hoffmann, T. and Opatz, T.: Secondary brown carbon formation via the dicarbonyl imine pathway: nitrogen heterocycle formation and synergistic effects, *Phys. Chem. Chem. Phys.*, 18(27), 18353–18364, doi:10.1039/C6CP03029G, 2016.
- Kaur, R. and Anastasio, C.: Light absorption and the photoformation of hydroxyl radical and singlet oxygen in fog waters, *Atmos. Environ.*, 164, 387–397, doi:https://doi.org/10.1016/j.atmosenv.2017.06.006, 2017.
- Kaur, R. and Anastasio, C.: First Measurements of Organic Triplet Excited States in Atmospheric Waters, *Environ. Sci. Technol.*, 52(9), 5218–5226, doi:10.1021/acs.est.7b06699, 2018.
- Kaur, R., Labins, J. R., Helbock, S. S., Jiang, W., Bein, K. J., Zhang, Q. and Anastasio, C.: Photooxidants from brown carbon and other chromophores in illuminated particle extracts, *Atmos. Chem. Phys.*, 19(9), 6579–6594, doi:10.5194/acp-19-6579-2019, 2019.

- Kim, H., Collier, S., Ge, X., Xu, J., Sun, Y., Jiang, W., Wang, Y., Herckes, P. and Zhang, Q.: Chemical processing of water-soluble species and formation of secondary organic aerosol in fogs, *Atmos. Environ.*, 200, 158–166, doi:<https://doi.org/10.1016/j.atmosenv.2018.11.062>, 2019.
- Kirchstetter, T. W. and Thatcher, T. L.: Contribution of organic carbon to wood smoke particulate matter absorption of solar radiation, *Atmos. Chem. Phys.*, 12(14), 6067–6072, doi:[10.5194/acp-12-6067-2012](https://doi.org/10.5194/acp-12-6067-2012), 2012.
- Kirchstetter, T. W., Novakov, T. and Hobbs, P. V.: Evidence that the spectral dependence of light absorption by aerosols is affected by organic carbon, *J. Geophys. Res. Atmos.*, 109(D21), doi:<https://doi.org/10.1029/2004JD004999>, 2004.
- Kirillova, E. N., Andersson, A., Han, J., Lee, M. and Gustafsson, Ö.: Sources and light absorption of water-soluble organic carbon aerosols in the outflow from northern China, *Atmos. Chem. Phys.*, 14(3), 1413–1422, doi:[10.5194/acp-14-1413-2014](https://doi.org/10.5194/acp-14-1413-2014), 2014.
- Laskin, A., Laskin, J. and Nizkorodov, S. A.: Chemistry of Atmospheric Brown Carbon, *Chem. Rev.*, 115(10), 4335–4382, doi:[10.1021/cr5006167](https://doi.org/10.1021/cr5006167), 2015.
- Laskin, J., Laskin, A., Nizkorodov, S. A., Roach, P., Eckert, P., Gilles, M. K., Wang, B., Lee, H. J. (Julie) and Hu, Q.: Molecular Selectivity of Brown Carbon Chromophores, *Environ. Sci. Technol.*, 48(20), 12047–12055, doi:[10.1021/es503432r](https://doi.org/10.1021/es503432r), 2014.
- Li, H., Zhang, Q., Jiang, W., Collier, S., Sun, Y., Zhang, Q. and He, K.: Characteristics and sources of water-soluble organic aerosol in a heavily polluted environment in Northern China, *Sci. Total Environ.*, 758, 143970, doi:<https://doi.org/10.1016/j.scitotenv.2020.143970>, 2021.
- Li, J., Zhang, Q., Wang, G., Li, J., Wu, C., Liu, L., Wang, J., Jiang, W., Li, L., Ho, K. F. and Cao, J.: Optical properties and molecular compositions of water-soluble and water-insoluble brown carbon (BrC) aerosols in northwest China, *Atmos. Chem. Phys.*, 20(8), 4889–4904, doi:[10.5194/acp-20-4889-2020](https://doi.org/10.5194/acp-20-4889-2020), 2020.
- Lim, Y. B. and Turpin, B. J.: Laboratory evidence of organic peroxide and peroxyhemiacetal formation in the aqueous phase and implications for aqueous OH, *Atmos. Chem. Phys.*, 15(22), 12867–12877, doi:[10.5194/acp-15-12867-2015](https://doi.org/10.5194/acp-15-12867-2015), 2015.
- Lin, P., Laskin, J., Nizkorodov, S. A. and Laskin, A.: Revealing Brown Carbon Chromophores Produced in Reactions of Methylglyoxal with Ammonium Sulfate, *Environ. Sci. Technol.*, 49(24), 14257–14266, doi:[10.1021/acs.est.5b03608](https://doi.org/10.1021/acs.est.5b03608), 2015.
- Lin, P., Aiona, P. K., Li, Y., Shiraiwa, M., Laskin, J., Nizkorodov, S. A. and Laskin, A.: Molecular Characterization of Brown Carbon in Biomass Burning Aerosol Particles, *Environ. Sci. Technol.*, 50(21), 11815–11824, doi:[10.1021/acs.est.6b03024](https://doi.org/10.1021/acs.est.6b03024), 2016.
- Liu, J., Bergin, M., Guo, H., King, L., Kotra, N., Edgerton, E. and Weber, R. J.: Size-resolved measurements of brown carbon in water and methanol extracts and estimates of their contribution to ambient fine-particle light absorption, *Atmos. Chem. Phys.*, 13(24), 12389–12404, doi:[10.5194/acp-13-12389-2013](https://doi.org/10.5194/acp-13-12389-2013), 2013.
- Ma, L., Worland, R., Jiang, W., Niedeck, Christopher Guzman, C., Bein, K., Zhang, Q. and

- Anastasio, C.: Predicting photooxidant concentrations in aerosol liquid water based on laboratory extracts of ambient particles., n.d.
- Matheson, I. B. C. and Lee, J.: CHEMICAL REACTION RATES OF AMINO ACIDS WITH SINGLET OXYGEN, *Photochem. Photobiol.*, 29(5), 879–881, doi:<https://doi.org/10.1111/j.1751-1097.1979.tb07786.x>, 1979.
- Mok, J., Krotkov, N. A., Arola, A., Torres, O., Jethva, H., Andrade, M., Labow, G., Eck, T. F., Li, Z., Dickerson, R. R., Stenchikov, G. L., Osipov, S. and Ren, X.: Impacts of brown carbon from biomass burning on surface UV and ozone photochemistry in the Amazon Basin, *Sci. Rep.*, 6(1), 36940, doi:10.1038/srep36940, 2016.
- Moschos, V., Kumar, N. K., Daellenbach, K. R., Baltensperger, U., Prévôt, A. S. H. and El Haddad, I.: Source Apportionment of Brown Carbon Absorption by Coupling Ultraviolet–Visible Spectroscopy with Aerosol Mass Spectrometry, *Environ. Sci. Technol. Lett.*, 5(6), 302–308, doi:10.1021/acs.estlett.8b00118, 2018.
- Niedek, C. R., Mei, F., Zawadowicz, M. A., Zhu, Z., Schmid, B. and Zhang, Q.: Quantitative Chemical Assay of Nanogram-Level PM Using Aerosol Mass Spectrometry: Characterization of Particles Collected from Uncrewed Atmospheric Measurement Platforms, *Atmos. Meas. Tech. Discuss.*, 2022, 1–23, doi:10.5194/amt-2022-246, 2022.
- Reisen, F., Meyer, C. P., Weston, C. J. and Volkova, L.: Ground-Based Field Measurements of PM<sub>2.5</sub> Emission Factors From Flaming and Smoldering Combustion in Eucalypt Forests, *J. Geophys. Res. Atmos.*, 123(15), 8301–8314, doi:<https://doi.org/10.1029/2018JD028488>, 2018.
- Reyes-Villegas, E., Priestley, M., Ting, Y.-C., Haslett, S., Bannan, T., Le Breton, M., Williams, P. I., Bacak, A., Flynn, M. J., Coe, H., Percival, C. and Allan, J. D.: Simultaneous aerosol mass spectrometry and chemical ionisation mass spectrometry measurements during a biomass burning event in the UK: insights into nitrate chemistry, *Atmos. Chem. Phys.*, 18(6), 4093–4111, doi:10.5194/acp-18-4093-2018, 2018.
- Saleh, R., Marks, M., Heo, J., Adams, P. J., Donahue, N. M. and Robinson, A. L.: Contribution of brown carbon and lensing to the direct radiative effect of carbonaceous aerosols from biomass and biofuel burning emissions, *J. Geophys. Res. Atmos.*, 120(19), 10,210-285,296, doi:<https://doi.org/10.1002/2015JD023697>, 2015.
- Scully, F. E. and Hoigné, J.: Rate constants for reactions of singlet oxygen with phenols and other compounds in water, *Chemosphere*, 16(4), 681–694, doi:[https://doi.org/10.1016/0045-6535\(87\)90004-X](https://doi.org/10.1016/0045-6535(87)90004-X), 1987.
- Seinfeld, John H. ; Pandis, S. N.: *Atmospheric Chemistry and Physics: From Air Pollution to Climate Change*, 3rd ed., 2016.
- Setyan, A., Zhang, Q., Merkel, M., Knighton, W. B., Sun, Y., Song, C., Shilling, J. E., Onasch, T. B., Herndon, S. C., Worsnop, D. R., Fast, J. D., Zaveri, R. A., Berg, L. K., Wiedensohler, A., Flowers, B. A., Dubey, M. K. and Subramanian, R.: Characterization of submicron particles influenced by mixed biogenic and anthropogenic emissions using high-resolution aerosol mass spectrometry: results from CARES, *Atmos. Chem. Phys.*, 12(17), 8131–8156, doi:10.5194/acp-12-8131-2012, 2012.

- Shamjad, P. M., Tripathi, S. N., Thamban, N. M. and Vreeland, H.: Refractive Index and Absorption Attribution of Highly Absorbing Brown Carbon Aerosols from an Urban Indian City-Kanpur, *Sci. Rep.*, 6(1), 37735, doi:10.1038/srep37735, 2016.
- Smith, J. D., Sio, V., Yu, L., Zhang, Q. and Anastasio, C.: Secondary Organic Aerosol Production from Aqueous Reactions of Atmospheric Phenols with an Organic Triplet Excited State, *Environ. Sci. Technol.*, 48(2), 1049–1057, doi:10.1021/es4045715, 2014.
- Smith, J. D., Kinney, H. and Anastasio, C.: Phenolic carbonyls undergo rapid aqueous photodegradation to form low-volatility, light-absorbing products, *Atmos. Environ.*, 126, 36–44, doi:http://dx.doi.org/10.1016/j.atmosenv.2015.11.035, 2016.
- Sumlin, B. J., Pandey, A., Walker, M. J., Pattison, R. S., Williams, B. J. and Chakrabarty, R. K.: Atmospheric Photooxidation Diminishes Light Absorption by Primary Brown Carbon Aerosol from Biomass Burning, *Environ. Sci. Technol. Lett.*, doi:10.1021/acs.estlett.7b00393, 2017.
- Sun, Y. L., Zhang, Q., Anastasio, C. and Sun, J.: Insights into secondary organic aerosol formed via aqueous-phase reactions of phenolic compounds based on high resolution mass spectrometry, *Atmos. Chem. Phys.*, 10(10), 4809–4822, doi:10.5194/acp-10-4809-2010, 2010.
- Sun, Y. L., Zhang, Q., Schwab, J. J., Yang, T., Ng, N. L. and Demerjian, K. L.: Factor analysis of combined organic and inorganic aerosol mass spectra from high resolution aerosol mass spectrometer measurements, *Atmos. Chem. Phys.*, 12(18), 8537–8551, doi:10.5194/acp-12-8537-2012, 2012.
- Tong, H., Arangio, A. M., Lakey, P. S. J., Berkemeier, T., Liu, F., Kampf, C. J., Brune, W. H., Pöschl, U. and Shiraiwa, M.: Hydroxyl radicals from secondary organic aerosol decomposition in water, *Atmos. Chem. Phys.*, 16(3), 1761–1771, doi:10.5194/acp-16-1761-2016, 2016.
- Tong, H., Lakey, P. S. J., Arangio, A. M., Socorro, J., Kampf, C. J., Berkemeier, T., Brune, W. H., Pöschl, U. and Shiraiwa, M.: Reactive oxygen species formed in aqueous mixtures of secondary organic aerosols and mineral dust influencing cloud chemistry and public health in the Anthropocene, *Faraday Discuss.*, 200(0), 251–270, doi:10.1039/C7FD00023E, 2017.
- Ulbrich, I. M., Canagaratna, M. R., Zhang, Q., Worsnop, D. R. and Jimenez, J. L.: Interpretation of organic components from Positive Matrix Factorization of aerosol mass spectrometric data, *Atmos. Chem. Phys.*, 9(9), 2891–2918, doi:10.5194/acp-9-2891-2009, 2009.
- Washenfelder, R. A., Attwood, A. R., Brock, C. A., Guo, H., Xu, L., Weber, R. J., Ng, N. L., Allen, H. M., Ayres, B. R., Baumann, K., Cohen, R. C., Draper, D. C., Duffey, K. C., Edgerton, E., Fry, J. L., Hu, W. W., Jimenez, J. L., Palm, B. B., Romer, P., Stone, E. A., Wooldridge, P. J. and Brown, S. S.: Biomass burning dominates brown carbon absorption in the rural southeastern United States, *Geophys. Res. Lett.*, 42(2), 653–664, doi:https://doi.org/10.1002/2014GL062444, 2015.
- Young, D. E., Kim, H., Parworth, C., Zhou, S., Zhang, X., Cappa, C. D., Seco, R., Kim, S. and Zhang, Q.: Influences of emission sources and meteorology on aerosol chemistry in a polluted urban environment: results from DISCOVER-AQ California, *Atmos. Chem. Phys.*,

16(8), 5427–5451, doi:10.5194/acp-16-5427-2016, 2016.

Yu, L., Smith, J., Laskin, A., Anastasio, C., Laskin, J. and Zhang, Q.: Chemical characterization of SOA formed from aqueous-phase reactions of phenols with the triplet excited state of carbonyl and hydroxyl radical, *Atmos. Chem. Phys.*, 14(24), 13801–13816, doi:10.5194/acp-14-13801-2014, 2014.

Yu, L., Smith, J., Laskin, A., George, K. M., Anastasio, C., Laskin, J., Dillner, A. M. and Zhang, Q.: Molecular transformations of phenolic SOA during photochemical aging in the aqueous phase: competition among oligomerization, functionalization, and fragmentation, *Atmos. Chem. Phys.*, 16(7), 4511–4527, doi:10.5194/acp-16-4511-2016, 2016.

ZEPP, R. G., WOLFE, N. L. E. E., BAUGHMAN, G. L. and HOLLIS, R. C.: Singlet oxygen in natural waters, *Nature*, 267(5610), 421–423, doi:10.1038/267421a0, 1977.

Zhang, Q., Jimenez, J. L., Canagaratna, M. R., Ulbrich, I. M., Ng, N. L., Worsnop, D. R. and Sun, Y.: Understanding atmospheric organic aerosols via factor analysis of aerosol mass spectrometry: a review, *Anal. Bioanal. Chem.*, 401(10), 3045–3067, doi:10.1007/s00216-011-5355-y, 2011.

Zhang, Y., Xu, J., Shi, J., Xie, C., Ge, X., Wang, J., Kang, S. and Zhang, Q.: Light absorption by water-soluble organic carbon in atmospheric fine particles in the central Tibetan Plateau, *Environ. Sci. Pollut. Res.*, 24(26), 21386–21397, doi:10.1007/s11356-017-9688-8, 2017.

Zhao, R., Lee, A. K. Y., Huang, L., Li, X., Yang, F. and Abbatt, J. P. D.: Photochemical processing of aqueous atmospheric brown carbon, *Atmos. Chem. Phys.*, 15(11), 6087–6100, doi:10.5194/acp-15-6087-2015, 2015.

Zhou, S., Collier, S., Xu, J., Mei, F., Wang, J., Lee, Y.-N., Sedlacek III, A. J., Springston, S. R., Sun, Y. and Zhang, Q.: Influences of upwind emission sources and atmospheric processing on aerosol chemistry and properties at a rural location in the Northeastern U.S., *J. Geophys. Res. Atmos.*, 121(10), 6049–6065, doi:https://doi.org/10.1002/2015JD024568, 2016.

Zhou, S., Collier, S., Jaffe, D. A., Briggs, N. L., Hee, J., Sedlacek III, A. J., Kleinman, L., Onasch, T. B. and Zhang, Q.: Regional influence of wildfires on aerosol chemistry in the western US and insights into atmospheric aging of biomass burning organic aerosol, *Atmos. Chem. Phys.*, 17(3), 2477–2493, doi:10.5194/acp-17-2477-2017, 2017.



## Supporting Information

**Table S1.** Information of PM<sub>2.5</sub> sample collection

Sample ID	Start Date of Sampling	Sampling Time (hr) <sup>e</sup>	Average PM <sub>2.5</sub> Concentration (μg m <sup>-3</sup> ) <sup>f</sup>	Estimated Equivalent Liquid Water Content (mg m <sup>-3</sup> ) <sup>g</sup>
11/12/2019	11/12/2019	168 (a week)	13.2	9.4
12/3/2019	12/3/2019	24	10.6	65.7
12/17/2019	12/17/2019	168 (a week)	9.0	9.4
1/2/2020	1/2/2020	24	10.2	65.7
1/3/2020	1/3/2020	168 (a week)	10.0	9.4
2/20/2020	2/20/2020	24	9.0	65.7
3/4/2020	3/4/2020	24	8.4	65.7
7/7/2020	7/7/2020	24	7.0	65.7
8/4/2020	8/4/2020	24	7.2	65.7
8/19/2020 <sup>a</sup>	8/19/2020	24	67.9	65.7
8/24/2020 <sup>a</sup>	8/24/2020	24	57.2	65.7
9/9/2020 <sup>a</sup>	9/9/2020	24	44.6	65.7
9/15/2020	9/15/2020	24	19.5	65.7
10/8/2020	10/8/2020	24	33.9	65.7
10/15/2020	10/15/2020	24	7.9	65.7
Summer <sup>b, d</sup>	/	28.8 (average)	49.3	38.3
Winter <sup>c, d</sup>	/	169.7(average)	9.1	6.6

a. Samples influenced by the wildfire occurred in Lake Berryessa area (See fire map in Figure S6).

b. A summer sample that evenly combines filters collected on 8/20/2020 (24 h), 8/21/2020 (40 hr), and 8/23/2020 (23 hr).

c. A winter sample that evenly combines filters collected on 2/5/2020 (a week), 2/13/2020 (a week), and 2/21/2020 (a week).

d. Samples extracted with 0.7 mL of water per filter cut while other samples were extracted with 1 mL of water per filter cut.

e. The air flow rate through each 10×8 inch filter was 40 cfm during sampling.

f. Average PM<sub>2.5</sub> concentration during each sampling period measured at the UC Davis sampling site by the California Air Resources Board.

g. The equivalent liquid water content (LWC, mg m<sup>-3</sup>) of each PM extract sample was calculated as:  $LWC = \frac{V_{\text{water}} \times \rho_{\text{water}}}{T \times Q \times \frac{A_{\text{cut}}}{A_{\text{filter}}}}$ . In this equation, V<sub>water</sub> is the volume (mL) of water used to extract each

square cut of filter, ρ<sub>water</sub> is the density (mg mL<sup>-1</sup>) of water, T is the sampling duration (hr) of the filter, Q is the air flow rate (m<sup>3</sup> hr<sup>-1</sup>) through the filter during sampling, A<sub>cut</sub> is the area (cm<sup>2</sup>) of the extracted filter cut, and A<sub>filter</sub> is the area (cm<sup>2</sup>) of the whole filter.

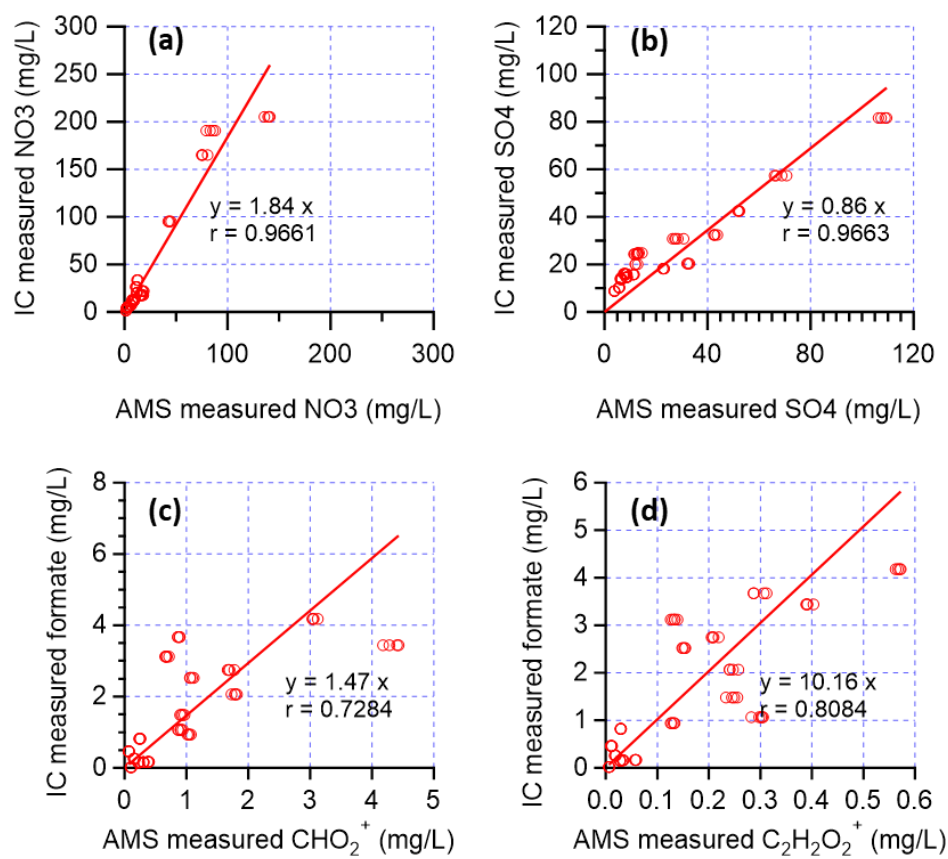


**Figure S1.** Scatter plots of IC- vs. AMS-measured (a) nitrate and (b) sulfate, and scatter plots of IC measured formate versus AMS acid tracer ions (c) CHO<sub>2</sub><sup>+</sup> and (d) C<sub>2</sub>H<sub>2</sub>O<sub>2</sub><sup>+</sup> in the PM extracts.

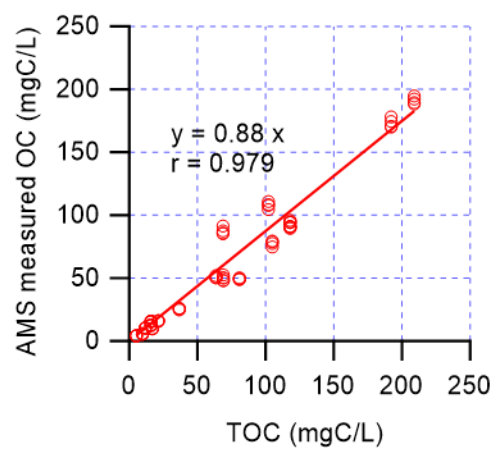


**Figure S2.** Scatter plots of AMS measured organic carbon versus that by TOC analyzer.

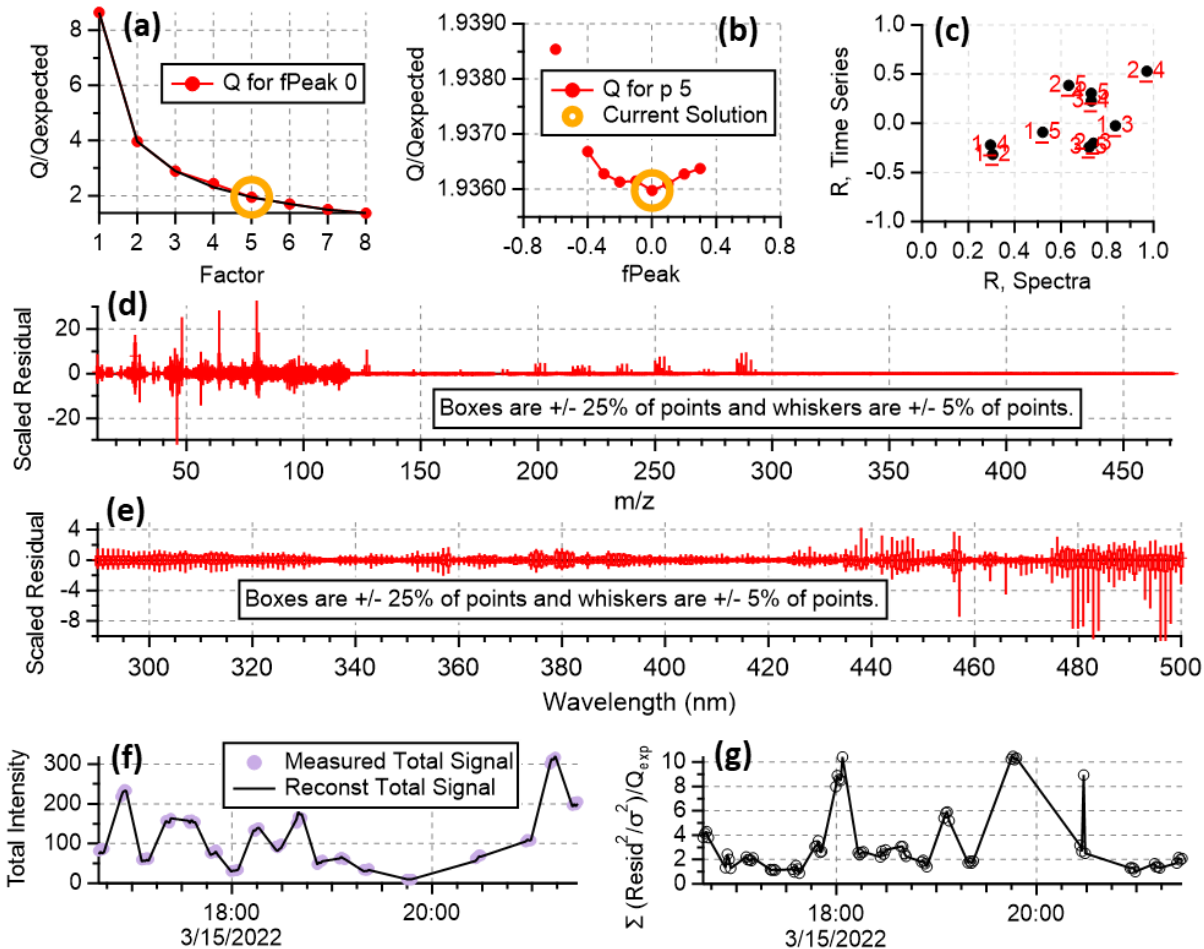


**Figure S3.** Summary of diagnostic plots for the five-factor solution for PMF analysis: (a)  $Q/Q_{\text{exp}}$  as a function of number of factors selected for PMF modeling. (b)  $Q/Q_{\text{exp}}$  as a function of  $f_{\text{Peak}}$ . (c) Correlations among PMF factors. (d) Box and whisker plot showing the distributions of scaled residuals for each AMS ion. (e) Box and whisker plot showing the distributions of scaled residuals for each light absorption wavelength. (f) Reconstructed and measured total signal for each sample. (g)  $Q/Q_{\text{exp}}$  for each sample.

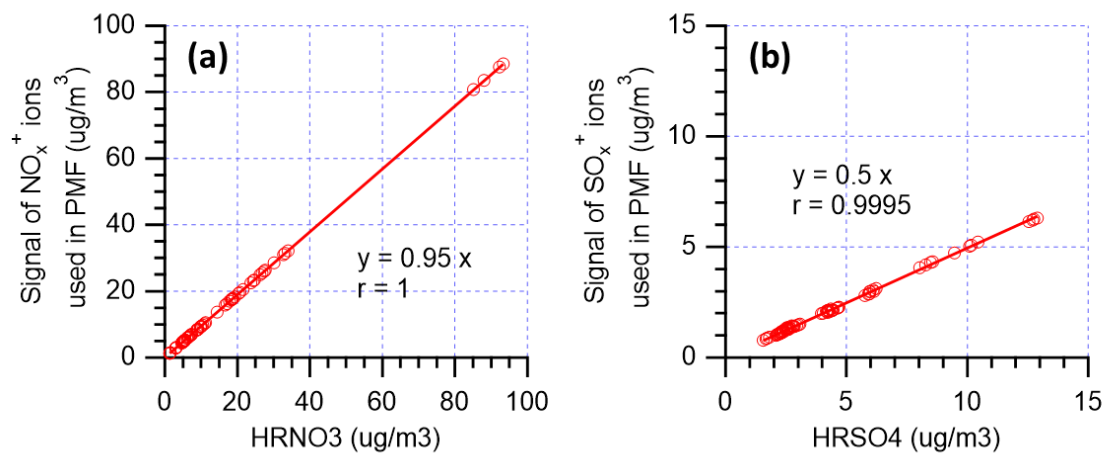


**Figure S4.** (a) Relationship between the signal of the  $\text{NO}_x^+$  ions used in PMF (i.e.,  $\text{NO}^+$  and  $\text{NO}_2^+$ ) and the total nitrate signal. (b) Relationship between the signal of the  $\text{SO}_x^+$  ions used in PMF (i.e.,  $\text{SO}^+$ ,  $\text{SO}_2^+$ ,  $\text{HSO}_2^+$ ,  $\text{SO}_3^+$ ,  $\text{HSO}_3^+$ ,  $\text{H}_2\text{SO}_4^+$ ) and the total sulfate signal.

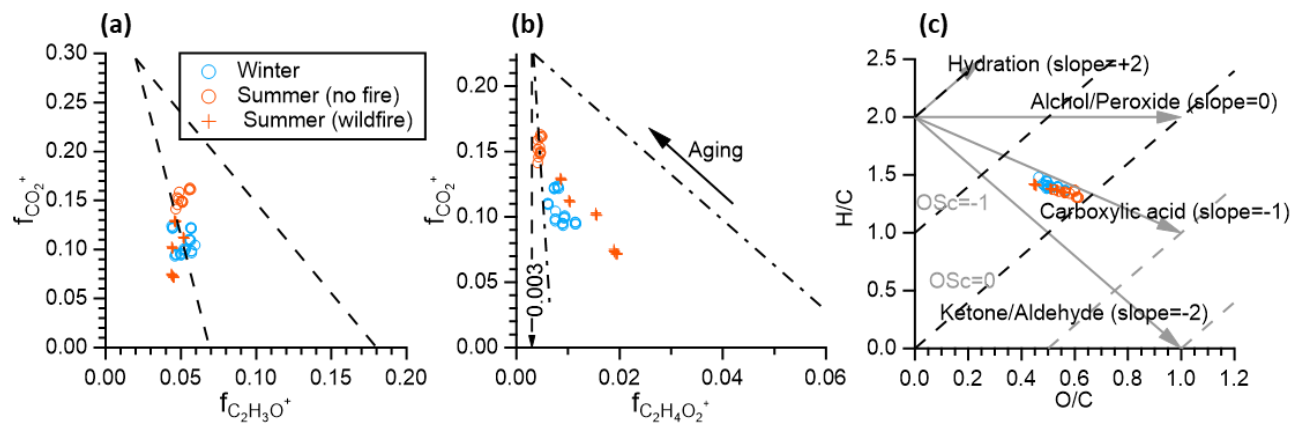


**Figure S5.** (a)  $f_{44}$  vs.  $f_{43}$ , (b)  $f_{44}$  vs.  $f_{60}$  and (c) Van Krevelen diagram for the WSOA in the PM extracts.

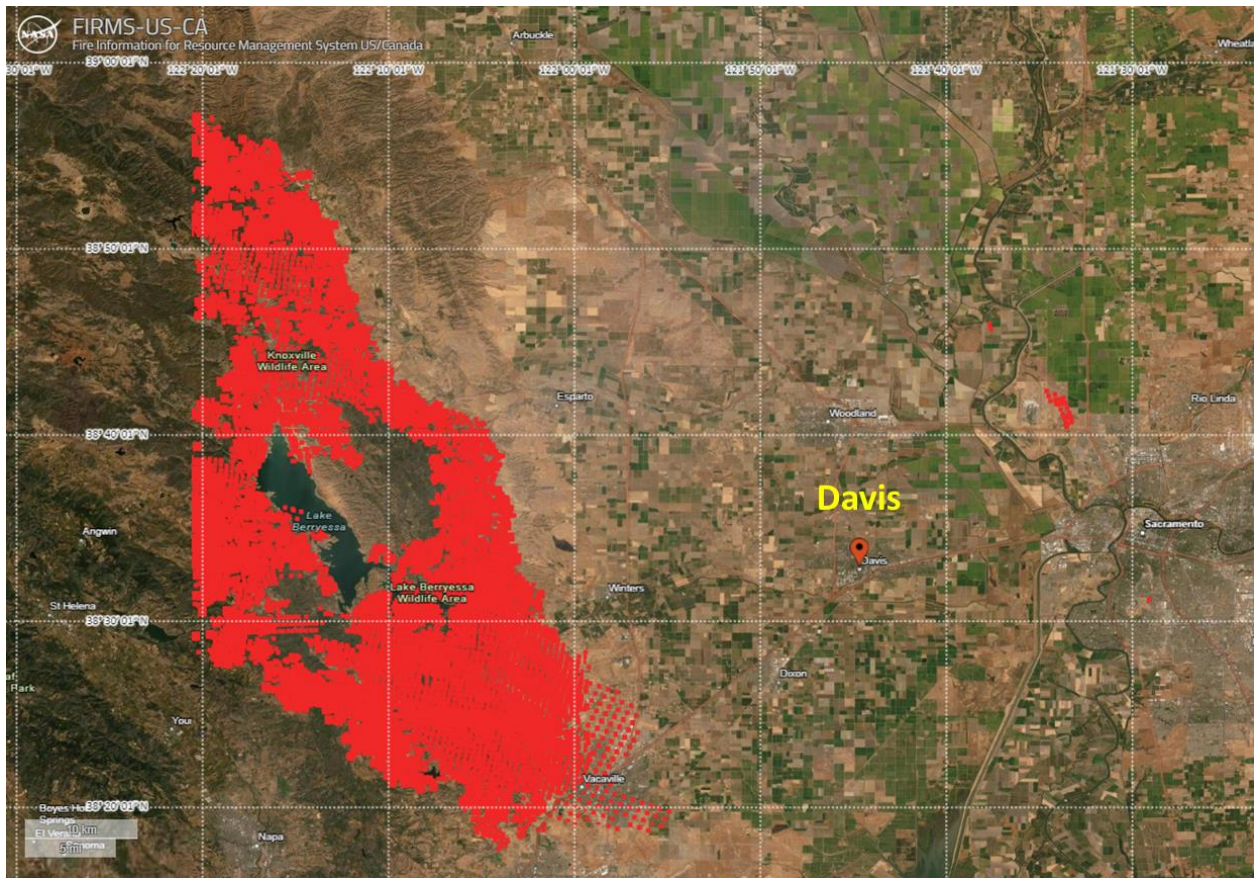


**Figure S6.** Map of the sample collection site (Davis) and the adjacent area in northern California, with wildfires detected by MODIS and VIIRS (red squares) from August 18 to September 9, 2020.



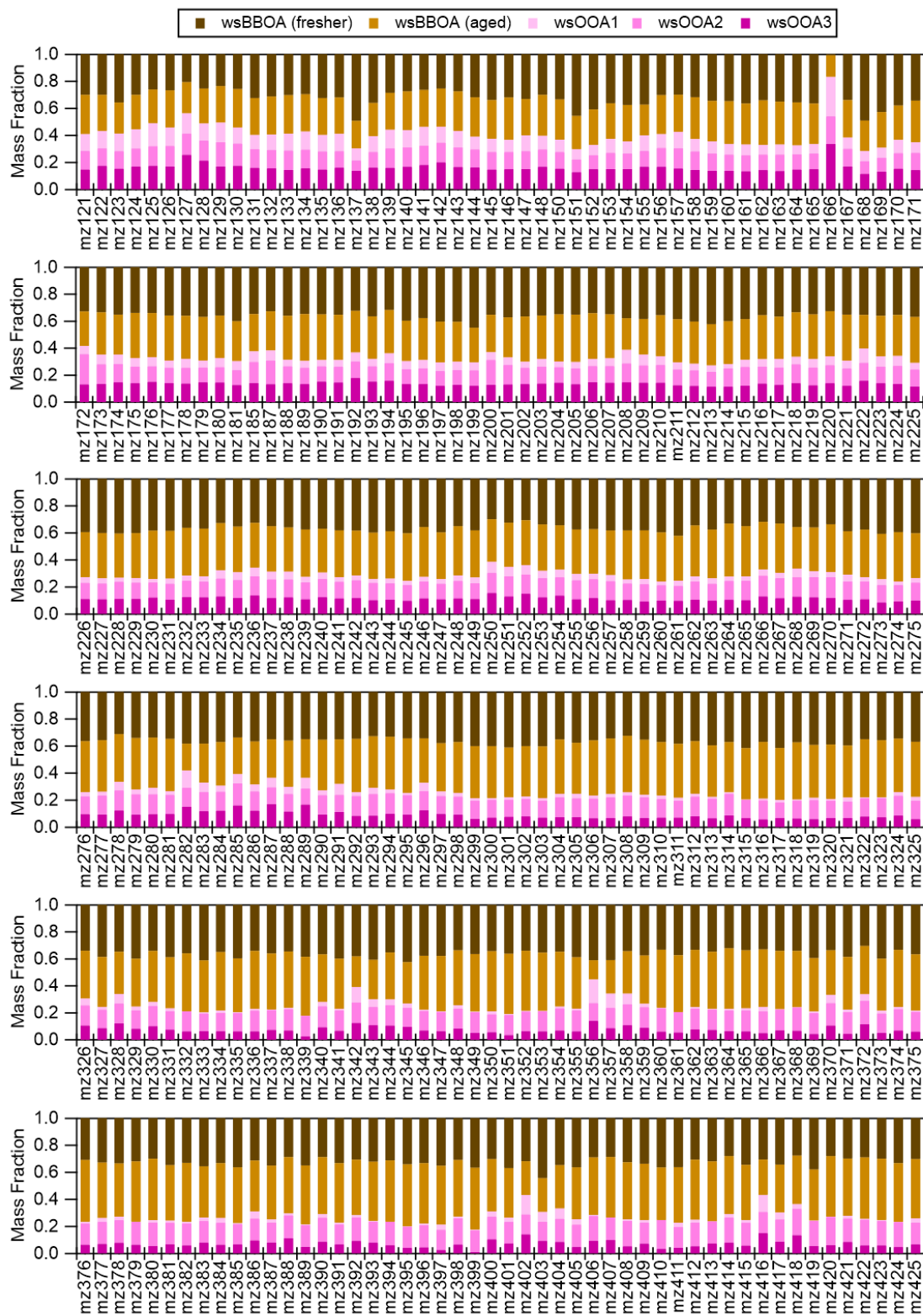


**Figure S7.** Contributions of the five WSOA factors to the high m/z ions (m/z > 120, unit mass resolution) in the PM extracts.



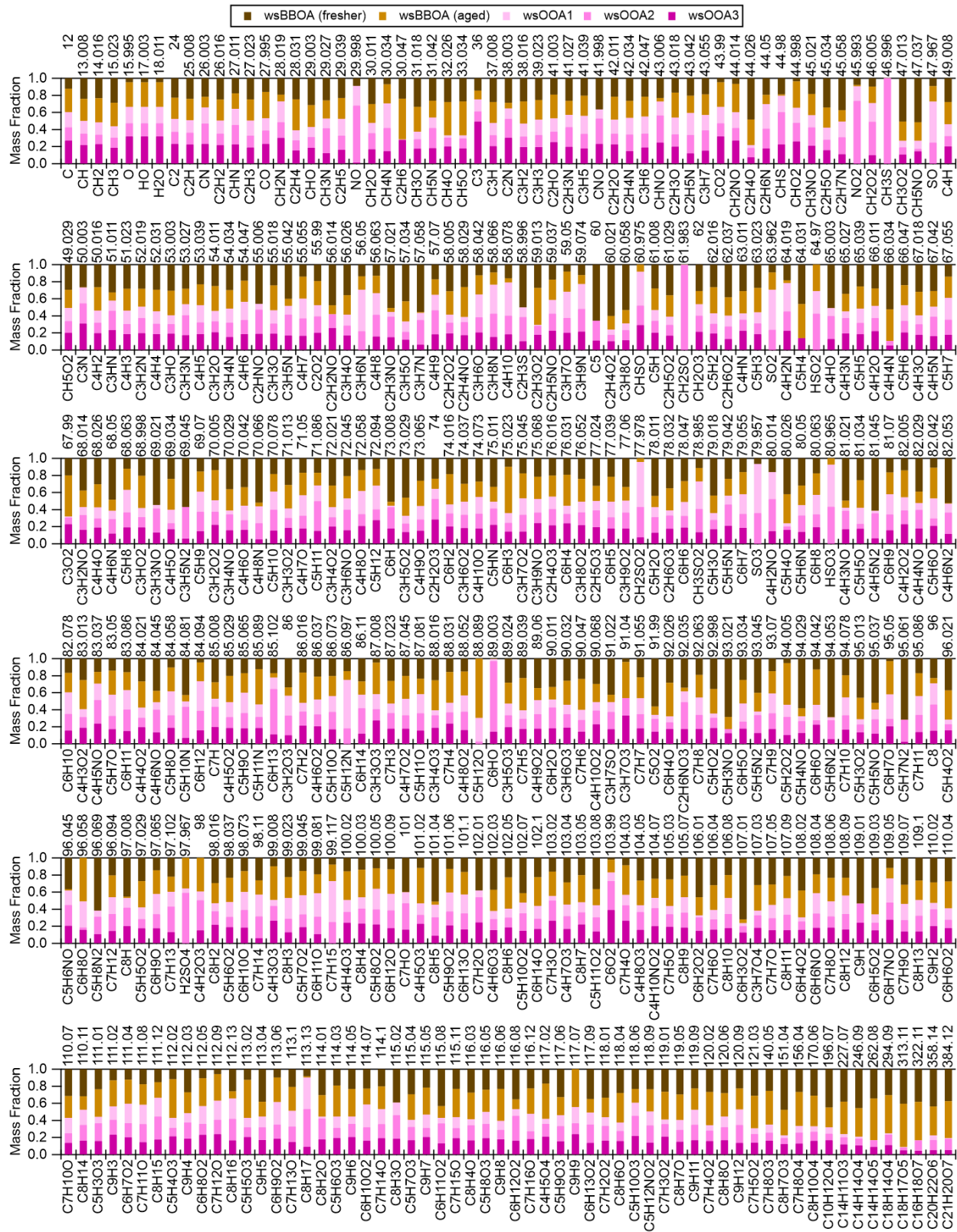


**Figure S8.** Contributions of the five WSOA factors to individual AMS ions in the PM extracts.

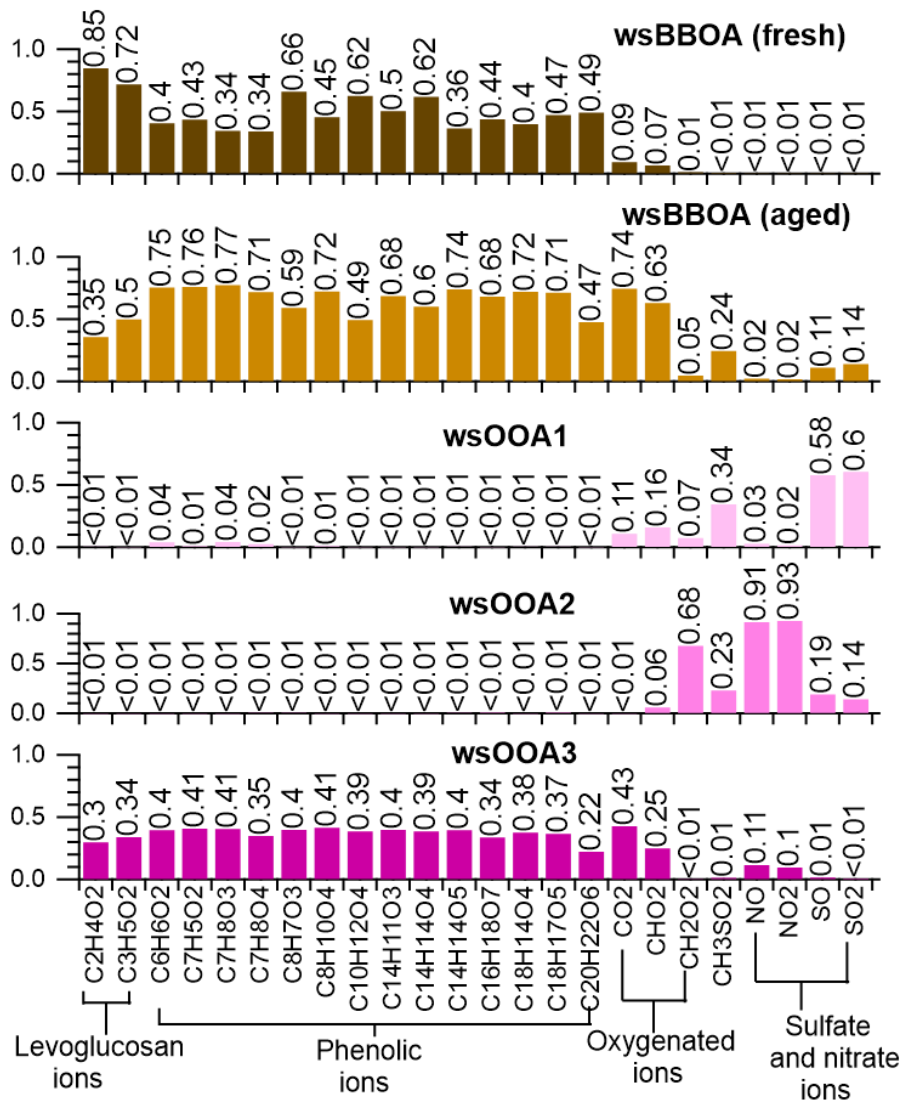


**Figure S9.** Correlations between WSOA factors and selected tracer ions, including fresh BBOA tracers, phenolic tracers, oxygenated organic tracers, and sulfate and nitrate tracers.

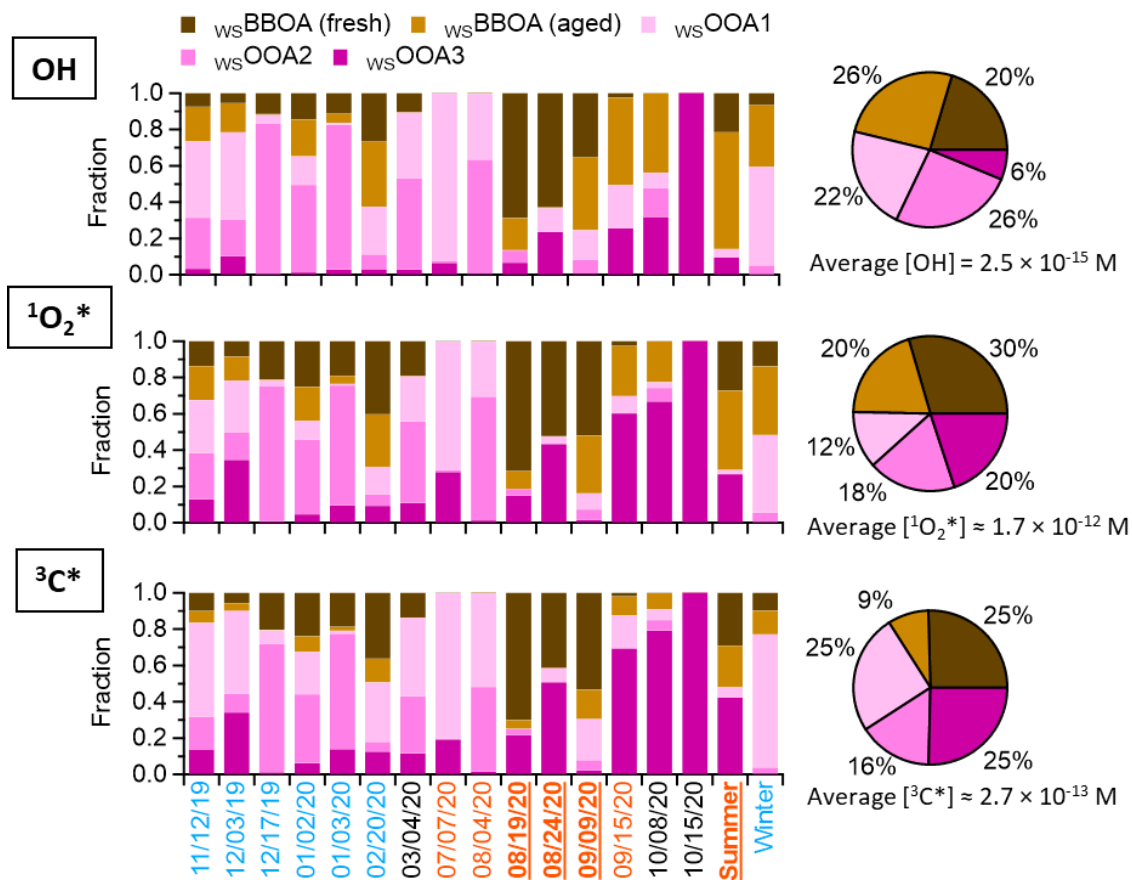


**Figure S10.** Fractional contributions of the five WSOA factors to oxidant ( $\bullet\text{OH}$ ,  $^1\text{O}_2^*$  and  $^3\text{C}^*$ ) concentrations in PM extracts.

## S1. Calculation of species concentration and mass absorption coefficient of PMF factors

The organic concentration of a PMF factor in solution ( $[\text{Org}]_i$ ,  $\mu\text{g mL}^{-1}$ ) was calculated as:

$$[\text{Org}]_i = f_{\text{org},i} \times [\text{Total Signal}]_i \quad (\text{Eq. S1})$$

where  $f_{\text{org},i}$  is the fraction of organic signals in the factor's spectral profile, and  $[\text{Total Signal}]_i$  is the total signal of the factor. The concentrations of nitrate and sulfate associated with a PMF factor ( $[\text{NO}_3]_i$  and  $[\text{SO}_4]_i$ ,  $\mu\text{g mL}^{-1}$ ) in solution were calculated as:

$$[\text{NO}_3]_i = \frac{f_{\text{NO}_x^+,i} \times [\text{Total Signal}]_i}{R_{\text{NO}_x^+/\text{HRNO}_3}} \quad (\text{Eq. S2})$$

and

$$[\text{SO}_4]_i = \frac{f_{\text{SO}_x^+,i} \times [\text{Total Signal}]_i}{R_{\text{SO}_x^+/\text{HRSO}_4}} \quad (\text{Eq. S3})$$

where  $f_{\text{NO}_x^+,i}$  is the fraction of  $\text{NO}_x^+$  ion signals in the factor's spectral profile,  $R_{\text{NO}_x^+/\text{HRNO}_3}$  is the ratio of the  $\text{NO}_x^+$  ions to the total nitrate signal (Figure S4a),  $f_{\text{SO}_x^+,i}$  is the fraction of  $\text{SO}_x^+$  ion signals in the factor's spectral profile, and  $R_{\text{SO}_x^+/\text{HRSO}_4}$  is the ratio of the  $\text{SO}_x^+$  ions to the total sulfate signal (Figure S4b). In addition, the species ambient concentrations can be calculated from the concentrations in solution using Eq. 6. The mass absorption coefficient of a PMF factor ( $\text{MAC}_{\lambda,i}$ ,  $\text{m}^2 \text{g}^{-1}$ ) was calculated as:

$$\text{MAC}_{\lambda,i} = 2.303 \times \frac{f_{\text{abs},\lambda,i} \times [\text{Total Signal}]_i}{[\text{Org}]_i} \times 100 \quad (\text{Eq. S4})$$

where  $f_{\text{abs},\lambda,i}$  is the fraction of the light absorption signal at wavelength  $\lambda$  in the factor's spectral profile, 2.303 is a conversion factor between  $\log_{10}$  and natural log, and 100 is for unit conversion.

## Chapter 6: Conclusions

SOA accounts for a substantial fraction of atmospheric aerosol and significantly impacts global climate and human health. A multitude of field and laboratory studies have been done to understand the formation, composition, properties and fate of SOA. However, due to the high complexity in precursors, reaction pathways and atmospheric conditions, thorough characterization of SOA is still challenging. This dissertation focuses on phenolic SOA formation and aging, as well as BrC formation in phenolic SOA. Apart from this, this dissertation also further explores the composition and properties of ambient water-soluble BrC aerosol. Important conclusions from this dissertation include:

- 1. The aqueous-phase photosensitized reaction of phenolic compounds with  $^3\text{C}^*$  is fast and produces aqSOA efficiently.** The atmospheric half-life of GA (a phenolic carbonyl model compound) corresponding to  $^3\text{C}^*$  reaction is on the order of hours in BB-impacted cloud/fog water, and this reaction produces aqSOA which is more oxygenated and more oxidized than the precursor with mass yield  $\sim 80\%$ .
- 2. The composition of the phenolic aqSOA evolves continuously, with oligomerization and functionalization dominating the initial formation, but fragmentation playing an important role in later periods.** The phenolic aqSOA gets increasingly more oxidized during formation. Three generations of aqSOA products are identified. The first generation, which grows rapidly upon irradiation, is the least oxidized and is enriched of high molecular weight products (e.g., oligomers of phenols). With the proceeding of the reaction, the 1<sup>st</sup>-generation products are transformed via hydroxylation, demethoxylation, and partial ring-opening to form functionalized monomers and dimers, and probably due to decreased precursor concentration, functionalization becomes increasingly important and competes

with oligomerization in the 2nd generation products. The 3rd generation products, which are the most oxidized, start to build up when the majority of the precursor reacts, and are dominated by lower molecular weight products (e.g., small carboxylic acids and other ring-opening products that don't retain the aromaticity).

- 3. Significant carboxylic acid production is involved in phenolic aqSOA formation.** Both AMS and IC analyses indicate continuous formation of carboxylic acids. The  $\text{CHO}_2^+$  signal detected by AMS correlates well with the IC-measured total concentration of five small carboxylic acids, suggesting that  $\text{CHO}_2^+$  can possibly be used as an AMS marker for carboxylic acids. Acid formation becomes increasingly important with the proceeding of the reaction, account for up to ~10% of the total aqueous organic carbon mass in the later periods of aqSOA formation. Among the determined small acids, oxalic acid plays an important role in phenolic aqSOA.
- 4. BrC compounds are formed in initial phenolic aqSOA formation.** Phenolic aqSOA formation exhibits an initial photo-enhancement of the aqueous phase followed by a slight photo-bleaching in the later periods. The initially formed oligomeric and hydroxylated products appear to be important BrC chromophores with absorption extended to ~ 400 nm. However, fragmentation and ring-opening reactions destroy the BrC chromophores.
- 5. Differences in composition and light absorption exist between the phenolic aqSOA formation from different oxidants.** Under the conditions of BB-influenced cloud/fog water, the photosensitized  $^3\text{C}^*$  reaction of phenols can be significantly faster and more efficient in producing low-volatility products than the  $\bullet\text{OH}$  reaction. When the phenolic precursor reacts out, the aqSOA formed from  $^3\text{C}^*$  reaction ( $^3\text{C}^*$ -aqSOA) shows more enhanced oligomeric and high molecular-weight products, while the aqSOA formed from

•OH reaction (•OH-aqSOA) is more oxidized and enriched of small, highly oxygenated species. Accordingly, the  $^3\text{C}^*$ -aqSOA can be more light-absorbing than the •OH-aqSOA.

- 6. Fragmentation and evaporation of volatile products dominates the prolonged photo-aging of phenolic aqSOA.** Significant phenolic aqSOA mass loss (i.e., 39% and 47% of the •OH-aqSOA and  $^3\text{C}^*$ -aqSOA, respectively) occurs in the prolonged photo-aging equivalent to several days in the atmosphere. Although the lifetime of cloud and fog drops is typically short, the low-volatility species (aqSOA products) in the droplets can remain in particles when the water evaporates, and the aerosol particles could then serve as condensation nuclei for cloud and fog which ensure re-dissolution of the water-soluble aqSOA products. This process may occur multiple times over the aerosol lifetime and leads to long time of atmospheric aging. The significant SOA mass loss observed in this study suggest that photochemical aging may serve as an important removal process for atmospheric aqSOA besides wet and dry deposition.
- 7. Prolonged photo-aging may lead to less oxidized aqSOA.** Although photochemical aging generally increases the oxidation degree of phenolic aqSOA, a slight decreased oxidation degree of •OH-aqSOA was observed after long time aging (i.e., 60 h of illumination in the experiment). This may be explained by evaporation of highly oxidized compounds induced by extended oxidation.
- 8. Significant loss of BrC chromophores in prolonged photo-aging of phenolic aqSOA.** Pronounced photobleaching occurs in prolonged photo-aging, and the phenolic aqSOA shifts from the weak BrC class to the very weak BrC class. In addition, our PMF analysis on combined AMS and UV-vis data suggests that the 2<sup>nd</sup>-generation phenolic aqSOA (which is moderately oxidized and enriched in functionalized phenolic monomers and

derivatives of phenolic oligomers with partial ring opening) represents the most light-absorbing phenolic aqSOA products in near-UV and visible range.

- 9. Elevated oxidant concentration during aging promotes the decay of phenolic aqSOA mass and BrC chromophores.** Increased OH and  $^3\text{C}^*$  concentration accelerates the chemical evolution of phenolic aqSOA, promotes fragmentation and eventually promotes evaporation of volatile products, resulting in faster aqSOA mass loss and bleaching. However, compared with  $\bullet\text{OH}$ , additional  $^3\text{C}^*$  exposure during aging may be capable of producing additional low-volatility functionalized products which can partially counteract the promoted mass and absorption decay.
- 10. Gas-phase reaction of phenols generates gasSOA showing different chemical compositions than phenolic aqSOA.** Gas-phase OH oxidation produces highly oxidized phenolic gasSOA soon after the reaction starts, whereas aqueous-phase oxidation initially produces less-oxidized aqSOA which gradually gets more oxidized in the continuing aqSOA formation. Oligomerization is an important pathway for phenolic aqSOA formation but is not observed in phenolic gasSOA. In addition, carboxylic acid formation is more significant in phenolic aqSOA compared with that in gasSOA. Although prolonged aging may eventually lead to similar composition for phenolic gasSOA and aqSOA, the significant compositional differences between initially formed phenolic gasSOA and aqSOA suggest the necessity to involve both gas-phase and aqueous-phase reaction mechanisms in model predictions for SOA formation.

In addition to the lab studies on phenolic SOA and BrC formation and aging, this dissertation also investigated the composition and properties of ambient BrC aerosols.



**11. WS-BBOA is more light-absorbing than WS-OOA and can be the most important contributor to the total WS-BrC absorption in North California.** PMF analysis was performed on combined AMS and UV-vis measurement data of PM extract samples collected in Davis over one year and resolved five WSOA factors (including a fresh and an aged WS-BBOA and three WS-OOA factors) with distinct mass spectral and light absorption spectral profiles. Fresh WS-BBOA is significantly more light-absorbing than the more aged WS-BBOA, suggesting atmospheric aging results in photobleaching of WS-BBOA. Both the fresh and the aged WS-BBOAs are more light-absorbing than the more oxidized WS-OOAs. The high light absorptivity together with the high abundance of WS-BBOA make biomass burning the most important contributor to the total WS-BrC absorption (~89%) in Davis.

**12. WS-BBOA and WS-OOA can be potent sources of photo-oxidants in atmospheric waters.** The BrC chromophores in WS-BBOA and WS-OOA serve as an important source of condensed-phase  $^1\text{O}_2^*$  and  $^3\text{C}^*$ . The oxidant production potentials of WS-BBOA and WS-OOA determined in this study were applied to a variety of ambient locations for oxidant concentration estimation, and due to the general higher abundance of WS-OOA, the results show WS-OOA can be a more important source of  $^1\text{O}_2^*$  and  $^3\text{C}^*$  than WS-BBOA.